

On the Use of Hydrogen Peroxide in Ignition Systems

Bioinspiration from the Bombardier Beetle

By:

Andreas Prongidis

Submitted in accordance with the requirements for the degree of

Doctor of Philosophy

The University of Leeds

School of Process Environmental and Materials Engineering

September 2011

The candidate confirms that the work published is his/her own and that appropriate credit has been given where reference has been made to the work of others.

This copy has been supplied in the understanding that it is copyright material and that no quotation from the thesis may be published without proper acknowledgment.

ABSTRACT

A novel ignition system was studied experimentally, in which small volumes of hydrogen peroxide -of the order of $\mu\text{l/s}$ - were injected at the immediate site of ignition, during the firing of a focus discharge igniter (FDI). Initially, the new ignition system was evaluated at an atmospheric expansion rig in the Mechanical Engineering of Leeds University. Afterwards, experiments were undertaken in an atmospheric testing facility with an industrial Rolls-Royce Olympus combustion chamber using kerosene Jet-A1 as the fuel and atmospheric air as the oxidizer. The study concentrated on the determination of the lean ignition limits of the kerosene-air mixture at various air mass flow rates with and without the addition of H_2O_2 . Notable improvements, from 6.5% to 44%, in the ignition limits of the fuel-air mixture were attainable by using only a maximum amount of $10.8\mu\text{l/s}$ of H_2O_2 during only the ignition process. The study suggests that these improvements are directly related to the increase in the ignition efficiency of the ignitor, by radical enhancement through the injection of the H_2O_2 plasma medium. Comparisons were made, between a fuel atomiser that was in normal service and of the same device but washed, in order to test the igniter's ability to initiate combustion under poor and high fuel spray qualities (FSQ). The results indicate an enhanced improvement in the ignitability limits during poor air-fuel mixing quality when using the H_2O_2 as described above. A biodiesel fuel was also selected to test the effect that the new ignitor system has in a low-volatility fuel. The question of how to create the small amounts of hydrogen peroxide that will be used for ignition was also approached. An idea of producing the required H_2O_2 came by studying the bombardier's beetle unique mechanism which produces H_2O_2 for defending itself from predators. Simulation work using Chemkin was conducted to investigate the production of H_2O_2 by passing hydrocarbon fuels through a catalyst. When passing propane-air through a platinum/ rhodium catalyst the simulations show that H_2O_2 production is possible in rates enough to supply the proposed novel ignition system. A more specialised study in the chemistry of the production of H_2O_2 , from gas-turbine fuels, is suggested. A cost effective method of an onsite H_2O_2 production in small amounts would be an ideal topic for further study.

Acknowledgments

I would like to acknowledge my supervisor, Prof. Andy C. McIntosh for the guidance and support he has so kindly offered me throughout this work. Many thanks should also go to Prof. Chris Wilson for his expert advice in the subject of combustion and for the tools he provided us to make this work exciting. I would like to thank Prof. A.C. McIntosh and Dr. N. Beheshti for their leading role in building the prototype of the μ Mist device and for all the good times we had as a team. I would like to acknowledge the help I received from the staff and especially Dr. T. Dolmansley in the Low Carbon Combustion Centre lab. I shouldn't also forget S. Caddick for sharing his technical skills and for building the required hardware equipment.

I would like to express my deepest gratitude to my parents Helen and Kostas for always being there for me. I would also like to thank my sister Lydia for the special role she plays in my life.

I would like to thank my friends in the U.K. for all the great memories during this journey and especially Eleftheria, Stanislav, Ariadni and George, Marianna and Giannis, Katerina, Pinelopi and Helen.

My thoughts are always with my best friends in Greece, Panos, Giannis and Katerina, George, George and Spyros for whom I am grateful to enjoy such a true friendship.

Last but not least, I would like to declare my appreciation to my dearest Eleftheria for her love and devotion.

PUBLICATIONS

1. Prongidis, A., McIntosh A.C., Wilson C. and Dolmanslaey T., *Enhancement of ignition of a gas turbine by the addition of small amounts of H₂O₂*. Institute of Mechanical Engineers, Part A: Journal of Power and Energy, **226**(1) pp.49-61, Feb. 2012, ISSN: 0957-6509.
2. McIntosh, A.C. and Prongidis A., *Further biomimetic challenges from the bombardier beetle- the intricate chemical production system*. Design and Nature V, Proc. of 5th Int. Conference on Design and Nature, Pisa, Italy, 28-30 June 2010, Eds. C.A. Brebbia and A. Carpi, WIT Transactions on Ecology and the Environment, **138**, pp 265-272, WIT Press, 2010.

-TABLE OF CONTENTS-

	DESCRIPTION	PAGE
1	CHAPTER 1 - INTRODUCTION	
1.1	Thesis Outline	1
1.2	Problem Description	1
1.3	Application and Orientation of Research	4
1.4	Importance of Research	5
1.5	Bio-inspiration from the Bombardier Beetle	9
2	CHAPTER 2 - GAS TURBINE THEORY	
2.1	Chapter Outline	13
2.2	Working Principles of the Gas Turbine	
2.2.1	Gas Turbine Design	14
2.2.2	Working Cycle of the Gas Turbine	16
2.3	Basic Equations and Physical Laws	
2.3.1	Open System Equations	19
2.3.2	General Thermodynamic Equations in Fluid Flow	19
2.3.3	2 nd Law of Thermodynamics - Entropy	21
2.3.4	The Ideal Gas Law	23
2.3.5	Perfect and Ideal Gas Equations	23
2.4	More Specific Equations	
2.4.1	Thrust Equation for the Gas Turbine	24
2.4.2	Enthalpy for Under Constant Pressure Processes	25
2.4.3	Entropy for Under Constant Pressure Processes	25
2.4.4	Ideal Gases Undergoing Isentropic Processes	
	Pressure Ratio	25
	Pressure Density Ratio	26
2.5	Normal Shockwave Relations	
	Propagation Speed of Sound Wave	26
	Speed of Sound	27
	Mach Number	27
2.5.1	Stagnation Terms	
	Stagnation Specific Enthalpy	28
	Stagnation Temperature	28
	Stagnation Pressure	28
2.6	Real Gas Turbines	
2.6.1	Real Cycle	29
2.6.2	Calculations for Real Gas Turbine Engines	31
2.6.3	Gas Turbine Efficiency and Performance	
	Propulsion Efficiency	32
	Thermal Efficiency	32
	Propeller Efficiency	33
	Overall Efficiency	33
	Take Off Thrust	34
	Specific Thrust	34
	Aircraft Range	34
	Thrust Specific Fuel Consumption	36
2.7	Calculations Example for a Turbojet Engine	
2.7.1	Known Parameters	38
2.7.2	Assumptions	38

2.7.3	Calculation 1 – Leading to Fuel to Air Ratio	39
2.7.4	Calculation 2 – Leading to Engine Exit Velocity	40
2.7.5	Calculation 3 – Leading to Specific Thrust, TSFC and Efficiencies	42
2.8	Parameters that Affect Gas Turbine Operation and Efficiency	
2.8.1	Constant Pressure Lines	43
2.8.2	Compression Ratio	44
2.8.3	Maximum Turbine Entry Temperature	44
2.8.4	Thermal Chocking due to Heating	44
2.8.5	Inlet Air Mass Flow Rate	45
	Increasing Engine Size	45
	Increasing Fuel Consumption	45
	Reducing the Lean Extension Limit of the Fuel	46
2.8.6	High Altitude	46
2.8.7	Other Factors Affecting Gas Turbine Design	
	The Fuel Tank Volume	48
	Pollution	48
3 CHAPTER 3 – GAS TURBINE COMBUSTORS		
3.1	Chapter Outline	50
3.2	Combustion Design Considerations	50
3.3	Combustor Design Requirements	51
3.4	Gas Turbine Combustor Components	
3.4.1	The Diffuser	
	Cold Pressure Drop	53
	Hot Pressure Drop	53
3.4.2	The Fuel Atomiser	54
3.4.3	The Liner or Combustion Chamber	54
3.4.4	The Primary Zone	55
3.4.5	The Intermediate Zone	
	Low Altitude	56
	High Altitude	56
3.4.6	The Dilution Zone	56
3.4.7	The Combustor Casing	57
3.5	Gas Turbine Combustor Types	
3.5.1	Tubular Combustor Single-Can or Multi-Can	57
3.5.2	Annular Combustor	59
3.5.3	Tuboannular Combustor	60
3.6	Fuels	
3.6.1	Hydrocarbon Categories	64
3.6.2	Terminology for Gas Turbine Fuels	65
3.6.3	Main Aviation Fuel Specification	67
3.6.4	Aviation Fuels	68
3.6.5	Fuels for Industrial Gas Turbines	
	Traditional Fuels	69
	Non-Traditional Fuels	69
4 CHAPTER 4 – IGNITION		
4.1	Gas Turbine Ignition Systems	71
4.2	Flame Out Situations	71
4.3	The Process of Ignition in Gas Turbines	
	Ignition Phase 1	72
	Ignition Phase 2	73

	Ignition Phase 3	73
4.4	Spark Igniter Types	
4.4.1	Surface Discharge Igniters (SDI)	74
4.4.2	Plasma Jet Igniters (PJI)	74
4.4.3	Focus Discharge Igniters (FDI)	75
4.5	Spark Ignition	
4.5.1	Capacitance Spark	76
4.5.2	Quenching Distance	76
4.5.3	Minimum Ignition Energy (MIE)	77
4.5.4	Pressure and Temperature Dependence on Ignition	78
4.6	Thermal Ignition and Some Chemical Concepts	
4.6.1	Arhenius and Rate of Reaction	79
4.6.2	Auto-Ignition	81
4.6.3	Ignition Delay Time	82
4.6.4	Ignition Limits and Auto-Ignition	82
4.6.5	Semenov's Thermal Ignition Theory	83
4.6.6	The Importance of Radicals in Ignition	85
4.7	A Review on Gas Turbine Plasma Ignition	
4.7.1	Plasma Formation	87
4.7.2	Plasma Motion	89
4.7.3	Plasma Motion and Electromagnetic Forces	89
4.7.4	Pressure Forces	
	Fluid Dynamics of Plasma Motion	90
	Igniter Orifice Diameter	91
	Static Pressure	92
	Combustor Fluid Dynamics and Trajectory of Plasma	92
4.7.5	Plasma Motion and Gravitational Forces	93
4.7.6	Radicals and Radical Augmentation in Plasma Ignition	93
4.7.7	Plasma Medium	94
4.7.8	Past Research on Plasma Mediums	94
4.7.9	Review on Plasma Ignition Performance	97
4.7.10	Thermal Efficiency - Thermal to Stored Energy	98
4.7.11	The Role of Stored Capacitor Voltage to the Efficiency and Life of the Igniter	99
5	CHAPTER 5 - IGNITION EXPERIMENTS IN THE STIRRED FAN REACTOR RIG	
5.1	Experiments in the Leeds Mechanical Engineering Stirred Fan Reactor Rig	
5.1.1	Objectives	102
5.1.2	Experimental Apparatus	103
5.1.3	Fuel Properties	105
5.1.4	Experimental Procedures	
	A. Main Operational Procedure	105
	B. Safety Procedure when Handling Hydrogen Peroxide	106
	C. Procedure for placing the H ₂ O ₂ to the FDI Igniter	107
5.1.5	H ₂ O ₂ Placement	107
5.1.6	Use of Wire Fitment to Igniter	108

6	CHAPTER 6 – STIRRED FAN REACTOR RIG EXPERIMENTAL RESULTS	
6.1	Chapter Outline	109
6.2	High Speed Images of the Propagating Ignition Front	110
6.3	Flame Radius Growth from Ignition	114
6.4	Kernel Radius Growth	115
7	CHAPTER 7 – IGNITION EXPERIMENTS IN A ROLLS ROYCE OLYMPUS GAS TURBINE COMBUSTOR	
7.1	Experiments in the Low Carbon Combustion Centre Labs, Sheffield	
7.1.1	Experimental Set-1 – Continuous Steady H ₂ O ₂ Injection (CSI)	116
7.1.2	Experimental Set-2 and Set-3 – Controlled Continuous Steady H ₂ O ₂ Injection (CCSI)	117
7.2	Modifications Made to the Focus Discharge Igniter	119
7.3	Experimental Apparatus	121
7.4	Reading Errors and Accuracy	125
7.5	Pump Calibration	
7.5.1	Pump Characteristics	127
7.5.2	Pump Calibration Procedure	127
7.5.3	Calibration Results	128
7.6	Experimental Procedures in the Olympus Rig	131
7.7	Olympus Control and Data Acquisition Program	
7.7.1	User Input Values	132
7.7.2	Olympus Engine Control and Experimental Procedure	133
7.8	Olympus Test Fuels and Specifications	134
8	CHAPTER 8 – ROLLS ROYCE OLYMPUS FACILITY EXPERIMENTAL RESULTS	
	Part A – Kerosene Jet A₁ Test Fuel	
8.1	Lean Ignition Limits with and without H ₂ O ₂ Addition – Mixture Strength Φ vs Air Mass Flow Rate	
8.1.1	Experimental Set-1 – Used Fuel Atomiser	138
8.1.2	Experimental Set-2 – Used Fuel Atomiser	139
8.1.3	Experimental Set-3 – Clean Fuel Atomiser	140
8.2	The Effect of Fuel Spray Quality in the Lean Ignition Limits	
8.2.1	Focus Discharge Igniter without H ₂ O ₂ Addition	143
8.2.2	Focus Discharge Igniter with H ₂ O ₂ Addition	144
8.3	Lean Ignition Limits with and without Water Addition	
8.3.1	Experimental Set-3 – Clean Fuel Atomiser	146
8.4	The Effect of Different H ₂ O ₂ Injection Rates in the Lean Ignition Limits	
8.4.1	Experimental Set-2 – Used Fuel Atomiser	147
8.4.2	Experimental Set-3 – Clean Fuel Atomiser	149
8.5	Energy Calculations at Time of Ignition for all Air Mass Flow Rates Studied. Results Only from Experimental Set-2 – Used Fuel Atomiser	152
8.6	Evolution of Exhaust Temperature After Ignition at Similar Equivalence Ratios for Different H ₂ O ₂ Injection Rates	
8.6.2	Results from Experimental Set-2 – Used Fuel Atomiser	154
8.6.3	Results from Experimental Set-3 – Clean Fuel Atomiser	155
	Part B – F.A.M.E. Biodiesel Test Fuel	
8.7	Lean Ignition Limits of F.A.M.E. Biodiesel with and without H ₂ O ₂ – Experimental Set-3 – Clean Fuel Atomiser	157

9 CHAPTER 9 – DISCUSSION OF EXPERIMENTAL RESULTS		
Discussion Part A		
Ignition Experiments in the Stirred Fan Reactor (Bomb) - Isooctane		
9.1	Equivalence Ratio Φ Calculations for the 'Bomb' Experiments	159
9.2	Images of the Propagation of the Ignition flame	160
9.3	Post Processing of the Image Data for the Flame Radius Growth	164
9.4	Flame Radius Growth	166
9.5	Errors in the Flame Radius Growth Calculations	167
9.6	Stirred Fan Reactor Work – Summary	168
Discussion Part B		
Ignition Experiments in the Olympus Gas Turbine Rig – Kerosene Jet A₁		
9.7	Data Post Processing Using Fortran-95	
9.7.1	Program 1 – Equivalence Ratio and Fuel Energy Calculator	169
9.7.2	Sorting the Data	
	Finding the Ignition Point and the H ₂ O ₂ Volume Pumped to Ignition Calculations	170 171
9.7.3	Program 2 – Temperature Increase after Ignition at Similar Equivalence Ratios	171
9.8	Equivalence Ratio Calculations	173
9.9	Ignition Limits of Kerosene Jet A ₁	
9.9.1	Experimental Set-1 – Used Fuel Injector and Continuous Steady H ₂ O ₂ Injection (CSI)	174
9.9.2	Experimental Set-2 – Used Fuel Injector and Controlled Continuous Steady H ₂ O ₂ Injection (CCSI)	177
9.9.3	Experimental Set-3 – Clean Fuel Injector and Controlled Continuous Steady H ₂ O ₂ Injection (CCSI)	180
9.10	The Effect of the Fuel Spray Quality (FSQ)	
9.10.1	Fuel Spray Quality (FSQ) with 'No H ₂ O ₂ ' Plasma Ignition	185
9.10.2	Fuel Spray Quality (FSQ) and H ₂ O ₂ Plasma Ignition	191
9.11	The Effect of Adding H ₂ O Instead of H ₂ O ₂	192
9.12	Energy at Time of Ignition	
9.12.1	Energy Calculations	194
9.12.2	Discussion on the Energy Addition by Introducing H ₂ O ₂ During Ignition	196
9.13	Discussion on the Differences of Set-1 with Set-2	198
9.14	Temperature Evolution as the Engine Pulls Away to Idle	200
9.15	Statistical Calculations – Ignition Time and Additional Costs From Hydrogen Peroxide Usage	
9.15.1	Ignition Time	206
9.15.2	Additional Costs From Hydrogen Peroxide Usage – Calculations from Experimental Data	207
Discussion Part C		
Ignition Experiments in the Olympus Gas Turbine Rig – F.A.M.E. Biodiesel		
9.16	Equivalence Ratio Calculations for the F.A.M.E. Biodiesel	209
9.17	Ignition Limits of F.A.M.E. Biodiesel Test Fuel	
9.17.1	Experimental Set-3 – Controlled Continuous Steady H ₂ O ₂ Injection (CCSI) and Clean Fuel Atomiser	210

Discussion Part D
Feasibility Study of the Proposed H₂O₂ Plasma Ignition System –
An Optional System for Producing H₂O₂

9.18	Feasibility Study	
9.18.1	H ₂ O ₂ Safety	212
9.18.2	Feasibility of the Proposed Ignition System and an Optional System for Producing H ₂ O ₂	214
10	CHAPTER 10 – SIMULATIONS ON THE H₂O₂ PRODUCTION	
10.1	Chapter Outline	
10.1.1	Bio-inspiration from the Bombardier Beetle	217
10.1.2	Simulation Work	217
10.2	Common Industrial Production of H ₂ O ₂ Today	
10.2.1	A Simple H ₂ O ₂ Production Scheme	218
10.2.2	A More Complex H ₂ O ₂ Production Scheme	218
10.3	The Bombardier Beetle's Defence Mechanism	
10.3.1	Reaction Chamber and Mechanism	
	Boxing Glove Shaped Reaction Chamber and Inlet Valve	221
	Reservoir and Thin Long Tube	222
	Outlet Valve	224
10.3.2	H ₂ O ₂ Production Mechanism	225
10.4	Simulations on the production of H ₂ O ₂	
10.4.1	Chemkin Pro	225
10.4.2	Detchem Mechanisms	226
10.4.3	Simulation Inputs in Chemkin	
	Honeycomb Catalyst Properties and Simulation Problem	227
	Catalyst Properties	228
	Honeycomb Properties	228
	Catalyst Species Specific Properties	228
	Source Inlet	229
	Product Settings	229
10.4.4	Simulation Procedure and Initial Conditions	229
11	CHAPTER 11 – CHEMKIN SIMULATIONS ON THE PRODUCTION OF H₂O₂ – RESULTS	
11.1	Varying the Catalyst Stagnation Pressure	
11.1.1	Passing Propane Over the Pt/Rh Catalyst	232
11.1.2	Passing Methane Over the Pt/Rh Catalyst	233
11.2	Varying the Catalyst Temperature	
11.2.1	Passing Propane Over the Pt/Rh Catalyst	234
11.2.2	Passing Methane Over the Pt/Rh Catalyst	236
11.3	Varying the Catalyst Inlet Mass Flow Rate	
11.3.1	Passing Propane Over the Pt/Rh Catalyst	237
11.3.2	Passing Methane Over the Pt/Rh Catalyst	238
11.4	Varying the Fuel Mixture Equivalence Ratio Φ	
11.4.1	Passing Propane Over the Pt/Rh Catalyst	239
11.4.2	Passing Methane Over the Pt/Rh Catalyst	240
12	CHAPTER 12 – DISCUSSION OF SIMULATION RESULTS ON THE PRODUCTION OF H₂O₂	
12.1	Study Outline	241

12.2	The Effect of Catalyst Stagnation Pressure to the Production of H ₂ O ₂	242
12.3	The Effect of Catalyst Temperature to the Production of H ₂ O ₂	244
12.4	The Effect of the Fuel-Air Mass Flow Rate to the Production of H ₂ O ₂	245
12.5	The Effect of the Fuel-Air Equivalence Ratio to the Production of H ₂ O ₂	246
12.6	Summary of Discussion on Chemkin Simulations on the Production of H ₂ O ₂	248
13 CHAPTER 13 – CONCLUSIONS AND SUGGESTIONS		
13.1	Conclusions from the Experimental Work	
	Conclusions from the Experiments with the Used Fuel Injector Device and Kerosene as the Test Fuel	250
	Conclusions from the Experiments with the Clean Fuel Injector Device and Kerosene as the Test Fuel	252
	Conclusions from the Experiments with the Clean Fuel Injector Device and F.A.M.E. Biodiesel as the Test Fuel	253
13.2	Simulations on the Production of H ₂ O ₂	253
13.3	Suggestions for Future Research	254
14 REFERENCES		
		257
APPENDIXES		
Appendix A	Focus Discharge Igniter (FDI) CAD Drawings – Original Dimensions and Modifications	264
Appendix B	Post Processing in Fortran-95 – Program 1 Equivalence Ratio Calculations	271
Appendix C	Post Processing in Fortran-95 – Program 2 Exhaust Temperature Evolution	276
Appendix D	Workbench Drawings of Olympus Rig from CFX Runs	286
Appendix E	Labview Programs – μ mist Device Control Programs	290
	Program 1	292
	Program 2	298
	Program 3	306
	High Speed Images of the Ejection Spray	317

-LIST OF FIGURES-

SHORT DESCRIPTION	PAGE
1. Figure 1.1: The Bombardier beetle and its hot-spray ejection mechanism	9
2. Figure 1.2: The prototype of the ejection device that mimics the beetle's mechanism	10
3. Figure 2.1: The basic design of the gas turbine engine with parts	14
4. Figure 2.2a: Enthalpy- entropy diagram for the gas turbine Brayton (open) cycle – Ideal Case	15
5. Figure 2.2b: Pressure-Volume diagram for the gas turbine open Brayton (open) cycle	15
6. Figure 2.3: Thrust production by a single jet	24
7. Figure 2.4: Sound Wave on a 2-D plane	26
8. Figure 2.5a: Ideal vs. real (red dashed line) enthalpy- entropy diagram for the simple gas turbine engine	29
9. Figure 2.5b: Pressure-Volume Diagram for the real gas turbine cycle	29
10. Figure 2.5c: Pressure, temperature and velocity distribution inside the gas turbine and its components	30
11. Figure 2.6: Typical Variation of the overall efficiency, lift-to-drag ratio and their product as function of Mach number for existing engine materials and the best design configurations	35
12. Figure 2.7: Ideal vs. real (red dashed line) enthalpy- entropy diagram for the simple gas turbine cycle (the turbojet).	37
13. Figure 2.8: A simple Turbojet Engine Design	38
14. Figure 2.9: Contrails across the English Channel	49
15. Figure 3.1: Gas Turbine Design- The combustor part. Main components	52

16. Figure 3.2: The Tubular Type Combustor: single-can and multi-can	58
17. Figure 3.3: The Annular type combustor	59
18. Figure 3.4: The Tuboannular type combustor	61
19. Figure 3.5: Net Specific energy of various fuels	63
20. Figure 4.1(a): Cross section of (i) Surface discharge igniter, (ii) Focus discharge igniter or plasma jet igniter	75
21. Figure 4.1(b): Cross section of a plasma jet igniter design, with feed line for supplying the plasma medium.	75
22. Figure 4.2: Spark ignition energy for kerosene Jet-A vapour mixtures at different temperatures	79
23. Figure 4.3: Plasma Jet Formation.	88
24. Figure 4.4: Ratio of Thermal to Stored Energy and igniter vs. arc length	99
25. Figure 5.1: The University of Leeds Mechanical Engineering 'Bomb' rig	104
26. Figure 5.2: The focus discharge igniter installed inside the 'bomb'	104
27. Figure 5.3: The Schlieren set-up that was used for the bomb experiments	104
28. Figure 6.1(a): Ignition without H ₂ O ₂ addition, $\Phi = 0.71$ Isooctane-Dry air. ($t \sim 0.16$ ms)	110
29. Figure 6.1(b): Ignition with H ₂ O ₂ addition, $\Phi = 0.71$ Isooctane-Dry air. ($t \sim 0.16$ ms)	110
30. Figure 6.2(a): Ignition without H ₂ O ₂ addition, $\Phi = 0.71$ Isooctane-Dry air. ($t \sim 6$ ms)	111
31. Figure 6.2(b): Ignition with H ₂ O ₂ addition, $\Phi = 0.71$ Isooctane-Dry air. ($t \sim 6$ ms)	111
32. Figure 6.2(c): Traces of liquid propelled outwards by the plasma motion	111
33. Figure 6.3(a): Ignition without H ₂ O ₂ addition, $\Phi = 0.71$	112

Isooctane-Dry air. ($t \sim 6\text{ms}$)	
34. Figure 6.3(b): Ignition with H_2O_2 addition, $\Phi = 0.71$ Isooctane-Dry air. ($t \sim 6\text{ms}$)	112
35. Figure 6.4(a): Ignition without H_2O_2 addition, $\Phi = 0.65$ Isooctane-Dry air. ($t \sim 6\text{ms}$)	113
36. Figure 6.4(b): Ignition with H_2O_2 addition, $\Phi = 0.65$ Isooctane-Dry air. ($t \sim 6\text{ms}$)	113
37. Figure 6.4(c): Traces of liquid propelled outwards by the plasma motion.	113
38. Figure 6.5: Flame radius growth against time, from time of ignition, with and without H_2O_2 . Isooctane-dry air: $\Phi = 0.8$	114
39. Figure 6.6: Flame radius growth against time, from time of ignition, with and without H_2O_2 . Isooctane-dry air: $\Phi = 0.6538$	114
40. Figure 6.9: Kernel radius growth against time, from time of ignition, with and without H_2O_2 . No fuel	115
41. Figure 7.1: The experimental focus discharge igniter and the modifications made. (i) Standard FDI igniter before modifications. (ii) Drawing of the modifications made to the standard FDI igniter showing the installation of the hypodermic tube. (iii) The modified FDI igniter	121
42. Figure 7.2: The Rolls-Royce Olympus combustion chamber	122
43. Figure 7.3: (a) The cylindrical casing that houses the liner. (b) A common Olympus diffuser and the place where the fuel injector mounts.	122
44. Figure 7.4: a) The fuel atomiser. b) cleaning of the fuel atomiser's parts.	123
45. Figure 7.5: The Endress and Hauser promass 60 coriolis used for measuring the fuel flow rate.	123
46. Figure 7.7: The Graseby 3100 syringe driver with the 25ml BD plastic syringe containing the hydrogen peroxide installed	126
47. Figure 7.8: The modified focus discharge igniter with the	126

attached hydrogen peroxide supply pipe	
48. Figure 7.9 Shows the volume of liquid ejected while increasing time for different flow rates. Pump Calibration	128
49. Figure 7.10: Repeated pump calibration run	129
50. Figure 7.11: The Graseby 3100 syringe driver and its design flaws.	130
51. Figure 7.12: The Labview environment which controls the engine and the data acquisition	133
52. Figure 8.1: Experimental set-1. Lean ignition limits for kerosene Jet A ₁ (used fuel injector cases). Average equivalence ratios against air mass flow rates. The H ₂ O ₂ rates studied are: 0 and 0.54μl/s. Ambient conditions	138
53. Figure 8.2(a): Experimental set-2. Lean ignition limits for kerosene Jet A ₁ (used fuel injector cases). Average equivalence ratios against air mass flow rates. The H ₂ O ₂ rates studied are: 0, 2.7, 5.4, 10.8μl/s. Ambient Conditions.	139
54. Figure 8.2(b): Same as figure 8.2(a) but showing all ignition attempts and <u>not averaged</u> equivalence ratio values.	140
55. Figure 8.3: Experimental set-3. Lean ignition limits for kerosene Jet A ₁ (Clean fuel injector cases). Average equivalence ratios against air mass flow rates. The H ₂ O ₂ rates studied are: 0, 2.7, 5.4, 10.8μl/s. Ambient Conditions	141
56. Figure 8.4: Lean ignition limits of Kerosene Jet A ₁ for all air mass flow studied using the modified igniter with no additive injected into its cavity. Comparison between the three experimental sets <u>All points show average values of Φ</u> . Different atmospheric conditions depending on the test day.	143
57. Figure 8.5(a): Lean ignition limits of Kerosene Jet A ₁ for all air mass flow studied using the modified igniter with 2.7 and 5.4μl/s of H ₂ O ₂ injected into its cavity. Comparison between the experimental set-1 and set-2.. <u>All points show average values of Φ</u> . Different atmospheric conditions depending on the test day	144
58. Figure 8.5(b): Lean ignition limits of Kerosene Jet A ₁ for all air mass flow studied using the modified igniter with 10.8μl/s of H ₂ O ₂ injected into its cavity. Comparison between the experimental set-1 and set-2. <u>All points show average values of Φ</u> . Different atmospheric conditions depending on the test day	145

59. Figure 8.6: Experimental set-3. Lean ignition limits for kerosene Jet A ₁ (Clean fuel injector cases. This case study shows how the limits are affected by the injection of 0 and 10.8 μl/s water into the focus discharge igniter cavity	146
60. Figure 8.7: Lean ignition limits of Kerosene Jet A ₁ for an air mass flow of 0.194(±0.003)kg/s at different hydrogen peroxide flow rates. Exp. set-2	147
61. Figure 8.8: Lean ignition limits of Kerosene Jet A ₁ for an air mass flow of 0.409(±0.008)kg/s at different hydrogen peroxide flow rates. Exp. set-2	148
62. Figure 8.9: Lean ignition limits of Kerosene Jet A ₁ for an air mass flow of 0.604(±0.009)kg/s at different hydrogen peroxide flow rates. Exp. set-2	148
63. Figure 8.10: Lean ignition limits of Kerosene Jet A ₁ for an air mass flow of 0.805(±0.012)kg/s at different hydrogen peroxide flow rates. Exp. set-2	149
64. Figure 8.11: Lean ignition limits of Kerosene Jet A ₁ for an air mass flow of 0.398(±0.004)kg/s at different hydrogen peroxide flow rates. Exp. set-3	149
65. Figure 8.12: Lean ignition limits of Kerosene Jet A ₁ for an air mass flow of 0.603(±0.007)kg/s at different hydrogen peroxide flow rates. Exp. set-3	150
66. Figure 8.13: Lean ignition limits of Kerosene Jet A ₁ for an air mass flow of 0.703(±0.005)kg/s at different hydrogen peroxide flow rates. Exp. set-3	150
67. Figure 8.14: Lean ignition limits of Kerosene Jet A ₁ for an air mass flow of 0.776(±0.001)kg/s at different hydrogen peroxide flow rates. Exp. set-3	151
68. Figure 8.15: Maximum net energy of fuel and hydrogen peroxide at the time of ignition and <u>at the lean ignition limits</u> . Exp. set-2	152
69. Figure 8.16: Comparison of average exhaust rig temperature evolution for similar equivalence ratios at 0.194(±0.003)kg/s inlet air. Exp. set-2.	154
70. Figure 8.17: Comparison of average exhaust rig temperature evolution for similar equivalence ratios at 0.604(±0.009)Kg/s inlet air. Exp. set-2	154

71. Figure 8.18: Comparison of average exhaust rig temperature evolution for similar equivalence ratios at 0.805(\pm 0.012)kg/s inlet air, Exp. set-2	155
72. Figure 8.19: Comparison of average rig temperature evolution after ignition for similar equivalence ratios at about 0.395kg/s air mass flow and at an equivalence ratio of about $\Phi=0.259$ of air-Jet A ₁ mixture (by keeping the fuel flow at 0.0069kg/s). Exp. set-3	155
73. Figure 8.20: Comparison of average rig temperature evolution after ignition for similar equivalence ratios at about 0.603kg/s air mass flow and an equivalence ratio of about $\Phi=0.169$ of air-Jet A ₁ mixture (by keeping the fuel flow at 0.0069kg/s). Exp. set-3	156
74. Figure 8.21: Comparison of average rig temperature evolution after ignition for similar equivalence ratios at about 0.703kg/s air mass flow and an equivalence ratio of about $\Phi=0.142$ of air-Jet A ₁ mixture (by keeping the fuel flow at 0.0069kg/s). Exp. set-3	156
75. Figure 8.22: Lean ignition limits of F.A.M.E. Biodiesel test fuel for all air mass flow studied using the modified igniter with 0 and 10.8 μ l/s H ₂ O ₂ additive injected into its cavity. Exp. set-3: Clean fuel atomiser	157
76. Figure 9.1: Examples of drawing the boundaries of an ignition flame front at different instances as it evolves	165
77. Figure 9.2: Examples of further processing of the image data (colour burned: black and white images)	165
78. Figure 9.3(a): % improvement in the ignition limits when comparing experimental set-1 with set-2 and set-3 with set-2 at \sim 0.4 and \sim 0.6kg/s	187
79. Figure 9.3(b): Detail from figure 8.4. The arrows explain which ignition limits are compared in order to obtain the points shown in figure 9.3(a)	187
80. Figure 9.4: The effect of the fuel spray quality (FSQ) in the lean ignition limits of kerosene jet-A ₁ . Experimental and calculated results at different air mass flow rates.	190
81. Figure 9.5: Drawing of tangents from figure 8.19 (exhaust temperature evolution plot) and comparison (purple box).	203
82. Figure 9.6: Drawing of tangents from figure 8.20 (exhaust temperature evolution plot) and comparison (purple box).	203

83. Figure 9.7: Drawing of tangents from figure 8.21 (exhaust temperature evolution plot) and comparison (purple box).	204
84. Figure 9.8: Max. Exhaust temperature gradients after ignition with different water or H ₂ O ₂ injection volume rates. The air mass are 0.4, 0.6 and 0.7kg/s. Exp. set-3: Clean fuel atomiser.	204
85. Figure 9.9: Compositions of H ₂ O ₂ that form ignitable vapour	213
86. Figure 9.10: A proposed ignition system with propane passing over a suitable catalyst and the product infused into the cavity of a focus discharge igniter.	216
87. Figure 10.1: Production of H ₂ O ₂ through the anthraquinone auto-oxidation (AQ) process	219
88. Figure 10.2: Electron photograph of the ejection mechanism inside the bombardier beetle.	221
89. Figure 10.3: Electron photograph of a dissected gland from a bombardier beetle	222
90. Figure 10.4: The Chemkin diagram interface	227
91. Figure 11.1: Graph of H ₂ O ₂ production volume rate against catalyst distance (varying the catalyst stagnation pressure). Propane-air	233
92. Figure 11.2: Graph of H ₂ O ₂ production volume rate against catalyst distance (varying the catalyst stagnation pressure). Methane-air	234
93. Figure 11.3: Hydrogen peroxide production volume rate against catalyst distance. Temperature parameter study at 3atm stagnation pressure. Propane-air	235
94. Figure 11.4: Hydrogen peroxide production volume rate against catalyst distance. Temperature parameter study at 4atm stagnation pressure. Propane-air	235
95. Figure 11.5: Hydrogen peroxide production volume rate against catalyst distance. Temperature parameter study at 3atm stagnation pressure. Methane-air	236
96. Figure 11.6: Graph of hydrogen peroxide production volume rate against catalyst distance. Inlet mass flow rate parameter study. Propane-air	237
97. Figure 11.7: Graph of hydrogen peroxide production volume rate against catalyst distance Inlet mass flow rate parameter	238

study. Methane-air

98. Figure 11.8: Graph of hydrogen peroxide production volume rate against catalyst distance. Equivalence ratio parameter study. Propane-air	239
99. Figure 11.9: Graph of hydrogen peroxide production volume rate against catalyst distance. Equivalence ratio parameter study. Methane-air	240
100. Figure 12.1: Main catalyst shapes. a) pellet type catalyst, b) ring type catalyst, c) ribbed or daisy type	243
101. Figure 12.2: Maximum H ₂ O ₂ production rates, within a specific catalyst length of 10cm, obtained by the Chemkin simulations in the passing of propane-air over a Pt/Rh catalyst	249

-LIST OF TABLES-

SHORT DESCRIPTION	PAGE
1. Table 2.1: The gas turbine working cycle explained	18
2. Table 2.2: The International Standard Atmosphere table	47
3. Table 3.1: Gas combustor design requirements.	51
4. Table 3.2: Hydrocarbon categories and description.	64
5. Table 3.3: Terminology for gas-turbine fuels	65-66
6. Table 3.4: Specifications for aviation fuels	67
7. Table 4.1: Main reasons for a flame-out in a gas-turbine engine	72
8. Table 5.1: Fuel properties for Isooctane.	105
9. Table 7.1: Calibration slopes of different injection rates for the Graseby 3100.	130
10. Table 9.1: Ignition improvement in the lean limits of the kerosene Jet-A ₁ fuel in terms of mixture strength Φ . Exp. set-1(used fuel injector. 0 and 0.54 μ l/s of H ₂ O ₂ into FDI). Summary of figure 8.1	176
11. Table 9.2: Ignition improvement in terms of fuel mixture strength Φ at the lean ignition limits Exp. set-2 (used fuel injector. 0, 2.7, 5.4, 10.8 μ l/s of H ₂ O ₂ into FDI). Summary of figure 8.2.	179
12. Table 9.3: Ignition improvement in terms of fuel mixture strength Φ at the lean ignition limits. Exp. set-3(clean fuel injector. 0, 2.7, 5.4, 10.8 μ l/s of H ₂ O ₂ into FDI). Summary of figure 8.3	183
13. Table 9.4: Ignition improvement in the lean limits of the kerosene Jet-A ₁ fuel in terms of mixture strength Φ . Experimental Set-3 (clean fuel injector. 0, 10.8 μ l/s H ₂ O). Summary of figure 8.4	193
14. Table 9.5: Statistical comparison of the maximum, minimum and mean <u>ignition times</u> of the kerosene fuel from the start of the ignition sequence between the four hydrogen peroxide	207

injection rate cases 0, 2.7, 5.4 and 10.8 μ l/s. Exp. set-2.

15. Table 9.6: Ignition improvement in the lean limits of the F.A.M.E. Bio-diesel test fuel in terms of mixture strength Φ . Experimental Set-3 (clean fuel injector. 0 and 10.8 μ l/s of H ₂ O ₂ into FDI). Summary of figure 8.22.	211
16. Table 9.7: Explosive power and sensitivity of various substances	213
17. Table 9.8: Minimum ignition energies in air and oxygen in mJ	213
18. Table 10.1: Physical properties of the catalyst	227
19. Table 10.2: Catalyst properties	228
20. Table 10.3: Honeycomb properties	228
21. Table 10.4: Catalyst Species	228
22. Table 10.5: Inlet Inputs	229
23. Table 10.6: Fuel properties for propane and methane	231
24. Table 10.7: Initial conditions for the Chemkin simulations on the production of H ₂ O ₂ by passing fuel over a Pt/Rh catalyst.	231
25. Table 12.1: Calculated fuel mass flow rate depending on the equivalence ratio used in the simulations	247

***On the Use of Hydrogen Peroxide in Ignition Systems –
Bioinspiration from the Bombardier Beetle***

“Dedicated to my family Helen and Kostas, Lydia and Vincent and little Philip”

CHAPTER 1- INTRODUCTION

1.1 THESIS OUTLINE

This study considers ways to improve current technologies of combustion systems in order to enhance combustion initiation and stability. The main aim is to investigate the use of a novel ignition system that will deploy small amounts of hydrogen peroxide to promote combustion. The idea of supplying hydrogen peroxide at the immediate site where the ignition spark develops, inside the cavity of a suitable igniter, is new. Past research in plasma-type ignition systems indicates that enhancement of the combustion initiation process is possible by increasing radical production [1, 2]. The phenomenon can be explained through the chain reaction theory where the free radicals are responsible for initiating a reaction [3]. This study is a bio-inspiration, following research on the Bombardier Beetle [4-6]; a combustion system found in nature. The Bombardier beetle creates hydrogen peroxide in its own “chemical plant”, combines it with hydroquinones and produces a hot caustic “gun” for defending itself against predators. The motive for this research is drawn from today’s demand for high power and reliable but in contrast fuel efficient engines.

1.2 PROBLEM DESCRIPTION

Over the past decades an increased interest has arisen in extending the lean operation limits of gas turbine engines. This trend for leaner mixtures has been stimulated by the potential for improving engine emission characteristics and for lowering the turbine inlet temperature; hence efficiency. More effective ignition

systems are one of the many ways to deal with these expectations. New ignition systems should be investigated in order to increase the ignition performance and to widen the operational abilities of current gas turbine technology.

Modern gas-turbines are built to operate for a large performance envelope, but such operating conditions can be met only by making some compromises. Examples of such compromises can be found by looking at the design differences between various types of engines; i.e. subsonic or supersonic-scramjets, tubular or annular, annular or can-annular, multi-can or single-can and many other types. The gas-turbine engine offers a great range of flexibility in design and that is why it is so widely used.

For land-based gas turbines, leaner mixtures are used in order to reduce their emissions and fuel usage. Apart from the difficulty in initiating combustion at fuel-air ratios well below the stoichiometric, a problem arises in maintaining the stability of the flame. Moreover, due to the use of a wide range of fuels in industrial applications, there is an increasing need for reliable ignition in order to ensure continuous operation even if the fuel atomisation quality drops before the scheduled maintenance. As cost is of more concern in industrial uses of gas turbines, more effective ignition systems will help to run the engine at lower fuel-air ratios and may prevent maintenance work and engine shut-down that is usually needed for cleaning the fuel injector devices.

For aero-engines, at high altitudes, the need to ignite a combustible mixture at low inlet temperatures and a poor degree of fuel atomisation- due to low pressures- is critical. Combustion termination may occur due to transient changes in the engine airflow during aircraft manoeuvres, gas exhaust ingestion following the release of a missile, severe ice, water or dust ingestion and other unpredictable situations. The situation of a flame-out during flight can be stressful and may become fatal in a short time by a bad follow-on decision. Although good training is essential for all pilots, human errors especially during such stressful situations are very possible. The high altitude re-lighting ability of aero-engines is a limiting factor for the operational envelope of an aircraft. The manufacturer cannot guarantee a successful re-light of the engine above a certain altitude. At some cases failure to re-ignite will lead to a high speed descent, stall of the compressor blades, loss of control of the aircraft, engine airflow disruptions, bad fuel-air mixing, low fuel atomisation and increasingly high loads on the aircraft control surfaces that make the recovery impossible etc. All these conditions make re-ignition of the engine even more difficult than what it already is. A quick re-ignition whilst the aircraft is still under control is essential for preventing all these situations from occurring, but for successful ignition the aircraft has to go below the altitude specified by the manufacturer. The altitude re-lighting characteristics of the engine depend strongly on its size and weight and in fact the size of an aircraft depends heavily upon such re-light characteristics. Near the ground (i.e. during take-off or landing), flame-outs are sure to be catastrophic because of the low proximity to the ground at high speeds that require impossible human reflexes.

It should be made clear to the reader, that although aviation will always gain from new knowledge on ignition, it is more likely that studies like this one will affect primarily industrial gas turbines.

The reason for this is straight forward. In aviation, the safety of the passengers will never be compromised. Even though it is desirable to use lean fuel-air mixtures for cleaner burning and low cost, safety will still be the greatest concern. A new ignition system may be installed in aircraft if the ignition efficiency is better overall and it is at least proven to be as reliable as the old. However, this should add to the overall safety of the aircraft without changing the operation of the engine.

On the other hand, the industrial gas turbine is more versatile in this respect. The cost and the environmental regulations coupled with the power efficiency are the most important. The use of leaner fuel mixtures is seen as one of many ways to tackle these issues. It is common knowledge that the use of lean mixtures at very low equivalence ratios renders the burning of the engine unstable. In this case the use of a better overall ignition system would be most beneficial. It should be highlighted, that although a reliable combustion system is always desirable in industrial engines, it is not a life-threatening concern. Therefore, the transition from a proven concept ignition system to an industrial application will be faster and more guaranteed than to an aviation application.

As all processes involved in the gas turbine operation, ignition is very important and ensures the reliable use of the engine. Unlike all other parts, the ignition system can have questionable performance and may result in catastrophic situations under some conditions, even if there is no apparent mechanical failure. Sometimes there is a thin line that separates the ignition from a 'no-ignition' condition. The reasons depend on many factors such as those that were described in the previous section and others that have to do more with the engine and how it works as a unit-system. Some of these factors are based on parameters like the combustor design, the airflow dynamics, the inlet temperature and velocity, the weather conditions, the altitude, the fuel atomiser, the size of the engine and of course the ignition system itself. As each engine design will have different characteristics, their behaviour cannot be fully assessed before testing a prototype.

To prevent problematic situations from happening, engine manufacturers produce stability loops that determine the engine's specifications. The ignitability loops lie within the flammability limits of the fuel and provide knowledge to the operators of the limiting conditions; when their engine will ignite or re-ignite without problems. But of course these stability loops are valid for a specific range of ignition plugs which the manufacturer recommends and they depend also on the fuel supplied.

Current ignition plugs have not evolved much after the appearance of the surface discharge igniters (SDI). Research on combustion has gone forward towards understanding it and considerable knowledge has been gained about the flame initiation process. Design-paths have been devised and are commonly used to both prevent flame-outs and help in the ignition procedure. These paths involve mainly design improvements of the combustor's layout and installation of better fuel injectors and not satisfactory improvements of the ignition plug. Hence, surface discharge igniters are used for more than five decades now.

Some of the well-known techniques that are used for improving ignition are:

- The protection of the flame from transient changes by a combustion chamber or liner.
- The creation of different zones of flow inside the liner.
- The aerodynamic manipulation of the primary zone to create a low velocity area that will be able to sustain a flame, even if at other areas combustion momentarily terminates.
- The atomisation of the fuel into finer droplets to better mix with the air.

It is apparent from studying ignition that there is a minimum energy that needs to reach the combustible mixture in order to ignite. The amount of this essential energy depends on factors like the combustor design, the engine airflow, the igniter's position, the temperature, the pressure and the mixture strength at the

point of ignition, the fuel, the fuel atomisation etc. However, the characteristics of the system that expels this energy –the igniter plug- (usually in the form of a spark) plays by itself a very crucial role. It is common knowledge that most of the energy created by the igniter's discharge is lost in vain. Consequently only about 10% of the total energy discharge of a surface discharge igniter reaches the fuel-air mixture [1, 7, 8]. The remainder energy is lost by conduction, radiation and shockwave dissipation [9].

The igniter plug as an energy delivery system that initiates combustion needs to be improved, but there are challenges. The difficulty is to understand what exactly happens during the ignition process. The timescales involved during the ignition process are of the order of microseconds and the temperatures that are present are very high. The dependency of the ignition process to all three dimensions and to the airflow dynamics make the use of a testing viewing window very difficult. Better understanding can be gained by the use of a high-speed camera if viewing is possible, but this is not essential and does not produce much useful information. Some of the more useful information that can be retrieved are the diameter of the hot kernel, the kernel speed and the process of ignition in general.

In most cases, it is difficult to relate the theory with what actually happens because of the many measurements that need to be taken, whilst the equipment is too expensive and almost impossible to be met by a common

research budget. The cost to run such experiments, usually done in only one of the combustion chambers taken from a real engine, can vary between **£1K to £25K per hour**; depending on the air mass flows studied. When testing under sub-atmospheric conditions, these costs can escalate even higher. Because of the particular problem being studied (i.e. the start-up of the engine), the high cost is usually related to the high energy needed by an external compressor to produce the air mass flows required for the one liner –or more- studied. The costs are related to the energy consumed by the air compressor (that is usually not connected to a turbine), the workmanship, the control equipment and programming, the components, the fuel, the safety equipment etc. These costs prevent a detailed investigation of the problem of ignition in a real engine, under a normal university PhD study. It is common practice for companies to develop their own knowledge data base. These experimental costs are very expensive and therefore, it would be difficult to share this knowledge without some kind of agreement. Because of the aforementioned difficulties, most of the ignition experiments involve the determination of the flammability limits and only some efforts to extend these limits by new ideas.

Other studies –mainly in research- concentrate on computational fluid dynamic (CFD) codes in order to simulate the process of ignition and combustion [10, 11]. CFD is a powerful tool and with today's technology, it is becoming a very important complimentary tool to experimental testing. CFD cannot make accurate predictions for all complex situations and combustion is regarded as one of the most complex situations in terms of fluid dynamics. Moreover, the need for real experiments to validate the codes will always exist.

For all these reasons, the development and testing of new ignition systems is considered important in building more knowledge on the subject of ignition. An improved performance system, in terms of energy delivered to the air-fuel mixture, would be very beneficial in the knowledge gained and would help towards extending the operational ability of the current gas turbine engines.

1.5 BIO-INSPIRATION FROM THE BOMBARDIER BEETLE

The project was inspired by studying the *Brachina Carabidae* beetles and in particular the Bombardier beetle species. As the name suggests, these beetles are 'bombarding' their predators with a hot ($\sim 100^{\circ}\text{C}$) caustic spray when they feel in danger (Figure 1.1).



Figure 1.1: The Bombardier beetle and its hot-spray ejection mechanism. [14]

These species are of particular interest because they are the only known living organisms that carry a reaction chamber, which they use to bring chemicals together to produce an exothermic reaction. The apparatus of their defence

mechanism has been studied extensively by Eisner and his research group at Cornell University in New York [12-14].

Furthermore, the physics behind this ejection mechanism was studied by the research group at the University of Leeds [5, 6, 15-18]. The ejection mechanism was reproduced successfully in the lab by building a scaled-up device that mimicked the beetle's valve system, but by using heaters to bring the liquid to the desired temperature. The device can be seen in Figure 1.2.

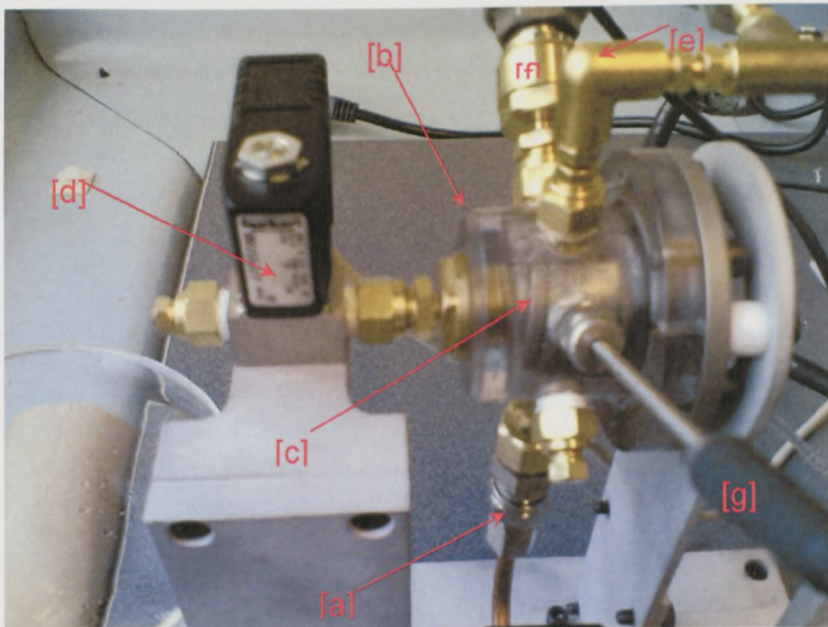


Figure 1.2: The prototype of the ejection device that mimics the beetle's mechanism. [a] Inlet Valve, [b] Chamber, [c] Heaters, [d] Ejection Valve, [e] Outlet Valve, [f] Pressure Transducer, [g] Thermocouple.

A Labview program that controlled the ejection device was built by the author during the initial stages of this research. This was very important in the process of understanding the beetle's mechanism. By using the ejection device, a droplet spray where 90% of the droplets are less than 5 μ m in diameter is

achievable. These droplet sizes were determined using a Malvern laser. Malvern lasers measure the individual droplet sizes of a spray that travels through their laser beam. The average droplet diameter of 90% of the droplets is then calculated. The Labview program and explanation of how it works, have been purposely placed in Appendix E as this is part of the authors PhD study. However, the reader should note that this labview program was written for a different device and is not for controlling the focus discharge igniter that is central to this thesis.

The beetle's ejection mechanism is not the only interesting feature in this small creature. There are other important engineering advantages that can be realised by studying the bombardier beetle. For example the material properties of the chamber and the external body of the beetle that sustain so high temperatures without burning, is one of the areas that require further investigation. Another interesting area which is hoped to be initiated by this work is how the beetle produces the reactive hydrogen peroxide. Some initial studies were published to highlight this area [4]. These are shown in more detail in Chapter 10.

The motivation for this work is to make an *on-site production of hydrogen peroxide* possible by passing the fuel through a catalyst and to promote the ignition process by the presence of H_2O_2 . This is inspired by the chemical production capabilities of the beetle.

In gas turbine igniters if we are able to achieve dissociation and breakdown locally of the hydrogen peroxide, by a high electrical current, temperature and pressure at the zone where the spark initiates, then it is expected to produce a radical increase to the reactive material (spark), which will eventually come into contact with the fuel-air mixture. With the addition of the hydrogen peroxide, the breakdown of the medium by the ignition spark will include quantities of O, OH and H radicals.

CHAPTER 2- GAS TURBINE THEORY

2.1 CHAPTER OUTLINE

Ignition and re-ignition ability is strongly related to the configuration of the engine's parts and how they work as a whole system. Inside a gas turbine engine, the energy paths, the continuity of the fluids involved, the physical and chemical paths are all combined by the human ingenuity in a way that fulfils one objective: the harnessing of the fuels into useful energy. In order to fully assess the ignition behaviour, one needs to understand the relationships that dictate the operation of the gas turbine.

As an example -to support the above statement- one can consider the aerodynamics in the primary zone of two different combustion chambers. Each design results in different mixing patterns of the injected fuel with the incoming air. One of the direct consequences will be that the air-fuel mixtures at the ignition zone will differ in uniformity and strength. It can be expected that the same igniter but installed at different combustion chambers will behave differently. Hence, the design of the combustor part plays an important role in achieving good ignition characteristics.

This chapter describes in some detail the working principles behind the gas turbine engine. This way, the reader should gain a more spherical

understanding of what might possibly change by increasing the efficiency of the ignition system.

2.2 WORKING PRINCIPLES OF THE GAS TURBINE

2.2.1 GAS TURBINE DESIGN

The gas turbine is usually an internal combustion engine. To build a simple back-yard gas turbine is mechanically much less complex than the piston engine because it has less moving parts. However, when efficiency is more important and at larger scales, the precision required, the materials that need to meet certain criteria make the construction of the gas turbine much more complicated than the piston engines. More sophisticated turbines may have multiple shafts, multiple turbine and compressor stages, movable blades, inlet diffuser and exhaust nozzle, complex piping for cooling and heat exchangers, and complex liners.

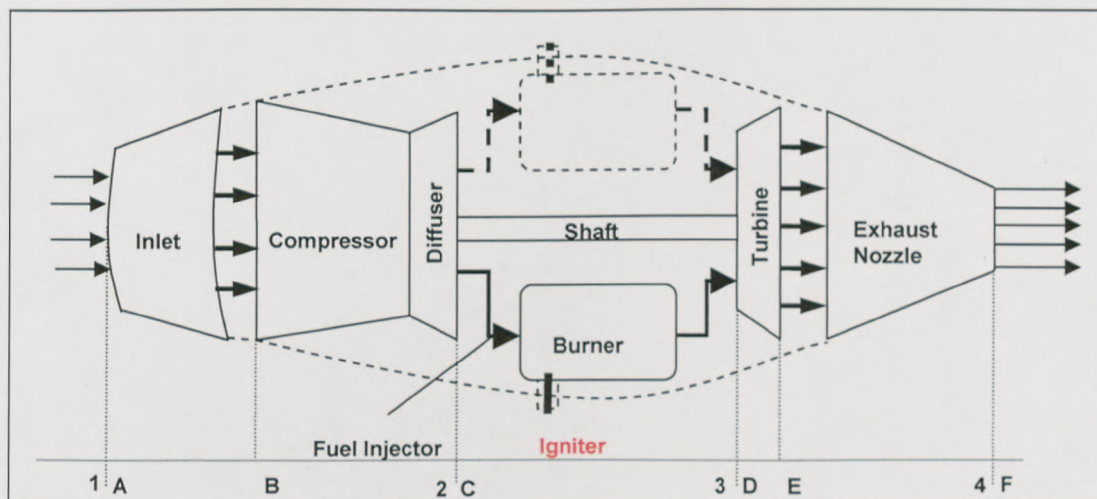


Figure 2.1: The basic design of the gas turbine engine with parts.

The gas turbine design makes use of the thermodynamic principles of fluids to accelerate the air- which is the working fluid- by heating it, in order to create

thrust [19]. In Figure 2.1 one can see a common design configuration of such an engine. Air enters the inlet from the outside. It then passes to the compressor where it is heated and compressed. Afterwards, the velocity of the air is decreased through the diffuser and enters a number of combustion chambers (the number depends on the design). In the combustion chamber, fuel is injected through the fuel injector and is mixed with the incoming air aerodynamically. The mixture is ignited by the ignition unit if it is not already light. The combustion chamber is designed in such a way that the mixture burns at almost constant pressure. The burning of the mixture increases the temperature of the working fluid and thus its kinetic energy. The accelerated fluid passes through the turbine, where some of its energy is transformed to shaft work which is instantly re-used to drive the compressor. Finally, the high kinetic energy fluid exits through the nozzle, where the exit pressure of the fluid leaving the nozzle is designed to be almost atmospheric. All parts are covered and protected by an outer casing (nacelle) which gives the engine an aerodynamically streamlined shape.

2.2.2 WORKING CYCLE OF THE GAS TURBINE

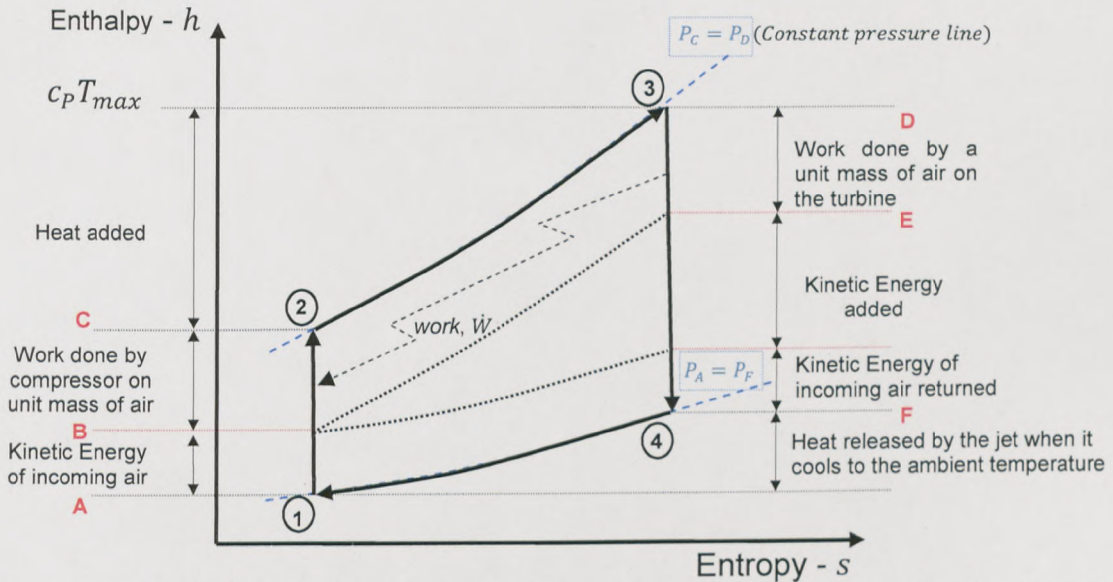


Figure 2.2a: Enthalpy- entropy diagram for the gas turbine Brayton (open) cycle - Ideal case.

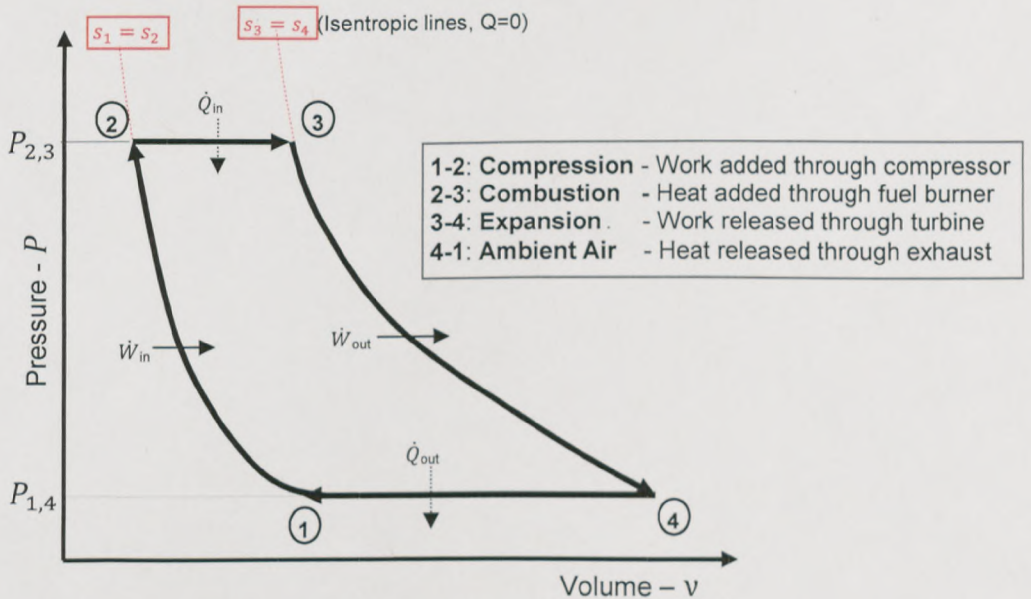


Figure 2.2b: Pressure-volume diagram for the gas turbine Brayton (open) cycle - Ideal case.

Figure 2.2a above, shows the working cycle of the gas turbine engine drawn in an enthalpy-entropy diagram. Figure 2.2b represents the same working cycle but drawn in a pressure-volume diagram. At point 1, air enters the engine at atmospheric pressure. Afterwards, it is compressed along the (isentropic) line 1-

2. From 2 to 3 heat is added to the air by introducing and burning fuel at constant pressure, therefore increasing considerably the volume of the air. From 3 to 4 the gases resulting in combustion expand adiabatically through the turbine and jet pipe back to the atmosphere. During this part of the cycle, some energy is turned into mechanical power by the turbine; the remainder, on its discharge to the atmosphere, provides a propulsive jet [20].

These two diagrams express the ideal cycle of the engine and as one would expect the real situation is a bit different. Nevertheless the ideal cycle is very useful in exploring the equations behind the operation of some parts and their interconnection with others. It is also useful because it shows that in a highly efficient system the cycle of the engine should be similar to Figures 2.2a,b. The theoretical -ideal- situation is a useful reference when interpolating the output data of a real gas turbine.

The ideal cycle of a gas turbine is further explained in Table 2.1. The cycle follows the fluid's path and the changes that happen to it. The numbers in Figures 2.2a,b and Table 2.1 express the change of state of the fluid and the letters indicate the passing of the flow from one component to the next.

From 1A to 1B:	Isentropic compression due to the high velocity air entering the inlet of the engine. This happens only if the engine is moving and not during start-up. The design of the inlet is crucial to achieve isentropic compression of the air.
From 1B to 2C:	Isentropic compression done by the compressor unit. $s_1 = s_2, P_1 < P_2$
From 2C to 3D:	Isobaric heat addition inside the combustion chamber. At this point the mass of the fluid is changed. The new mass equals to the mass of the air plus the mass of the fuel. $s_2 < s_3, P_2 = P_3$ or $P_C = P_D$
From 3D to 3E:	Isentropic decompression. The accelerated gas-mixture passes through the turbine. The turbine extracts from the mixture the energy needed to drive the compressor fan. The energy is transmitted as shaft work back to the compressor.
From 3E to 4F:	Isentropic decompression. The hot gas decompresses through the nozzle and exits the engine in an accelerated stream. At the exit of the nozzle the pressure of the mixture is ambient (assuming the nozzle is in the design regime). If the engine is moving then some of the kinetic energy of the fluid will be returned to the air in order to achieve equilibrium of the system. $s_3 = s_4, P_3 > P_4$
From 4F to 1A:	As the hot gas leaves the engine, it cools down to the ambient temperature at a constant pressure P_1 . $s_4 < s_1, P_4 = P_1$ or $P_F = P_A$

Table 2.1: The gas turbine working cycle explained.

2.3 BASIC EQUATIONS AND PHYSICAL LAWS

The basic equations are shortly listed here. For more information and derivations the reader is encouraged to read the relevant textbooks referred.

2.3.1 OPEN SYSTEM EQUATIONS

Unsteady continuity equation[21]:

$$\frac{\partial \rho}{\partial t} + \nabla \cdot (\rho \mathbf{V}) = 0 \quad \left[\frac{kg}{s} \right] \quad (2.1)$$

Momentum –x direction[21]:

$$\frac{\partial(\rho u)}{\partial t} + \nabla \cdot (\rho u \mathbf{V}) = -\frac{\partial p}{\partial x} + \rho f_x + (x)_{viscous} \quad (2.2)$$

Momentum Balance[21]:

$$F = \frac{d}{dt}(m\mathbf{V}) \quad (2.3)$$

2.3.2 GENERAL THERMODYNAMIC EQUATIONS IN FLUID FLOW

1st Law of Thermodynamics[21]:

$$dQ = dE + dW \quad [J] \quad (2.4)$$

Full energy equation[21]:

$$\begin{aligned} & \frac{\partial}{\partial t} \left[\rho \left(e + \frac{V^2}{2} \right) \right] + \nabla \cdot \left[\rho \left(e + \frac{V^2}{2} \right) \mathbf{V} \right] \\ & = \rho \dot{q} - \nabla \cdot (p\mathbf{V}) + \rho(\mathbf{f} \cdot \mathbf{V}) + \dot{Q}_{viscous} + \dot{W}_{viscous} \quad [W] \end{aligned} \quad (2.5)$$

Specific energies (defined as energies per unit mass):

$$q \equiv \frac{Q}{m}, e \equiv \frac{E}{m}, w \equiv \frac{W}{m}, h \equiv \frac{H}{m}, s \equiv \frac{S}{m} \quad \left[\frac{J}{kg} \right] \quad (2.6)$$

Work energy [22]:

$$w = Pdv \quad \left[\frac{J}{kg} \right] \quad (2.7)$$

Specific Volume:

$$v \equiv \frac{V}{m} = \frac{1}{\rho} \quad \left[\frac{m^3}{kg} \right] \quad (2.8)$$

Specific heat capacity for under constant volume heating process[22]:

$$c_v = \left(\frac{\partial q}{\partial T} \right)_v = \left(\frac{\partial e}{\partial T} \right)_v \quad \left[\frac{J}{kgK} \right] \quad (2.9)$$

Specific heat capacity for under constant pressure heating process[22]:

$$c'_p = \left(\frac{\partial q}{\partial T} \right)_p = \left(\frac{\partial e}{\partial T} \right)_p + p \left(\frac{\partial v}{\partial T} \right) \quad \left[\frac{J}{kgK} \right] \quad (2.10)$$

Enthalpy

Enthalpy is a defined term. It is the energy that is required to bring the system to a certain state. From definition[22]:

$$c'_p = \left(\frac{\partial h}{\partial T} \right)_p \quad \left[\frac{J}{kgK} \right] \quad (2.11)$$

Hence:

$$h = e + pv \quad \left[\frac{J}{kg} \right] \quad (2.12)$$

Also:

$$dh = de + Pdv + vdP \quad \left[\frac{J}{kg} \right] \quad (2.13)$$

And [22]:

$$dh = dq + vdP \quad \left[\frac{J}{kg} \right] \quad (2.14)$$

2.3.3 2ND LAW OF THERMODYNAMICS – ENTROPY

Definition of entropy[23]:

$$ds = \frac{dq}{T} \quad \left[\frac{J}{kgK} \right] \quad (2.15)$$

Entropy is a (defined) term which describes the energy required by the system to undergo a natural process. There are two possible routes:

1. $s_1 = s_2$. An isentropic or adiabatic and reversible process.

Although there is a change of state in the system, the entropy remains constant. A reversible path is the one that is obtained by connecting all the intermediate equilibrium states [22]. All ideal cases are considered isentropic.

2. $s_1 \neq s_2$. An irreversible process.

The system will change to a state with higher entropy in order to achieve equilibrium. In an irreversible process, the system cannot change back to the previous state without extra energy addition. There is a loss of energy from within the system to the surroundings by the change of state. This energy escapes the system and cannot be used to reverse the process which changed its state. All real cases are considered irreversible.

From equation (2.14) into (2.15):

$$ds = \frac{dh + v dP}{T} \quad \left[\frac{J}{kgK} \right] \quad (2.16)$$

Helmholtz free energy [22]:

$$\alpha = e - Tds \quad \left[\frac{J}{kg} \right] \quad (2.17)$$

At a constant volume if e and Tds are not fixed, they will adjust so as a is minimum.

Gibbs free energy [22]:

$$f' = h - Ts = a + Pv \quad \left[\frac{J}{kg} \right] \quad (2.18)$$

For a reversible process [22]:

$$f' = vdP - sdT \quad \left[\frac{J}{kg} \right] \quad (2.19)$$

2.3.4 THE IDEAL GAS LAW

Equation of state:

$$P = \rho \frac{R}{w} T \quad [Pa] \quad (2.20)$$

Or:

$$Pv = \frac{R}{w} T \quad \left[\frac{J}{kg} \right] \quad (2.21)$$

Also from (2.19) the free energy change of an ideal gas associated with a constant temperature compression is [22]:

$$df' = vdP = \frac{R}{w} T \frac{dP}{P} \quad \left[\frac{J}{kg} \right] \quad (2.22)$$

Hence:

$$f'_2 - f'_1 = \frac{R}{w} T \ln \frac{P_2}{P_1} \quad \left[\frac{J}{kg} \right] \quad (2.23)$$

2.3.5 PERFECT AND IDEAL GAS EQUATIONS

Definition of perfect and Ideal gas [23]:

A perfect gas is defined as a hypothetical gas with molecules of negligible size that exert no intermolecular forces. From equation (2.4) it can be deduced that the internal energy of a perfect gas is depended only in temperature.

An ideal gas is defined as a gas that obeys the ideal gas law (equation (2.20)) exactly. The ideal gas constants and their relationships are described below:

Specific Heat Ratio :

$$\gamma = \frac{C'_p}{C'_v} \quad (2.24)$$

Specific Gas Constant:

$$\frac{R}{w} = c'_p - c_v \quad \left[\frac{J}{kgK} \right] \quad (2.25)$$

Specific Heat at Constant Volume:

$$c_v = R - C'_p \quad \left[\frac{J}{kgK} \right] \quad (2.26)$$

Specific Heat at Constant Pressure:

$$c'_p = \frac{\gamma R}{\gamma - 1} \quad \left[\frac{J}{kgK} \right] \quad (2.27)$$

2.4 MORE SPECIFIC EQUATIONS

2.4.1 THRUST EQUATION FOR THE GAS TURBINE

Figure 2.3 shows the control volume of the engine as a whole system. The thrust equation is expressed by considering the momentum flux (equation

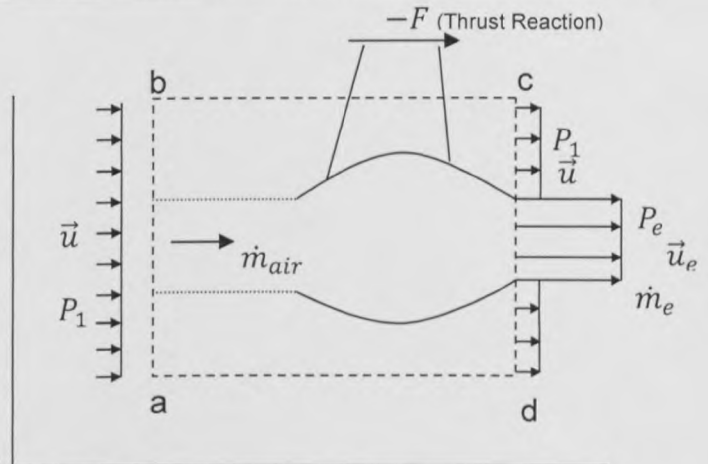


Figure 2.3: Thrust production by a single jet.

(2.3)) balance at the sides of ab and cd. It is assumed that the thrust force is parallel to the velocity of the incoming flow and that the pressure and velocity on side cd outside the jet coincide with their values far upstream- so nacelle drag can be neglected. Also the exit mass of the jet \dot{m}_e is equal to the mass of the air plus the mass of the fuel [24].

$$\vec{F} = \dot{m}_{air}[(1 + f)\vec{u}_e - \vec{u}] + (P_e - P_1)A_e \quad [N] \quad (2.28)$$

(Note: The exit pressure P_e may not be equal to P_1 during supersonic flight)

Where f is the fuel to air mass ratio:

$$f = \frac{\dot{m}_f}{\dot{m}_{air}} \quad [\text{non - dimensional}] \quad (2.29)$$

2.4.2 ENTHALPY FOR UNDER CONSTANT PRESSURE PROCESSES

From the definition of the enthalpy term (2.11) under constant pressure:

$$dh \equiv c_p dT \quad [J] \quad (2.30)$$

2.4.3 ENTROPY FOR UNDER CONSTANT PRESSURE PROCESSES

Substituting equations (2.30),(2.14) into (2.15) :

$$ds = c_p \frac{dT}{T} \quad \left[\frac{J}{kgK} \right] \quad (2.31)$$

For the gas undergoing constant pressure heating in a combustion chamber, equation (2.31) becomes:

$$s_3 - s_2 = C_p \ln \frac{T_3}{T_2} \quad \left[\frac{J}{kgK} \right] \quad (2.32)$$

2.4.4 IDEAL GASES UNDERGOING ISENTROPIC PROCESSES

PRESSURE RATIO

Taking isentropic compression or decompression of the gas (i.e. $S_2 = S_1$) in equation (2.16) and using equations(2.30), (2.22) and (2.27), the pressure ratio can be calculated as[23]:

$$\frac{P_1}{P_2} = \frac{P_4}{P_3} = \left(\frac{T_1}{T_2}\right)^{\gamma/(\gamma-1)} = \left(\frac{T_4}{T_3}\right)^{\gamma/(\gamma-1)} \quad [\text{non - dimensional}] \quad (2.33)$$

(Note: Equation (2.33) applies in the ideal isentropic case. In a real case the compression ratio $P_{rc} = \frac{P_{1B}}{P_{1C}}$ will be predefined by the compressor specifications.)

PRESSURE DENSITY RATIO

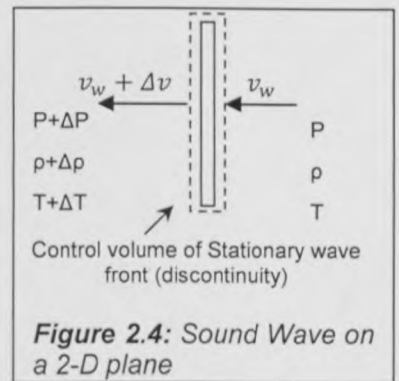
From the entropy equation(2.15), using the equation of state (2.20) with equation (2.27) and differentiating in an isentropic process $ds = 0$, [23]:

$$\frac{P}{\rho^\gamma} = \text{constant} \quad \left[\frac{J}{kg}\right] \quad (2.34)$$

2.5 NORMAL SHOCKWAVE RELATIONS

PROPAGATION SPEED OF A SOUND WAVE v_w

Assuming adiabatic conditions at the control volume of Figure 2.4 and using the continuity equation (2.1) and the momentum balance equation (2.3), the propagation speed of the pressure wave can be determined[25]:



$$v_w^2 = \frac{\Delta P}{\Delta \rho} \left(1 + \frac{\Delta \rho}{\rho}\right) \quad \left[\left(\frac{m}{s}\right)^2\right] \quad (2.35)$$

SPEED OF SOUND c

At the speed of sound c the wave is considered very weak and is approximated as infinitesimally small. Thus all changes across the discontinuity are approximately zero ($\frac{\Delta P}{P} \rightarrow 0, \frac{\Delta \rho}{\rho} \rightarrow 0, \frac{\Delta T}{T} \rightarrow 0$). From equation (2.35) and using equation (2.34) and the equation of state (2.20) [25]:

$$c = \sqrt{\frac{dP}{d\rho}} = \sqrt{\gamma \frac{R}{w} T} \quad \left[\frac{m}{s} \right] \quad (2.36)$$

MACH NUMBER M

The Mach number is defined as the velocity of an object compared to the speed of sound:

$$M = \frac{v}{c} \quad [non\ dimensional] \quad (2.37)$$

2.5.1 STAGNATION TERMS

The stagnation terms are defined as imaginary values of a compressible fluid ($M \geq 0.3$). They express the condition that the fluid would be if it was brought to rest in a steady adiabatic process.

STAGNATION SPECIFIC ENTHALPY h_0

Using the full energy equation (2.4) applying mass continuity (2.1) (steady state, invicid, with no body forces fluid flow) and the equation for enthalpy (2.12) (with $n = 1,2,3 \dots$) [23]:

$$h + \frac{V^2}{2} = \text{constant} \quad \left[\frac{J}{kg} \right] \quad (2.38)$$

Hence the stagnation term is:

$$h_0 = h_n + \frac{v_n^2}{2} \quad \left[\frac{J}{Kg} \right] \quad (2.39)$$

STAGNATION TEMPERATURE T_0

From equation(2.39), using equations (2.30), (2.27), (2.36) and (2.37) [25]:

$$T_0 = T \left(1 + \frac{(\gamma - 1)}{2} M^2 \right) \quad [K] \quad (2.40)$$

STAGNATION PRESSURE P_0

Taking equation (2.40) along with equations (2.34) and (2.33)[25]:

$$P_0 = P \left(1 + \frac{(\gamma - 1)}{2} M^2 \right)^{\frac{\gamma}{\gamma - 1}} \quad [Pa] \quad (2.41)$$

2.6.1 REAL CYCLE

In real engines the processes are not reversible. Accordingly the Brayton cycle changes in a way that at the end of each process the entropy is somewhat greater than what it would be in the ideal case (Figures 2.5a and 2.5b).

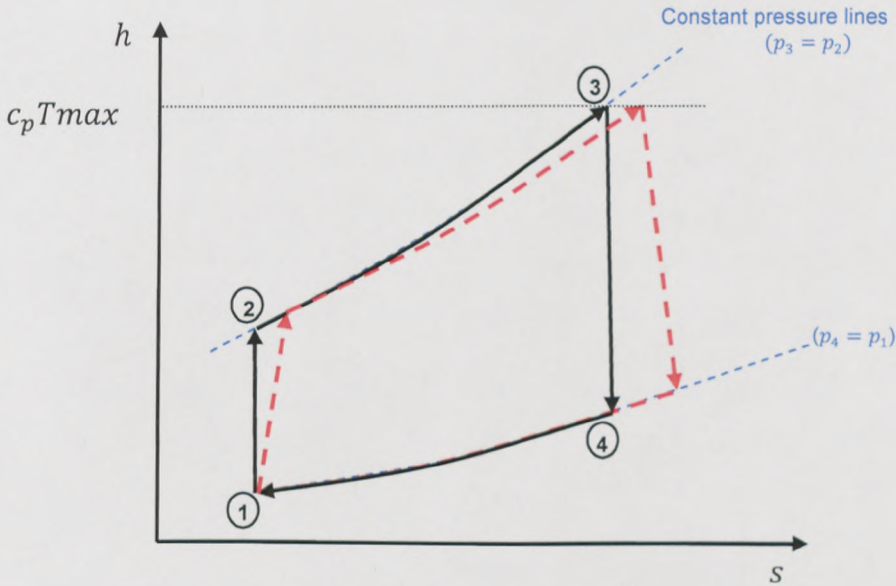


Figure 2.5a: Ideal vs. real (red dashed line) enthalpy- entropy diagram for the simple gas turbine engine (the turbojet).

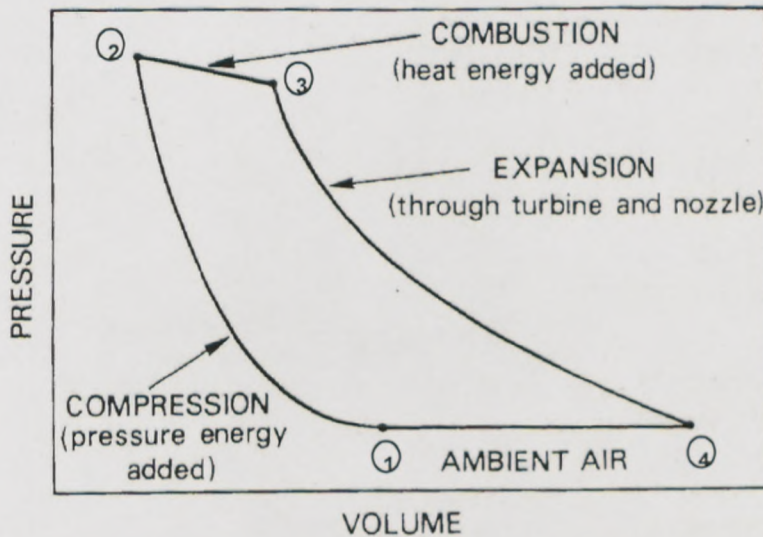


Figure 2.5b: Pressure-Volume diagram for the real gas turbine cycle [20].

Figure 2.5c shows typical values of temperature, pressure and velocity inside the gas-turbine engine. The changes in the temperature and pressure of the air can be traced using figure 2.2c. With the airflow being continuous, the volume changes are shown up as changes in velocity. The efficiency with which these changes are made will determine to what extent the desired relations of pressure, volume and temperature are attained [20].

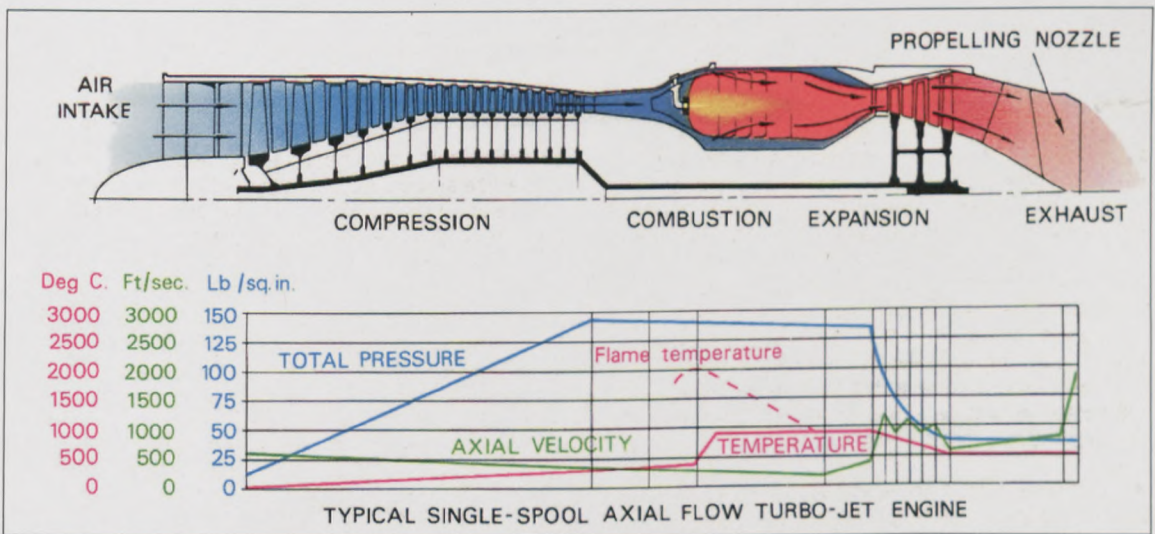


Figure 2.5c: Pressure, temperature and velocity distribution inside the gas turbine and its components [20].

The efficiency of the real gas turbine depends on many factors and components. It is practically impossible to extract 100% efficiency from the compressor and turbine and therefore it is not possible to achieve a completely adiabatic process. The reasons for this are the energy losses due to friction, conduction and turbulence. For these two components (compressor and turbine), 90% efficiency is a good value [20]. Meanwhile, the aerodynamic and energy requirements in the ducts and passages of the engine demand changes in the velocity and pressure of the flow. The design of these passages and

nozzles is of great importance for improving the efficiency with which the energy changes are affected. Any interference with the smooth airflow creates a loss in efficiency [20]. Finally, pressure losses will be sustained in the combustion chamber. The efficiency of each combustor is affected primarily by the magnitude of the pressure drop and the amount of complete burning of the reactants.

2.6.2 CALCULATIONS FOR REAL GAS TURBINE ENGINES

In addition to the above, in real engines due to combustion and temperature changes, the chemical composition of the gas varies. This can be approximately taken into account by using different values of γ and R (equations (2.24) and (2.25) in the ideal case) for different components.

Fortunately, since the heat transfer between the engine and the air can be neglected, there is only one parameter that is required in order to describe the deviation of the real performance from the ideal.

For engine components in which the stagnation pressure does not change in the ideal case (diffusers, burners and nozzles) the performance may be characterized by stagnation pressure ratios: $r_d = \frac{P_{0d}}{P_{0a}}$, $r_b = \frac{P_{0b}}{P_{0d}}$, $r_n = \frac{P_{0e}}{P_{0t}}$ (d : diffuser, b : burner, n : nozzle, e : exit, t : turbine) [26].

2.6.3 GAS TURBINE EFFICIENCY AND PERFORMANCE

PROPULSION EFFICIENCY n_p

Propulsion efficiency is defined as the work done by thrust per unit time or the thrust power to rate of production of propellant kinetic energy [24, 27].

$$n_p = \frac{Fu}{\dot{m}_a \left[(1+f) \frac{u_e^2 - u^2}{2} \right]} \quad [-] \quad (2.42)$$

Assuming: a) $f \ll 1$ (usually), b) $p_e \approx p_a \stackrel{a,b}{\Rightarrow} F = \dot{m}_a(u_e - u)$

$$n_p = \frac{2 \frac{u}{u_e}}{1 + \frac{u}{u_e}} \quad [-]$$

Note that maximizing propulsion efficiency n_p , by taking $\frac{u}{u_e}$ close to unity, means large air mass flow \dot{m}_a for finite thrust. (Turboprop engines use this approach.)

THERMAL EFFICIENCY n_{th}

Thermal efficiency is defined as the rate of addition of kinetic energy to the propellant per energy consumption rate $\dot{m}_f q_R$. Where q_R is the heat of reaction of the fuel [24, 27].

$$n_{th} = \frac{\dot{m}_a \left[(1+f) \frac{u_e^2 - u^2}{2} \right]}{\dot{m}_f q_R} \quad [non\ dimensional] \quad (2.43)$$

For turboprop and turboshaft engines, the output is largely shaft power P_{shaft} .

For these two cases the thermal efficiency is defined as:

$$n_{th} = \frac{P_{shaft}}{\dot{m}_f q_R} \quad [non\ dimensional] \quad (2.44)$$

PROPELLER EFFICIENCY n_{pr}

Propeller efficiency is the ratio of thrust power to shaft power [24]:

$$n_{pr} = \frac{F_{pr} u}{P_{shaft}} \quad [non\ dimensional] \quad (2.45)$$

Turboprops may produce a fraction of thrust from the hot exhaust which may need to be taken into account.

OVERALL EFFICIENCY n_o

The overall efficiency is defined as the ratio of thrust power to the rate of energy consumption [24, 27].

$$n_o = \frac{Fu}{\dot{m}_f q_R} \quad [non\ dimensional] \quad (2.46)$$

TAKE OFF THRUST F_{TO}

At take-off: a) $u = 0$, b) $f \ll 1$, c) $p_e \approx p_a$

Taking the thermal efficiency equation (2.43) with the assumptions above then the take off thrust can be defined in terms of efficiency [27]:

$$F_{TO} = \dot{m}_a(u_e - u) = \frac{2\eta_{th}q_R\dot{m}_f}{u_e} \quad [N] \quad (2.47)$$

For a given fuel consumption rate, take-off thrust is inversely proportional to the exhaust velocity. For a given take-off thrust, smaller u_e means smaller engine size.

SPECIFIC THRUST

An important engine characteristic, defined as [27]:

$$\text{specific thrust} = \frac{F}{\dot{m}_a} \quad \left[\frac{m}{s}\right] \quad (2.48)$$

If a certain engine design ensures higher specific thrust, then for the same thrust a smaller air mass flow is required and hence a reduced engine size.

AIRCRAFT RANGE - S

This equation is known as the Breguet's Range Formula.

Noting that the fuel consumption rate can be expressed as:

$$\dot{m}_f = \frac{dm_f}{dt} = -u \frac{dm_f}{ds} \quad \left[\frac{kg}{s} \right] \quad (2.49)$$

Where ds is the differential of distance for equation (2.49) only.

At constant speed the thrust is:

$$F = \frac{mg}{\frac{L}{D}} \quad [N] \quad (2.50)$$

Substituting equations (2.49) and (2.50) into (2.46) the Brequet's Range formula is found in terms of overall efficiency [27]:

$$S' = n_o \frac{D}{L} \frac{Q_R}{g} \ln \frac{m_{f1}}{m_{f2}} \quad [m] \quad (2.51)$$

Where 1 and 2 express the initial and final states respectively. S' denotes the distance and is used for equation (2.51) only.

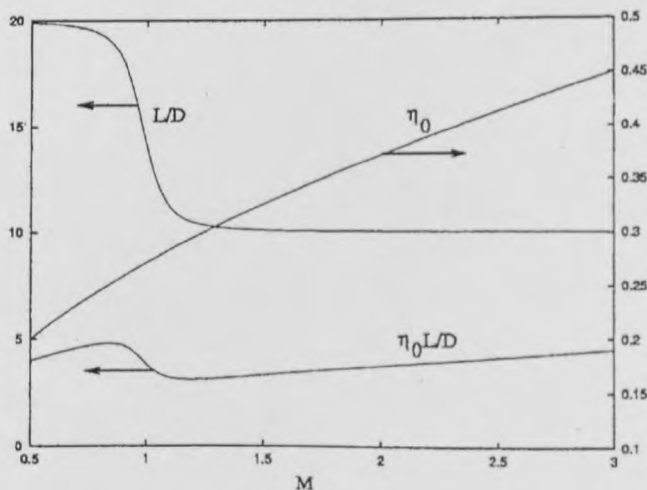


Figure 2.6: Typical Variation of the overall efficiency, lift-to-drag ratio and their product as function of Mach number for existing engine materials and the best design configurations [23]

Long range aircraft fly at high subsonic Mach numbers. As M increases it causes an increase in the thermal efficiency η_o and mechanical loads $\frac{L}{D}$ on the aircraft structure which hence has to be heavier [27, 28] (Figure 2.6 [24]).

THRUST SPECIFIC FUEL CONSUMPTION $TSFC$

$TSFC$ is defined as the ratio of the fuel mass flow rate over thrust [24, 27, 28]:

$$TSFC = \frac{\dot{m}_f}{F} \quad \left[\frac{s}{m} \right] \quad (2.52)$$

Using this equation and the overall efficiency definition (2.46), the Breguet range formula (2.51) reduces to:

$$S' = \frac{L u}{D g} \frac{1}{TSFC} \ln \frac{m_1}{m_2} \quad [m] \quad (2.53)$$

Where 1 and 2 express the initial and final states respectively. S' denotes the distance and is used for equation (2.53) only.

For a given flight speed the range of an aircraft is inversely proportional to $TSFC$. Typical values are: Ramjet engines ($M = 2$) $TSFC = 0.17 - 0.26 \left(\frac{kg}{Nhr} \right)$, Turbojet engines (static) $TSFC = 0.075 - 0.11 \left(\frac{kg}{Nhr} \right)$, Turbofan engines (static) $TSFC = 0.03 - 0.05 \left(\frac{kg}{Nhr} \right)$

For turboprop engines, a brake specific fuel consumption (*BSFC*) is used instead: $BSFC = \frac{\dot{m}_f}{P_s}$, with P_s : shaft power. Typical values for *BSFC* are 0.27 – 0.36 $\left(\frac{kg}{kWh}\right)$.

2.7 CALCULATIONS EXAMPLE FOR A TURBOJET ENGINE

In this example, it is shown how from theory one can calculate the basic parameters that comprise a gas turbine engine. The turbojet engine (Figure 2.8) is a simple and very basic gas-turbine configuration. Figure 2.7 shows the real and ideal working cycle of a turbojet. The procedure involves first solving for the ideal case and then moving to the real case.

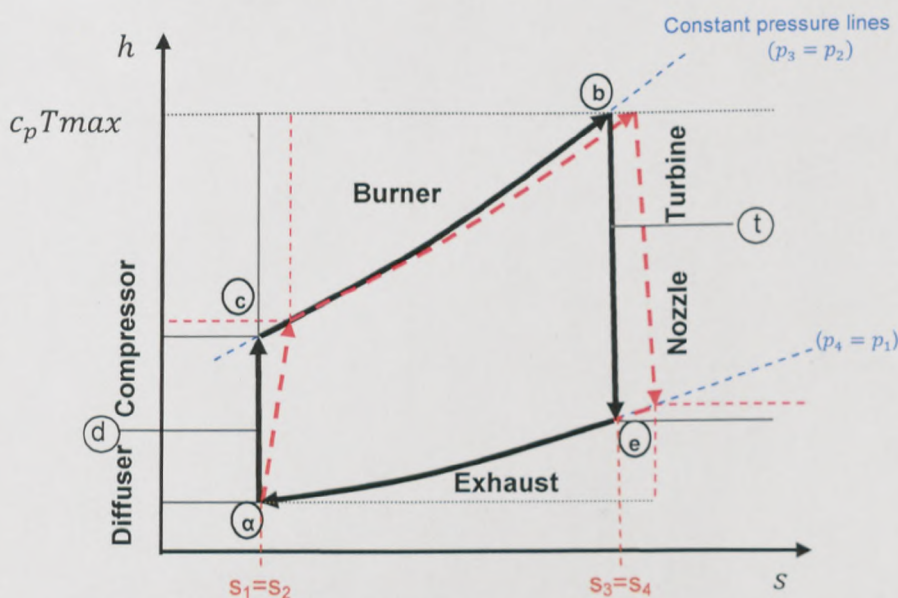


Figure 2.7: Ideal vs. real (red dashed line) enthalpy- entropy diagram for the simple gas turbine cycle (the turbojet).

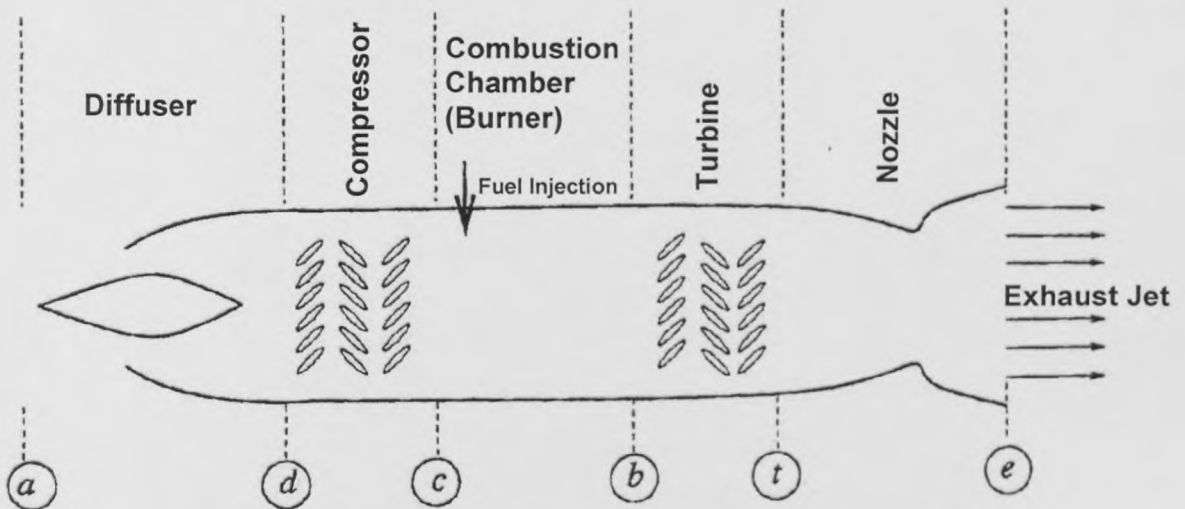


Figure 2.8: A simple Turbojet Engine Design. These symbols are used in the example to denote exit of component or state (α : ambient, d : diffuser, c : compressor, b : burner, t : turbine, e : exit).

2.7.1 KNOWN PARAMETERS

At least the following parameters should be known:

- Flight Mach number M
- Burner exit temperature T_b (or maximum turbine entry temperature)
- Heat of reaction of fuel q_R
- Specific heat ratio γ
- Specific heat at constant pressure C_p ($C_p = \frac{\gamma R}{(\gamma-1)}$)
- Compressor pressure ratio P_{rc} ($P_{rc} = \frac{P_b}{P_d}$)

2.7.2 ASSUMPTIONS

The assumptions are:

- Isentropic adiabatic flow in the diffuser and in the nozzle (i.e. $s_1=s_2$ and $s_3=s_4$)

- Zero velocity and constant pressure in the combustor (hence stagnation variable equals local variable, i.e. $T_{0b} = T_b$)
- Nozzle is inside the design regime (i.e. $P_e = P_a$)

ENERGY CONSERVATION FORM

Energy conservation law (equation (2.4)), for an open system with a steady flow and no losses, takes the form:

$$\dot{W} + \sum_{outlets} \dot{m}_{out} h_{0out} = \dot{Q} + \sum_{inlets} \dot{m}_{in} h_{0in} \quad (2.54)$$

2.7.3 CALCULATION 1 – LEADING TO FUEL TO AIR RATIO f

A. Stagnation temperature at diffuser exit.

- **Diffuser:** Isentropic compression

$$T_{0d} = T_a \left(1 + \frac{\gamma-1}{2} M^2 \right)$$

B. Stagnation pressure at diffuser exit.

- **Diffuser:** Isentropic compression

$$\frac{P_{0d}}{P_a} = \left(\frac{T_{0d}}{T_a} \right)^{\frac{\gamma}{\gamma-1}} \Rightarrow P_{0d} = P_a \left(\frac{T_{0d}}{T_a} \right)^{\frac{\gamma}{\gamma-1}} = P_a \left(1 + \frac{\gamma-1}{2} M^2 \right)^{\frac{\gamma}{\gamma-1}}$$

C. Stagnation pressure at compressor exit

- **Compressor:** Isentropic compression

$$\frac{P_{0c}}{P_{0d}} = \frac{P_c \left(\frac{T_{0c}}{T_c} \right)^{\frac{\gamma}{\gamma-1}}}{P_d \left(\frac{T_{0d}}{T_d} \right)^{\frac{\gamma}{\gamma-1}}} = \frac{P_b \left(\frac{T_c \left(1 + \frac{\gamma-1}{2} M^2 \right)}{T_c} \right)^{\frac{\gamma}{\gamma-1}}}{P_d \left(\frac{T_d \left(1 + \frac{\gamma-1}{2} M^2 \right)}{T_d} \right)^{\frac{\gamma}{\gamma-1}}} = P_{rc} \Rightarrow P_{0c} = P_{rc} P_{0d}$$

D. Stagnation temperature at compressor exit

- **Compressor:** Isentropic compression

$$\frac{T_{0c}}{T_{0d}} = \left(\frac{P_{0c}}{P_{0d}}\right)^{\left(\frac{\gamma-1}{\gamma}\right)} \Rightarrow T_{0c} = P_{rc}^{\left(\frac{\gamma-1}{\gamma}\right)} T_{0d} \Rightarrow T_{0c} = P_{rc}^{\left(\frac{\gamma-1}{\gamma}\right)} T_a \left(1 + \frac{\gamma-1}{2} M^2\right)$$

E. Fuel air ratio at burner $f = \frac{\dot{m}_f}{\dot{m}_a}$

➤ **Burner:** Heat addition at constant pressure and $\dot{W}_b = 0$

From the energy equation (2.54):

$$\dot{W} + \sum_{outlets} \dot{m}_{out} h_{0out} = \dot{Q} + \sum_{inlets} \dot{m}_{in} h_{0in}$$

$$\Rightarrow (\dot{m}_f + \dot{m}_a) h_{0b} = \dot{m}_f q_R + \dot{m}_a h_{0c}$$

$$\Rightarrow (1 + f) h_{0b} = f q_R + h_{0c}$$

$$\Rightarrow f = \frac{T_{0b} - T_{0c}}{\frac{q_R}{C_p} - T_{0b}} = \frac{T_{0b} - P_{rc}^{\left(\frac{\gamma-1}{\gamma}\right)} T_a \left(1 + \frac{\gamma-1}{2} M^2\right)}{\frac{q_R}{C_p} - T_{0b}}$$

2.7.4 CALCULATION 2 - LEADING TO ENGINE EXIT VELOCITY u_e

A. Stagnation Temperature at turbine exit

➤ **Turbine** work equals **compressor** work

$$\dot{W}_t = \dot{W}_c$$

$$\Rightarrow h_{0c} - h_{0d} = h_{0b} - h_{0t}$$

$$\Rightarrow C_p(T_{0c} - T_{0d}) = C_p(T_{0b} - T_{0t})$$

$$\Rightarrow T_{0t} = T_{0b} - (T_{0c} - T_{0d})$$

$$\Rightarrow T_{0t} = T_{0b} - (P_{rc}^{\left(\frac{\gamma-1}{\gamma}\right)} T_{0d}) - T_{0d}$$

$$\Rightarrow T_{0t} = T_{0b} - \left(P_{rc}^{\left(\frac{\gamma-1}{\gamma}\right)} - 1\right) T_a \left(1 + \frac{\gamma-1}{2} M^2\right)$$

B. Stagnation pressure at turbine exit

➤ **Turbine:** Isentropic expansion

$$\frac{P_{0t}}{P_{0b}} = \left(\frac{T_{0t}}{T_{0b}}\right)^{\frac{\gamma}{\gamma-1}} \Rightarrow P_{0t} = P_{0b} \left(\frac{T_{0t}}{T_{0b}}\right)^{\frac{\gamma}{\gamma-1}} = P_{0c} \left(\frac{T_{0t}}{T_{0b}}\right)^{\frac{\gamma}{\gamma-1}} = P_{rc} P_{0d} \left(\frac{T_{0t}}{T_{0b}}\right)^{\frac{\gamma}{\gamma-1}}$$

$$\Rightarrow P_{0t} = P_{rc} P_a \left(1 + \frac{\gamma-1}{2} M^2\right)^{\frac{\gamma}{\gamma-1}} \left(\frac{T_{0b} - \left(P_{rc}^{\frac{\gamma-1}{\gamma}} - 1\right) T_a \left(1 + \frac{\gamma-1}{2} M^2\right)}{T_{0b}}\right)^{\frac{\gamma}{\gamma-1}}$$

$$\Rightarrow P_{0t} = P_{rc} P_a \left[\left(1 + \frac{\gamma-1}{2} M^2\right) \left(\frac{T_{0b} - \left(P_{rc}^{\frac{\gamma-1}{\gamma}} - 1\right) T_a \left(1 + \frac{\gamma-1}{2} M^2\right)}{T_{0b}}\right) \right]^{\frac{\gamma}{\gamma-1}}$$

C. Temperature at nozzle exit

➤ **Nozzle:** Isentropic expansion

$$\frac{T_e}{T_{0t}} = \left(\frac{P_e}{P_{0t}}\right)^{\frac{\gamma-1}{\gamma}} = \left(\frac{P_a}{P_{0t}}\right)^{\frac{\gamma-1}{\gamma}}$$

D. Jet velocity at nozzle exit

➤ **Nozzle:** Isentropic expansion

From the energy conservation law:

$$h_{0t} = h_{0e} + \frac{1}{2} u_e^2$$

$$\Rightarrow u_e^2 = 2C_p(T_{0t} - T_e)$$

$$\Rightarrow u_e^2 = 2C_p T_{0t} \left(1 - \left(\frac{P_a}{P_{0t}}\right)^{\frac{\gamma-1}{\gamma}}\right)$$

$$\Rightarrow u_e^2 = 2C_p T_{0t} \left(1 - \left(\frac{P_a}{P_{rc} P_a \left(1 + \frac{\gamma-1}{2} M^2\right) \left(\frac{T_{0t}}{T_{0b}}\right)^{\frac{\gamma}{\gamma-1}}}\right)^{\frac{\gamma-1}{\gamma}}\right)$$

$$\Rightarrow u_e^2 = 2C_p T_{0t} \left(1 - \frac{P_{rc}^{\frac{\gamma}{\gamma-1}}}{\left(1 + \frac{\gamma-1}{2} M^2\right) \left(\frac{T_{0t}}{T_{0b}}\right)} \right)$$

$$\Rightarrow u_e^2 = 2C_p \left(T_{0t} - \frac{P_{rc}^{\frac{\gamma}{\gamma-1}}}{\left(1 + \frac{\gamma-1}{2} M^2\right) \left(\frac{1}{T_{0b}}\right)} \right)$$

$$\Rightarrow u_e =$$

$$= \sqrt{2C_p \left(\left(T_{0b} - \left(P_{rc}^{\frac{\gamma-1}{\gamma}} - 1 \right) T_a \left(1 + \frac{\gamma-1}{2} M^2 \right) \right) - \frac{P_{rc}^{\frac{\gamma}{\gamma-1}}}{\left(1 + \frac{\gamma-1}{2} M^2 \right) \left(\frac{1}{T_{0b}} \right)} \right)}$$

2.7.5 CALCULATION 3 - LEADING TO SPECIFIC THRUST, THRUST SPECIFIC FUEL CONSUMPTION TSFC AND EFFICIENCIES

A. Velocity at inlet

$$u = M \sqrt{\gamma R T_a}$$

B. Specific Thrust

$$\frac{F}{\dot{m}_a} = (1 + f) u_e - u$$

$$\Rightarrow \frac{F}{\dot{m}_a} =$$

$$(1 + f) \sqrt{2C_p \left(\left(T_{0b} - \left(P_{rc}^{\frac{\gamma-1}{\gamma}} - 1 \right) T_a \left(1 + \frac{\gamma-1}{2} M^2 \right) \right) - \frac{P_{rc}^{\frac{\gamma}{\gamma-1}}}{\left(1 + \frac{\gamma-1}{2} M^2 \right) \left(\frac{1}{T_{0b}} \right)} \right)} - M \sqrt{\gamma R T_a}$$

C. Thrust Specific Fuel Consumption TSFC

$$TSFC = \frac{\dot{m}_f}{F} = \frac{f}{\frac{F}{\dot{m}_a}}$$

D. Efficiencies

The efficiencies for the turbojet can then be calculated in terms of the known parameters using the above equations:

➤ **Propulsive efficiency:**
$$n_p = \frac{Fu}{\dot{m}_a \left((1+f) \frac{u_e^2}{2} - \frac{u^2}{2} \right)}$$

➤ **Thermal efficiency:**
$$n_{th} = \frac{\dot{m}_a (1+f) \left(\frac{u_e^2}{2} - \frac{u^2}{2} \right)}{\dot{m}_f q_R}$$

➤ **Overall efficiency:**
$$n_o = n_p n_{th}$$

2.8 PARAMETERS THAT AFFECT GAS TURBINE OPERATION AND EFFICIENCY

2.8.1 CONSTANT PRESSURE LINES

In a $h - s$ diagram (i.e. Figure 2.2) the constant pressure curves of a perfect gas take the exponential form $h = C \exp\left(\frac{s}{c_p}\right)$ which is derived by using equations (2.30) and (2.32). So, the difference between two constant pressure curves a and b -in terms of the enthalpy h - is at any point, $h_{n_b} - h_{n_a} = (C_b - C_a) \exp\left(\frac{s_n}{c_p}\right)$ [19]. Thus as entropy s increases, the difference $h_{n_b} - h_{n_a}$ also increases exponentially. Therefore in Figure 2.2a the distance between points 3-4 is greater than 1-2, which implies that the kinetic energy of the working fluid is greater at the exhaust than at the inlet and thrust is created.

2.8.2 COMPRESSION RATIO

As a consequence, the compression ratio $\frac{P_2}{P_1}$ of the gas, before entering the combustion chamber, is an important parameter. In Figure 2.2 it can be deduced that higher $\frac{P_2}{P_1}$ will result in higher thermal efficiency.

2.8.3 MAXIMUM TURBINE ENTRY TEMPERATURE

Theoretically as the compression ratio increases, the thrust increases exponentially. However, there is a limit in the kinetic energy that exits the engine. The limit corresponds to the thermal resistance of the turbine's material. The turbine can reach to a maximum temperature before its structural properties change. Above such temperature the structural bonds of the material are not stable. This can lead to the formation of a crack and eventually to a catastrophic damage of the blades (due to the high stress loads experienced, while the turbine rotates by the passing of the high-speed/ high-temperature gas). The maximum turbine entry temperature corresponds to point 3 in Figure 2.2. (For more on compressors and turbines the reader is encouraged to read further in [29-31])

2.8.4 THERMAL CHOKING DUE TO HEATING

During ignition and engine pull-away, there is a limitation of how much heat can be added to the system which is known as thermal choking. In the engine ducts, if the flow becomes sonic, adding more heat will only decrease the velocity of the air. This is explained by the different properties of the flow as it becomes

supersonic. The reader is encouraged to read references [32, 33] for further information on this subject.

2.8.5 INLET AIR MASS FLOW RATE

INCREASING ENGINE SIZE

The size of the engine could increase in order to host more mass of air inside. It is logical to assume that the size is directly related to the weight of the engine as the material properties will remain the same and only the quantity of the materials change. So increasing the size will proportionally increase the weight of the engine [19]. (*Note: In an aircraft engine this factor is more important than in an industrial generator.*)

INCREASING FUEL CONSUMPTION

The fuel to air ratio f should not fall below the lean extinction limit of the fuel. At a low f the flame is not self-sustainable and combustion is not possible. Hence to keep the fuel to air ratio f within the flammability limits of the fuel, while increasing the air mass flow, means that the fuel consumption will have to increase. In addition, the flammability limits of the fuel depend on the air mass velocity inside the combustor. This problem can be dealt by a diffuser that will slow down the air entering the combustor and by increasing the number of combustion chambers.

REDUCING THE LEAN EXTINCTION LIMIT OF THE FUEL

If feasible, a decrease in the lean extinction limit of the fuel could be very beneficial in terms of ignition performance, consumption and power. If the turbine entry temperature is not affected by a reduction in the fuel to air ratio f – as a result of reducing the extinction limit and therefore increasing the air mass flow whilst keeping the fuel flow constant- then the thrust (equation (2.28)) is bound to increase. The lean extinction limit of a fuel is different to the lean ignition limit. If, when reducing the ignition limit, the flame is still self-sustainable or stable, then similar to the above, there will be a gain in thrust. As already mentioned, the main objective of this study is to reduce the lean ignition limit by increasing the efficiency of current igniter technology.

2.8.6 HIGH ALTITUDE

Another parameter that affects engine performance is the altitude. At higher altitudes the density of the air decreases. Since the density and volume of a fluid are interconnected properties ($v = \frac{1}{\rho}$) the specific volume of the ambient air will increase. In the pressure volume diagram in figure 2.2b, one can see that when the ambient air starts at a higher specific volume at the intake, then the output thrust is bound to decrease. In table 2.2, one can see the International Standard Atmosphere table from 1,000 ft below sea level to 65,000ft. At a normal cruising altitude of 11,000ft, it can be seen that the temperature and pressure drop 21.79°C and 343mbar each from sea level standards. The ambient density can be determined from table 2.2 using the equation of state (2.20) and assuming the air is an ideal gas.

THE INTERNATIONAL
STANDARD ATMOSPHERE (I.S.A.)

ALTITUDE (h)		AMBIENT TEMPERATURE (To)			AMBIENT PRESSURE (Po)		SPEED OF SOUND (ao)		
Feet	Metros	Deg. K.	Deg. C.	Deg. F.	lb./sq. in.	millibars	ft./sec.	knots	m./sec.
-1,000	-304.8	290.13	+16.98	62.6	15.24	1050.4	1120.3	663.3	341.5
0	0	288.15	15.00	59.0	14.69	1013.2	1116.6	661.1	340.3
+1,000	+304.8	286.17	13.02	55.4	14.17	977.1	1112.6	658.8	339.1
2,000	609.6	284.19	11.04	51.9	13.66	942.1	1108.7	656.5	337.9
3,000	914.4	282.21	9.06	48.3	13.17	908.1	1104.9	654.2	336.8
4,000	1219.2	280.23	7.08	44.7	12.69	875.1	1100.9	651.9	335.6
5,000	1524.0	278.24	5.09	41.2	12.23	843.0	1097.1	649.6	334.4
6,000	1828.8	276.26	3.11	37.6	11.78	811.9	1093.2	647.8	333.2
7,000	2133.6	274.28	1.13	34.0	11.34	781.8	1089.3	644.9	332.0
8,000	2438.4	272.30	-0.85	30.5	10.92	752.6	1085.3	642.6	330.8
9,000	2743.2	270.32	-2.83	26.9	10.51	724.3	1081.4	640.3	329.6
10,000	3048.0	268.34	-4.81	23.3	10.11	696.8	1077.4	637.9	328.4
11,000	3352.8	266.36	-6.79	19.8	9.72	670.2	1073.4	635.6	327.2
12,000	3657.6	264.38	-8.77	16.2	9.35	644.4	1069.4	633.2	325.9
13,000	3962.4	262.39	-10.76	12.6	8.98	619.4	1065.4	630.8	324.7
14,000	4267.2	260.41	-12.74	9.1	8.63	595.2	1061.4	628.4	323.5
15,000	4572.0	258.43	-14.72	5.5	8.29	571.7	1057.3	626.0	322.3
16,000	4876.8	256.45	-16.70	1.9	7.97	549.1	1053.3	623.6	321.1
17,000	5181.6	254.47	-18.68	-1.6	7.65	527.2	1049.2	621.2	319.8
18,000	5486.4	252.49	-20.66	-5.2	7.34	505.9	1045.1	618.8	318.5
19,000	5791.2	250.51	-22.64	-8.8	7.04	485.6	1040.9	616.4	317.3
20,000	6096.0	248.53	-24.62	-12.3	6.75	465.6	1036.9	613.9	316.1
21,000	6400.8	246.54	-26.61	-15.9	6.48	446.4	1032.7	611.5	314.8
22,000	6705.6	244.56	-28.59	-19.5	6.21	427.9	1028.6	609.0	313.5
23,000	7010.4	242.58	-30.57	-23.0	5.95	409.9	1024.4	606.5	312.2
24,000	7315.2	240.60	-32.55	-26.6	5.69	392.7	1020.2	604.1	310.9
25,000	7620.0	238.62	-34.53	-30.2	5.45	375.9	1015.9	601.6	309.7
26,000	7924.8	236.64	-36.51	-33.7	5.22	359.9	1011.8	599.1	308.4
27,000	8229.6	234.66	-38.49	-37.3	4.99	344.3	1007.5	596.6	307.1
28,000	8534.4	232.68	-40.47	-40.9	4.78	329.3	1003.2	594.0	305.8
29,000	8839.2	230.69	-42.46	-44.4	4.57	314.8	998.9	591.5	304.5
30,000	9144.0	228.71	-44.44	-48.0	4.36	300.9	994.7	588.9	303.2
31,000	9448.8	226.73	-46.42	-51.6	4.17	287.4	990.3	586.4	301.9
32,000	9753.6	224.75	-48.40	-55.1	3.98	274.5	986.0	583.8	300.5
33,000	10058.4	222.77	-50.38	-58.7	3.80	261.9	981.7	581.2	299.2
34,000	10363.2	220.79	-52.36	-62.3	3.63	249.9	977.3	578.7	297.9
35,000	10668.0	218.81	-54.34	-65.8	3.46	238.4	972.9	576.1	296.5
36,000	10972.8	216.83	-56.32	-69.4	3.29	227.3	968.5	573.4	295.2
36,089	11000.0	216.65	-56.50	-69.7	3.28	226.3	968.1	573.2	295.1
37,000	11277.6	Ambient temperature remains constant from this point up to 65,617 ft.			3.14	216.6	Speed of sound remains constant from this point up to 65,617 ft.		
38,000	11582.4				2.99	206.5			
39,000	11887.2				2.85	196.8			
40,000	12192.0				2.72	187.5			
45,000	13716.0				2.14	147.5			
50,000	15240.0				1.68	115.9			
55,000	16764.0				1.32	91.2			
60,000	18288.0				1.04	71.7			
65,000	19812.0				0.82	56.4			

Table 2.2: The International Standard Atmosphere table adopted from [20].

2.8.7 OTHER FACTORS AFFECTING GAS-TURBINE DESIGN

There are some other practical factors that affect the gas turbine design:

THE FUEL TANK VOLUME

This is not so important for industrial engines. For an aircraft though, an increase in fuel tank volume means an increase in weight due to both the change in dimensions and the heavier fuel load. The change in tank dimensions will also imply a change in shape and in the aerodynamics of the whole aeroplane or a less useable space inside it.

POLLUTION

Pollution is a broad area that is only mentioned here. More can be found in various books about gas-turbine engines (i.e. reference [19]). One example for more thought is an environmental issue that is not so obvious and concerns the contrails of aircraft engines. The contrails form high in the atmosphere when the mixture of water vapour of the aircraft exhaust and the air condenses and freezes. The contrails dissolve very slowly at high altitudes and soot particles are trapped inside them. At air corridors where commercial flights are very frequent, the contrails are persistent and can spread into extensive cirrus clouds. The contrails like other clouds trap radiation waves that would otherwise escape the earth's atmosphere, thus reinforcing the green-house effect. The contrails are created solely by the human activity and this raises a lot of concern. Due to the increased demands in commercial flying this activity is

expected to increase dramatically over the years. A good example of such frequent flight activity can be found over the English Channel in Figure 2.9 [34].



Figure 2.9: Contrails across the English Channel. Satellite image courtesy of NASA Visible Earth [34]

CHAPTER 3- GAS TURBINE COMBUSTORS

3.1 CHAPTER OUTLINE

Chapter 3 aims in the understanding of the combustor as a component. Some of the experiments carried out in this PhD study concern work done on a real Olympus Rolls Royce Combustion Chamber. It is the purpose of this work to bring forward more understanding and help the reader by gathering the basic knowledge involving the ignition problem. The relationship between combustor design and ignition is very close.

3.2 COMBUSTOR DESIGN CONSIDERATIONS

The combustor serves as the component where the heat addition takes place by burning the fuel with the air- ideally at a constant pressure. Inside it, the fuel mixes with the air and then burns, releasing in that way the stored energy of the fuel (calorific value) as heat to the mixture.

The shape of the combustor is driven mainly by the desire to keep the length and the front within a space set by other engine components and by the desirability to use efficiently all the available space.

3.3 COMBUSTOR DESIGN REQUIREMENTS

The main design requirements for a burner are summarised in Table 3.1 [19] below:

1.	<u>A High combustion efficiency.</u> The fuel must be burned completely to ensure that all the chemical energy is released as heat.
2.	<u>Operation at various conditions.</u> For this to be achieved, the flame must be kept alight over a wide range of pressures, velocities and air/fuel ratios.
3.	<u>Tolerance during pressure pulsations and other combustion induced instabilities.</u>
4.	<u>Reliable, smooth ignition and re-ignition.</u> It is required to achieve ignition of the mixture at usual situations like low ambient temperatures, or at extreme ones after a flameout at high attitude.
5.	<u>Operation with low pressure losses.</u> It is important to minimize the pressure loss induced by the insertion of the compressed air into the combustor and the pressure drop created by the sudden addition of heat to the high velocity mixture.
6.	<u>Recovery of dynamic pressure losses by slowing down the flow smoothly prior to burning.</u>
7.	<u>Specific temperature distribution at the exit that will ensure the maximum life of the turbine blades and also the nozzle guide vanes.</u>
8.	<u>Sustaining of low emissions of smoke, unburned fuel and pollutants.</u>
9.	<u>Operation with minimum cost.</u>
10.	<u>Accessibility to ensure easy maintenance.</u>
11.	<u>Size and shape that suites the design criteria of the engine.</u>
12.	<u>High-life expectancy of combustor.</u>
13.	<u>Light and compact (mainly for aircraft GT).</u>
14.	<u>Low fuel consumption and high power (mainly for industrial GT).</u>

Table 3.1: Gas combustor design requirements [19]

3.4 GAS TURBINE COMBUSTOR COMPONENTS

The criteria and choices for designing a combustor system are dictated by the operational requirements of the engine. There are numerous geometries and a wide range of parts to help achieve the desired result: high combustion efficiency over wide operational conditions and an even temperature distribution at the exit. The possibilities in the way that the components can be configured are endless. This versatility and the high efficiencies that can be achieved are two of the main advantages of the gas turbine engine [19].

The main components of the gas turbine combustor can be seen in Figure 3.1. The airflow leaves the compressor blades through the guide vanes and enters the combustor's diffuser.

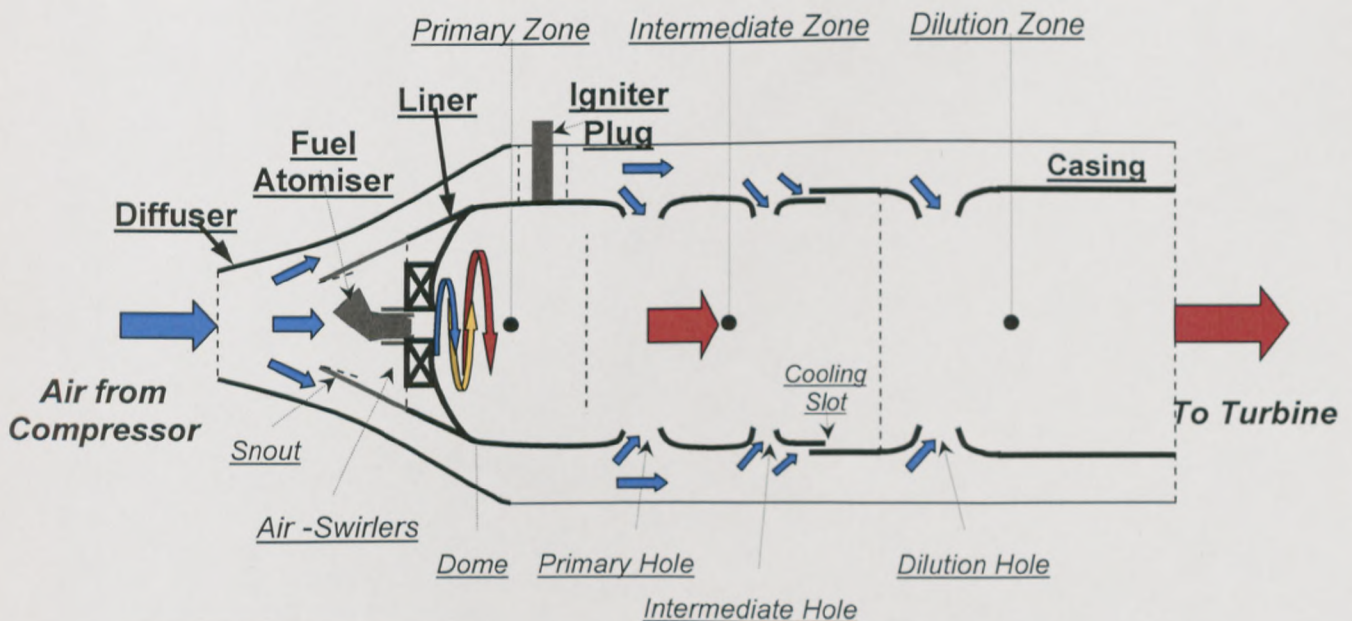


Figure 3.1: Gas Turbine Design- The combustor part. The main components are: 1: the combustor casing, 2: the liner, 3: the diffuser, 4: the fuel atomiser and 5: the igniter plug. The liner is divided into three zones: 2.1: primary, 2.2: intermediate and 2.3: dilution zone.

3.4.1 THE DIFFUSER

The diffuser slows down the velocity of the incoming air. It helps to minimise the pressure drop that will emerge after the exposure of the high velocity fluid to the heat energy released.

The pressure drop that is suffered across the combustor can be explained as the result of two different actions [19]:

COLD PRESSURE DROP

The cold pressure drop emerges by the resistance found by the air when flowing inside the combustor. It represents the sum of the losses experienced in the diffuser and the liner. Some pressure drop and particularly that incurred by the liner wall can be manifested as turbulence and mixing which is beneficial for burning. The cold pressure drop can be measured experimentally by running a cold test of the combustor. Typical values of cold pressure losses in combustors range between 2% and 6%.

HOT PRESSURE DROP

The hot pressure drop results by the sudden heat addition to the cold incoming air, as mentioned previously. The fundamental pressure loss due to combustion is proportional to the square of the incoming air velocity and is described by the expression [19]:

$$\Delta P_{hot} = 0.5\rho U^2 \left(\frac{T_4}{T_3} - 1 \right) \quad [Pa]$$

The diffuser prevents a large hot pressure drop by slowing down the incoming flow and keeps the loss to an acceptable level. It is also used to provide a stable flow of air to the liner. On the other hand, the pressure lost by the use of the diffuser cannot be retrieved and care should be taken during the design process. The velocity of the incoming air is usually reduced by about a factor of 5 by the diffuser [19].

3.4.2 THE FUEL ATOMISER

The fuel atomiser is the device that is responsible for reducing the fuel into a high quality, micro-size droplet spray. The small size of the droplet is important for achieving a quick evaporation rate. The spray is obtained by either forcing the fuel through a fine orifice under pressure or by utilizing the pressure differential across the liner wall to create a high speed jet of air that shatters the fuel into fine droplets and carries it to the primary combustion zone. The quality of the spray (i.e. the droplet size) is critical for ensuring good ignition characteristics. It is indicative to say that a slight deterioration of the quality of the spray will cause a large increase in the minimum ignition energy [19] (Section 4.5.1).

3.4.3 THE LINER OR COMBUSTION CHAMBER

The liner is the part where the main combustion takes place. It is also called a combustion chamber. Some of the airflow inside the diffuser flows through the snout and is guided towards the air swirlers and into the dome of the liner. From

there, the injected fuel mixes with the high-speed recirculating air and is then ignited in the primary zone by the creation of sparks through the ignition plug or by the release of heat due to the continuous burning when in operation. The introduction of air from the combustor casing to various zones inside the liner, is a creative way to achieve the desired high combustion efficiency [35].

3.4.4 THE PRIMARY ZONE

The role of the primary zone is to maintain the flame and to prevent it from extinction. The introduction of air through the primary holes is used to create the desirable airflow pattern that will ensure high quality mixing of the air with the fuel and will provide low-velocity zones that hold the flame. At high altitudes, the burning of the mixture in the primary zone is usually incomplete [19].

3.4.5 THE INTERMEDIATE ZONE

The intermediate zone as the name suggests hosts the advanced stage of the burning. The insertion of air through the intermediate holes is utilised to provide “fresh” oxygen to the hot gas exiting the primary zone. This extra stage of combustion guarantees a longer residence time of the mixture inside the combustor. Hence, it prevents losses due to the chemical dissociation of the primary combustion products and presents a higher chance for any unburned fuel to mix with oxygen and burn. Thus, the intermediate zone is critical for achieving higher combustion efficiencies and for keeping the hot pressure drop to minimum, by smoothening the evolution of the flame [19].

The intermediate zone serves two main functions depending on the altitude [19]:

LOW ALTITUDE

To decrease the temperature to an intermediate level by the insertion of air from the combustor casing to the liner, prior to the dilution zone. To complete the burning of any carbon monoxide and partly burned fuel that escaped the primary zone.

HIGH ALTITUDE

At high altitudes, the intermediate zone is used as an extension of the primary zone in order to allow an increased exposure time at high temperatures prior to the cooling of the reaction in the dilution zone.

The length of the intermediate zone is therefore strongly related to the overall combustion efficiency.

3.4.6 THE DILUTION ZONE

The gases exiting the intermediate zone, pass to the last stage of combustion in the liner; the dilution zone. The dilution zone is used mainly to decrease the temperature of the gas that exits the combustor to a temperature that can be tolerated by the turbine blades. The amount of air available for dilution is usually

between 20% and 40% of the total combustor airflow [19]. It is of primary importance to achieve a pattern-like temperature distribution at the exit. The requirement is to achieve a minimum temperature at the turbine root which is subject to very high loads and to protect the sealing material at the turbine tip.

3.4.7 THE COMBUSTOR CASING

The combustor casing occupies the space between the liner and the combustor wall. The main role of the combustor casing is to cool the liner wall and to provide “fresh” air to the main combustion chamber.

3.5 GAS TURBINE COMBUSTOR TYPES

There are three main combustor types. These are the tubular, annular and tubo-annular [19, 35]. Their categorisation depends on how the liner is configured inside the combustor casing and the shape of the combustor.

3.5.1 TUBULAR COMBUSTOR: SINGLE-CAN AND MULTI-CAN

The tubular combustor is the type that has a cylindrical liner concentrically positioned inside a cylindrical casing. The single-can, as the name suggests, is an engine that operates with one combustion chamber. This configuration is used mainly in small gas turbines, for applications that do not require a high power output.

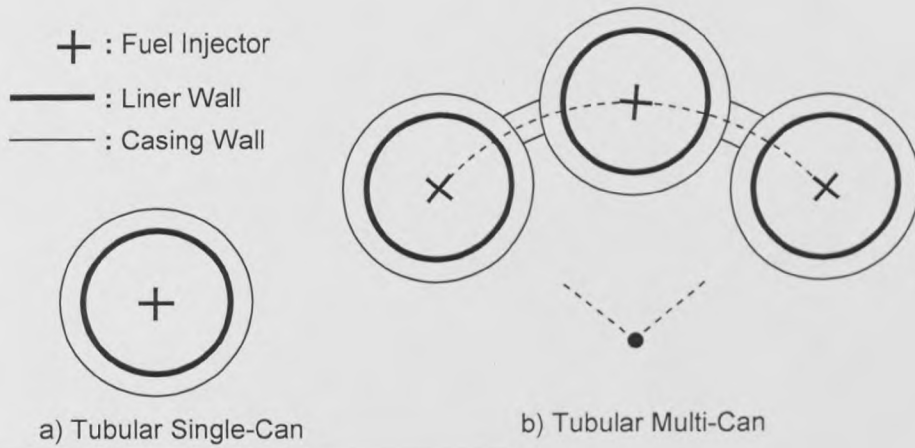


Figure 3.2: *The Tubular Type Combustor: a) single-can and b) multi-can configurations*

Designs of the tubular type are generally more mechanically robust. Their structural properties ensure a longer life for the combustor in conjunction with low maintenance costs. In terms of experimenting costs, the tubular combustor can be tested without running a full engine test. Usually, only one of the combustion chambers is enough for testing. The air mass flow is therefore reduced to the requirements of the test specimen. The cylindrical shape of the liner and the casing, together with the ability to test at smaller scales, allows for an easier prediction and manipulation of the flow. Another advantage of the tubular type is also the high mixing strength of fuel and air that can be achieved. Moreover, due to the shape of the liner that nurses the flame and due to the gas dynamics of the primary zone, the combustor is more tolerable to sudden pressure variations.

The multi-can configuration is deployed in applications that require high power and make use of the advantages previously mentioned. In gas turbine engines of this type the number of chambers varies from seven to sixteen [19].

The tubular type, although it allows for a very strong structure, it loses ground to other types in terms of power to weight output and bulkiness. This kind of design suffers from large pressure losses and requires flame connectors when it is of a multi-can type. Also, in the multi-can combustor, the frontal area is quite large due to the shape.

The multi-can configuration is not preferred in aircraft gas turbine engines because of the disadvantages discussed.

3.5.2 ANNULAR COMBUSTOR

The annular type has an annular liner fitted concentrically inside an annular casing.

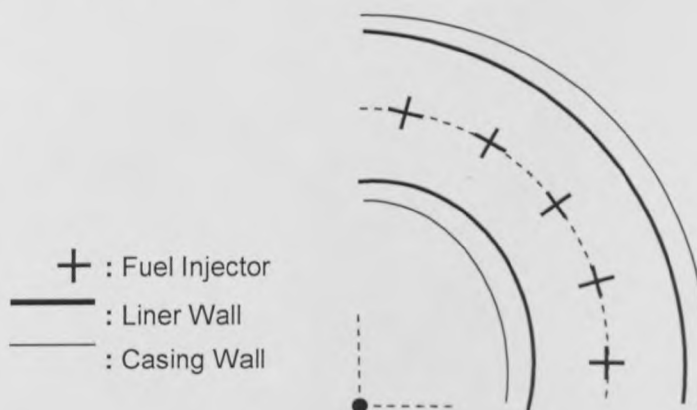


Figure 3.3: The Annular type combustor

This type of design is considered to sustain a small pressure drop due to the aerodynamically more efficient shape of the liner and the casing. It can also be quite compact and for this reason it is preferred when weight and space are of

importance. Another advantage of the annular configuration is that the shape allows for a small frontal area. Since the combustor is 'wrapped' around the engine, the power to weight output that can be achieved is quite high.

Although the annular type solves some design problems in terms of weight and space, there are compromises in other areas. For example, it is difficult to do experiments on a combustor of this design because the tests will require running a full engine air mass flow. It is therefore much more difficult to make predictions and to manipulate the flow. Nowadays CFD simulations are becoming more commercial and due to high power computers this problem is less important. However, the shape of the liner makes the flame more prone to sudden pressure changes and this is not easily predictable. Another but very important disadvantage of the annular type is the heavy buckling load of the annular liner. Finally due to the configuration, any variation of the flow characteristics when entering the engine may change the temperature distribution at the turbine inlet.

3.5.3 TUBOANNULAR OR CAN-ANNULAR COMBUSTOR

The tuboannular or can-annular type combustor is a 'hybrid' design that combines characteristics from both the annular and the tubular combustors. The combustor case is of the annular type but instead of having a single annular liner inside, it is comprised by a number of cylindrical liners; similar to the tubular multi-can type.

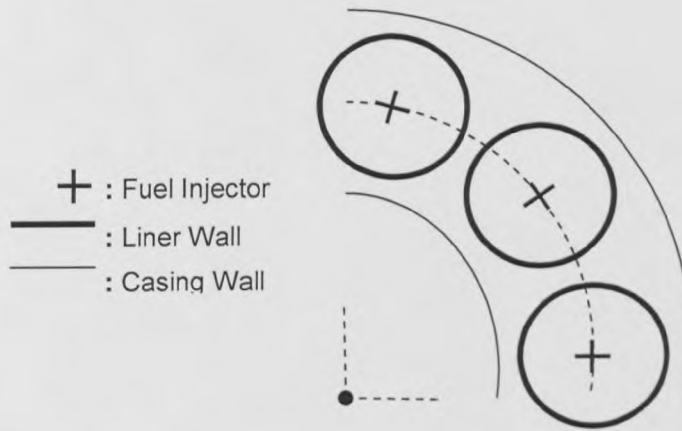


Figure 3.4: *The Tuboannular type combustor*

These 'hybrid' designs bring together advantages that would normally be in conflict with each other in the other two combustor types. Like the tubular configuration, they are considered to be mechanically robust structures, that achieve good air-fuel mixing and they maintain operation at various conditions with stable flame characteristics. Because of the annular shape, these combustors are lighter and more compact compared to the tubular kind. The shape allows for a more aerodynamically efficient flow and thus, sustains a small pressure loss. Most importantly, the tuboannular type permits for a considerable reduction of cost in combustor development. Like in the tubular design, the need to run a full engine test is greatly minimised by testing a section of the combustor instead (i.e. usually one liner is enough), at scaled air mass flows.

The main disadvantage of the can-annular configuration is the difficulty of providing consistent airflow characteristics throughout the annular casing and

inside the liners. Thus, the design of the diffuser is very crucial for achieving the desired result. It is also less compact and heavier compared to the annular type and the liner requires flame connectors, similar to the tubular multi-can combustor.

The tuboannular combustors are used extensively, although modern combustors tend to be of the annular type [19].

3.6 FUELS

The realisation that the fossil fuels are reducing with rapid pace and that the oil wells are draining raises great concern for the future of a world that has never again been so energy dependent. These two phenomena, by today's standards, come in contrast with the fact that the world population is growing exponentially and that more and more countries become industrialised.

State of the art engineering is deployed to make the changes required in order for a wide variety of fuels to be compatible with gas turbine engines and fuel system requirements. The current portfolio of fuels, considered suitable for gas turbines, is shown in Figure 3.5 [36]. A classification of the main aviation fuels has been attempted in Table 3.4 [19].

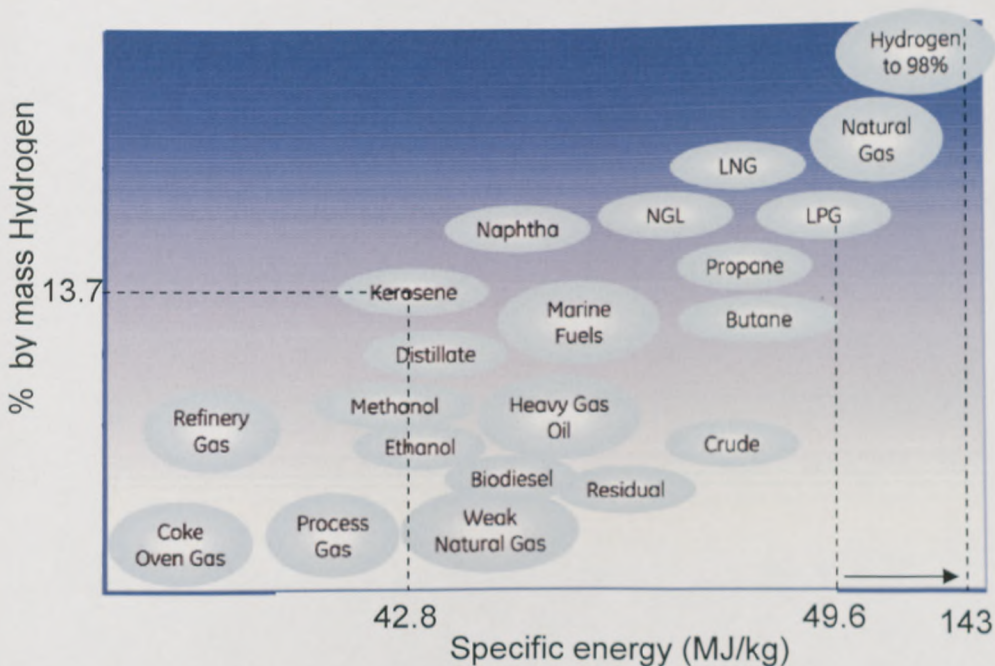


Figure 3.5: Possible fuels for gas-turbine usage [36]

3.6.1 HYDROCARBON CATEGORIES

Table 3.2 below, describes the four main groups of hydrocarbon compounds [19, 37].

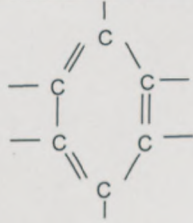
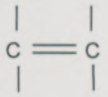
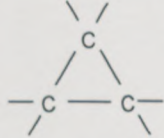
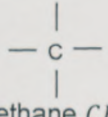
Name	Description	Simplest Structure
<i>Aromatics</i>	Hydrocarbons with characteristic formula C_nH_{2n-6} containing carbon-rings	 <p>(Benzene C_6H_6)</p>
<i>Napthalenes</i>	Aromatic Hydrocarbon $C_{10}H_8$	
<i>Olefins</i>	Hydrocarbons with characteristic formula C_nH_{2n} (very active chemically- not desired in gas turbine fuels)	 <p>(Ethylene C_2H_4)</p>
<i>Napthenes</i>	Hydrocarbons with characteristic formula C_nH_{2n} containing carbon rings	 <p>(Cyclopropane C_3H_6)</p>
<i>Paraffins</i>	Hydrocarbons with characteristic formula C_nH_{2n+2}	 <p>(Methane CH_4)</p>

Table 3.2: Hydrocarbon categories and description.

3.6.2 TERMINOLOGY FOR GAS-TURBINE FUELS

Table 3.3 [19] below defines some common properties of fuels and characteristics that are useful for specifying the requirements that must be met by the fuel manufacturers (next Table 3.4).

Name	Description
Gum Formation	Oxidation of inorganic elements that exist in the fuel. In the initial oxidation period, the gum in the fuel appears to have a yellowish colour and in later stages it turns into sludge. Gum is undesirable as it can clog filters, fuel lines and fuel injector nozzles. It may interfere with fuel flow and engine system control, increase carbon deposition and can deposit on surfaces that are used for cooling [19].
Water Reaction	Measure of the materials that are readily extractable by water (<i>separation rating</i>) or have a tendency to absorb water such as <i>surfactants</i> (<i>interface rating</i>). Water exists in all distillate fuels depending on their composition, temperature and storage history. Water droplets in the fuel may also form by passing the fuel through pumps and mixers or during flights with low fuel temperatures [19]. At temperatures below zero water tends to form ice crystals and may block filters, fuel lines and fuel injector nozzles.
Surfactants	Materials that reduce the effectiveness of coalescers (water separators) and fuel filters. Prolonged storage of fuels that contain surfactants may lead to the formation of water pools in the fuel tank.
WSIM	Water separation Index Modified. Measure of water separation characteristics and of the surfactant content of a fuel.
Distillation Range	Because of the nature of fuels, being a mixture of many compounds, a boiling temperature range is recorded. The first point is recorded when the most volatile compound evaporates, passes to a connected ice-cold container and begins to condense. The final point is recorded when there is no more fuel to evaporate. This process is called ASTM distillation test [19].
Reid Vapour Pressure	Common measure of the volatility of <u>gasoline-type</u> fuels.

Table 3.3: Terminology for gas-turbine fuels .Definitions mainly from reference [19]

Name	Description
Flash Point	Minimum temperature at which the fuel vaporises at a sufficient rate to form a flammable mixture with air. Flash point and vapour pressure are inversely related, whilst volatility is directly related. The flash point is used to assess the fire-hazards involved when handling a fuel.
Freezing Point	The temperature at which the fuel starts to form solid particles due to a decrease of its temperature.
Smoke Point	The maximum height of smokeless flame. This distance is determined by burning the fuel in a special wick lamp and increasing the height of the flame until it begins to smoke [19]. The larger the distance, the lower is the tendency of the fuel to form smoke.
Net Specific Energy	The low energy value of a fuel which is available to be released as heat by the complete combustion of 1kg of fuel with oxygen. The net energy is equal to the gross energy of the fuel less the energy (latent heat) that was spent to vaporise the water quantity, formed by the combustion reaction.
Wobbe Index	Provides information for the energy quantity that can be released by a given fuel when knowing the size of the fuel nozzle. It is a useful number as it allows for comparisons to be made between different fuels [36]. $Wobbe\ Index = \frac{energy\ density}{relative\ density} \left[\frac{MJ}{m^3} \text{ or } \frac{Btu}{ft^3} \right]$
Static-Dissipator Additive	Increases the conductivity of the fuel in order to dissipate a charge and thus prevent the occurrence of a spark due to static electricity.
Corrosion Inhibitor-Lubricity Additive	Protects Fe metals in fuel handling systems –i.e. pipelines and tanks- from corrosion and improves the lubricating properties of certain jet-fuels.

Table 3.3(continued): Terminology for gas-turbine fuels. Definitions mainly from reference [19]

3.6.3 MAIN AVIATION FUEL SPECIFICATIONS

<u>Specification:</u>	<u>Wide-Cut Gasoline</u>	<u>Kerosene</u>	<u>High-Flash Kerosene</u>
<u>Designation:</u>	<u>Avtag</u> (Military) <u>JP4</u> (Military) <u>Jet-B</u> (Civil)	<u>Avtur</u> <u>Jet-A</u> <u>Jet-A1</u>	<u>Avcat</u> <u>JP5</u>
<u>Aromatics</u> (max %by volume)	25.0	22.0	25.0
<u>Napthalenes</u> (max %by volume)	-	3.0	-
<u>Sulphur</u> (max %by mass)	0.3	0.3	0.3
<u>Olefins</u> (max %by volume)	5.0	5.0	5.0
<u>Existent Gum</u> (max mg/100ml)	7.0	7.0	7.0
<u>Water Reaction:</u>			
Separation Rating ^b	2	2	2
Interface Rating (max)	1	1	1
<u>Water-Separation- Index-Modified</u> (min WSIM)	70 ^a 85 ^b	70 ^a 85 ^b	70 ^c 85 ^d
<u>Density</u> (kg/l at 288K)	0.751 (min) 0.802 (max)	0.775 (min) 0.830 (max)	0.788 (min) 0.845 (max)
Viscosity (max m ² /s at 253K)	-	8.0x10 ⁻⁶	8.0x10 ⁻⁶
<u>Distillation Range:</u>			
10% boiling point	-	478	478
Final point (max K)	543	573	573
<u>Reid Vapour Pressure</u> (kPa at 311K)	14 (min) 21 (max)	- -	- -
<u>Flash Point</u> (min K)	-	311	333
Freezing Point (max K)	215	226	227
Smoke Point (min mm)	21	20	20
Net Specific Energy (min MJ/kg)	42.8	42.8	42.6

Table 3.4: Specifications for aviation fuels [19]

^aWith static-dissipator additive, ^bwithout static-dissipator additive, ^cwith corrosion inhibitor-lubricity improving additive, ^dwithout corrosion inhibitor-lubricity improving additive.

3.6.4 AVIATION FUELS

Aviation fuels are high-grade fuels. Military requirements differ from commercial ones due to the unlike operating conditions, but still remain the same in terms of aircraft performance, safety, reliability and ease of handling. In contrast with commercial airliners, for military aircrafts fuel cost is of secondary importance compared with availability, supply logistics and the need for stable operation over more demanding conditions [19, 38]. A summary of the main fuels used for aircraft gas turbines is shown in Table 3.4 [19]. It is interesting to note that JP4 (U.S.) or Avtag (U.K.) wide-cut gasoline is a direct result of strategic military decisions in order to minimize problems of availability during wartime. A study of this issue concluded that the best source of fuel which can prove substantial during times of war by denying access to the civilian sector, is motor gasoline[38].

3.6.5 FUELS FOR INDUSTRIAL GAS TURBINES

The improvements and the fuel flexibility that have developed over the years for ground-engines of this kind have given to the gas turbine a leading role in industrial applications. The key parameters for choosing the right gas turbine and the operating fuel -or fuels- are the cost of the plant, the cost of the fuel, the availability of the fuel, maintenance considerations, fuel handling and pollution. The choice is decided usually by the end-user after considering the available options. Although power generation is the main application for industrial gas turbines, other uses include pumps and drilling machines. The fuels that are

considered are split into two categories: traditional fuels and non-traditional ones [19, 36].

TRADITIONAL FUELS FOR INDUSTRIAL GAS TURBINES

- Natural Gas (NG)

Natural gas has been a significant fuel source for power generation and is expected to continue to be a very important fuel for the near future [36]. Natural gas resources are not distributed equally around the globe.

- Liquefied Natural Gas (LNG)

Adding globally sourced LNG to the fuel mixture used for power generation, adds a degree of complexity to the control system of the gas turbine. LNG can have increased content of inert gases (i.e. N_2) and higher hydrocarbons, especially ethane (C_2); depending on the source. To surpass this problem, the Wobbe Index of the fuel mixture is used to simulate the gas turbine operability boundaries (e.g. emissions, combustion dynamics, etc.) in a real time basis, while the turbine is running and sends them to the control system, where appropriate decisions are taken with minimum user input[36].

NON-TRADITIONAL FUELS FOR INDUSTRIAL GAS TURBINES

- Refiner Residuals

The realisation of using refiner residuals in gas turbines for power generation has proved very attractive for the refining industry. These industries, once

concerned with what to do with the waste from refining processes, are now able to invest in gasification technologies to improve refining and overall production [36]. These technologies can also produce residuals such as aviation kerosene Jet A₁.

- By-Products of Industrial Processes (LCV-Low Calorific Value Fuels)

These can be used to produce energy onsite instead of wasting them. The cost of maintaining the plant should be weighted with the energy that can be produced.

- Syngas and Synfuels

These fuels are mainly hydrogen based. They are usually processed products of coal, lignite, petroleum coke, heavy oil and waste materials [19, 36].

- Renewable Bio-liquid Fuels

Renewable fuels can be produced from many bio-materials such as Corn, soy, palm, rapeseed and jatropha. The main components of the product fuel are hydrogen and carbon monoxide. The most popular are: Vegetable oils (VO) - virgin or recycled-, alcohols, Esterified VO or Fatty Acid Alkyl Esters [36]. Concerns have been raised on the sustainability of these fuels and the energy that is required to process and supply such a fuel. Moreover growing plants for fuel usage means that large quantities of water are used for energy purposes. The increasing demand of non-forest land for farms and vegetable growing comes in contrast with growing plants as fuel sources.

CHAPTER 4 – IGNITION

4.1 GAS TURBINE IGNITION SYSTEMS

The role of the ignition system is to provide the extra energy that is required by the combustible mixture to initiate the chemical reaction that is commonly known as burning. Inarguably, the ignition system is an important part of the engine and reliable ignition is crucial for ensuring that the flame is sustained during operation. As one can deduct, reliable performance of the ignition system is life-critical for aircraft engines, whilst for industrial engines, although continuous burning is essential, a flame-out is not catastrophic. For this reason, most ignition research is focused on aircraft engines (as they are more demanding in this respect) but applies also to industrial applications.

4.2 FLAME OUT SITUATIONS

Although the main role of the combustor's primary zone is to shelter the flame and to prevent it from extinction, sometimes combustion suddenly terminates. There are some particular situations that the probability of a flame-out is high. These fall into six main categories which are summarised in Table 4.1 [19].

Flame-Out Situations	
1	Pressure variations when the airflow is transient during flight manoeuvres or under adverse climatic conditions.
2	Excessive water or ice ingestion by taking off from a wet runway or by flying into bad weather.
3	Excessive dust ingestion due to a natural event. A recent example of such natural event was the ash cloud that was formed by the explosive activity of Iceland's Eyjafjallajökull volcano.
4	Gas-exhaust ingestion following the release of a missile in military aircrafts.
5	Deterioration of the fuel-spray quality while running, due to the high altitude or because of a fuel injector blockage. It is unlikely that the later situation occurs in an aircraft engine due to the strict rules that apply for high quality aviation fuels.
6	Flame instability due to the use of lean air-fuel mixtures or low quality fuels in industrial applications.

Table 4.1: Main reasons for a flame-out in a gas-turbine engine

4.3 THE PROCESS OF IGNITION IN GAS TURBINES

The process of ignition in a gas turbine can be divided into three distinct phases [10]. In phase no. 1 the spark initiates and forms a flame kernel of roughly spherical volume. If the kernel temperature and volume are high enough then the flame propagates in phase no. 2 to the whole of the primary zone. If the combustor is of a tubular multi-can or tuboannular type, then in phase no. 3 the flame spreads to all other chambers through the flame connectors. A failure in any single phase translates to a failure in ignition.

IGNITION PHASE 1

The successful outcome of phase no. 1 depends on whether the rate of heat release exceeds the rate of heat loss during the initiation of the flame kernel. The effective air-fuel mixture strength in the area adjacent to the igniter plug,

the energy and the duration of the spark are all considered to influence the rate of heat released by ignition. The rate of heat loss is subject to the flow conditions and the turbulence intensity that exist near the point of ignition [19].

IGNITION PHASE 2

Through phase no. 2, the flame develops to its full potential inside the primary zone. The main factor that affects this phase is the position of the igniter inside the liner. The ignition kernel from phase no. 1 should ideally be directed/ projected into the recirculation area of the primary zone. An increase in pressure, a decrease in primary zone flow velocity, an increase in air-fuel mixture strength or in the velocity of the kernel are all factors that affect positively phase no. 2 [19].

IGNITION PHASE 3

The success of phase no. 3, the propagation of the flame to all other liners, depends solely on the position and the shape of the flame connectors. The inlet of the connector should be ideally at a position where the burning gas is higher in temperature. When exiting the flame connector, the hot gas should fall into the recirculation area of the next liner [19]. The shape of the connector is found to be an important parameter in the propagation of the flame to the other combustion chambers. The flame connectors should be short in length and wide enough to facilitate a large flame area.

4.4.1 SURFACE DISCHARGE IGNITERS (SDI)

A common igniter used in gas turbine engines is the surface discharge igniter (SDI) [19, 39, 40]. The design of the SDI comprises a central electrode and an outer electrode separated by a semiconductor. The igniter expels the plasma electromagnetically [41, 42]. Only 10% of the energy is transferred to heat the mixture from the 2-3 Joules which are provided to the spark [7]. The remainder energy is lost by conduction, radiation and shockwave dissipation [43].

4.4.2 PLASMA JET IGNITERS (PJI)

The plasma jet igniter is a modification of the SDI. In the PJI the central electrode is placed below the outer electrode in a way that, at its end, there is a gap between the cylindrical inner and outer electrodes and the electrodes are separated by a semiconductor. This has the effect of lengthening the distance between the inner and outer electrodes and better matching the impedance of the ignitor and spark source. The inner electrode of the igniter is recessed within a ceramic cavity [42]. PJI igniters usually feed continuous gas into the cavity of the igniter (continuous plasma jet CPJ) [44, 45]. A 'soup of ions' is formed by an arc discharge within this cavity from which it is expelled by a large pressure gradient created between the medium in the cavity and the unburned gas [42, 44]. The advantages of these igniters are found to be the higher velocities and reaction rates and the increased production of radicals, which are proven to chemically augment the combustion and stability of the system.

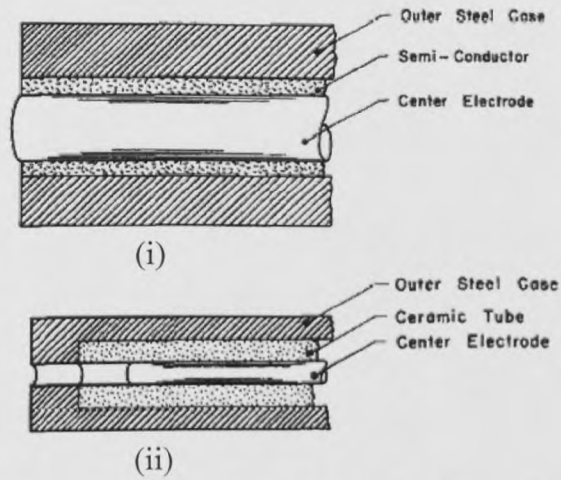


Figure 4.1(a): Cross section of (i) Surface discharge igniter, (ii) Focus discharge igniter or plasma jet igniter. [42]

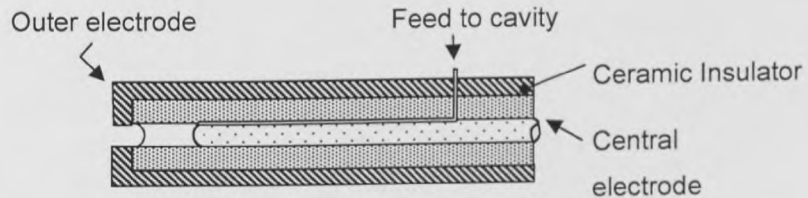


Figure 4.1(b): Cross section of a plasma jet igniter design with feed line for supplying the plasma medium.

4.4.3 FOCUS DISCHARGE IGNITERS (FDI)

One similar to the plasma jet, but not so well known igniter, is the focus discharge igniter (FDI) [7]. The difference is not so much in the design of the plug but mainly on the medium that is supplied and creates the plasma. The FDI's create a plasma discharge with whatever exists in the cavity of the igniter during the operation of the engine [7]. The design can be considered similar to a simplified pulsed plasma jet igniter (PPJ) [45, 46], as the discharge is not continuous but rather pulsating.

4.5.1 CAPACITANCE SPARK

These are the sparks produced by discharging a charged condenser. The total energy required to produce a capacitance spark is [47]:

$$E_c = \frac{1}{2} C (\mathcal{V}_2^2 - \mathcal{V}_1^2) \quad [J] \quad (4.1)$$

E_c : Energy dissipated in the spark

C : Capacitance of discharged condenser (farads)

\mathcal{V}_1 : Extinction potential remaining after the spark has been dissipated (volts).

Usually $\mathcal{V}_1 \ll \mathcal{V}_2$ and may be disregarded.

\mathcal{V}_2 : Circuit potential immediately before the passage of the spark (volts)

It should be highlighted that not all electrical energy is dissipated as heat in the spark. There are many sources of electrical loss. The actual proportion of the total energy converted into heat in the spark may be as low as one tenth [47] (see also Section 4.7.10 for more references).

4.5.2 QUENCHING DISTANCE

The 'quenching distance' d_q is defined as the minimum separation of between parallel plates that will just allow a flame to pass [47, 48]. A popular procedure for determining the quenching distance is to confine the combustible mixture between parallel flat plates and to find the minimum separation before extinction [48]. From Lefebvre [19] for a low turbulence intensity v' :

$$d_q = \frac{10\lambda}{c_p \rho_0 (v_0 - 0.16v')} \quad [m] \quad (4.2)$$

See equation (4.3) for an explanation of the λ and v_0 terms.

4.5.1 MINIMUM IGNITION ENERGY (MIE)

The minimum ignition energy requirement is defined through the use of pre-mixed flames. The MIE describes the minimum energy added to the gas to heat a slab about as thick as a steadily propagating adiabatic laminar flame to the adiabatic flame temperature [48]. It should be noted that the MIE describes the total energy before losses to the ignition plug. These losses account to about 90% from the total energy (Section 4.7.10). Because of the definition of the MIE, through the premixed flame theory, these values are mostly used in safety studies for handling and storing chemicals. In real flowing gases where turbulence is high and the fuel-air is not uniformly mixed, the MIE is much lower than the real energy requirement for ignition (Section 4.7.9). Moreover in spray combustion, the effect of the fuel droplet size (or the fuel spray quality (FSQ)) along with other factors [47] -some being the local pressure and temperature of the mixture at the immediate site of ignition (but not only)- will dominate the energy requirement for ignition. J.F. Griffiths [49] notes that the spark energy required to initiate ignition in premixed fuel and air is dependent on pressure composition and temperature, factors which are governed primarily by the chemical reactivity of the fuel. The effect of temperature and pressure on reaction is expressed by the Vant Hoff equation [50]. Theoretically the minimum ignition energy *MIE* per unit area is expressed by [48]:

$$\frac{MIE}{A_{slab}} = \frac{\lambda(T_{\infty} - T_0)}{v_0} \quad \left[\frac{J}{m^2} \right] \quad (4.3)$$

A_{slab} : Area of slab

λ : Average thermal conductivity of gas

v_0 : Adiabatic laminar burning velocity

There are many variations of equation (4.3) [48] and some of them include the quenching distance d_q [19]:

$$MIE = \pi d_q^2 \frac{\lambda}{v_0} (T_b - T_0) \quad [J] \quad (4.4)$$

4.5.2 PRESSURE AND TEMPERATURE DEPENDENCE OF IGNITION

The main factor for determining the ignition energy is the composition and the concentration of the fuel in vapour. The concentration in vapour of the fuel (X_{fuel}) when in equilibrium is proportional to the ratio of the fuel vapour pressure over the ambient pressure (equation (4.5)[51]). The fuel vapour pressure depends primarily on the fuel liquid temperature inside the vessel and less on the amount of liquid and history of handling. The dependence of the ignition energy of the kerosene Jet-A fuel with temperature at a fixed ambient pressure is shown in Figure 4.2[51].

$$X_{fuel} = \frac{p_{fuel}(T_{fuel})}{p_a} \quad \left[\frac{kmol}{m^3} \right] \quad (4.5)$$

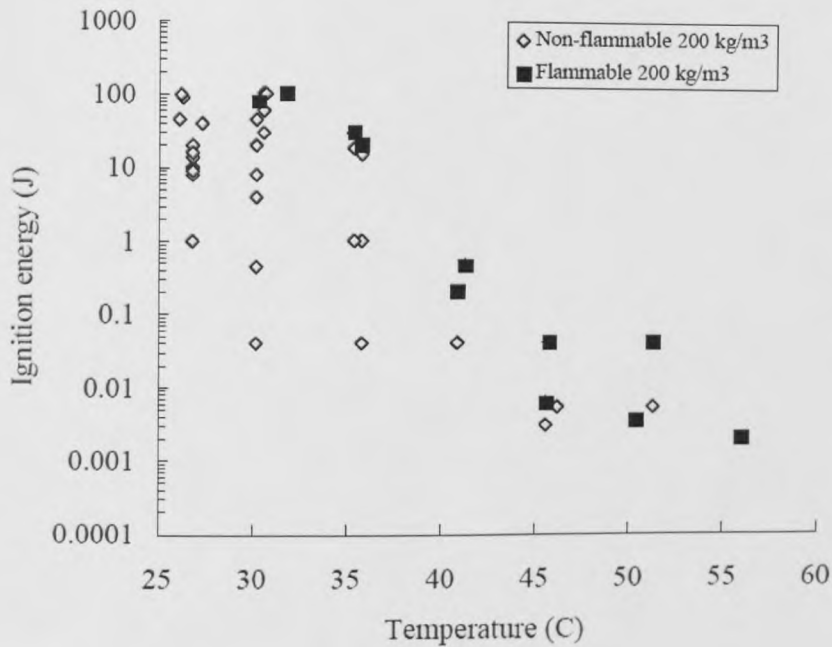


Figure 4.2: Spark ignition energy for kerosene Jet-A vapour mixtures at different temperatures at an initial pressure of 0.585bar and a fuel mass loading of 200kg/m³ (fuel quantity-density) [51]

4.6 THERMAL IGNITION AND SOME CHEMICAL CONCEPTS

4.6.1 ARRHENIUS AND RATE OF REACTION

“Every combustion or explosion process is above all a chemical reaction between the components of the combustible mixture, accompanied by the liberation of heat and various kinds of motion in gases.” Semenov [52].

Chemical reactions are the direct result of collisions between the reactive species that come into contact with each other. However, not all molecules have the energy that is required for the reaction to occur – i.e. for the collisions between reactants to lead to a reaction. Only active species are capable of causing a reaction. The term active species is used to denote those species that poses energies higher than an amount E per mole of reactant [53]. The

total energy of the species should be higher than the activation energy E_A for the reaction to proceed. The activation energy is found experimentally.

The number of collisions per unit time is directly proportional to the initial concentration of the reactive species. The rate of the reaction is also directly proportional to the number of collisions per unit time between the reactive species. The reaction rate \mathcal{R} for an n^{th} order reaction is expressed by [54]:

$$\mathcal{R} = K C_1^{x_1} C_2^{x_2} \dots C_n^{x_n} \quad \left[\frac{\text{mol}}{\text{ls}} \right] \quad (4.6)$$

C_n : Concentration of n reactant $\left[\frac{\text{mol}}{\text{l}} \right]$.

K : Reaction rate constant $[\text{mol}^{(1-n)} \text{l}^{(n-1)} \text{s}^{-1}]$.

x_n : Empirical coefficient for n reactant

It follows from equation (4.6) that the reaction rate decreases as the initial concentration of the reactive species reduces; while the reaction progresses and the reactants are converted into products.

The Arrhenius' equation is considered as the most satisfactory expression of the influence of temperature on the velocity of the chemical reaction[55]:

$$\frac{d(\ln K)}{dt} = \frac{E}{RT^2} \Leftrightarrow K = A' e^{-\frac{E_A}{RT}} \quad \left[\frac{\text{mol}}{\text{ls}} \right] \quad (4.7)$$

Equation (4.7) implies that the plot of the log of the reaction rate constant ($\ln K$) against the inverse of temperature ($\frac{1}{T}$) is a straight line and is found to be true for many homogeneous and heterogeneous chemical reactions [55]. The activation energy E_A can be interpreted by knowing the reaction rate constant K at two or more temperatures and then by drawing the straight line of $\ln K$ against ($\frac{1}{T}$) which expresses the line ($-\frac{E_A}{R}$). The dependence of temperature on the reaction rate is well known. An increase in temperature results in heat energy being absorbed by the reactive molecules. The additional energy input increases the concentration of active species per unit time, thus forcing the reaction to proceed faster [55].

4.6.2 AUTO-IGNITION

According to Arrhenius' equation, the heat created by the reaction increases the velocity of reaction. The existence of such retroaction between temperature and reaction velocity is characteristic of most phenomena of the combustion process. The effect of the reaction on the generation of heat in the mixture, but also on the increase in reaction velocity due to this higher generated heat, initiates a self-accelerating surge of heat which is known as auto-ignition [52]. Moreover, because of the dissipation of heat on the walls of the reaction vessel, auto-ignition is possible only under certain conditions that are all (parameters) reflected in the temperature of auto-ignition. This temperature is a function of kinetic and thermal parameters of the reaction, namely the order of reaction, the activation energy, the density and composition of the combustible mixture, the heat of reaction and the dissipation of heat on the vessel walls.

4.6.3 IGNITION DELAY TIME

The time difference between the instance of contact of the reactive materials and the onset of the reaction is called ignition delay time. The ignition delay time (τ) can be roughly calculated by using the Arrhenius' equation and by assuming that τ represents a fraction of the time of the completed reaction at a given pressure. According to this assumption, the delay time will be inversely proportional to the reaction rate constant $\left(\frac{1}{K}\right)$ so that:

$$\tau = Ae^{\frac{E_A}{RT}} \quad [s] \quad (4.8)$$

This equation holds for a number of homogeneous reactions although the assumption used is not very accurate[55].

4.6.4 IGNITION LIMITS AND AUTO-IGNITION

The limits of ignition are drawn as loops in a way that inside them, ignition is always guaranteed for a particular type of engine. However, ignition is not impossible below the lean limit or above the rich limit. In general, the ignition limits and their use in combustion represent a conservative approach on the problem of ignition according to which, when within them, the auto-ignition of a combustion reaction is guaranteed.

4.6.5 SEMENOV'S THERMAL IGNITION THEORY

Semenov's theory employs the approximation that the reactants are at same constant temperature T' higher than the outside ambient temperature T_a . The heat production and heat loss terms can therefore be calculated:

Heat Production term:

$$\Phi_+ = \rho Q C A e^{-\frac{E_A}{RT}} \quad [W] \quad (4.9)$$

Heat Loss term:

$$\Phi_- = \frac{hS}{V} (T' - T_a) \quad [W] \quad (4.10)$$

There are three possible routes that the reaction will follow according to the famous plot in Figure 4.3 produced by Semenov[56].

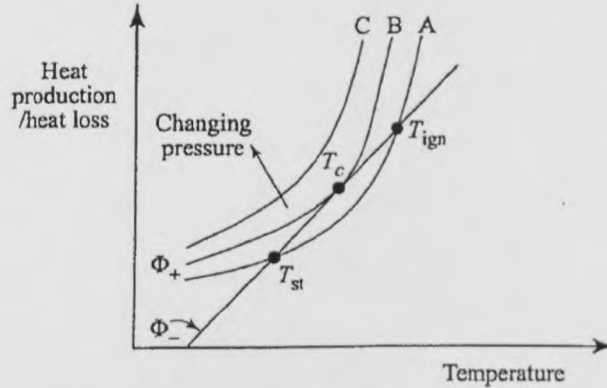


Figure 4.3: Curves of heat production and heat loss terms of a reaction against temperature [56]

The first route is the heat loss term to be greater than the heat production term (curve A). Then the reactants will heat up until a stable temperature T_{st} is reached where no further self-heat is released. If the reaction is heated externally until a temperature T_{ign} is reached then instability is induced and the

thermal runaway takes over. If the temperature of the reactants is greater than T_{st} but smaller than the ignition temperature T_{ign} then if the reaction is left to itself, the temperature will decrease back to T_{st} .

The second route is the heat loss and heat production terms to be balanced (curve B). In such a case there will be a critical temperature that the reaction will heat up to, above which rapid acceleration in temperature is bound to take place. At that critical temperature $T_c = T_{st} = T_{ign}$. It follows that the critical temperature represents the lower temperature at which the reaction can be initiated by thermal means.

The third route is the heat production term to be greater than the heat loss term (curve C). In this case the reaction will be explosive whatever the temperature of the reactants is.

By equating the heat production (4.9) and heat loss (4.10) terms and solving the second order polynomial equation for the temperature function, the critical temperature T_c can be evaluated. Although the second order polynomial equation has two solutions only one is found to be physically possible. Hence the only physical solution for the critical temperature is expressed by equation (4.11).

$$T_C \approx T_a + \frac{RT_a^2}{E_A} + \dots \quad [K] \quad (4.11)$$

4.6.6 THE IMPORTANCE OF RADICALS IN IGNITION

The introduction of the chain reaction theory evolved the knowledge of ignition. It provided a tool for understanding the initial stages of combustion through chemical sub-reactions; something that was missing before from the complex problem of ignition. According to the chain reaction theory the general reaction mechanism is actually divided into many step-reactions. The radicals are products of previous reactions that are passed into new reactions ahead. The radicals are neutral chemical species that contain an odd number of electrons and thus have a single unpaired electron in one of its orbitals [57]. The radicals are the main driving force for preceding a chain reaction and for increasing the overall rate of the reaction. There are three mechanisms of chain reactions[54]:

- i) Chain initiation reactions: Involve the initiation of radicals from stable species.
- ii) Chain propagating reactions: Involve the same number of radical species on both reactant and product sides such that the radical pool is propagated.
- iii) Chain branching reactions: In these reactions more radicals are produced than consumed. In the chain branched reactions the radicals will increase the overall reaction rate exponentially, causing an abrupt and violent reaction

In combustion, if the key radicals are supplied to the chemical initiation process, of the fuel-oxidation reaction, then it is anticipated that they will aid the ignition of the mixture by increasing the reaction rate and hence, reducing the minimum ignition energy requirement. Radicals typically absorb energy from collision. In combustion, oxidation usually begins with O_2 molecules acquiring sufficient energy to break the C-H bond which is weaker compared to the C-C bond [54]. However, due to the difficulty in envisioning the very first steps of the initiation process the mechanism is not yet fully understood. Research has shown that all the O,H and OH radicals play a key role in promoting the combustion process. Furthermore, the addition of N radicals during combustion has been reported to destroy exhaust NO_x polluting compounds that are formed due to incomplete burning (i.e. lean burning) [58, 59].

4.7 A REVIEW ON GAS TURBINE PLASMA IGNITION

Plasma jet (PJI) igniters are not a new concept. They have been studied extensively from the mid-seventies and onwards. The process by which the plasma promotes flame propagation and stabilization is not yet fully understood. However, it is widely accepted that the charged plasma will include some quantities of free radicals. There are many parameters affecting the plasma igniter performance; some influence the properties of the plasma itself, some the dynamics of the jet, and also others play a significant role in changing the reaction rates of the system (i.e. the choice of plasma medium).

4.7.1 PLASMA FORMATION

The mechanism of plasma formation which occurs in a plasma jet plug is shown in Figure 4.3[60]. The igniter is fired by discharging energy into a small cavity existing between the central electrode and the orifice plate. When the voltage in the capacitor reaches the required level, the high energy is released to the igniter plug [61]. The high energy discharge causes the rapid breakdown of the electrodes. The charged capacitor is discharged into the igniter's cavity by passing a high voltage across the gap in a short space of time [62]. A narrow conducting channel forms inside the cavity which consists of ionized gas at high temperatures. The extremely intense currents of electrons produced by the discharge increase further the temperature ($\sim 5,000K$) and consequently the pressure. The production of the reactive plasma (charged ions) inside the short electrode gap (or cavity), suddenly increases the number of molecules in the region so there is a sharp ejection of mass away from the igniter. As a result, a high velocity jet of hot plasma is ejected through the orifice [8, 63]. The charged plasma promotes the electrical conductivity of the gas and creates a preferred path through which the ions travel. The electrical currents produce also a transient magnetic field.

Following the sudden energy release by the spark (electrode breakdown), a shockwave is created and separates from the plasma boundary, moving outward with a velocity greater than the spread of plasma.

Past work indicates the characteristics of FDI and Plasma igniters [19, 64]. The arc discharge appears to heat only a relatively small fraction of the gas to very high temperatures. This results in the formation of small hot pockets of highly active species/radicals [58, 64, 65]. Moreover the pressure increase inside the cavity due to the discontinuity created by the 'electrode breakdown' should ensure that the radical 'soup' will reach the combustible mixture. A turbulent boundary layer is formed between the hot gases and the surroundings due to the dissipation of energy of the high speed plasma as it travels through the cold gases. When the hot gases move away from the tip there is less conductive heat loss to the solid surface of the igniter [41]. Hence ignition should ideally be initiated away from the chamber walls in order to reduce the quenching of the reaction by the cold walls [66].

The dimensions of the cavity play an important role in producing a longer plasma plum [62]. Considerable efforts have gone into determining the optimum relation between cavity dimensions and length of plasma plum (plasma jet) [8, 9, 46, 67].

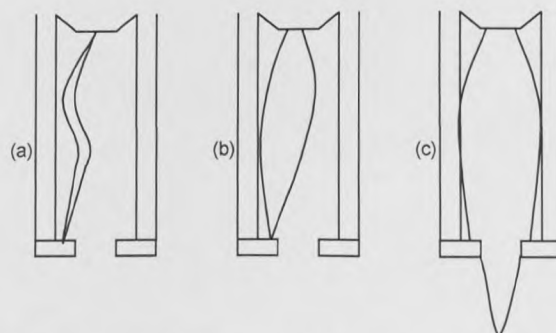


Figure 4.3: Plasma Jet Formation. From left to right: (a) High voltage, low current discharge. (b) Heating up of gases in the cavity by high current discharge. (c) Hot gases expansion through the orifice (plum) [60]

4.7.2 PLASMA MOTION

The motion of the plasma, as one would expect, is outwards in the axes of the centre electrode. The high velocities (of the hot plasma ejections) realized by the plasma jet play a significant role in improving ignition. By achieving high velocities, the hot plasma is more successful in penetrating into a zone inside a combustion system where the mixture of the fuel and air is suitable to initiate combustion. These zones are the more quiescent regions towards the centre of the recirculation pattern, in the primary region of the liner. There are three parameters that influence the plasma motion (described in Sections 4.7.3-4.7.5).

4.7.3 PLASMA MOTION AND ELECTROMAGNETIC FORCES

Pioneering research at Leeds University [41] demonstrated that the spark kernel itself is not related to any motion. By placing two electrodes in line with each other the researchers created sparks that initiated and extinguished, at the centre between the two electrodes, with no apparent effect to the movement of the kernel. Furthermore they noted that by placing the electrodes in parallel to each other the plasma moved away from the electrodes in the outward direction. This motion was the result of magnetic field forces induced by the current flowing along the electrodes. This observation led to the conclusion that the bodily movement of the kernel can be affected by electromagnetic forces. It also suggested that there exists a theoretical influence of the mean spark current upon kernel displacement. Moreover experiments with a solenoid field showed that the electromagnetic forces created are more effective in opposing

than accelerating the motion of the kernel. Nevertheless the addition of the solenoid, when this force is reinforcing the motion revealed -although not significant- improved travelling distances for the plasma [41, 67]. The application of an external magnetic field has been used by newer studies to achieve rapid mixing of gasses fed into the cavity of the plasma jet igniter [53, 68].

It should be made clear that the force arising from such a magnetic induction, created by the current flowing along parallel electrodes, is not the main driving force of the motion of the plasma produced by a common PJI. Furthermore Fitzgerald and Breshears [53] in a patent application proposed a plasma igniter device where electromagnetic forces will be the main driving force of the outward plasma motion. Even though the study in reference [41] investigates the influence of this magnetic force to the kernel, other parameters like the fluid dynamics of the jet and the pressure increase inside the cavity, where the formation of the plasma takes place, were not taken into account [9].

4.7.4 PRESSURE FORCES

FLUID DYNAMICS OF PLASMA MOTION

The dominant force responsible for the outward ejection of plasma is the pressure arising by the extreme increase in temperature at the time the electrodes breakdown. The gases initially within the cavity expand instantly by the high-energy release of the igniter. Moreover the discontinuity, created by the

instantaneous addition of energy to the gases, causes a shock wave to initiate around it. The shock wave and the plasma itself are restricted by the cavity walls which force them to expand towards the only route that is available, the igniter orifice. In [42] the authors state that even for an igniter designed to optimize the magnetic forces required for improved ejection throw ratios (Fitzgerald igniter [53]), the main outward driving force of the plasma motion is the pressure within the cavity. Only a very small portion, of the percentage of the total stored electrical energy directed as kinetic energy of the jet, is due to electromagnetic induction.

ORIFICE DIAMETER

One of the main parameters influencing the speed and displacement of the plasma is the orifice diameter. Decreasing the diameter results in increasing the velocity and hence the distance travelled by the kernel. Thus, it is a convenient parameter for controlling the movement of the kernel and for reaching different specified conditions for flame initiation. However, there is a limitation to choosing the nozzle diameter. Designers should avoid choosing a sonic nozzle because of the large heat losses at the nozzle throat [69]. The choice of orifice size is dictated by the fuel, the spray atomisation (FSQ), the fuel to air ratio and the plasma medium fed into the igniter cavity.

STATIC PRESSURE

Moreover the static pressure at the point where the igniter is positioned, inside a dynamic combustion system, plays an important role to the motion of the plasma. It should be noted that the pressure inside the throat of the igniter, before an ejection occurs, is the same as the static pressure of the main flow [69]. Increasing the static pressure of the combustion chamber has a counterproductive effect to the distance travelled by the plasma, as one would expect. The high pressure restricts the propagation of the hot gases, which results in the plasma appearing more uniform [70]. Along with the restriction in the velocity and the motion of the plasma, an increased static pressure will cause an increase in the curvature of the flame front. Hence, the plasma will be less penetrating to the surrounding flowing mixture, and will require higher minimum energies for a successful ignition [60, 67, 70].

COMBUSTOR FLUID DYNAMICS AND TRAJECTORY OF PLASMA

As the hot kernel leaves the igniter end, it is ejected into a very dynamic system which is important in mixing the sprayed fuel with air. This passage through the high-velocity boundary layers, formed inside a practical combustor, modifies the initial trajectory of the plasma by the fluid motion. High speed pictures of the plasma movement inside a combustor show the horizontal movement away from the plasma jet igniter [42, 69].

4.7.5 PLASMA MOTION AND GRAVITATIONAL FORCES

Gravitational forces also appear to affect the trajectory of the plasma. The high-speed pictures reveal that injected plasma which travels at some distance without instantly initiating ignition flows towards and along the bottom of the chamber [69]. The downward component of force though is not as significant, in influencing the plasma motion, as the parameters discussed above.

4.7.6 RADICALS AND RADICAL AUGMENTATION IN PLASMA IGNITION

It is widely accepted that the improvement in flame initiation and combustion propagation is also attributed to the existence of free radicals; specifically O, H, N and OH [19]. These radicals are generated in the plasma by the discharge, which both heats the medium and dissociates its molecules.

Radicals appear to contribute to the promotion of combustion through the acceleration of the initial stage of oxidation [69]. It is widely accepted, that the supply of radicals through the creation of some reactive plasmas contributes in the ignition process. Any conceivable model in the chemistry of the ignition process relies heavily on the existence of certain radical species as well as their energy [71]. The importance of the first steps in the chain reaction and of the involvement of free radicals is well acknowledged [3, 54].

Radicals involved in the ignition process of a plasma jet igniter (PJI) are said to promote reactions and to enlarge the combustion region [72]. An increase in the reaction rate can be achieved and maintained during flame propagation in normally non flammable mixtures [43, 65, 69, 73]. Flame stabilisation and combustion [72] is also augmented by the production of radicals in the mixing zone and by the heat and mass transfer from plasmas [69].

4.7.7 PLASMA MEDIUM

It has been observed by many researchers that by feeding different media to the plasma jet igniter, the ignition characteristics change. Furthermore a different handling approach should be considered between gas and liquid feeds. The introduction of liquid into the bleed cavity will seal or partially seal the otherwise open gap through which the medium is introduced into the igniter cavity and therefore improves the characteristics of ignition.

4.7.8 PAST RESEARCH ON PLASMA MEDIUMS

Experiments with feeding oxygen [64, 72, 74-76], hydrogen [65, 71, 76-78], nitrogen [58, 59, 65, 69, 71] and hydrocarbon gases [76, 78] to the cavity of the igniter have shown that they change the ignition performance of a fuel. It was concluded that the supply of their associated radicals (i.e. the plasma medium) is crucial. Some media enhance combustion whilst others (i.e. argon [43, 72]) do not affect the ignition characteristics of the engine [71, 72, 74, 77]. All studies agree that the free radicals O, HO and H, produced by the plasma, play an important role in ignition.

It was demonstrated over various comparison studies [65, 69, 71] that the hydrogen plasma is much more effective than the nitrogen for improved ignition. This can be explained by the higher thermal conductivity of hydrogen when compared with nitrogen. Hence, the heat losses experienced in the igniter are higher for the nitrogen and the lifetime of the hydrogen is shorter [69]. In fact, the best choice in media should be determined by the extent of mixing in the system. If the fuel/air in the chamber is not well mixed then the large diffusion coefficient of the hydrogen should confer an advantage that will overcompensate for those of the nitrogen atoms [65].

Furthermore, it is suggested in references [65, 79] that the hydrogen radicals play a major role in augmentation of the ignition-combustion process and that relevant plasma mediums improve burn rates in accordance with their atomic hydrogen content. Although this suggestion has some basis through experimental findings, the full relationship between ignition augmentation and fed plasma medium is yet to be fully understood.

On hydrocarbon fed plasma mediums, it is interesting to note that previous research has gone into the possibility of a locally stratified mixture which is chemically different from one layer of fuel-air mixture to the other [80]. This possibility implies that the injection of a hydrocarbon medium into the igniter cavity changes the mixture strength locally, decreasing therefore the minimum spark energy requirement for ignition. However, the conclusion in reference [80] was that ignition was enhanced at low plasma medium injection rates and when

the fed plasma did not over-flood the cavity of the igniter. The implication of their conclusion is that the igniter performance is optimum at low plasma injection rates. Therefore local stratification of the mixture is not the main cause of the ignition improvement because the hydrocarbon medium does not escape the cavity prior to the creation of the plasma. Hence, the creation of some relevant to the medium free radicals is more important.

In another study [74] water was used as a plasma medium. It was shown that the water does not produce the desired effect in promoting combustion and this was attributed to the high energy spend in the formation of water vapour. Experiments with water plasma additive were also conducted during this thesis work. The results are shown in Section 8.3.

It is interesting to note that most of the past work presented here, has not focused on the flow rate that the medium is supplied to the cavity of the igniter. A parameter that the author believes is crucial for comparing between researches. All previous studies do not show a relationship between this parameter and the ignition performance. The author suggests that the free radicals that augment ignition are produced in concentrations that are associated with both the kind of the plasma medium and the amount that this medium is fed to the igniter.

4.7.9 REVIEW ON PLASMA IGNITION PERFORMANCE

The performance of the plasma jet igniter is judged by its ability to ignite a combustible mixture depending on the minimum total energy spent. Moreover the minimum ignition energy is set as the minimum electrical energy needed to ignite such a mixture, with the electrodes set to the optimum value. The minimum ignition energy is therefore the energy delivered by the plasma to the fuel/air mixture at the point where combustion initiation is most feasible. Clearly the minimum ignition energy decreases rapidly with an increase in air temperature or an increase in fuel to air ratio towards the stoichiometric [60]. Due to the energy losses involved in an igniter system, the minimum ignition energy accounts just as a percentage of the total energy supplied to the igniter. Hence the question arises of how the manner in which ignition energy is delivered affects the minimum ignition energy (i.e. less losses → lower MIE).

It appears that when the injected plasma flows along the bottom plate, inside a combustion chamber, some of its energy is lost in vain [69]. Some degradation of the high temperature thermal energy happens due to the drag forces, characterised by the generation of turbulence at the kernel boundary [41]. Also a reduction in pressure is going to increase the amount of spark energy required for effective ignition [60] (see also Sections 4.5.1-4.5.2).

Another important point is that although the temperatures in the spark channel are well above the needed to initiate local ignition, it is the dynamics of the propagating flame front that dictate the minimum energy required for complete

ignition [70]. The minimum energy requirement is limited by flame propagation criteria at the stage when the curvature of the flame kernel is so great that the flame front is unable to propagate without additional energy [67]. It should be reminded that combustion can be also sustained by the continuous supply of (ignition) energy to the chemical reaction. This method requires a type of continuous ignition system and has obvious implications in aiding the combustion process [67].

4.7.10 THERMAL EFFICIENCY $\frac{E_{th}}{E_s}$ – THERMAL TO STORED ENERGY

The above observations impose the need to link ignition circuit and igniter design with the fluid dynamics of the combustion process. Some energy is bound to be lost to the external circuit [42]. It is characteristic that approximately 90% of the total energy supplied to the PJ igniter ends up as heat in the igniter body or is lost to the surroundings. Only 10% of the stored energy is released in the plasma upon firing the igniter [2, 8, 9, 47, 48]. Energy conversion efficiency depends mainly on igniter design [42]. Low conversion efficiency is a result of energy losses in the viscous boundary layer within the cavity, heat transfer to the cold igniter and perhaps to the surrounding gas [42]. Stored capacitive energy should be mostly shared between the circuit and plasma resistances in proportion to their magnitudes [62] but in practice the hot gas within the cavity has to work to expand out into the combustor and it is bound to lose heat to the cavity walls [62]. A linear relationship exists between thermal efficiency ($\frac{E_{th}}{E_s}$ – thermal to stored energy) and igniter resistance (Figure 4.4 [62]). The resistive

losses of the gas in the cavity are directly proportional to the ceramic length of the inner electrode [62].

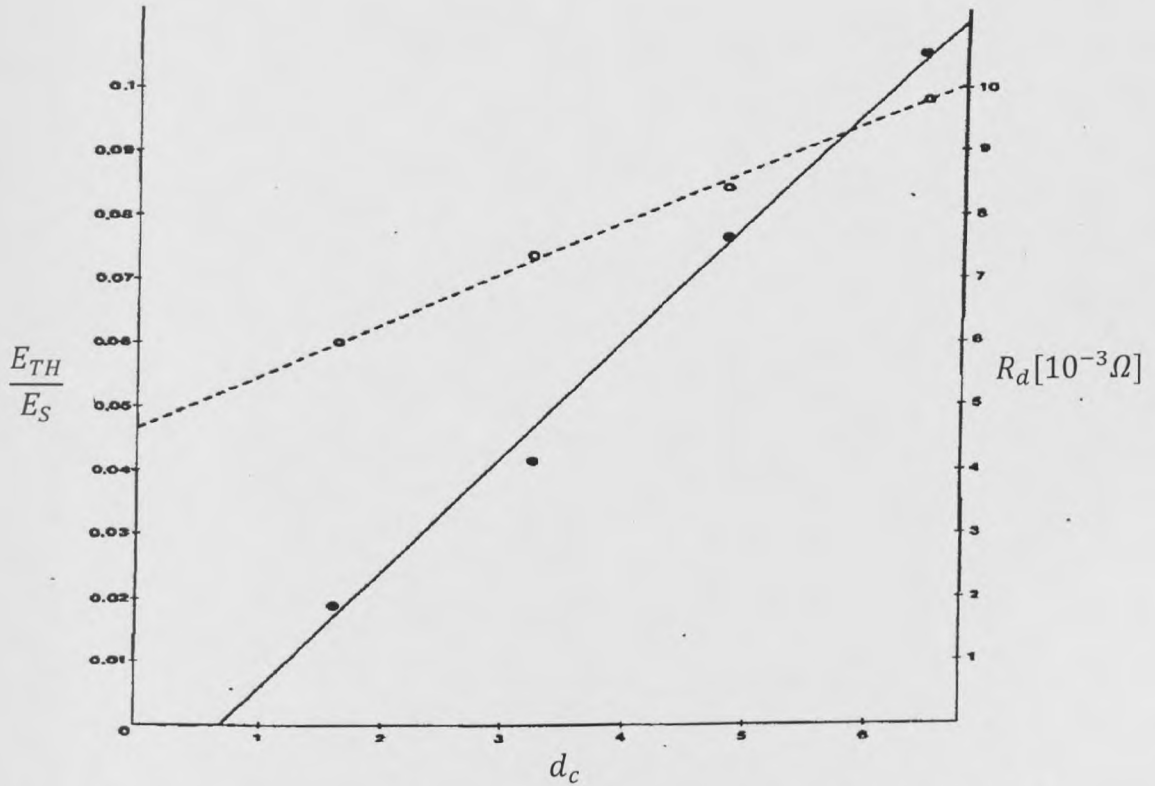


Figure 4.4: Ratio of Thermal to Stored Energy (solid line) and igniter resistance (broken line) vs. arc length [62]

4.7.11 THE ROLE OF STORED CAPACITOR VOLTAGE TO THE EFFICIENCY AND LIFE OF THE IGNITER

In most ignition circuits the voltage of the stored capacitor is generally less than 1kV and the stored energy lies in the range of 1-12J depending on the system requirements [61, 62]. Ignition performance decreases substantially at stored energies below 1J, but on the other hand no significant improvement in efficiency can be produced above 4J [64]. In another study [45], it was observed that ignition efficiency dropped significantly with increasing voltage and that igniter lifetime was improved. There is a strong relationship between total charge flow and electrode erosion. In reference [42] the authors conclude that

lower plug erosion is experienced when using high storage voltages and that lifetime and efficiency have opposing voltage requirements. As the authors state the only reason for increasing the storage voltage is that the lifetime of the plug appears to be a more limiting factor in the application of these igniters [42]. On the other hand high-voltage circuits are more complex, expensive and less reliable than low-voltage ones.

CHAPTER 5- IGNITION EXPERIMENTS IN THE STIRRED FAN REACTOR RIG

5.1 EXPERIMENTS IN THE LEEDS MECHANICAL ENGINEERING STIRRED FAN REACTOR RIG

Initial experiments were done in the Leeds stirred fan reactor rig under atmospheric pressures. The experiments were designed to give a better understanding of the operation of the focus discharge igniter and to initially test the behaviour of the igniter when adding liquid hydrogen peroxide. The placement of the hydrogen peroxide was also varied in order to test this effect. The liquid H_2O_2 was placed at the igniter before the start of each experiment using a syringe with a needle.

This rig is commonly known in combustion techniques as a 'bomb' [81] and is widely used in ignition experiments because of the low running costs involved. The 'bomb' used was a cylindrical vessel with two viewing windows opposite to each other. The liquid fuel (in this case isooctane) can be injected into the vessel through a syringe connected to a valve. There are four fans inside the 'bomb' placed diagonally, two at the top and two at the bottom, to stir the fuel mixture and to create turbulence if required.

A simple Schlieren technique was used alongside a high speed video camera to visualise the ignition process and to capture the creation and travelling of the kernel. The video data were then post-processed using imaging techniques and a Fortran 77 program [82] that counted black and white pixels in an image. The

post-processing gave some insight into the kernel diameter growth and the rate of the reaction in time.

As hydrogen peroxide is toxic, health and safety issues were raised in handling it in a confined laboratory space. These concerns made the experimental techniques used much more complicated than common ignition experiments. During the experiments, the laboratory had to be evacuated and only two persons were allowed to operate the rig by wearing respiration masks and protective gear. The second person helped to ensure that all safety procedures were followed. The experiments undertaken were crucial in familiarising with the handling of the H_2O_2 and were proven to be helpful, although the experiments were time consuming because of the safety concerns.

5.1.1 OBJECTIVES

The objectives of the Leeds 'bomb' experiments are summarised below:

1. To illustrate successful and repeatable ignitions when adding hydrogen peroxide to the cavity of a focus discharge igniter.
2. To test the hypothesis that hydrogen peroxide will augment combustion.
3. To familiarize with the handling and safety issues of hydrogen peroxide.

4. To gain some expertise through these experiments in preparation of new and more complicated ones.

5.1.2 EXPERIMENTAL APPARATUS

The hardware equipment used is as follows. The stirred fan reactor rig (Figure 5.1) is described in detail by another work in reference [83]. The same rig was also used in ignition experiments with various focus discharge igniters in a, relevant to this thesis, study made by C. Wilson [2]. The focus discharge igniter used here, is shown in Figure 5.2 and is the same igniter plug used throughout the research (see also Section 7.2 and Appendix A (before modifications) for more information on the FDI). No modifications were made to the igniter at the start of the particular study but a wire was fitted at a later stage. The wire was rounded at its end and was used to hold a droplet of H_2O_2 above the igniter. The power source used to drive the igniter was the same as in C. Wilson's study [2]. The power unit fired only one discharge per ignition. A solution of liquid hydrogen peroxide at 60% by mass composition was used throughout these experiments. The total used H_2O_2 quantity was a little bit above 50ml by the end of the experiments. Water was also tested as an additive for comparison reasons. A Solarc 600W light beam was used as the light source for the Schlieren imaging together with optical lenses that manipulated this light, as shown in Figure 5.3. A Photron Ultima APX high speed camera completed the Schlieren set-up.

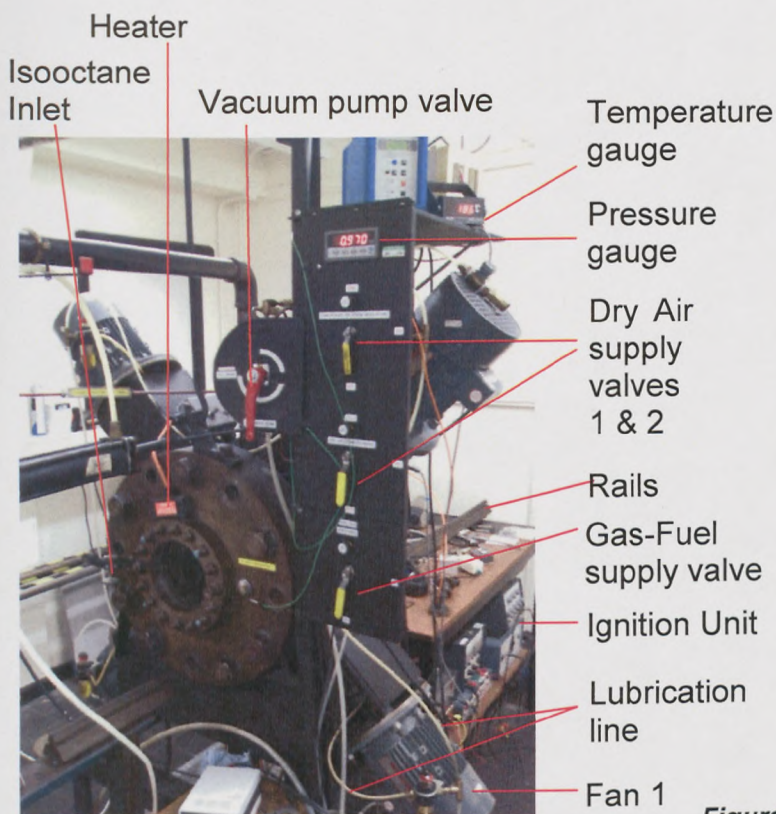


Figure 5.1: The University of Leeds' Mechanical Engineering 'Bomb' facility.



Figure 5.2: The focus discharge igniter installed inside the 'bomb'. Parts of the two bottom fans are also visible.

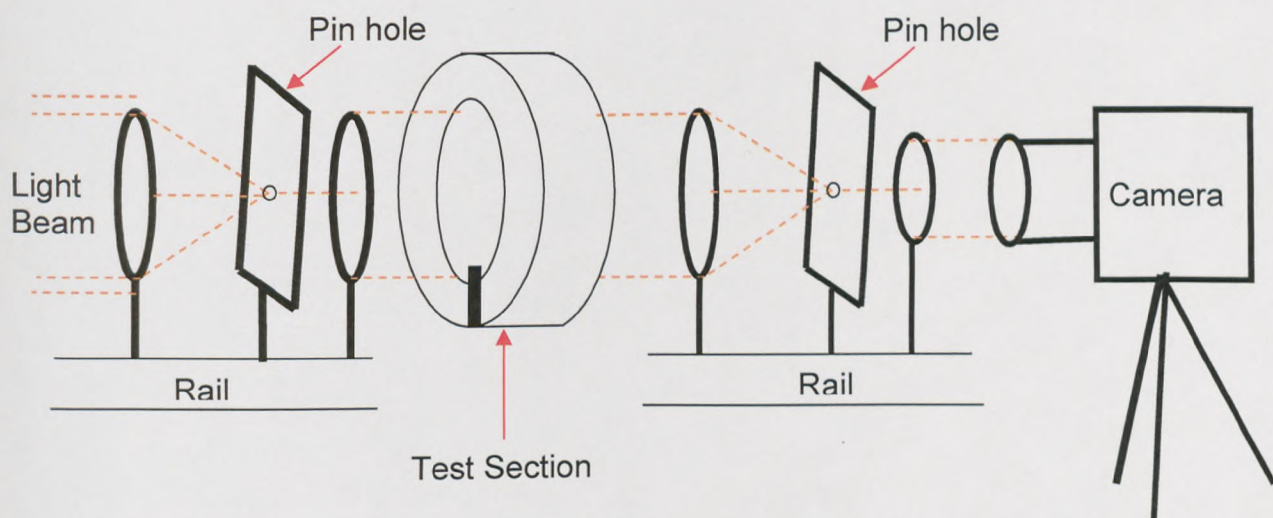


Figure 5.3: The Schlieren set-up used in the 'bomb' experiments

5.1.3 FUEL PROPERTIES

The fuel that was deployed in the 'bomb' experiments was isooctane. The oxidizer used throughout this initial study was dry air. The fuel properties are summarized in Table 5.1.

Name	Isooctane (liq.)
Chemical Formula	C_8H_{18}
%vol stoichiometric air	1.08
Molecular Weight ($\frac{g}{mol}$)	114.23
Density ($\frac{kg}{m^3}$)	688
Melting point (K)	166
Boiling point (K)	372
Flash point(K)	277.88
Auto-ignition temperature (K)	690.4
Heat of combustion ($\frac{MJ}{kg}$)	94.836

Table 5.1: Fuel properties for Isooctane.

5.1.4 EXPERIMENTAL PROCEDURES

A. MAIN OPERATIONAL PROCEDURE

The following is the main procedure that was followed in all experiments for operating the 'bomb'. The vessel at this point was tightly closed and ready for an ignition experiment. The air compressor was turned on and its associated valve was opened in order to supply lubrication to the fans seals through the lubrication line (this step was done only once a day). After sufficient lubrication, the fans were turned on and were operated at 1500 rpm. The heater module was used manually to bring the vessel to the desired operating temperature, which was about 30°C. After reaching this temperature, the heater was turned-off and the vacuum pump was started together with opening the connected valve to vacuum the vessel. At about 0.02bar the 'bomb' was then isolated by

changing the valve position to closed. After reaching almost vacuum conditions the liquid or gas fuel was introduced into the reaction vessel. The amount of fuel was pre-calculated to the desired equivalence ratio for a total pressure of 1.00bar. After inserting the fuel, dry air was supplied into the vessel until the pressure reached 1.00bar. After ensuring that the fuel and air were well mixed, the fans were turned off. At this point the video recording was initiated together with a 10s count-down which automatically fired the focus discharge igniter. After each ignition attempt the vessel was always vacuumed and then flushed with dry air to ensure that all residues were extracted from the vessel.

B. SAFETY PROCEDURE WHEN HANDLING HYDROGEN PEROXIDE

Safety procedures were always followed when handling the liquid H_2O_2 . The hydrogen peroxide was placed inside a larger open-top container to contain any spills when pumping a small amount of H_2O_2 through the syringe. A large container with water was positioned near the area where hydrogen peroxide was handled so as to quickly flash any accidental spills. Only the operator and one observer were allowed to be present in the facility when conducting the experiments. A no-entrance sign was indicated at the laboratory door. Disposable respiration masks and protective clothing were worn at all times by both personnel when experimenting with hydrogen peroxide. The respiration masks were worn mainly because there was insufficient circulation of outside air; to prevent a toxic accident in the case that traces of hydrogen peroxide vapour resided in the experimental environment. A 60% by mass hydrogen peroxide solution is considered highly toxic. Thick protective gear was a

preventative measure in the case of spillage whilst handling the hydrogen peroxide.

C. PROCEDURE FOR PLACING THE HYDROGEN PEROXIDE TO THE FDI IGNITER

The procedure below was followed in all experiments that were done with H_2O_2 . Before any handling, the operator should ensure that the fans were not operating. After opening the reaction vessel and whilst following all safety procedures (procedure B) a droplet of hydrogen peroxide was placed at the focus discharge igniter by gently squeezing the syringe that contained the solution. After successfully placing the H_2O_2 droplet at the required location, the reaction vessel was firmly closed. If the droplet was not placed at the correct position or the cavity of the igniter was over-saturated with H_2O_2 , then the igniter was dried by heating-up the reaction vessel and the same procedure C was followed from the beginning. After the successful placement of the H_2O_2 the fans were turned-on to 1500rpm. After this point, the procedure was the same as the main procedure A.

5.1.5 H_2O_2 PLACEMENT

When planning the 'bomb' experiments the questions relating to this project were many. The main concern was how to modify the focus discharge igniter and where to place the liquid hydrogen peroxide. The spark initiation of the FDI igniter with H_2O_2 placed inside its cavity was also questionable. For this reason the H_2O_2 was placed in three different positions during the tests: inside the cavity, at the tip and above the igniter at the path of the ignition kernel.

5.1.6 USE OF WIRE FITMENT TO IGNITER

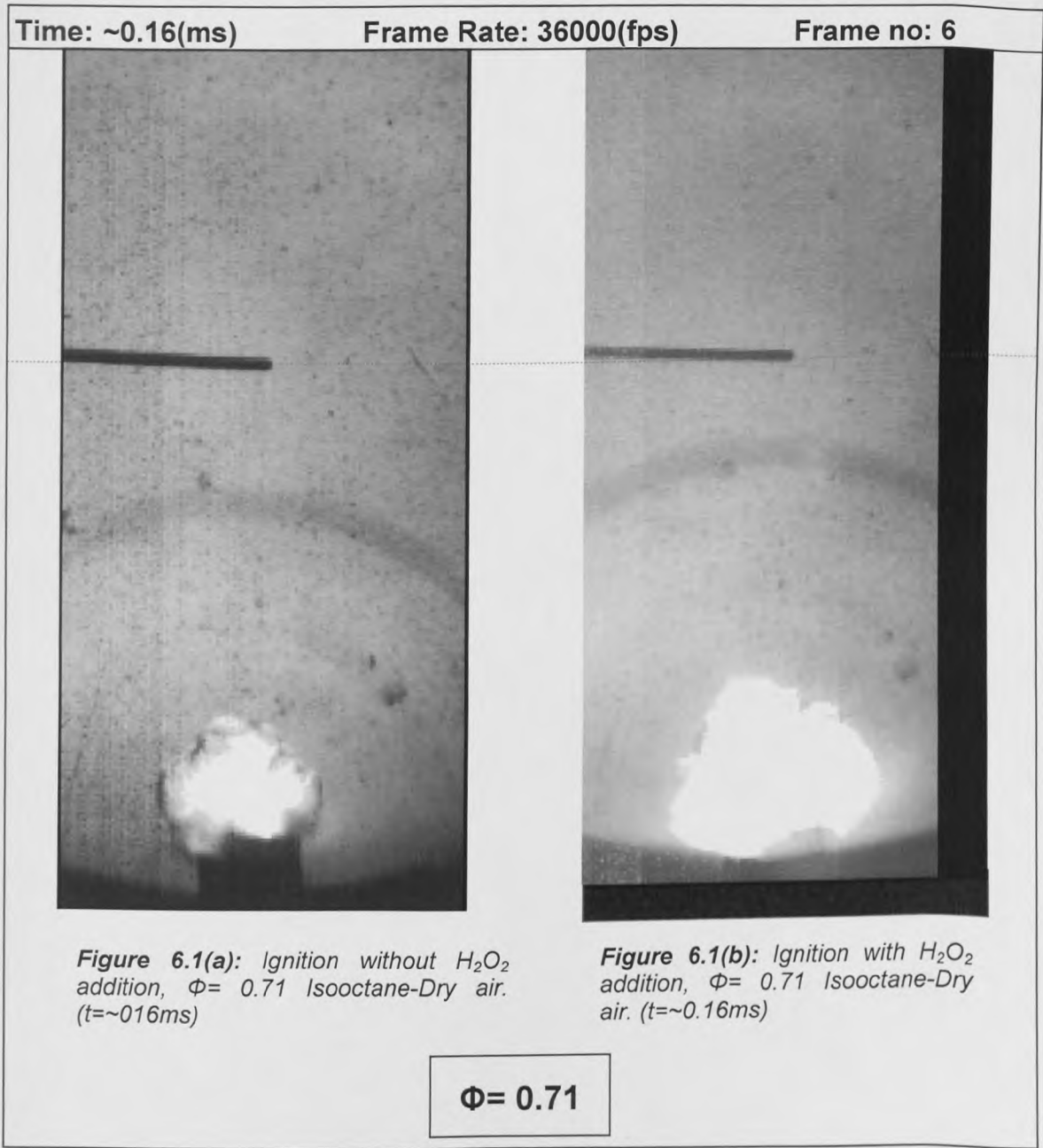
A wire was attached to the focus discharge igniter that was used to hold a H_2O_2 droplet above the FDI. The tip of the wire was made circular (i.e. like the common bubble toys). The diameter of the circular end was almost equal to half the diameter of the cavity of the igniter. The circular end was positioned horizontally to the tip of the igniter at a height of about 1mm.

The reason for fitting this droplet holder directly into the path of the travelling hot kernel was to test the ability of the igniter to dissociate the H_2O_2 . Of course the wire was expected to interfere with the ignition kernel as it was into its path but experiments with the wire were done for both cases; with and without H_2O_2 . This way the study compared only the effect of the hydrogen peroxide and eliminated the wire parameter with its associated losses in ignition energy.

6.1 CHAPTER OUTLINE

Chapter 6 presents the results acquired from the 'bomb' experiments. Figures 6.1-6.4, show still images of the propagating ignition front with and without the addition of H_2O_2 . The equivalence ratios of the isooctane and dry air mixture that are shown in the images are $\phi=0.71$ and 0.65. Figure 6.1 shows the growing reactive material at an early stage (at $t=0.16ms$), before the plasma escapes the igniter. Figures 6.5 and 6.6 are graphical representations of the increasing flame radius of the fuel-air mixture, with and without the H_2O_2 additive, from the time of ignition, at $\phi=0.8$ and 0.65 respectively. Figures 6.7 and 6.8 are plots of the flame speed of the same mixtures that correspond to Figures 6.5 and 6.6. The FDI igniter was also fired without any fuel inside the test rig at a pressure of 1 atmosphere of dry air. Figure 6.9 displays the kernel growth radius of the plasma igniter from ignition with no fuel, with and without the addition of H_2O_2 and also with and without the wire fitment.

6.2 HIGH SPEED IMAGES OF THE PROPAGATING IGNITION FRONT



Time: ~6(ms)

Frame Rate: 15000(fps)

Frame no: 100

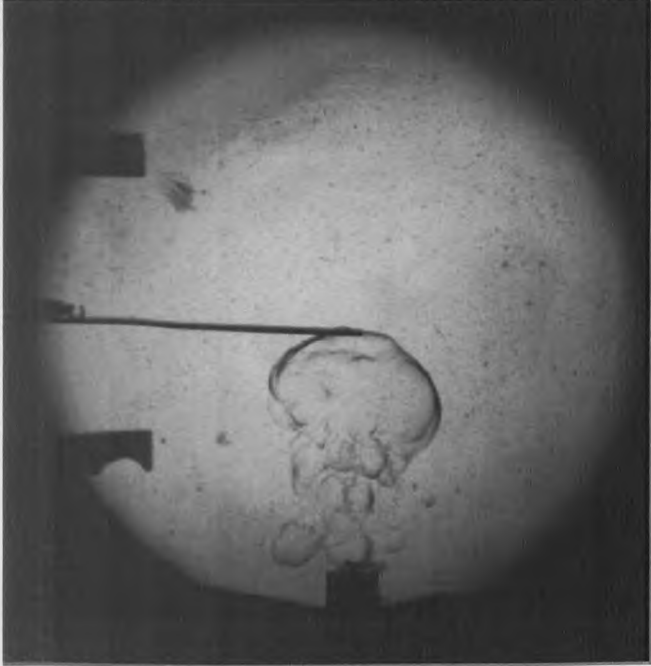


Figure 6.2(a): Ignition without H_2O_2 addition, $\Phi = 0.71$ Isooctane-Dry air. ($t \sim 6ms$)

$\Phi = 0.71$

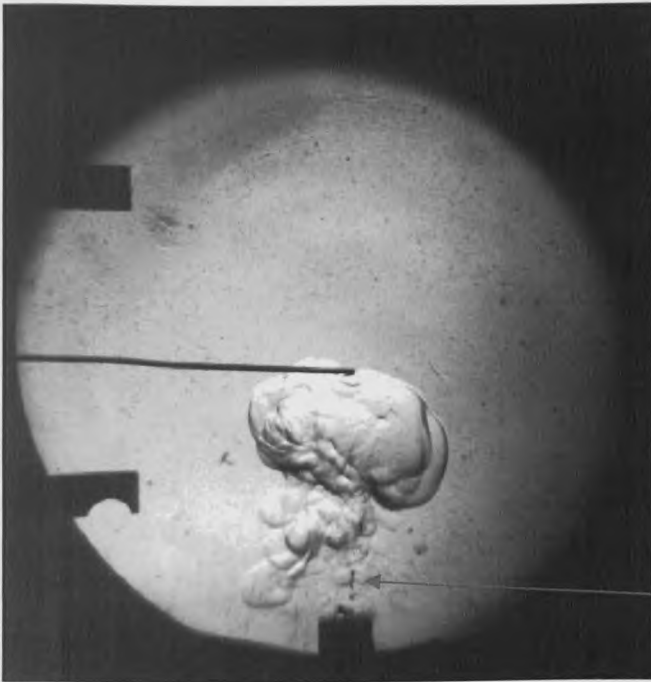


Figure 6.2(b): Ignition with H_2O_2 addition, $\Phi = 0.71$ Isooctane-Dry air. ($t \sim 6ms$)

Figure 6.2(c): Traces of liquid propelled outwards by the plasma motion. After the plasma passes through the liquid these later seen traces do not take part in the ignition process.

Time: ~6(ms)

Frame Rate: 15000(fps)

Frame no: 100

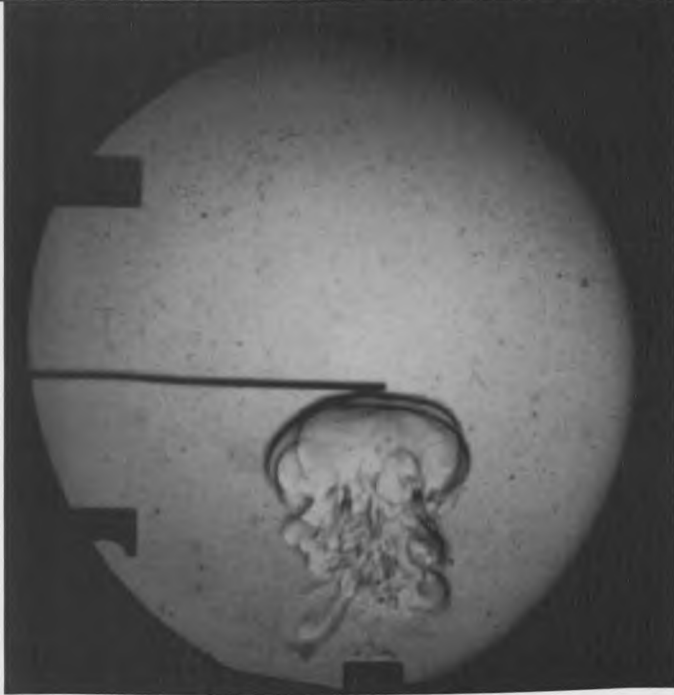


Figure 6.3(a): Ignition without H_2O_2 addition, $\Phi = 0.71$ Isooctane-Dry air. ($t \sim 6ms$)

$\Phi = 0.71$

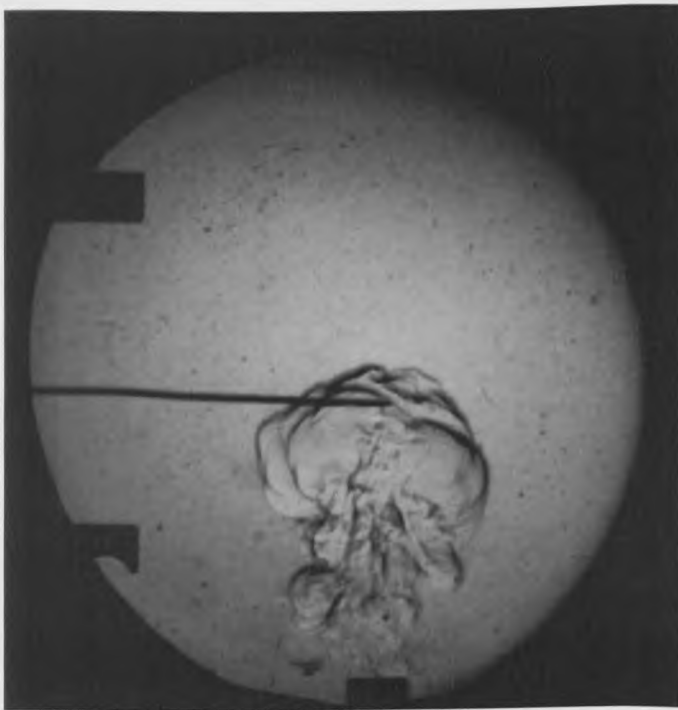


Figure 6.3(b): Ignition with H_2O_2 addition, $\Phi = 0.71$ Isooctane-Dry air. ($t \sim 6ms$)

Time: ~6(ms)

Frame Rate: 15000(fps)

Frame no: 100

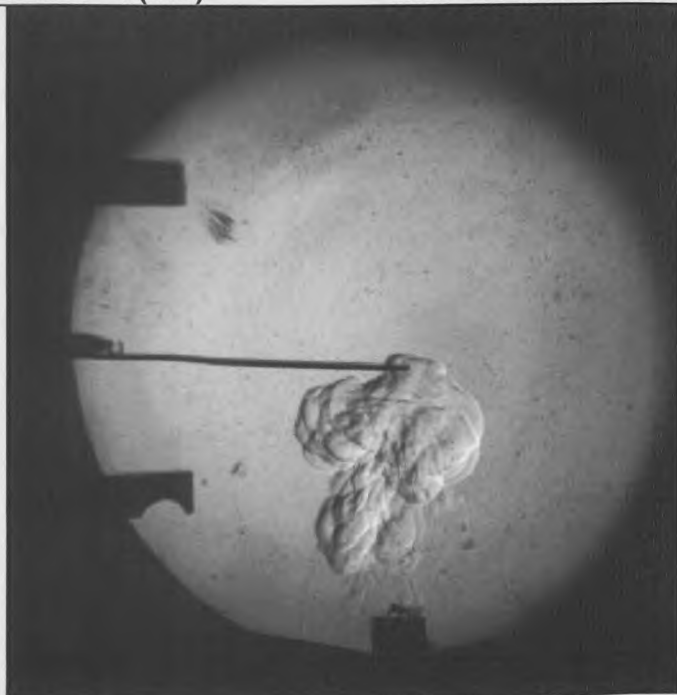


Figure 6.4(a): Ignition without H_2O_2 addition, $\Phi = 0.65$ Isooctane-Dry air. ($t \sim 6ms$)

$\Phi = 0.65$

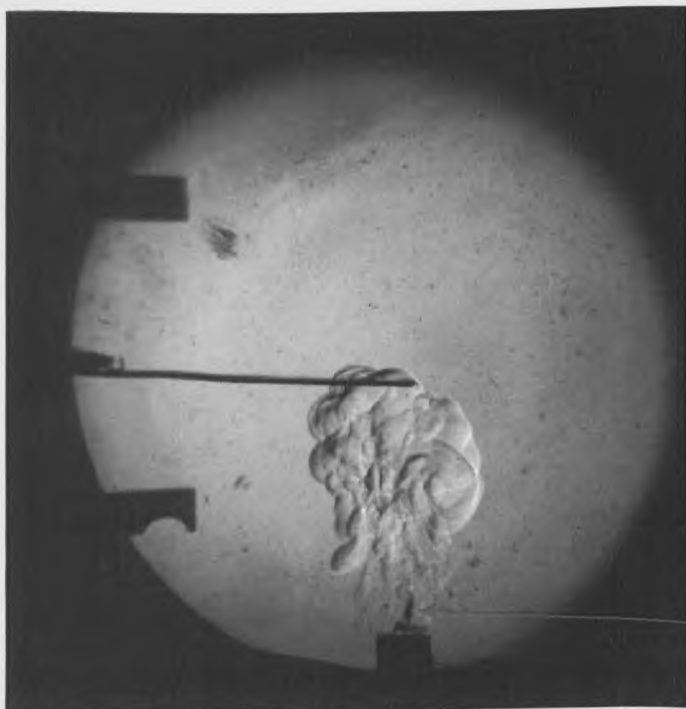


Figure 6.4(b): Ignition with H_2O_2 addition, $\Phi = 0.65$ Isooctane-Dry air. ($t \sim 6ms$)

Figure 6.4(c): Traces of liquid propelled outwards by the plasma motion. After the plasma passes through the liquid these later seen traces do not take part in the ignition process.

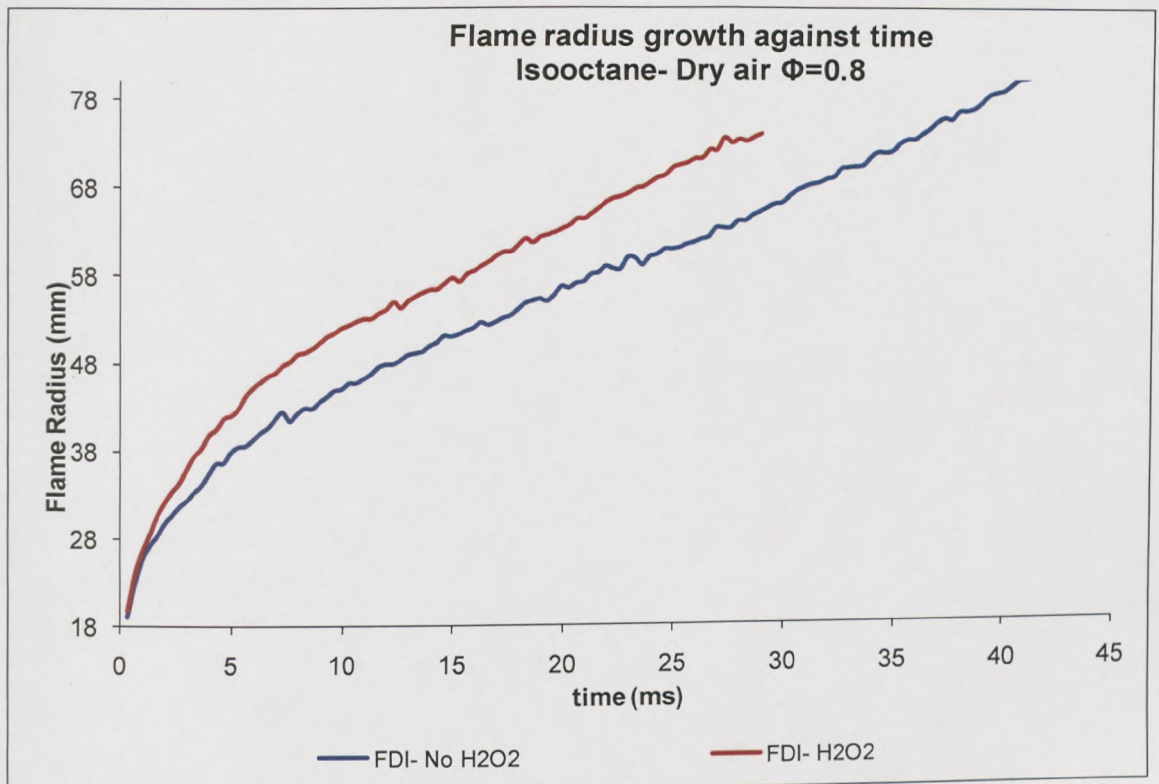


Figure 6.5: Flame radius growth against time, from time of ignition, with and without H_2O_2 . The fuel is Isooctane and the oxidizer is dry air, at a mixture strength of 0.8

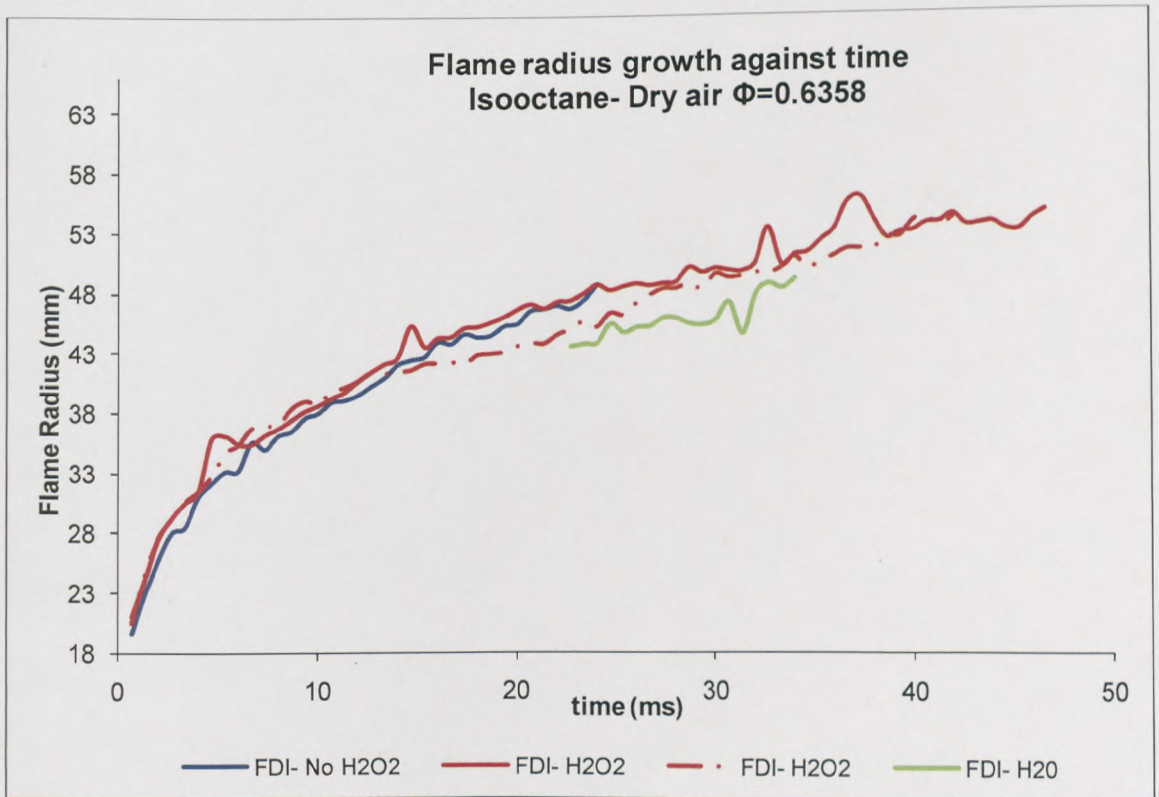


Figure 6.6: Flame radius growth against time, from time of ignition, with and without H_2O_2 and also with water addition. The fuel is Isooctane and the oxidizer is dry air, at a mixture strength of 0.6358

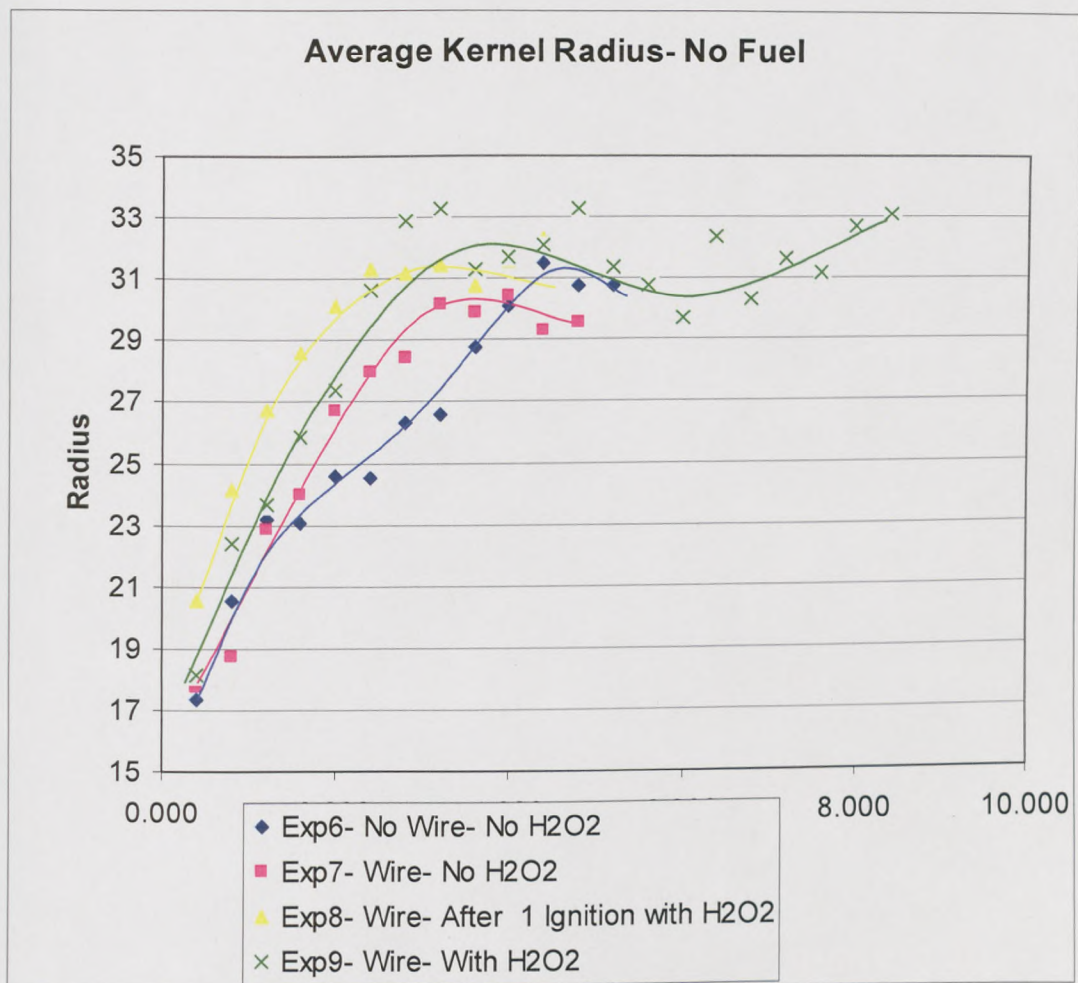


Figure 6.7: Kernel radius growth against time, from time of ignition, with and without H_2O_2 and no fuel. Only dry air was present at the reaction vessel.

CHAPTER 7 – IGNITION EXPERIMENTS IN A ROLLS ROYCE OLYMPUS GAS-TURBINE COMBUSTOR

7.1 EXPERIMENTS IN THE LOW CARBON COMBUSTION CENTRE LABS, SHEFFIELD

Following the initial study in the 'bomb' facility, the project moved towards more realistic situations by experimenting with the new ignition system into a real Olympus combustion chamber. For these gas-turbine ignition experiments, the focus discharge igniter was modified in order to feed the liquid peroxide into the igniter's cavity. After conducting and analysing the 'bomb' results, this modification was a logical step forward. Moreover, the installation of the igniter into a real combustion chamber and the conduction of dynamic experiments necessitated a direct method of feeding the igniter with the liquid hydrogen peroxide. The experiments were done in three sets at different times. The break-up of the experiments in three sets although not entirely on purpose has helped in the optimisation of the experimental techniques and in bringing forward more ideas for each next set, after processing the results of the previous.

7.1.1 EXP. SET-1 - CONTINUOUS STEADY H₂O₂ INJECTION (CSI)

In the first set, the experiments involved firing the modified focus discharge igniter, first without the addition of H₂O₂ to determine the lean ignition limits of the fuel. The fuel used was aviation kerosene Jet A₁ (composition is discussed in Section 3.6.3) and it was provided by Shell. In this set, H₂O₂ was injected continuously into the cavity of the igniter by the use of a medical syringe driver.

The outcome of the first set was encouraging as it showed an enhancement in the ignition efficiency of the focus discharge igniter. The results are discussed in Chapter 9. After the first set showing significant ignition enhancement by the use of the H_2O_2 , the need to measure and control the injected H_2O_2 liquid became more evident.

7.1.2 EXP. SET-2 AND SET-3 - CONTROLLED CONTINUOUS STEADY H_2O_2 INJECTION (CCSI)

In the second experimental set the operation of the medical syringe driver was controlled by the main Labview program that also controlled the engine. The operation of the program is discussed further at Section 7.7. The only difference between the engine control programs for set-1 and set-2 is the addition of a pump control loop for the H_2O_2 injection. The result was the ability to quantify the maximum amount of energy that was added to the ignition system by the dissociation of the H_2O_2 . The program controlled and recorded when the medium was injected into the igniter and also the period of the injection.

In set-3, the experiments involved ignition tests under same conditions as the second set but using a clean fuel atomiser. In the previous two tests the same fuel atomiser was used but tested under normal service conditions and not when clean. Set-3 highlighted the importance of the fuel injection device and most importantly, of the quality of the spray during the ignition procedure and under normal operation. Moreover during these experiments, water was also injected into the cavity of the igniter at a volume rate of $10.8\mu\text{l/s}$. The tests with

the water additive were done in order to demonstrate the difference in the ignition performances that is obtained by the two, similar in chemistry, additives (H_2O and H_2O_2). The Labview program used for this set was the same as in set-2 but this time the fuel injection was also controlled through the computer, by pre-setting the desired fuel flow rate. This change helped to reduce the experimental time and hence the cost, because of the quicker adjustment of the fuel injection rate during the ignition experiments. After the tests with Shell Jet-A1 kerosene, the test fuel was changed to biodiesel. Again, the lean ignition limits of the biodiesel fuel was investigated using the test igniter; with and without the addition of H_2O_2 . The reasons for choosing a biodiesel fuel for testing the proposed ignition device are quite straight forward. Biodiesel is considered more difficult to ignite than other gas-turbine fuels. Because of its renewable characteristics, it is regarded as a good extender to fuel of future.

All tests for each experimental set were conducted on the same day in order to eliminate atmospheric temperature and pressure differences (between cold, hot or more humid) days and also to minimise the cost. The next section describes the changes made to the focus discharge igniter

The focus discharge igniter tested in this study was an experimental device with identification number 1606, made by Smiths Industry. It was used previously by Wilson [2] as a PhD study in Leeds and the current study is a continuation of this research, but into the plasma - radical production area and especially into the enhancement of ignition by using radicals that are created by the addition of the H_2O_2 , at the site of ignition.

In order to modify the igniter it was necessary to acquire the dimensions of the exterior and interior parts. The problem of finding the dimensions of the inner parts was bypassed by cutting lengthwise a similar focus discharge igniter which came to the end of its useful life. The igniter dimensions are shown in Appendix A. Another issue with the igniter's modification was that the igniter plug had to fit into the standard fitment which was used for the surface discharge igniter. The advantage with setting this restriction as a design parameter is that the end result becomes a straight forward ignition solution. The modified ignition plug can be integrated into existing gas-turbine engine designs without the need for other modifications. The thickness of the hypodermic tube was decided according to this restriction.

The main modification was the installation of a thin hypodermic tube which runs along the outer electrode of the igniter and then passes around the tip and into

its cavity. The outer electrode of the igniter, where the hypodermic tube sits, was cut lengthwise by a laser cutter to the desired depth which was less than the thickness of the electrode. Precise cutting was necessary to avoid damaging the outer electrode and thus the igniter. Part 1 and part 2 (Figure 7.1 and CAD drawings in Appendix A) comprise the necessary standard fitment of the igniter into the gas turbine. The fitment is split into two parts because in this way, it allows the user to change the fitment or the hypodermic tube without damaging any of the parts involved. Therefore, whilst part 2 is screwed onto the igniter, part 1 just fits as a collar around the outer electrode of the igniter and sits on part 2. Although in Figure 7.1 (and Appendix A) part 1 and part 2 are shown to be held together by screws, it was later decided to weld the parts together as this action is also reversible and has the same effect. Part 1 was cut lengthwise and along its width to create a C shape in order to manipulate the shape of the hypodermic tube and then to pass it outside the igniter and the gas-turbine; as it is shown in Figure 7.1. The most difficult issue was with the silver braising of the hypodermic tube to the fitment in order to seal its exit. The hypodermic tube passes from a hole at the edge of part 1 and above part 2. The difficulty arises from the fact that the tube is very thin. By silver braising such a thin tube there is the possibility of melting the tube and therefore blocking the inner hole. This problem was overcome by inserting the hypodermic tube inside a piece of tube which had the inner diameter equal to the main tube's outer diameter and then silver braising both of them together into the hole of part 1. The hypodermic tube end was connected by a thick silicon tube to a plastic BD syringe containing the hydrogen peroxide. The syringe was controlled by a Graseby 3100 syringe driver. Section 7.5.1 describes the syringe driver.

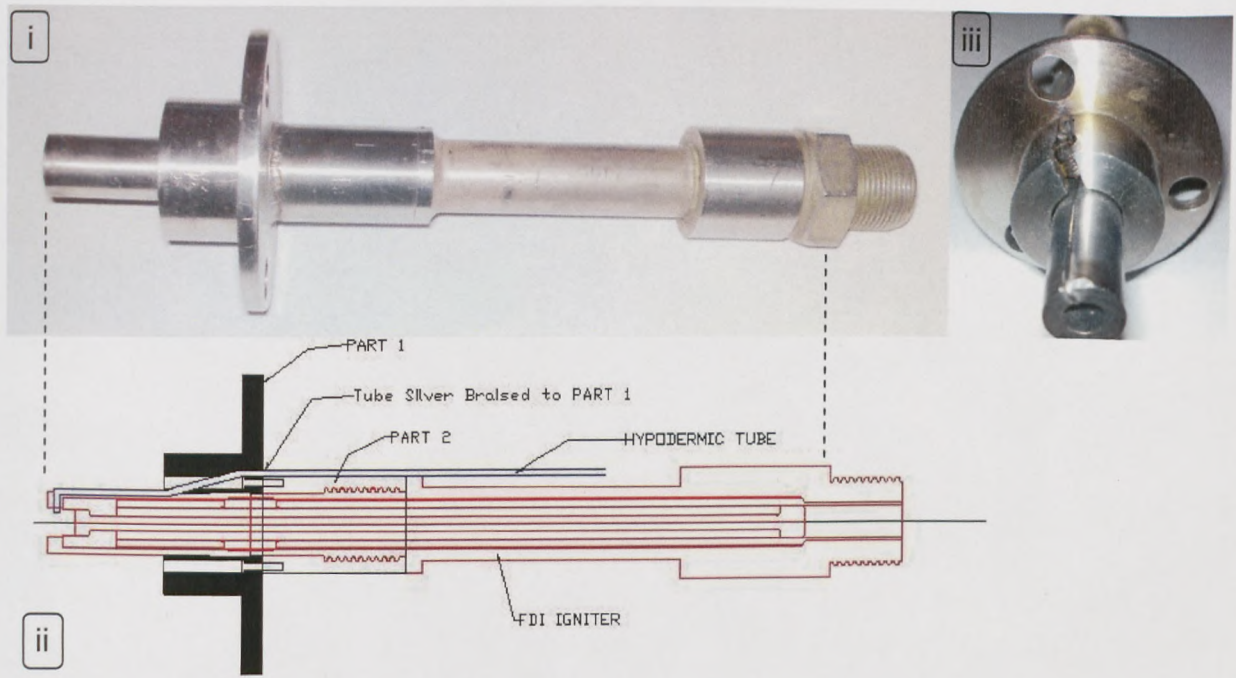


Figure 7.1: The experimental focus discharge igniter and the modifications made. i) Standard FDI igniter before modifications. ii) Drawing of the modifications made to the standard FDI igniter showing the installation of the hypodermic tube. iii) The modified FDI igniter. [65]

7.3 EXPERIMENTAL APPARATUS

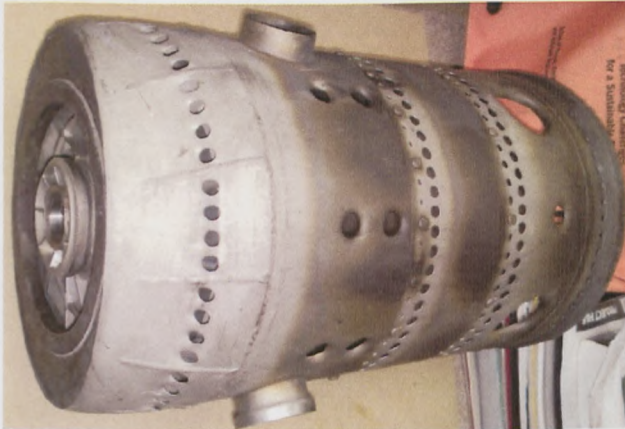
Experiments were made at the Low Carbon Combustion Centre laboratories in Sheffield U.K. The experiments were conducted in a testing facility of an industrial Rolls Royce Olympus liner (Figure 7.2) with kerosene or bio-diesel fuel and air as the oxidizer. Figure 7.1 shows the FDI igniter that was used throughout the experiments.



(a)



(b)



(c)

Figure 7.2: The Rolls-Royce Olympus combustion chamber. a) Front view with air swirlers, b) back and inside view, c) outer view with air holes and flame connectors.

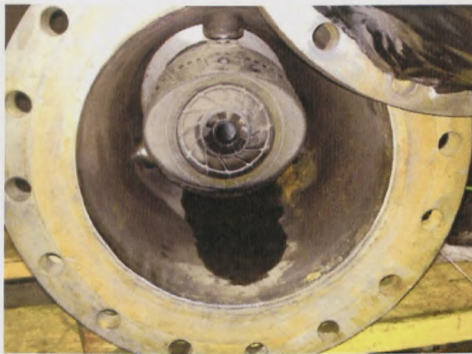


Figure 7.3: a) The cylindrical casing that houses the liner. b) A common Olympus diffuser and the place where the fuel injector mounts.

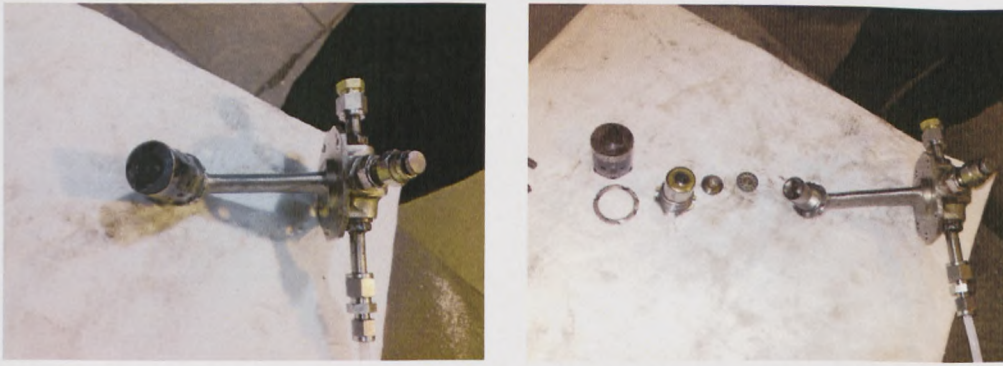


Figure 7.4: a) The fuel atomiser. b) cleaning of the fuel atomiser's parts.

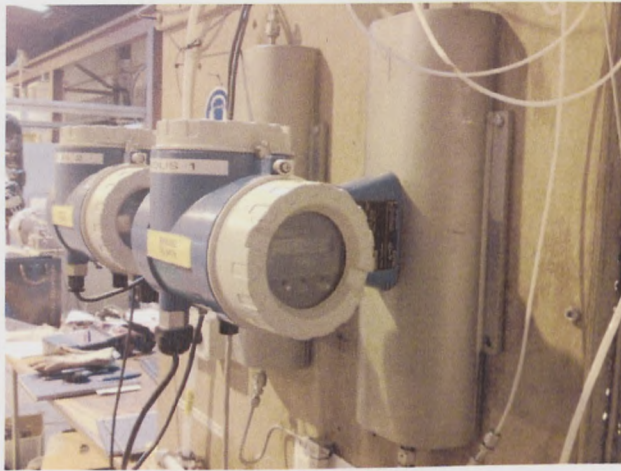


Figure 7.5: The Endress and Hauser promass 60 coriolis used for measuring the fuel flow rate.

The liner was placed inside a cylindrical casing which at the end was connected to a nozzle. At the front, the liner was connected to its standard Olympus diffuser. A high-power compressor was used to deliver the air mass flows needed for the experiments. The compressed air was fed into the test-section through a straight cylindrical pipe of the same diameter as the casing. The pipe was long enough to ensure that turbulence was kept at a minimum. The fuel injector was a standard atomiser mechanism that is commonly used with the Olympus gas turbines. During the experimental sets 1 and 2, the fuel atomiser was not cleaned in order to test the igniter's ability to initiate combustion under poor fuel atomisation. Poorer fuel atomisation is expected as the fuel injector

works under normal service. For experimental set 3, the fuel atomiser was then cleaned. This allowed for a better understanding of the ignition process and enhanced the importance of the experimental results which are in favour of the new ignition system.

Liquid hydrogen peroxide was selected because the radicals that can be created by the presence of the hydrogen peroxide near the zone where the spark initiates are all expected to augment combustion. The liquid hydrogen peroxide is assumed to vaporise after being inserted into the combustion chamber and it is assumed to dissociate whilst passing through the spark ignition zone during ignition.

The concentration of the hydrogen peroxide used throughout these experiments was a 50% by weight solution in water. The rate of injection of the hydrogen peroxide was controlled by a medical syringe driver Graseby 3100. The pump was calibrated prior to the conduction of the experiments. The 25ml syringe that contained the H_2O_2 was connected to the hypodermic tube using a thick silicon pipe. It should be highlighted that the modified igniter was installed to the combustor without any other modifications. The ignition spark was generated by a standard Lodge S26631 ignition unit, which was the original power source of the Olympus testing facility. The position of the igniter was at 90° relative to the horizontal plane.

The air mass flow rate was measured using an orifice plate method to BS EN ISO 5167;2003. The pressure drop across the rig was measured using a ABB 600T series pressure transmitter. The fuel flow was measured using an Endress and Hauser promass 60 coriolis. The exhaust temperature was measured using two K type thermocouples with cold junction compensation where it was connected to Labview. The position of the thermocouples was 20mm away from the combustor end at 225° and 315° each with respect to the horizontal plane and 50mm inside the combustor casing. All of the sensors used were calibrated to a traceable, independently audited system and according to UKAS standards.

7.4 READING ERRORS AND ACCURACY

All reading accuracy errors were considered in this study for the ranges handled. The mass flow rate error is within $\pm 1.5\%$. The fuel flow rate reading error is $\pm 1\%$. The pressure transmitter is accurate to $\pm 2\%$.



Figure 7.7: The Graseby 3100 syringe driver with the 25ml BD plastic syringe containing the hydrogen peroxide installed. The supply pipe that attaches to the igniter is also visible.

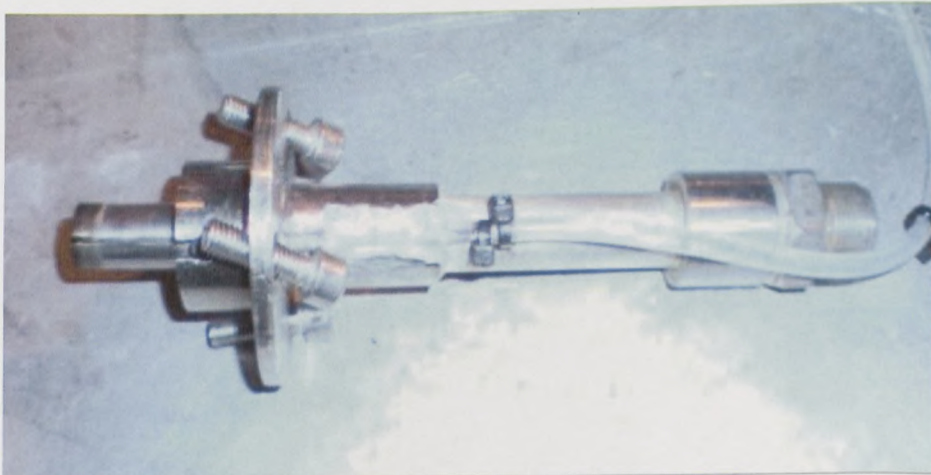


Figure 7.8: The modified focus discharge igniter with the attached hydrogen peroxide supply pipe.

7.5 PUMP CALIBRATION

7.5.1 PUMP CHARACTERISTICS

In preparation for the experiments in Eptec Labs, a used syringe pump was calibrated to inject an exact volume of liquid. The Graseby 3100 (Figure 7.7) was employed to drive a predetermined amount of liquid hydrogen peroxide into the cavity of the igniter.

The pump accepts only 25,30,50 and 60 ml plastic syringes and drives the installed syringe with a constant set rate. This infusion rate can be changed from 0.1ml/hr to 199.9ml/hr in 0.1ml/hr increments. After turning the pump in the on position, the device recognises the syringe type (provided there is a syringe) and then asks to input the rate. The rate can be changed only when the pump is paused.

7.5.2 PUMP CALIBRATION PROCEDURE

The calibration of the pump was made for 2, 8, 10, 14 and 20ml/hr infusion rates. The syringe used was a standard 20ml BD Plastic syringe. Volume measurements were taken by driving the liquid into a 2ml pipette through a silicon pipe; the same pipe which is used in the experiments. The pipe was connected to a pipette at the other end. The volume of the pipette is labelled in increments of 0.01ml. The position of the syringe's moving part was set at the point where the liquid was at the first labelled line of the pipette. This is taken therefore as the zero point.

The device was calibrated by leaving the pump to continuously insert liquid into the pipette. A stopwatch was used to take the times the device was infusing constant volumes of the liquid. The time counter was started at exactly the same time the start button was pressed. Each time was noted for every increase of 0.05ml in volume. Each calibration was repeated to make sure that the results are consistent.

7.5.3 CALIBRATION RESULTS

Figures 7.9 and 7.10 are the graphical representation of the results from the calibration runs. Each data point expresses the ejected volume of the test liquid at each corresponding time from the time the pump was started.

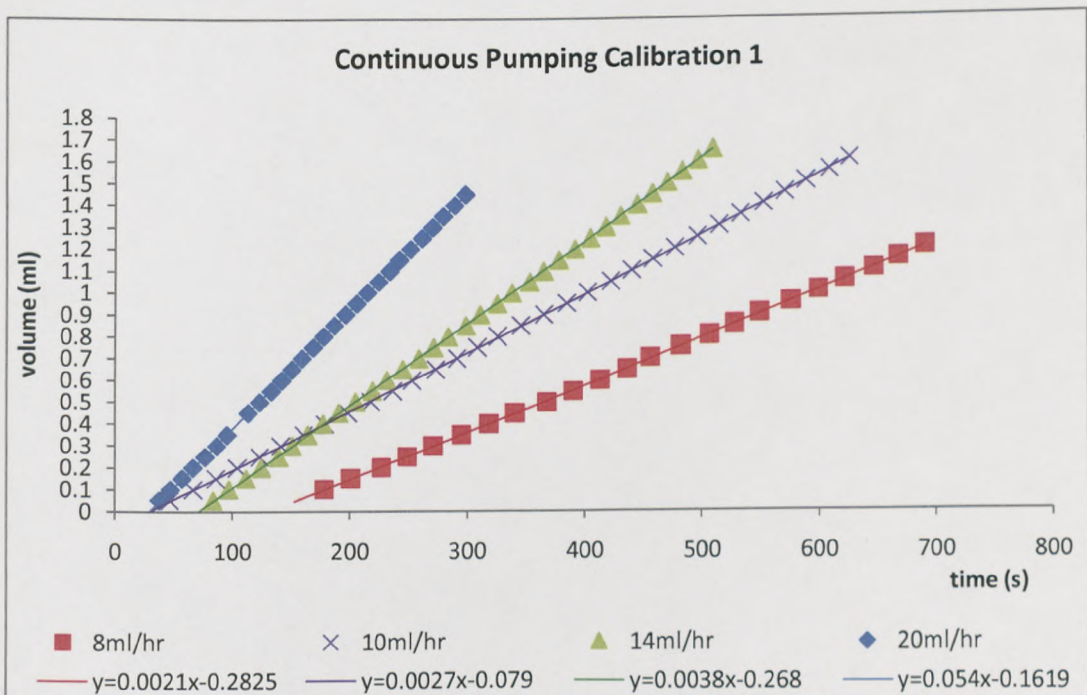


Figure 7.9 Shows the volume of liquid ejected while increasing time for different flow rates

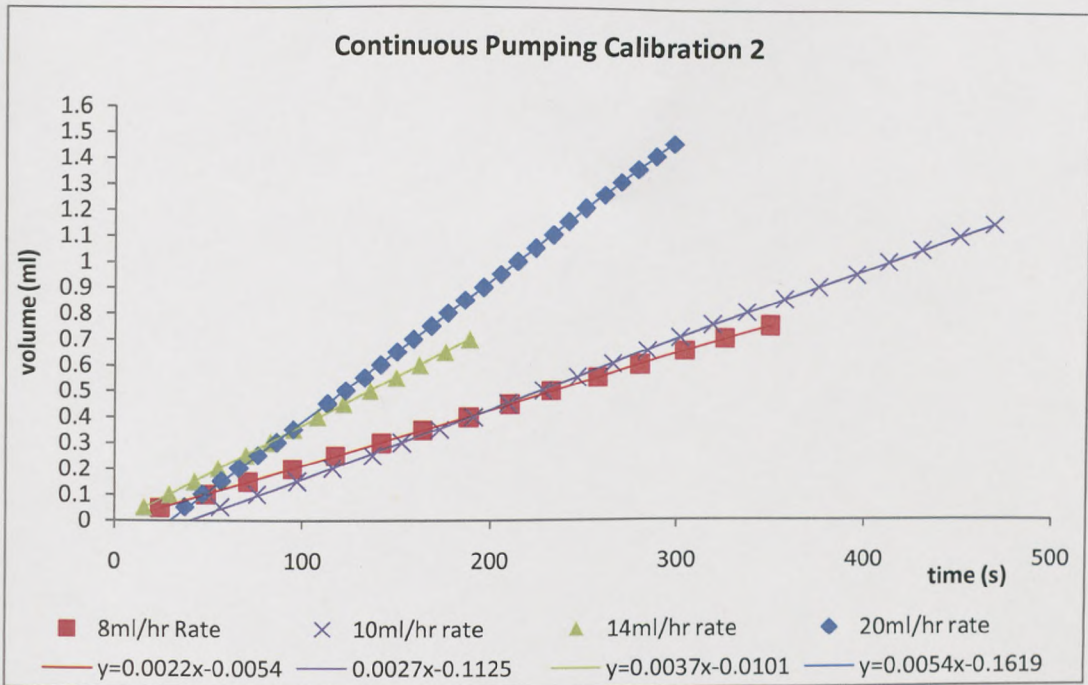


Figure 7.10: Repeated calibration run. The graph shows similarity with Figure 7.9

From the data obtained, it is shown in the two calibration graphs that the volume ejected by the Graseby 3100 pump increases linearly with time during continuous pumping. By comparing the graphs in Figures 7.9 and 7.10, it becomes clear that each calibration shows different results but almost identical slopes. Hence, it is only the start-up time that differs for each run. The reason for this difference is that for each calibration the syringe had to be re-filled with the liquid and therefore the clamp of the driver had to be opened and moved back in order to remove and then re-fit the syringe to the device. A careful inspection of the device exposes two crucial flaws in the design of the driver which are shown in Figure 7.11. Due to the nature of the pump that is used in conjunction with syringes, the start up time is not immediate. Time is required

for the syringe to seat in a stable position after installing it to the device. As one would expect this time is smaller for higher flow rates. Hence, whenever the syringe was installed to the pump care was taken to operate the driver for a short time prior to the conduction of the ignition experiments.

Pump Rate	Equation derived from Calibration Graphs $V(\text{ml}), t(\text{s})$	Actual Pump Rate
8ml/hr	$V = 0.00215t$	7.74ml/hr
10ml/hr	$V = 0.0027t$	9.72ml/hr
14ml/hr	$V = 0.00375t$	13.5ml/hr
20ml/hr	$V = 0.0054t$	19.44ml/hr

Table 7.1: Calibration slopes of different injection rates for the Graseby 3100.

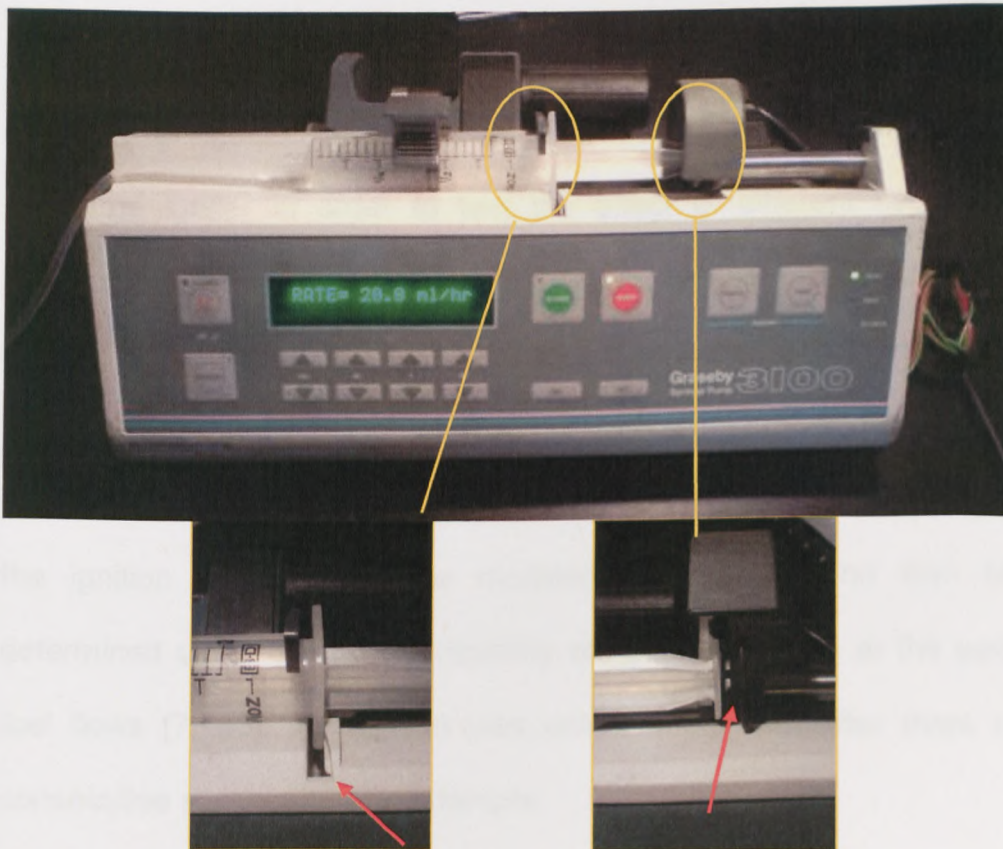


Figure 7.11: The Graseby 3100 syringe driver and its design flaws.

A Labview program was devised to control, the engine, the ejection of the liquid hydrogen peroxide into the igniter and to accumulate data for each ignition attempt. Air and fuel flow rates were controlled manually for experimental set1 and set 2. For the experimental set 3, the air and fuel mass rates were controlled by the Labview program and this later addition gave a better control of the fuel flow rate and decreased the time to adjust the fuel rate to the required value. The importance of this modification to the test engine is better understood by saying that the fuel could not be pre-adjusted manually to the fine quantity required to find the best value of the ignition limit and that the fuel valve was shut-off by the program after each ignition attempt. The air mass flow was controlled through a pneumatic butterfly valve. The fuel flow was controlled with a pneumatic needle valve.

7.7.1 USER INPUT VALUES

The inputs to the rig by the Labview program were air mass flow, fuel flow, hydrogen peroxide injection, electrical ignition delay, ignition time and total burn time after ignition. For set-1 and set-2 the fuel flow input was used as a stable value that the program should detect in order to start the ignition sequence.

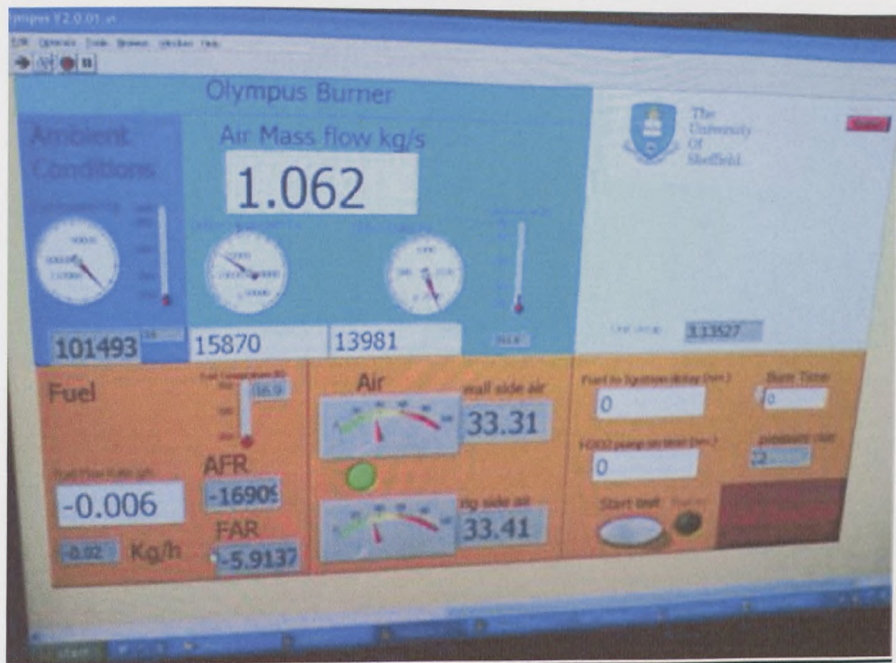


Figure 7.12: The Labview environment which controls the engine and the data acquisition

7.7.2 OLYMPUS ENGINE CONTROL AND EXPERIMENTAL PROCEDURE

By the start of each experiment the automated program had to start the fuel flowing and wait for 4.5s, time which was sufficient to achieve stability of the fuel supply. During this time the H_2O_2 infusion pump was started 1.8s before triggering the igniter at the pre-set hydrogen peroxide flow rate. After the first 4.5s the igniter was fired and was kept discharging for 10s at a pulse rate of 108 discharges per minute. If the ignition attempt was successful, then the rig was left running for 10s before the fuel supply was shut-off to ensure that the light was stable. The ignition sequence could only be initiated if the exhaust temperature was below $50^\circ C$ to prevent ignition enhancement due to the elevated temperature. Between no-light attempts the engine was left with only the air running for more than 20s, time sufficient to clear out any unburned fuel or H_2O_2 .

Both experimental set-1 and set-2 tested the ignition limits of kerosene Jet-A₁ with different rates of H₂O₂. In experimental set-3, the study investigated the ignition limits of the same kerosene Jet-A₁ and a biodiesel test fuel under the clean fuel atomiser condition. On the biodiesel, it should be noted that the fuel was provided by the lab with no further information except that it was a fatty acid methyl ester (F.A.M.E). diesel. The biodiesel was later analysed to obtain the composition in hydrocarbons for calculating the equivalence ratio values from the fuel and air mass flow data. For kerosene, the supplier provided the information for the fuel. The following are specifications regarding the fuels used:

- Kerosene Jet-A₁

The general specifications for the Jet-A₁ fuel are provided in Section 3.6.3 Table 3.4. For the kerosene test fuel the net specific energy was 43.21(MJ/kg). The density of the Jet-A₁ was 801.9(kg/m³). These values were used for calculating the net available energy at the time of ignition (Section 9.12). The chemical formula C₁₁H₂₁ is considered a good approximation for kerosene [84]. This formula was used for calculating the fuel-air mixture strength ϕ (or equivalence ratio).

- Biodiesel Fuel

An analysis of the test biodiesel was done to reveal the main composition of the fuel. The composition was found to be: carbon: 86.53%, hydrogen: 13.41%, nitrogen: 0.06% in by weight percentages. Hence the chemical formula C_{7.2}H_{13.4}

results from the analysis of the fuel. This composition was used when calculating the equivalence ratios of the fuel-air mixtures. In general, the calorific value of biodiesel fuels lies between 37.27 and 39.9 MJ/kg. The density of methyl ester derived biodiesels is usually in the region of 880kg/m³. It is common knowledge that the biodiesel depends strongly on the initial feedstock used. In fatty acid methyl esters the transesterification process of the feedstock involves methanol fuel. The feedstock used in the production of biodiesel can be either vegetable oil or animal fat.

PART-A – KEROSENE JET A₁ TEST FUEL

The results presented in this chapter summarise the ignition experiments that were conducted using the Rolls Royce Olympus reaction chamber at atmospheric conditions. These experiments were designed mainly to test the ignitability of a fuel when using the modified focus discharge igniter, in conjunction with the particular reaction chamber. The modifications allowed the user to inject the hydrogen peroxide into the cavity of the igniter at a pre-specified rate. More on the experimental apparatus and procedures can be found at the previous chapter. The experimental results are categorised depending on the fuel used. Part-1 presents the results acquired by testing the ignition of the kerosene Jet-A₁ fuel. Part-2 presents the results that were obtained from the biodiesel runs.

8.1 LEAN IGNITION LIMITS WITH AND WITHOUT H₂O₂ ADDITION - MIXTURE STRENGTH ϕ VS. AIR MASS FLOW RATE

A series of experiments were conducted in the Olympus test rig in order to determine the lean ignition limits of the kerosene Jet-A₁ fuel using this research's modified focus discharge igniter. Only tests during the same day are directly compared in the graphs below. Figures 8.1-8.3 and Figure 8.6 are a summary of all Jet-A₁ cases examined and therefore show both light and failed light attempts (referred to as no-light attempts). The ignition limits are found using the 60% probability of ignition criterion out of a total of 5 ignition attempts. In the modified FDI, H₂O₂ is continuously injected into the cavity of the igniter at 0 μ l/s and 0.54 μ l/s volume rates. Each circle indicates the equivalence ratio ϕ that represents one ignition limit (60% probability of ignition criterion), for each air mass flow rate studied. The crosses represent failed ignition attempts and the squares show all other attempts where combustion was initiated (light attempts) but were either above the lean limit or, if below, did not pass the 60% probability of ignition criterion.

Figures 8.1-8.3 show the lean ignition limit lines of the Jet A₁ fuel that were obtained using different H₂O₂ injection rates at each air mass flow studied.

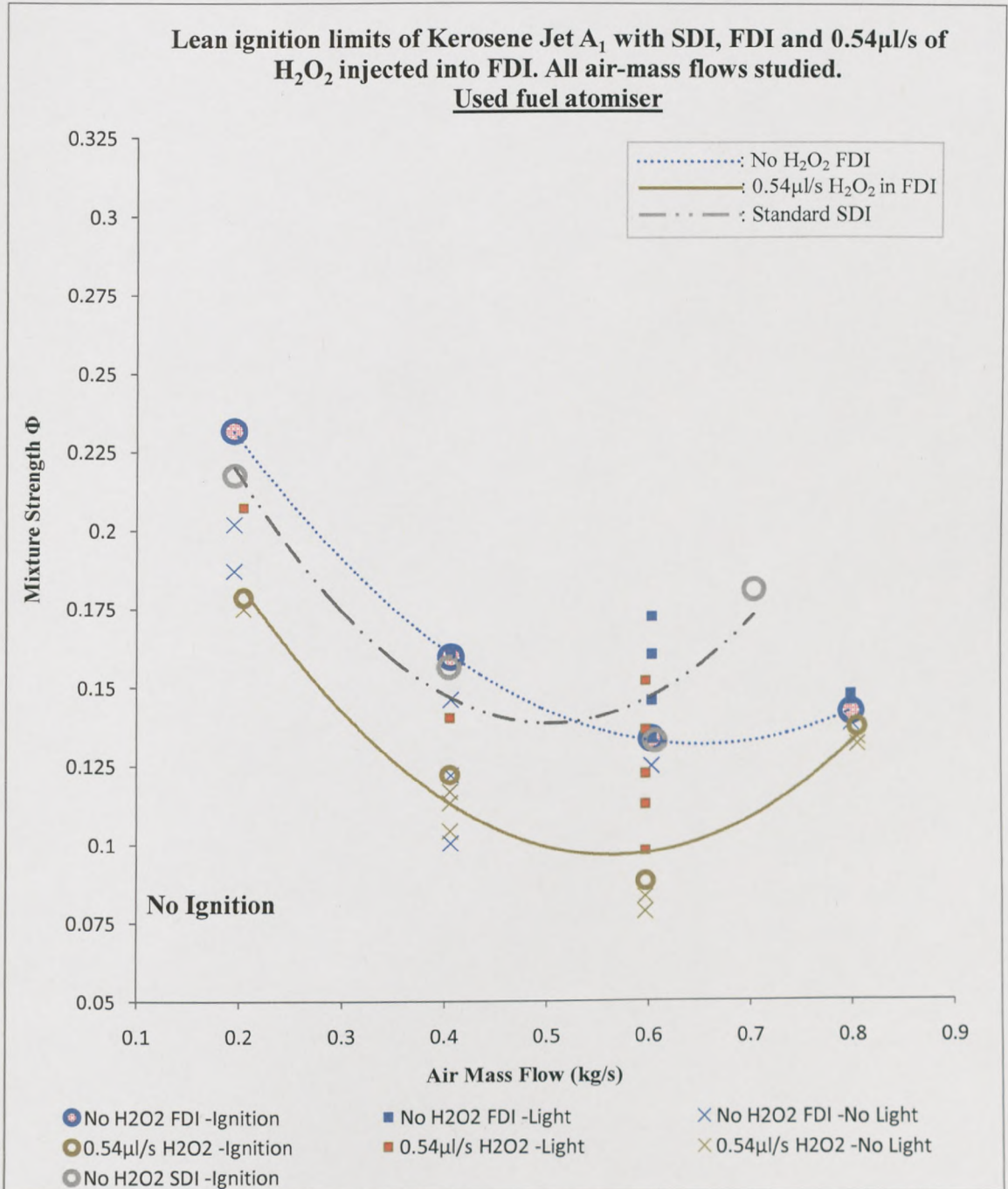


Figure 8.1: Experimental set-1. Lean ignition limits for kerosene Jet A₁ (used fuel injector cases). Equivalence ratios against air mass flow rates. The lines represent 2nd order polynomials passing approximately near the data points which correspond to the ignition limits for each hydrogen peroxide volume flow rate. All points show average values of Φ . Each circle indicates 3 consecutive successful ignitions (60% probability of ignition criterion) at the limit of ignition for each H₂O₂ and air mass flow case. (FDI: Focus Discharge Igniter. SDI: Surface Discharge Igniter). Ambient conditions.

See also Appendix A for more information on the modified FDI.

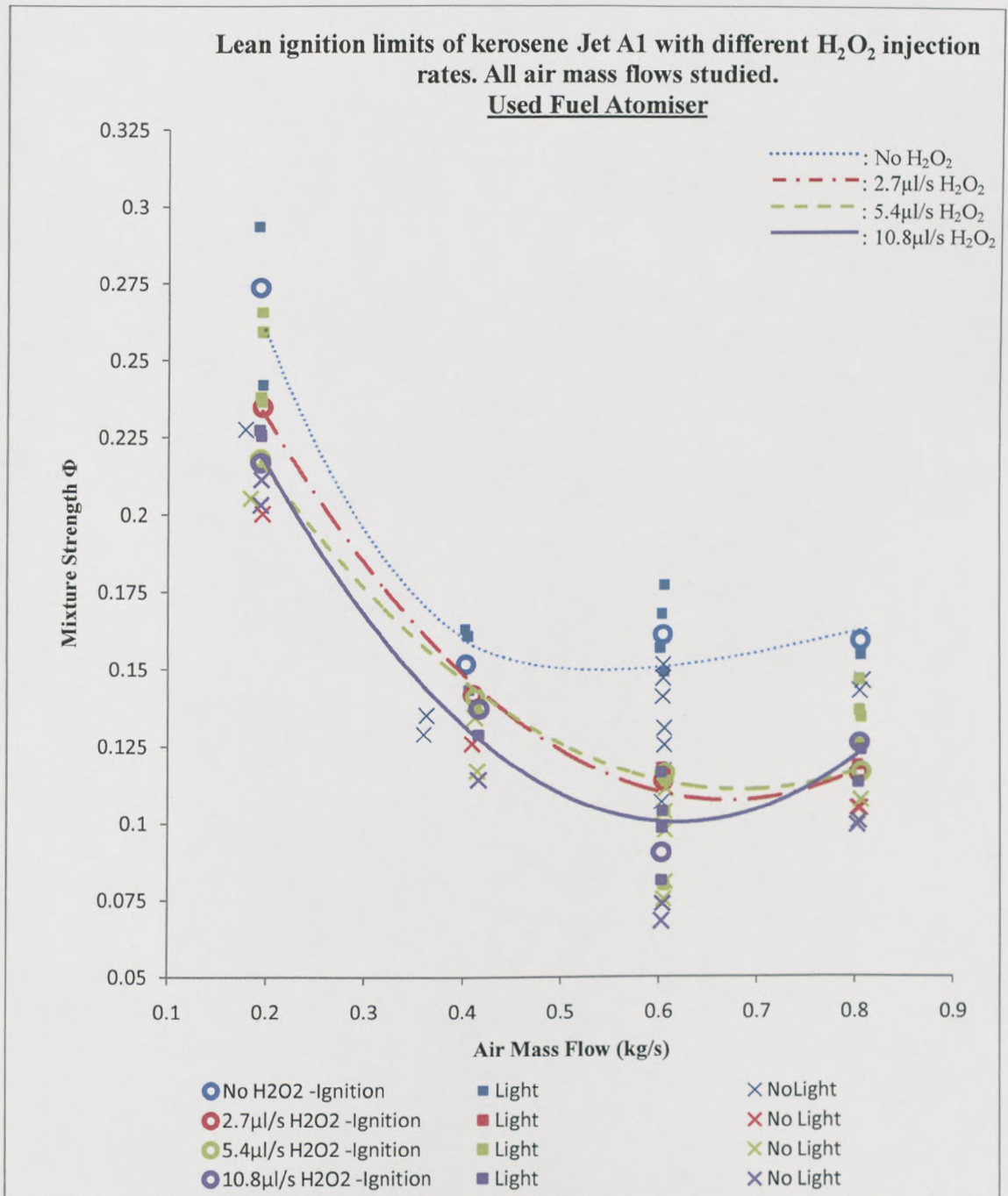


Figure 8.2(a): Experimental set-2. Lean ignition limits for kerosene Jet A1 (used fuel injector cases). Equivalence ratios against air mass flow rates. The lines represent 2nd order polynomials passing approximately near the data points which correspond to the ignition limits for each hydrogen peroxide volume flow rate. All points show average values of Φ . Each circle indicates 3 consecutive successful ignitions (60% probability of ignition criterion) at the limit of ignition for each H₂O₂ and air mass flow case. The H₂O₂ rates studied are: 0, 2.7, 5.4, 10.8 μ l/s. FDI igniter-Ambient Conditions.

Lean ignition limits of kerosene Jet A1 with different H₂O₂ injection rates. All air mass flows studied.

Used fuel atomiser

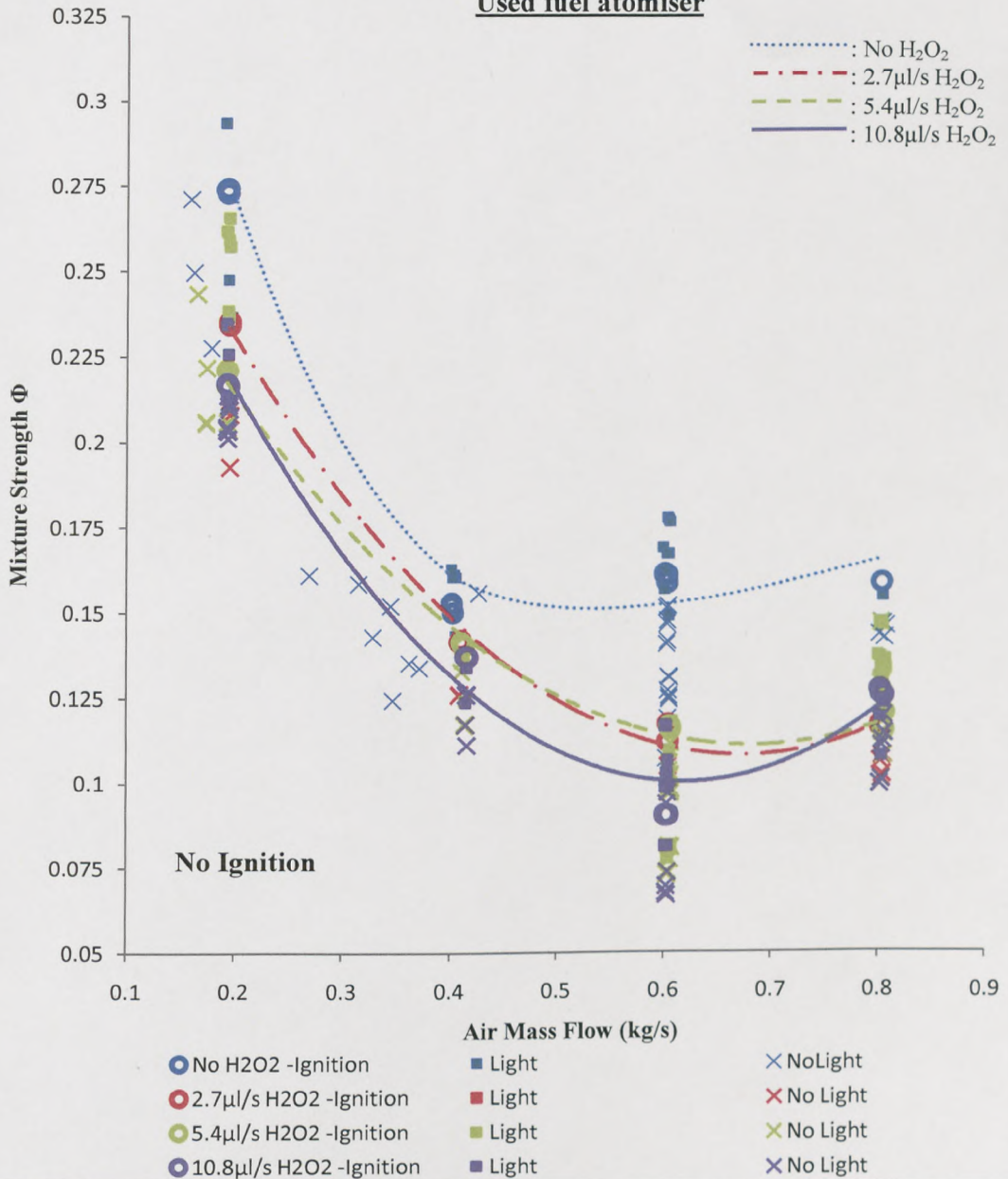


Figure 8.2(b): Same as Figure 8.2(a) but showing all ignition attempts and *not averaged* equivalence ratio values. The 3 consecutive successful ignitions (60% probability of ignition criterion) at the lean limits of ignition are shown to be very close or coincide for each hydrogen peroxide case. The H₂O₂ rates studied are: 0, 2.7, 5.4, 10.8 μ l/s. Results from experimental set-2: Used fuel injector- FDI igniter -Ambient Conditions. [65]

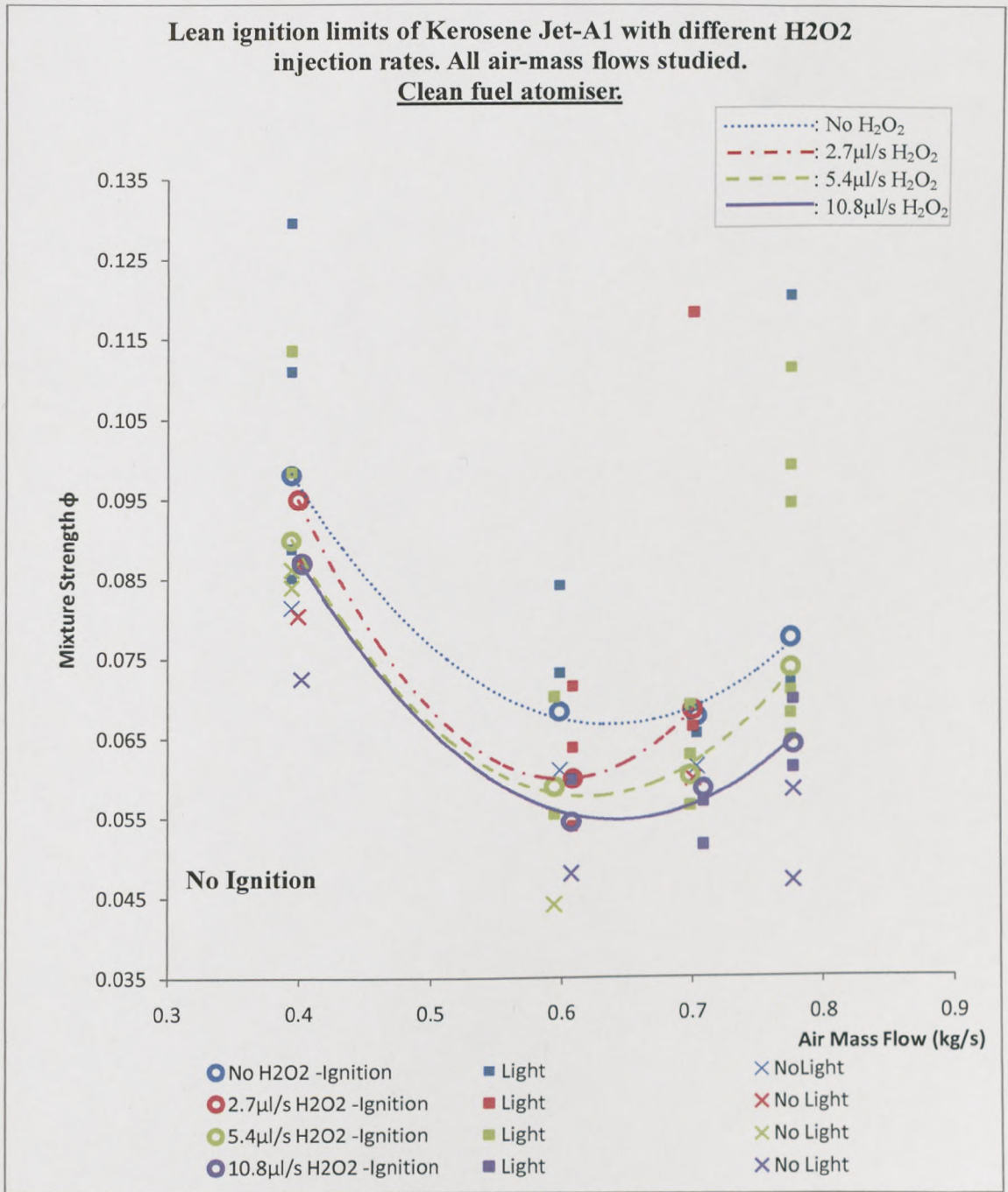


Figure 8.3: Experimental set-3. Lean ignition limits for kerosene Jet A1 (Clean fuel injector cases). Equivalence ratios against air mass flow rates. The lines represent 2nd order polynomials passing approximately near the data points which correspond to the ignition limits for each hydrogen peroxide volume flow rate. All points show average values of ϕ . Each circle indicates 3 consecutive successful ignitions (60% probability of ignition criterion) at the limit of ignition for each H₂O₂ and air mass flow case. The H₂O₂ rates studied are: 0, 2.7, 5.4, 10.8 μ l/s. FDI igniter- Ambient Conditions

8.2 THE EFFECT OF FUEL SPRAY QUALITY IN THE LEAN IGNITION LIMITS.

Figures 8.4 and 8.5 underline the importance of the fuel atomiser in lowering the lean ignition limits of the Jet A₁ fuel. Comparisons of the ignition limits are made between the experimental sets one, two and three, separately for the lowest and highest H₂O₂ injection rate cases; i.e. 0μl/s and 10.8μl/s H₂O₂. The importance of the fuel spray quality, in order to achieve better ignition characteristics, is emphasised in both graphs of this section. The graphs indicate that the lean ignition limits of the Jet A₁ have been dramatically reduced by the use of the clean fuel injector. Figure 8.4 is considered particularly useful in this interpretation as it compares data from experiments that were done without the use of the H₂O₂ additive during ignition.

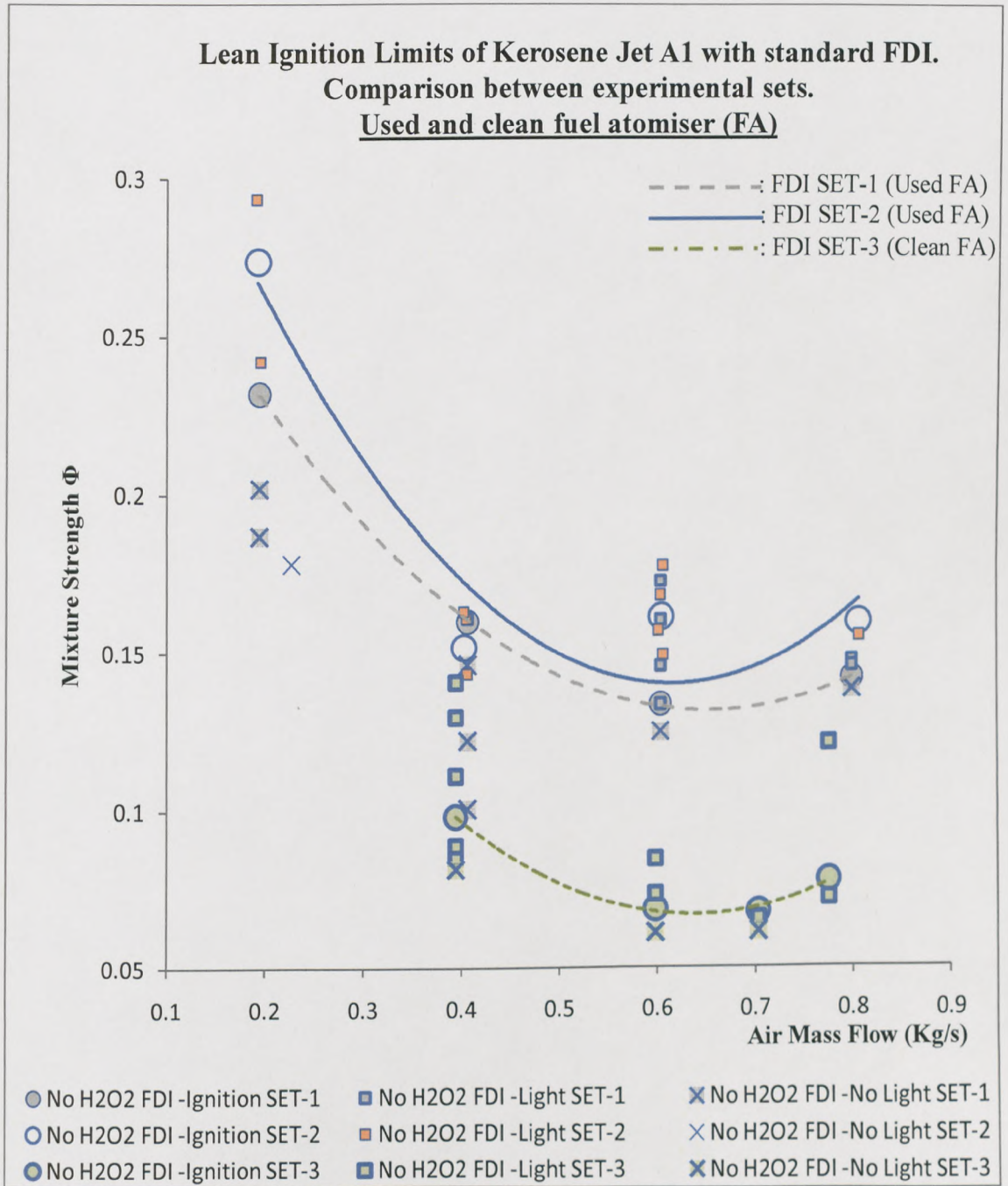


Figure 8.4: Lean ignition limits of Kerosene Jet A₁ for all air mass flow studied using the modified igniter with no additive injected into its cavity. Comparison between the three experimental sets where the only controlled parameter that changes is that the fuel atomiser was cleaned for set-3. All points show average values of Φ . FDI igniter- Different atmospheric conditions depending on the test day.

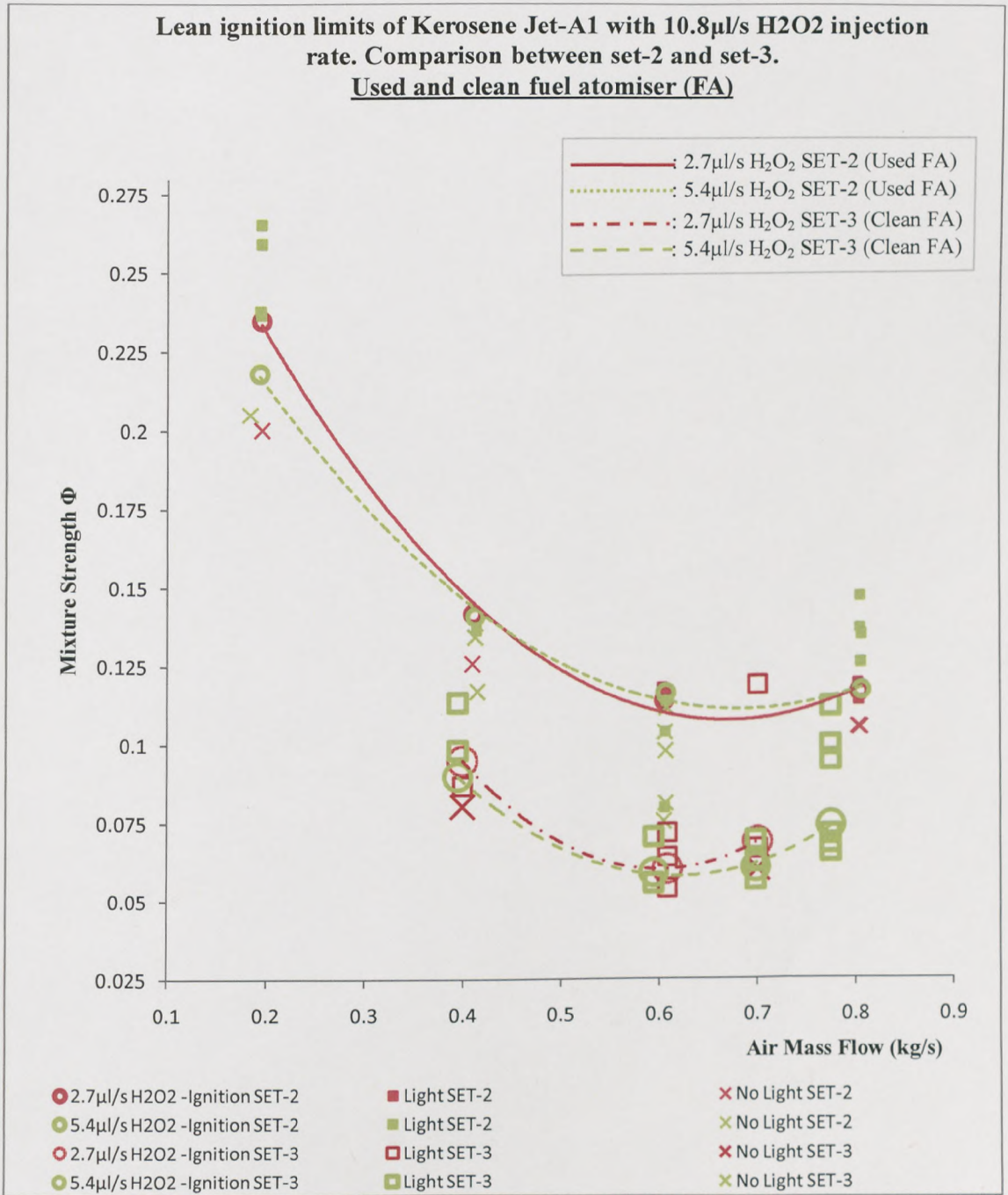


Figure 8.5(a): Lean ignition limits of Kerosene Jet A₁ for all air mass flow studied using the modified igniter with 2.7 and 5.4μl/s of H₂O₂ injected into its cavity. Comparison between the three experimental sets where the only controlled parameter that changes is that the fuel atomiser was cleaned for set-3. All points show average values of Φ . FDI igniter-Different atmospheric conditions depending on the test day

**Lean ignition limits of Kerosene Jet-A1 with 10.8 μ l/s H₂O₂ injection rate. Comparison between set-2 and set-3.
Used and clean fuel atomiser (FA)**

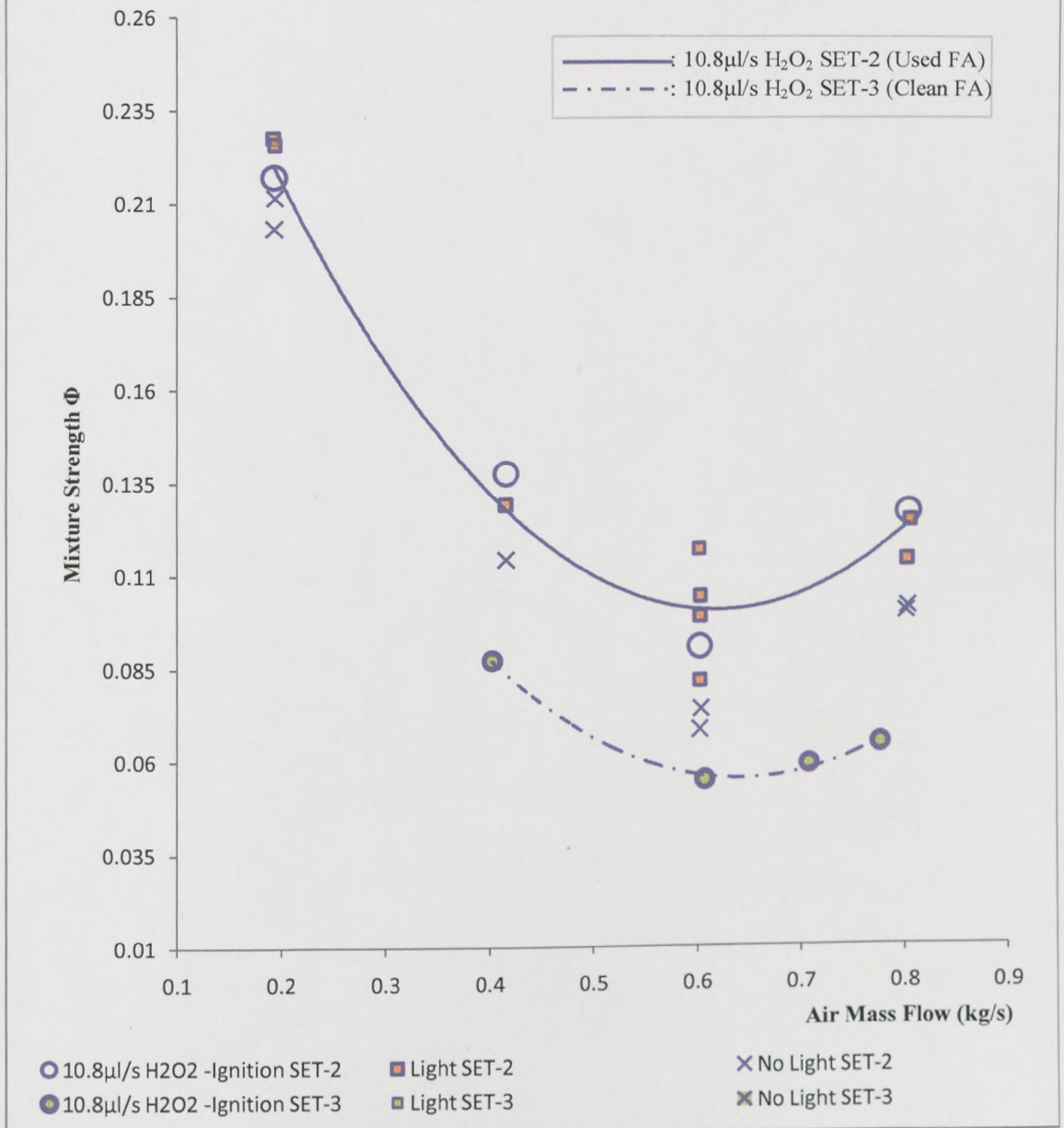


Figure 8.5(b): Lean ignition limits of Kerosene Jet A₁ for all air mass flow studied using the modified igniter with 10.8 μ l/s of H₂O₂ injected into its cavity. Comparison between the three experimental sets where the only controlled parameter that changes is that the fuel atomiser was cleaned for set-3. Atmospheric conditions are also expected to affect the lean limits but not by much. All points show average values of Φ . FDI igniter- Different atmospheric conditions depending on the test day

8.3 LEAN IGNITION LIMITS WITH AND WITHOUT WATER ADDITION

8.3.1 EXPERIMENTAL SET-3 – CLEAN FUEL ATOMISER

Figure 8.6 shows how the lean ignition limits are affected by adding water instead of H_2O_2 into the cavity of the FDI igniter.

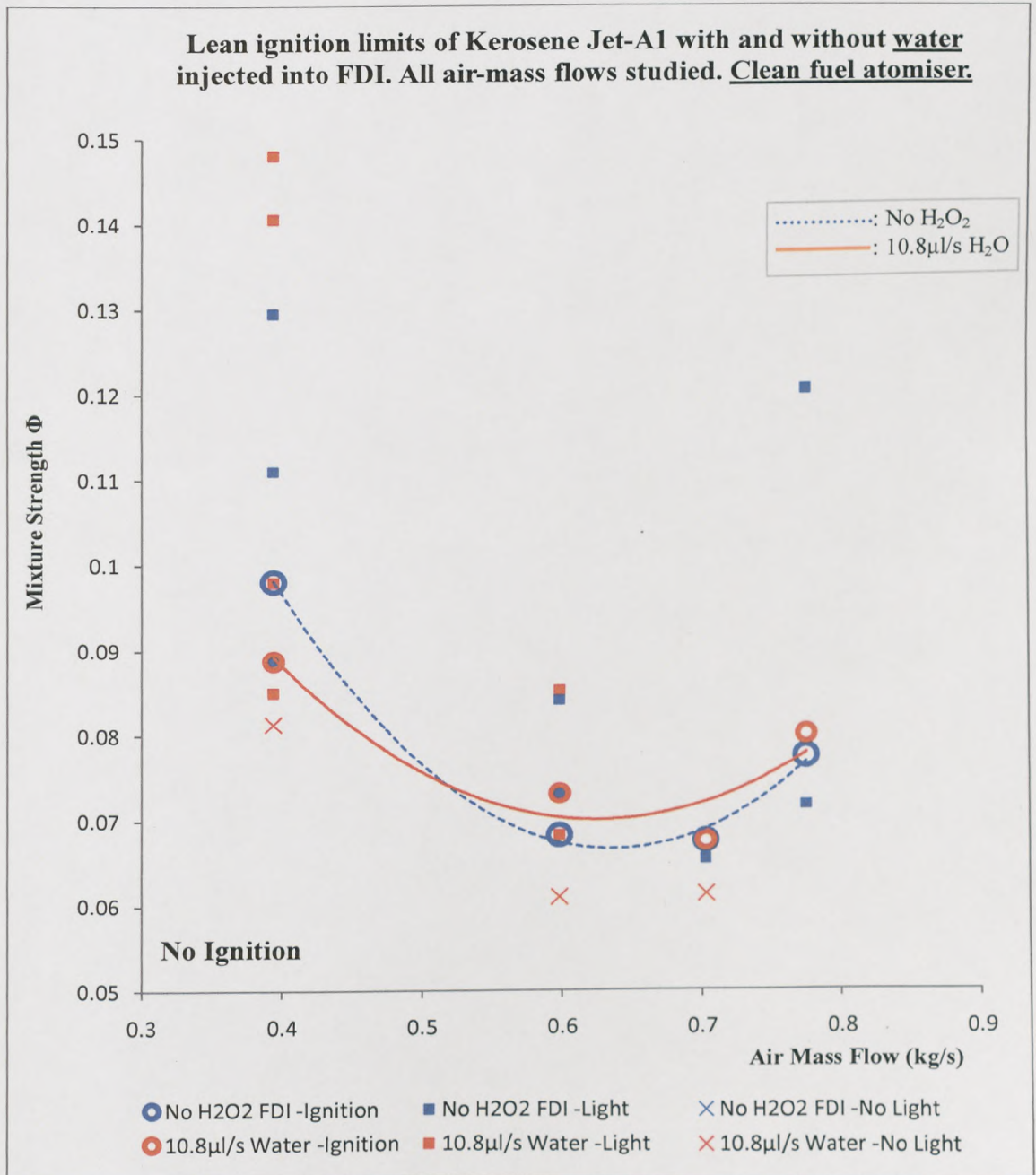


Figure 8.6: Experimental set-3. Lean ignition limits for kerosene Jet A1 (Clean fuel injector cases) Equivalence ratios against air mass flow rates. The lines represent 2nd order polynomials passing approximately near the data points which correspond to the ignition limits for each hydrogen peroxide volume flow rate. All points show average values of Φ . Each circle indicates 3 consecutive successful ignitions (60% probability of ignition criterion) at the limit of ignition for each case. This case study shows how the limits are affected by the injection of 0 and 10.8 $\mu\text{l/s}$ water into the focus discharge igniter cavity. FDI igniter- Ambient conditions

8.4 THE EFFECT OF DIFFERENT H₂O₂ INJECTION RATES IN THE LEAN IGNITION LIMITS OF THE KEROSENE JET A₁ FUEL - MIXTURE STRENGTH Φ VS. H₂O₂ VOLUME RATE

8.4.1 EXPERIMENTAL SET-2 – USED FUEL ATOMISER

The plots in Figures 8.7-8.14 show how the lean ignition limits are affected by changing the H₂O₂ injection volume rate. Each plot summarises the results for each of the air mass flow rates studied and only between same fuel injector characteristics. The H₂O₂ volume rates injected were 0, 2.7, 5.4 and 10.8 $\mu\text{l/s}$ for each of the air mass flow rates tested. Figures 8.7-8.10 are plots from the data collected in experimental set-2 (experiments with a used fuel injector). Figures 8.11-8.14 show the data collected from experimental set-3 for the Jet A₁ fuel case; where, prior to its use, the fuel injector was serviced (clean fuel injector).

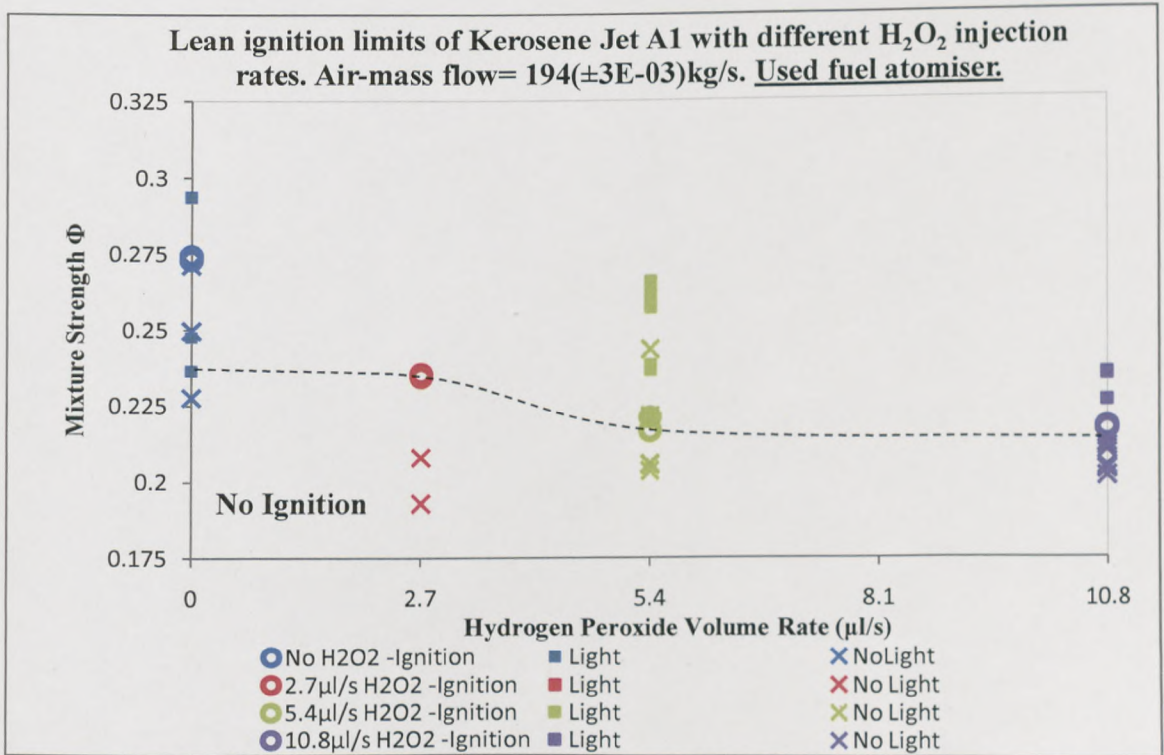


Figure 8.7: Lean ignition limits of Kerosene Jet A₁ for an air mass flow of 0.194(±0.003)kg/s at different hydrogen peroxide flow rates. The circles indicate 3 consecutive successful ignitions (60% probability of ignition criterion) at the limit of ignition for each case. Test conditions are ambient. All data points- FDI igniter [65]

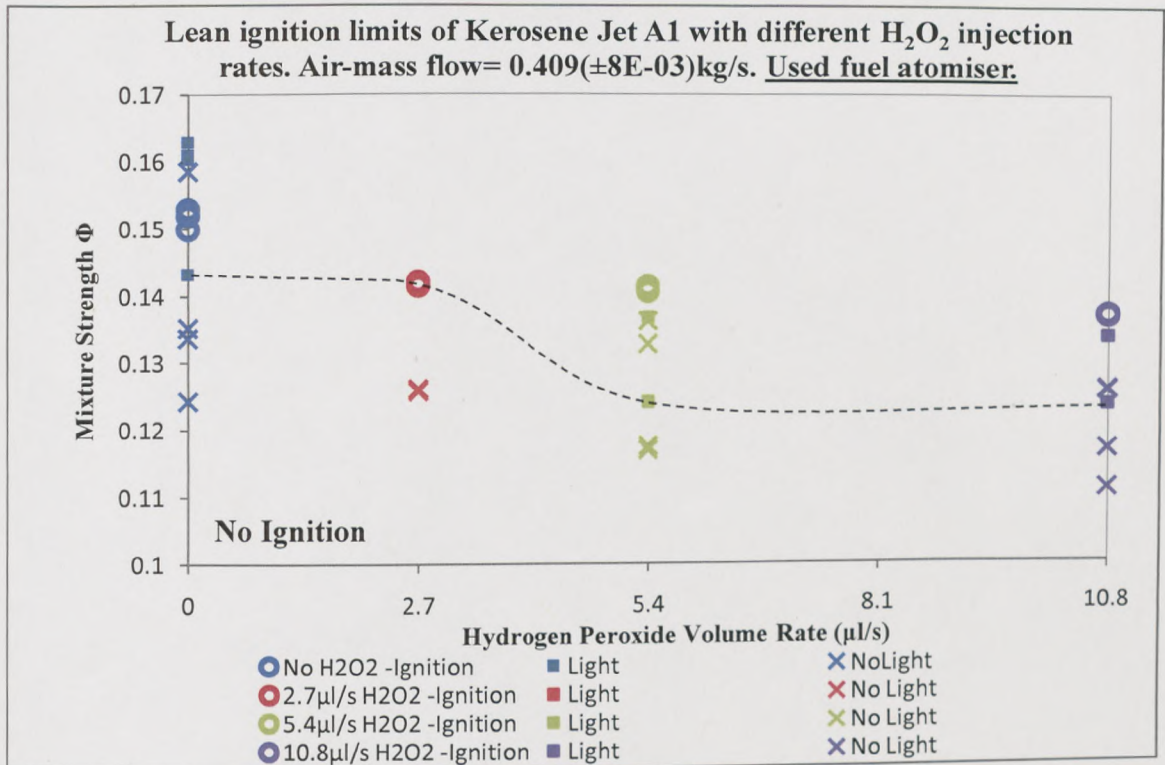


Figure 8.8: Lean ignition limits of Kerosene Jet A₁ for an air mass flow of 0.409(±0.008)kg/s at different hydrogen peroxide flow rates. The circles indicate 3 consecutive successful ignitions (60% probability of ignition criterion) at the limit of ignition for each case. Test conditions are ambient. All data points- FDI igniter [65]

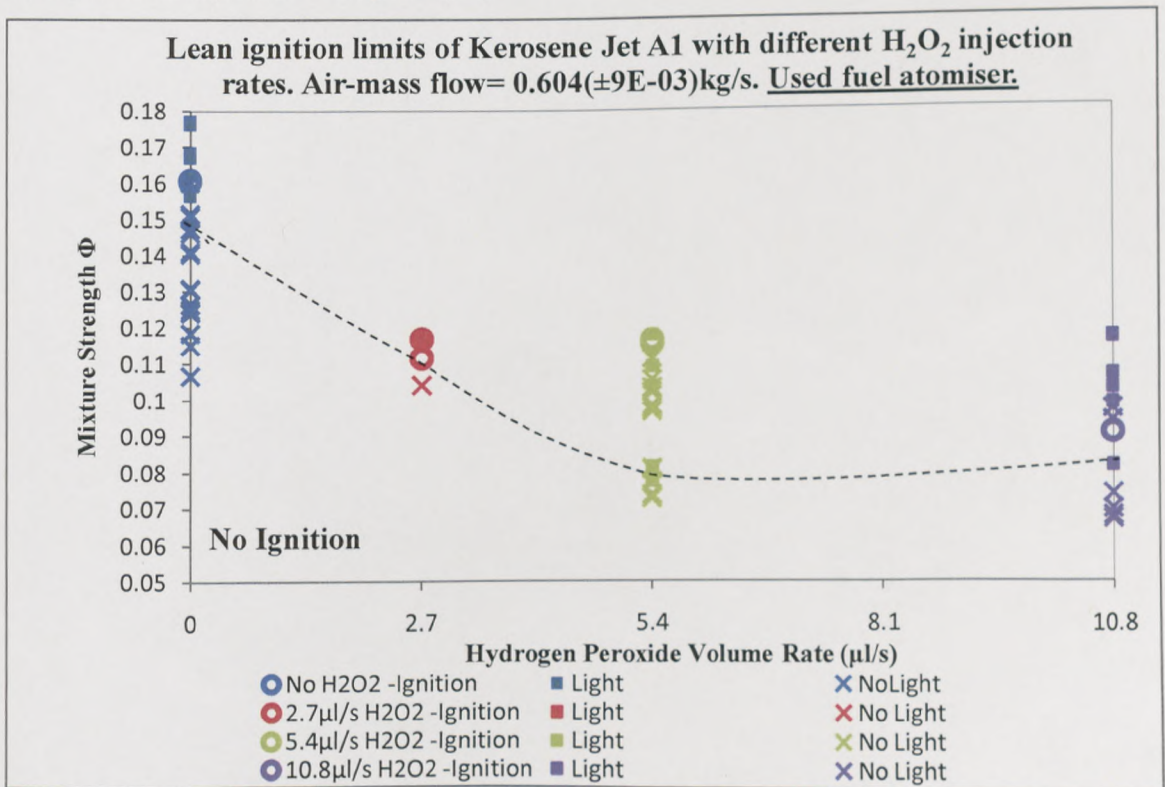


Figure 8.9: Lean ignition limits of Kerosene Jet A₁ for an air mass flow of 0.604(±0.009)kg/s at different hydrogen peroxide flow rates. The circles indicate 3 consecutive successful ignitions (60% probability of ignition criterion) at the limit of ignition for each case. Test conditions are ambient. All data points- FDI igniter [65]

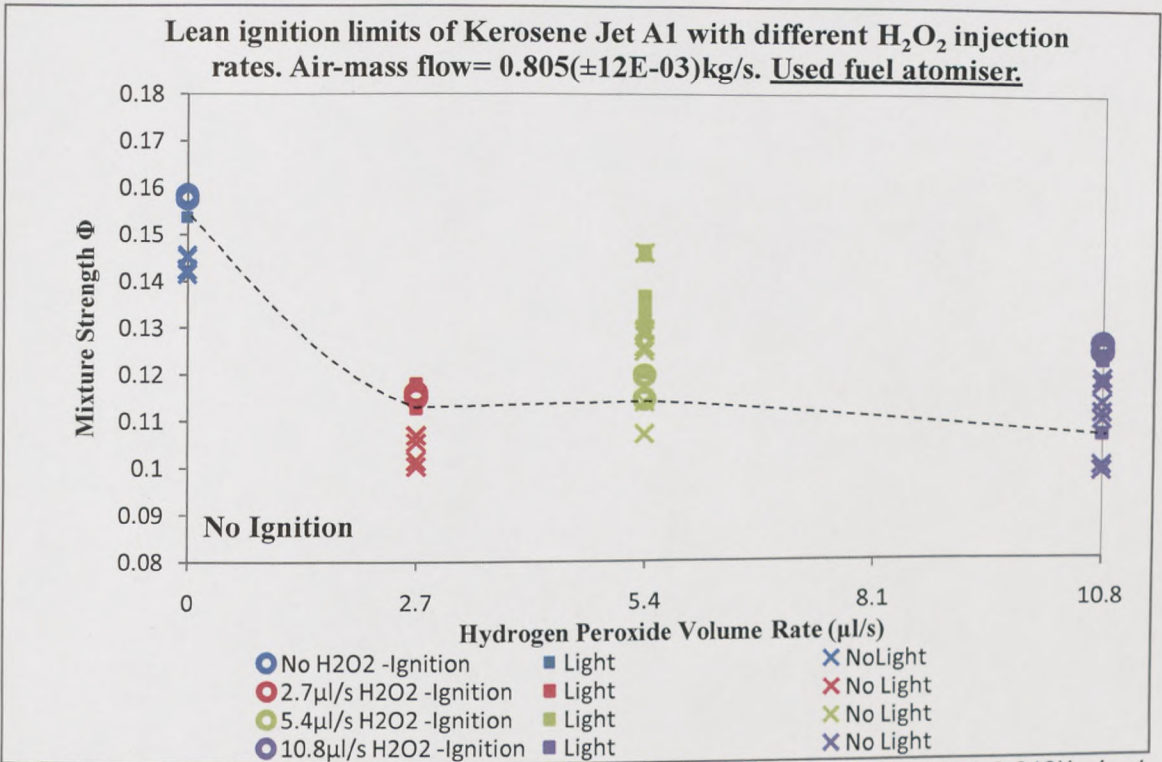


Figure 8.10: Lean ignition limits of Kerosene Jet A₁ for an air mass flow of 0.805(±0.012)kg/s at different hydrogen peroxide flow rates. The circles indicate 3 consecutive successful ignitions (60% probability of ignition criterion) at the limit of ignition for each case. Test conditions are ambient. All data points- FDI igniter [65]

8.4.2 EXPERIMENTAL SET-3 – CLEAN FUEL ATOMISER

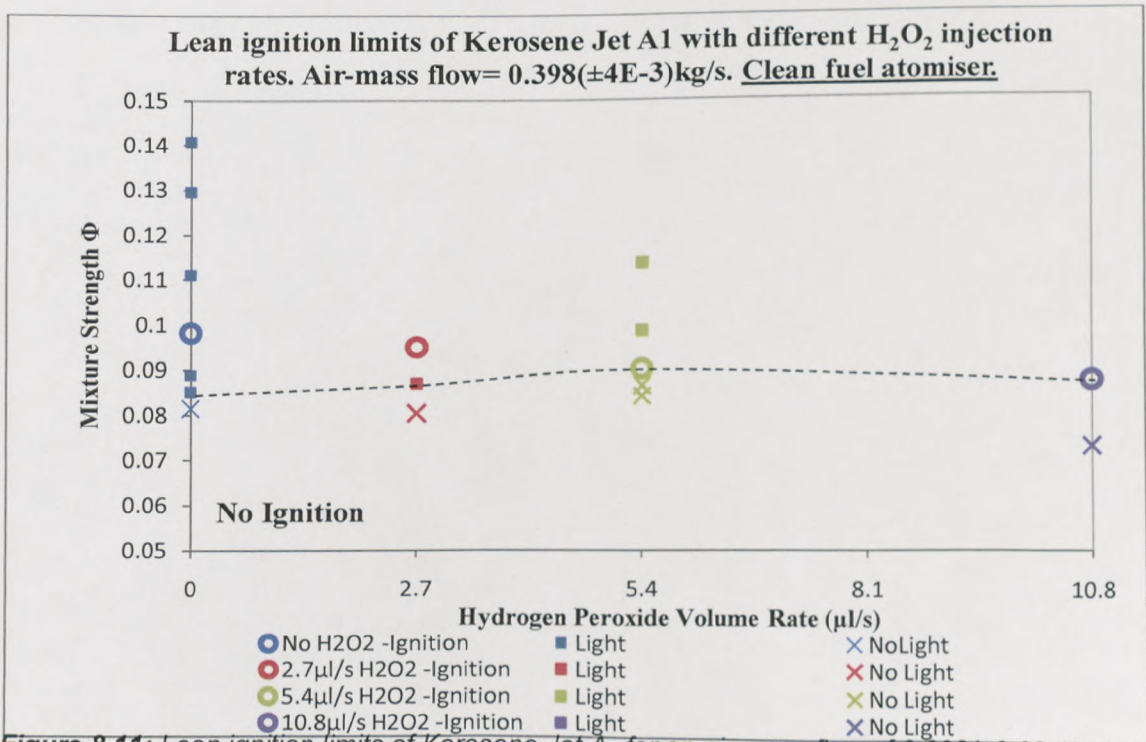


Figure 8.11: Lean ignition limits of Kerosene Jet A₁ for an air mass flow of 0.398(±0.004)kg/s at different hydrogen peroxide flow rates. Each circle indicates 3 consecutive successful ignitions (60% probability of ignition criterion) at the limit of ignition for each case. Test conditions are ambient. All points show average values of Φ- FDI igniter

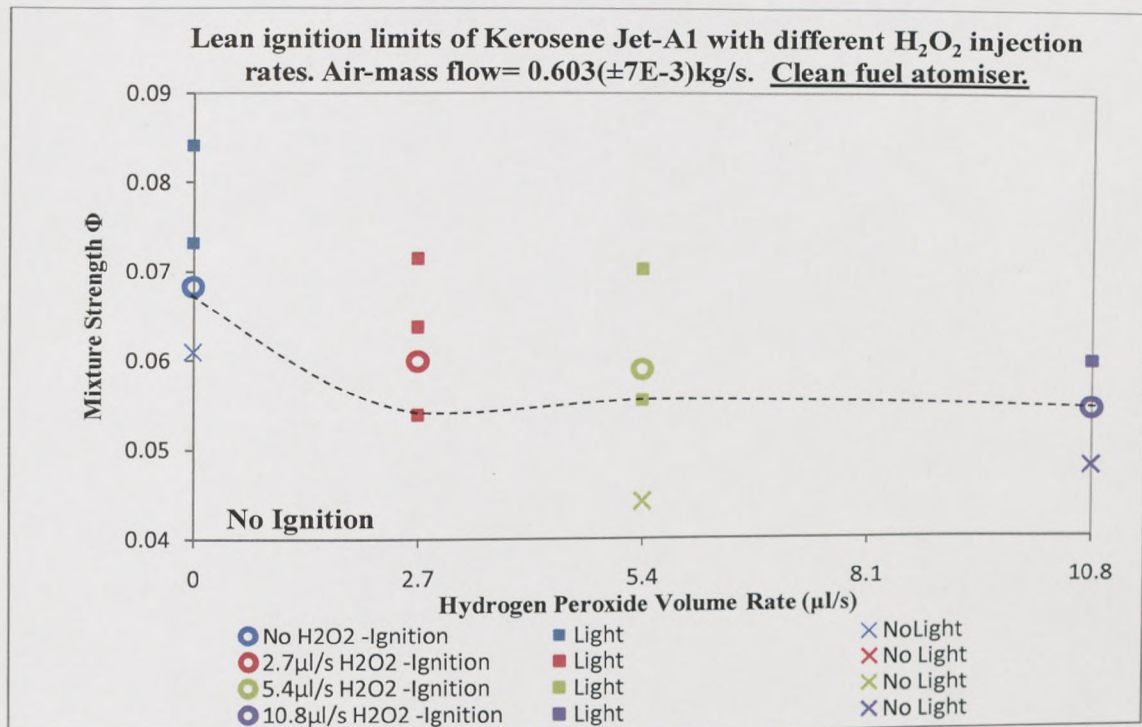


Figure 8.12: Lean ignition limits of Kerosene Jet A₁ for an air mass flow of 0.603(±0.007)kg/s at different hydrogen peroxide flow rates. Each circle indicates 3 consecutive successful ignitions (60% probability of ignition criterion) at the limit of ignition for each case. Test conditions are ambient. All points show average values of Φ- FDI igniter

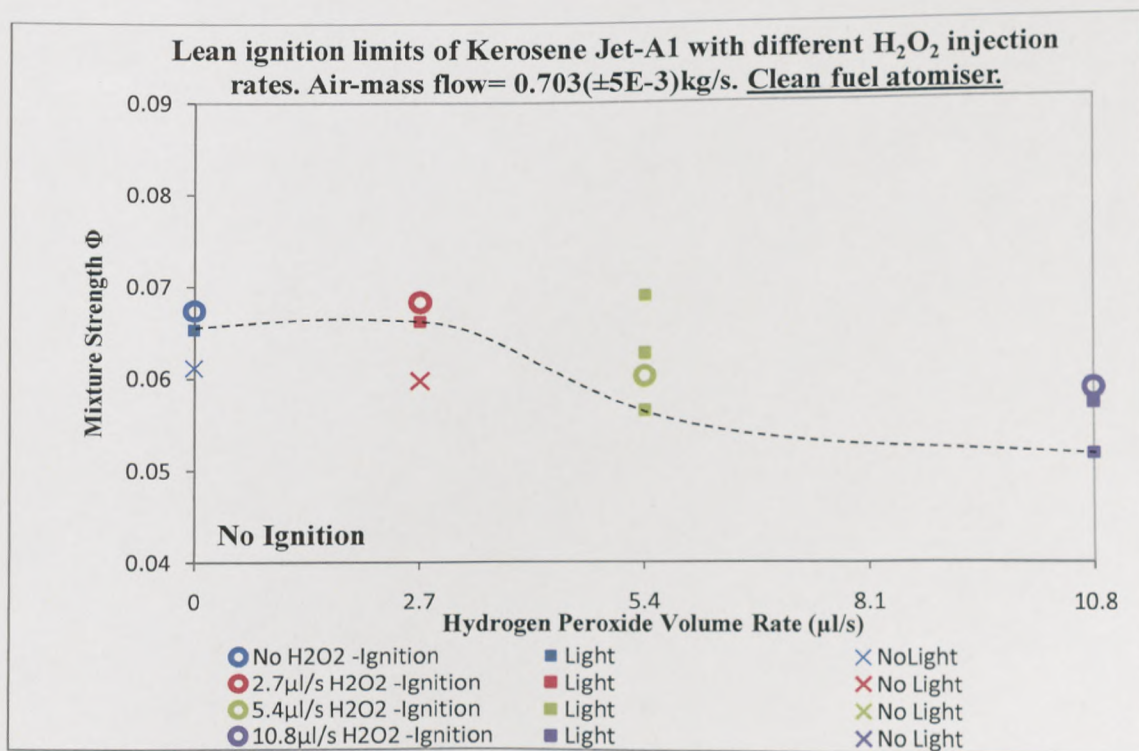


Figure 8.13: Lean ignition limits of Kerosene Jet A₁ for an air mass flow of 0.703(±0.005)kg/s at different hydrogen peroxide flow rates. Each circle indicates 3 consecutive successful ignitions (60% probability of ignition criterion) at the limit of ignition for each case. Test conditions are ambient. All points show average values of Φ- FDI igniter

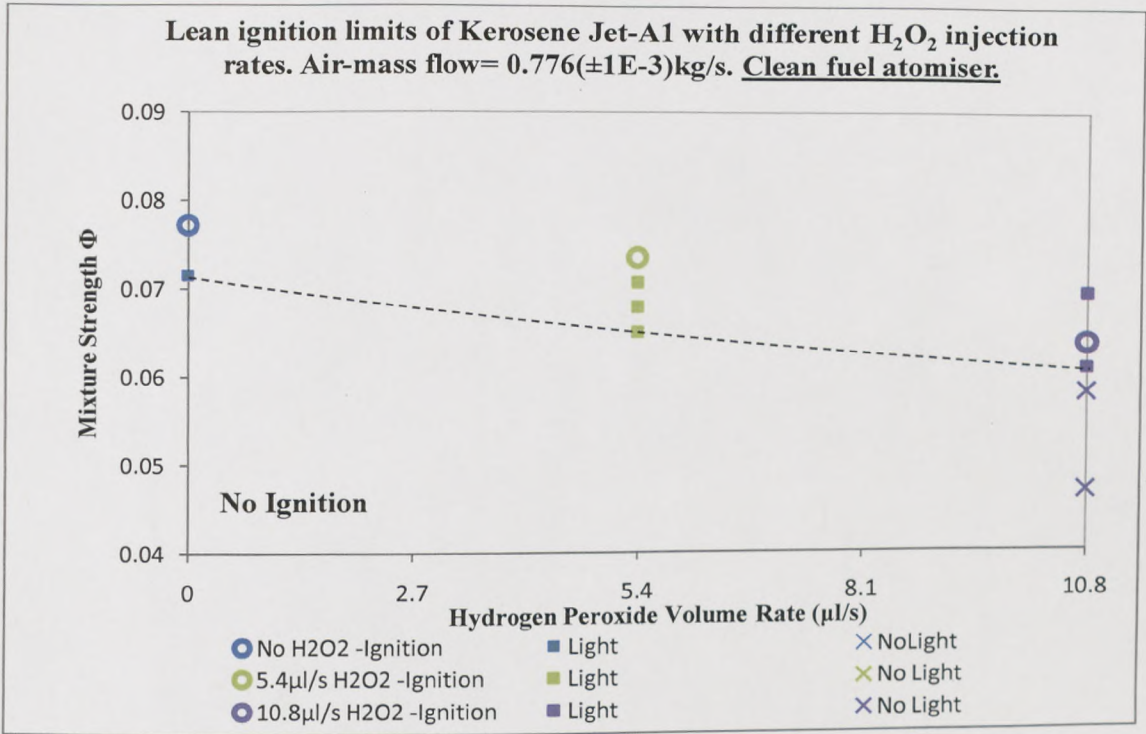


Figure 8.14: Lean ignition limits of Kerosene Jet A₁ for an air mass flow of 0.776(±0.001)kg/s at different hydrogen peroxide flow rates. Each circle indicates 3 consecutive successful ignitions (60% probability of ignition criterion) at the limit of ignition for each case. Test conditions are ambient. All points show average values of Φ- FDI igniter

8.5 ENERGY CALCULATIONS AT TIME OF IGNITION FOR ALL AIR MASS FLOW RATES STUDIED. RESULTS ONLY FROM EXPERIMENTAL SET-2 – USED FUEL ATOMISER

Figure 8.15 shows the maximum energy of the fuel that is available inside the combustion chamber at the instance of ignition. The available energy originates usually only from the high calorific fuel that is injected into the combustion chamber. In the cases of the ignitions that were aided by adding hydrogen peroxide, the available energy at the time of ignition is assumed to be higher because of the chemical properties of the additive.

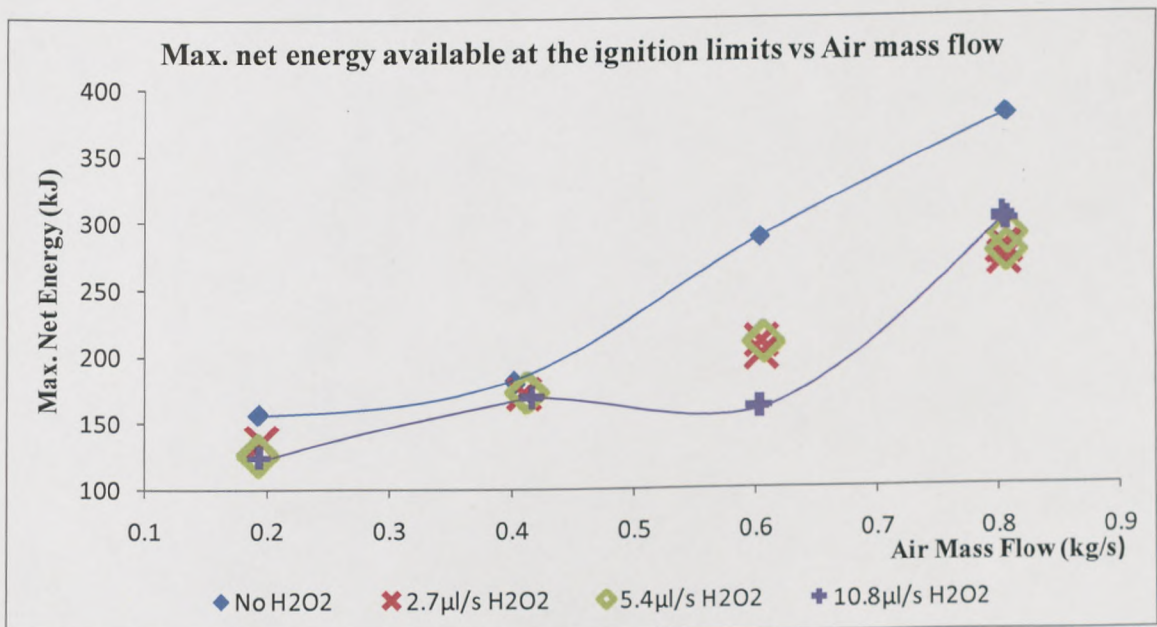


Figure 8.15: Maximum net energy of fuel and hydrogen peroxide at the time of ignition and at the lean ignition limits. The maximum energy is calculated using the hydrogen peroxide volume that was ejected up to the time of ignition. As the hydrogen peroxide rate increases the equivalence ratio at the lean limit of ignition decreases and the maximum net energy available at the time of ignition is also decreased. Results from Experimental set-2: Used fuel injector- FDI igniter [65]

The hydrogen peroxide is known to release energy from its bonds when it dissociates. With the presence of the H_2O_2 at the zone where the ignition spark initiates, it is assumed that the hydrogen peroxide dissociates during the ignition

sequence. Because the exact amount of the dissociated hydrogen peroxide cannot be quantified a maximum for each case is calculated by using the known values of the H_2O_2 injection rate, the H_2O_2 injection time and the combustor residence time inside the combustor. It is clear from Figure 8.15 that the maximum available energy at the time of ignition was reduced dramatically even when there was H_2O_2 dissociation, at the lean ignition limits.

8.6 EVOLUTION OF EXHAUST TEMPERATURE AFTER IGNITION AT SIMILAR EQUIVALENCE RATIOS ϕ FOR DIFFERENT H_2O_2 INJECTION RATES

One physical quantity that should be affected by the ignition system and the H_2O_2 plasma is the exhaust temperature from ignition and after. If the reaction rate of the combustion is affected by the H_2O_2 addition, then it is expected that the temperature of the reaction and therefore the exhaust temperature will be affected in a proportional manner. Figures 8.16-8.18 are plots from random light-cases from the experimental set-2, where the equivalence ratio was very similar in value between the study cases, at the same air mass flow. Figures 8.19-8.21 again show the temperature increase from ignition against time from light-cases that were specially designed for this purpose, in experimental set-3. In the third set, temperature tests were conducted at a standard fuel flow rate of about 6.8kg/s for all the air mass flow rates studied, all the H_2O_2 settings and also for the experiment where water was used as an ignition additive. All the temperature data plotted below are averaged values between the readings of the two thermocouples that are situated at opposite positions at the end of Olympus test section near its walls. The difference in how the temperature of

the exiting gas evolves with time and therefore the reaction rate during ignition is visible in the graphs below. The results are discussed in Section 9.14.

8.6.1 RESULTS FROM EXPERIMENTAL SET-2 - USED FUEL ATOMISER

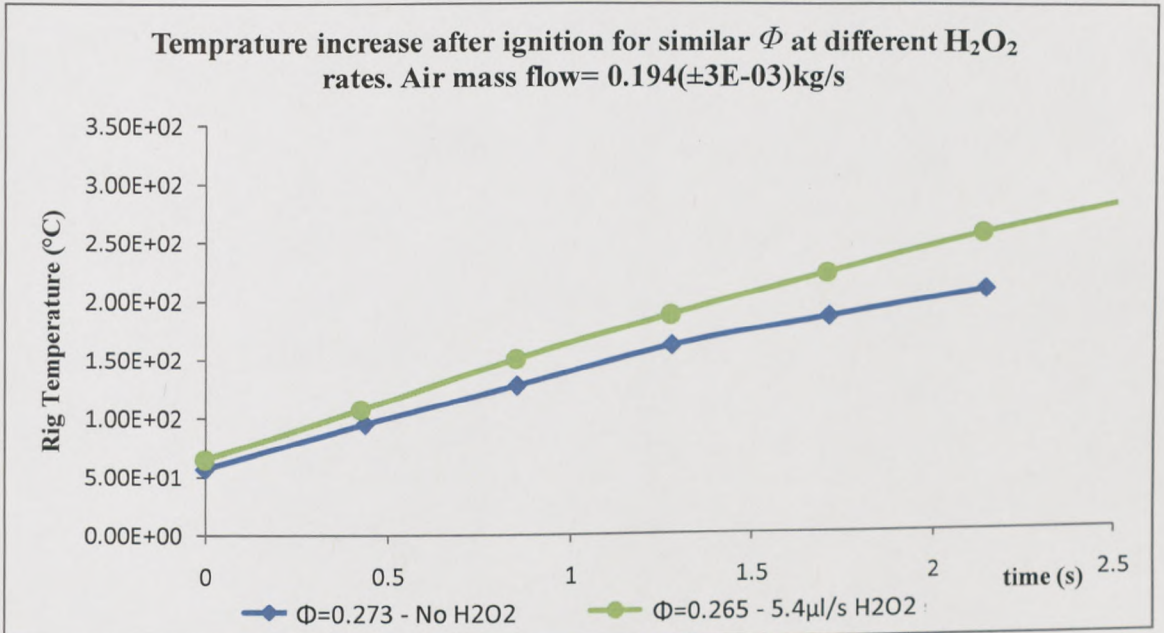


Figure 8.16: Comparison of average exhaust rig temperature evolution for similar equivalence ratios at $0.194(\pm 0.003)$ kg/s inlet air. The hydrogen peroxide ejection rates are 0μ l/s with equivalence ratio $\Phi=0.273$ and 5.4μ l/s with equivalence ratio $\Phi=0.265$ respectively for each plot. Experiments with a used fuel injector. Exp. set-2 [65]

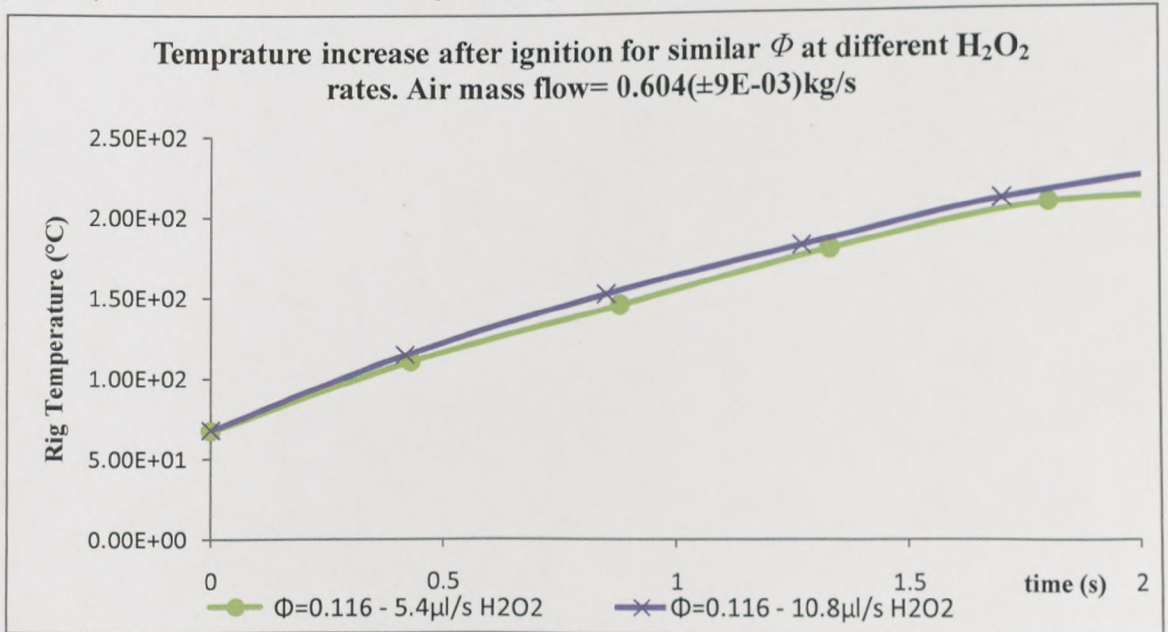


Figure 8.17: Comparison of average exhaust rig temperature evolution for similar equivalence ratios at $0.604(\pm 0.009)$ Kg/s inlet air. The hydrogen peroxide ejection rates are 5.4μ l/s with equivalence ratio $\Phi=0.116$ and 10.8μ l/s with equivalence ratio $\Phi=0.116$ respectively for each plot. Experiments with a used fuel injector- FDI igniter. Exp. set-2 [65]

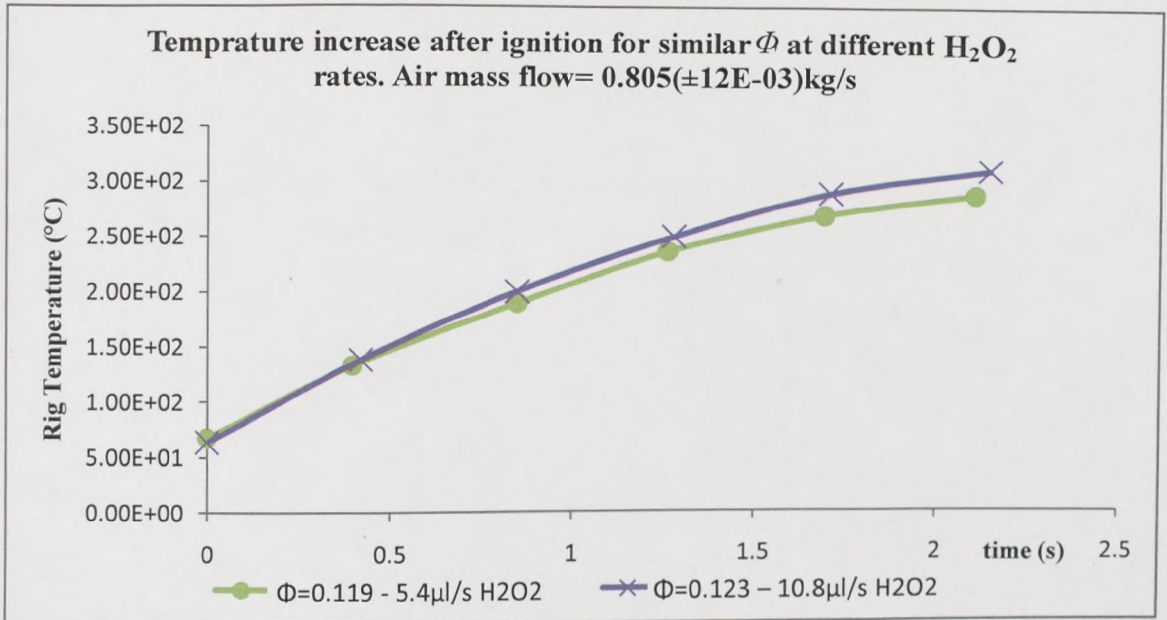


Figure 8.18: Comparison of average exhaust rig temperature evolution for similar equivalence ratios at $0.805(\pm 0.012)$ kg/s inlet air. The hydrogen peroxide ejection rates are $5.4\mu\text{l/s}$ with equivalence ratio $\Phi=0.119$ and $10.8\mu\text{l/s}$ with equivalence ratio $\Phi=0.123$ respectively for each plot. Experiments with a used fuel injector- FDI igniter. Exp. set-2 [65]

8.6.2 RESULTS FROM EXPERIMENTAL SET-3 - CLEAN FUEL ATOMISER

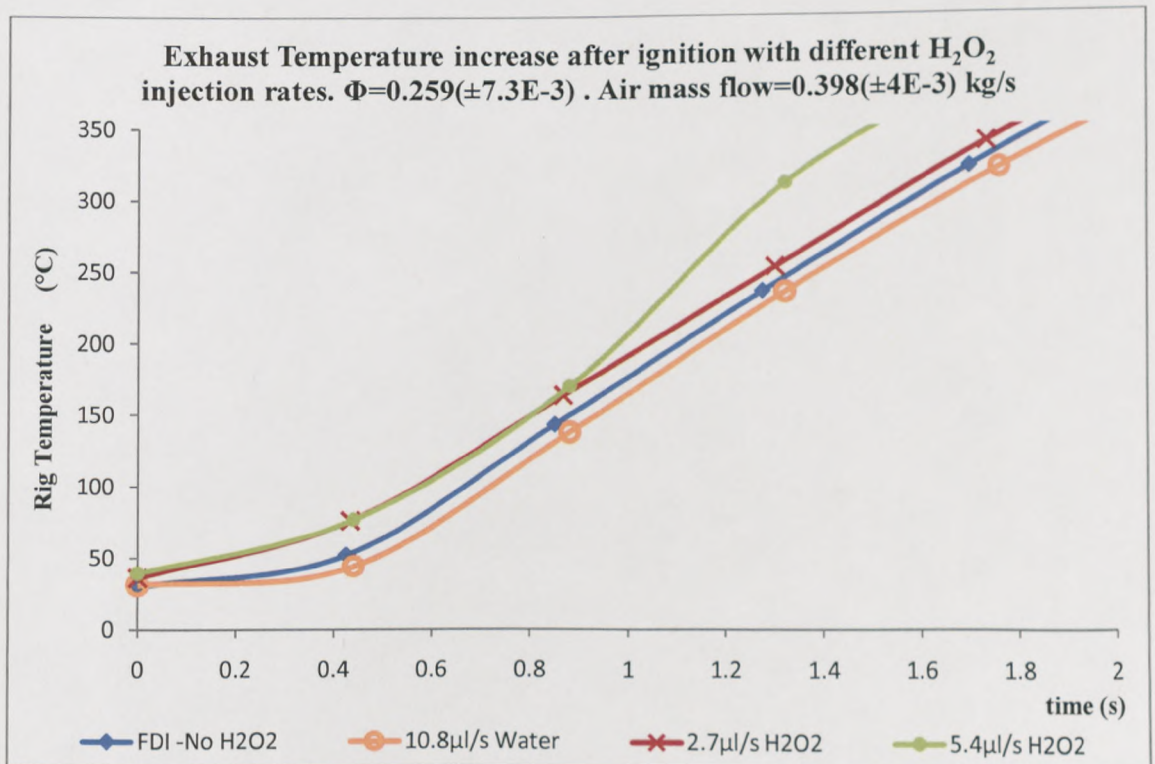


Figure 8.19: Comparison of average rig temperature evolution after ignition for similar equivalence ratios at about 0.395 kg/s air mass flow and at an equivalence ratio of about $\Phi=0.259$ of air-Jet A₁ mixture (by keeping the fuel flow at 0.0069 kg/s). Experiments are with $10.8\mu\text{l/s}$ water and with $0, 2.7, 5.4\mu\text{l/s}$ H_2O_2 injected into the igniter. The kerosene was injected using a clean fuel atomiser- FDI igniter. Exp. set-3

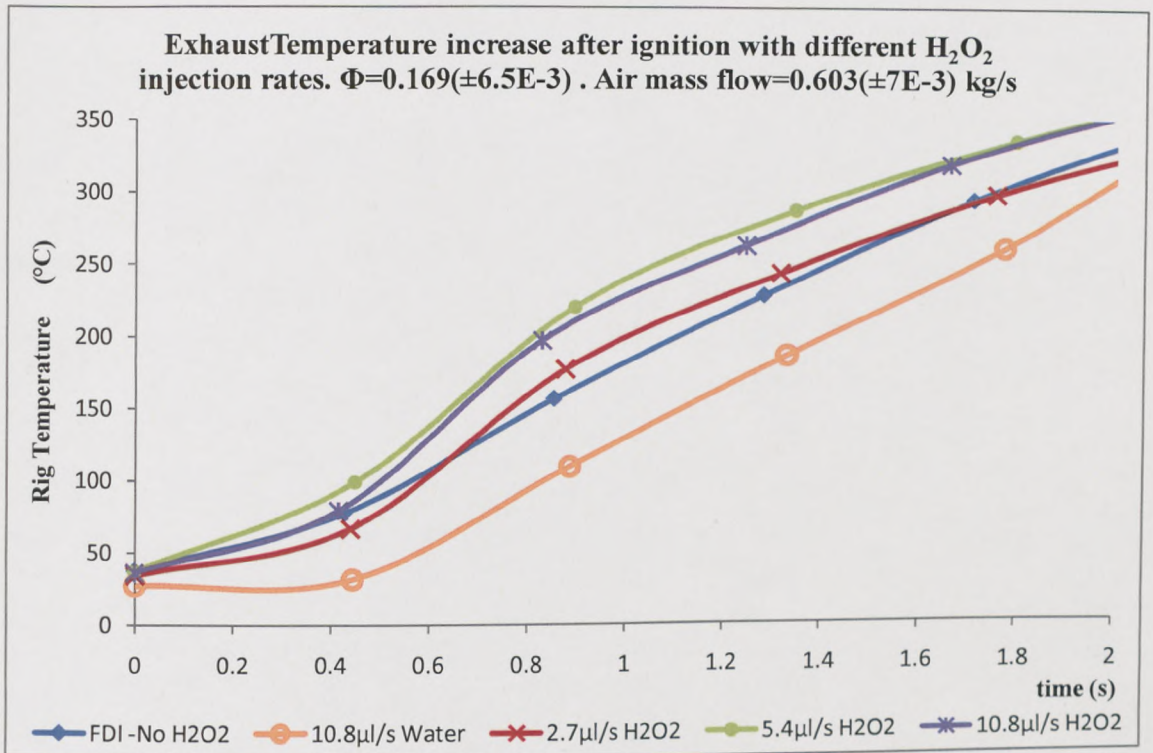


Figure 8.20: Comparison of average rig temperature evolution after ignition for similar equivalence ratios at about 0.603kg/s air mass flow and an equivalence ratio of about $\Phi=0.169$ of air-Jet A₁ mixture (by keeping the fuel flow at 0.0069kg/s). Experiments are with 10.8µl/s water and with 0, 2.7, 5.4µl/s H₂O₂ injected into the igniter. The kerosene was injected using a clean fuel atomiser- FDI igniter. Exp. set-3

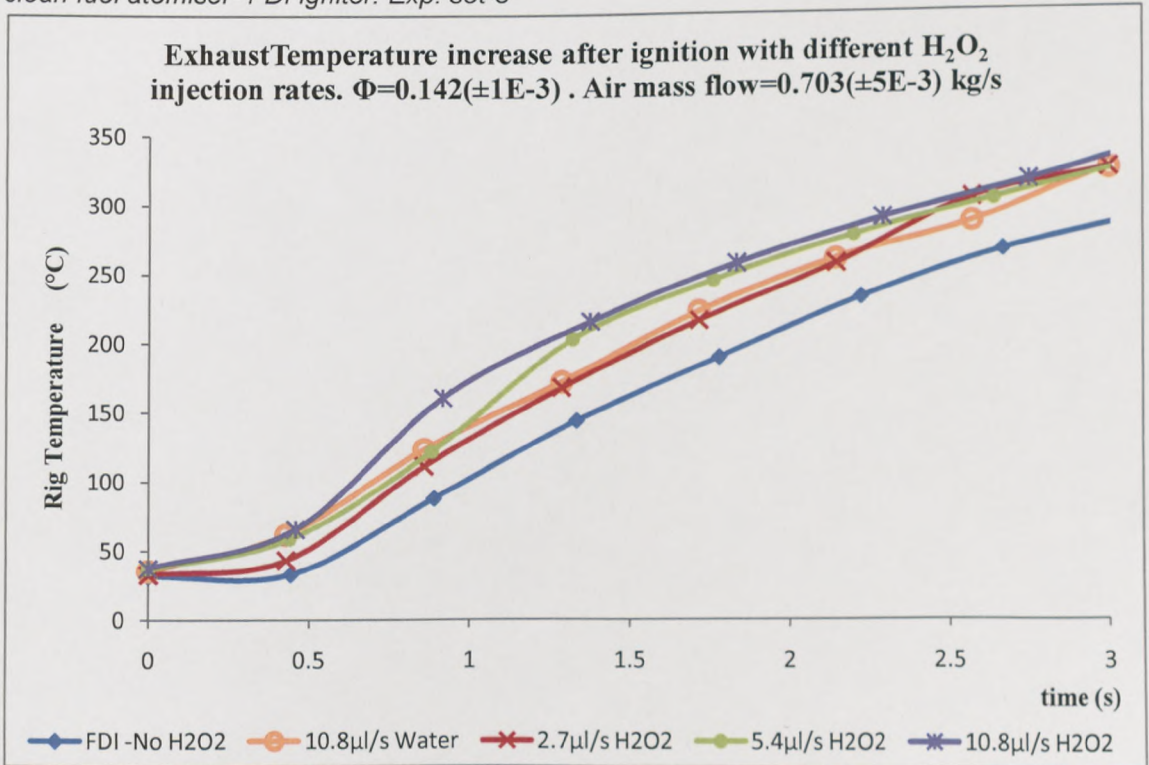


Figure 8.21: Comparison of average rig temperature evolution after ignition for similar equivalence ratios at about 0.703kg/s air mass flow and an equivalence ratio of about $\Phi=0.142$ of air-Jet A₁ mixture (by keeping the fuel flow at 0.0069kg/s). Experiments are with 10.8µl/s water and with 0, 2.7, 5.4µl/s H₂O₂ injected into the igniter. The kerosene was injected using a clean fuel atomiser- FDI igniter. Exp. set-3

PART-B - F.A.M.E. BIODIESEL TEST FUEL

8.7 LEAN IGNITION LIMITS OF F.A.M.E. BIODIESEL WITH AND WITHOUT H₂O₂ - EXPERIMENTAL SET-3 - CLEAN FUEL ATOMISER

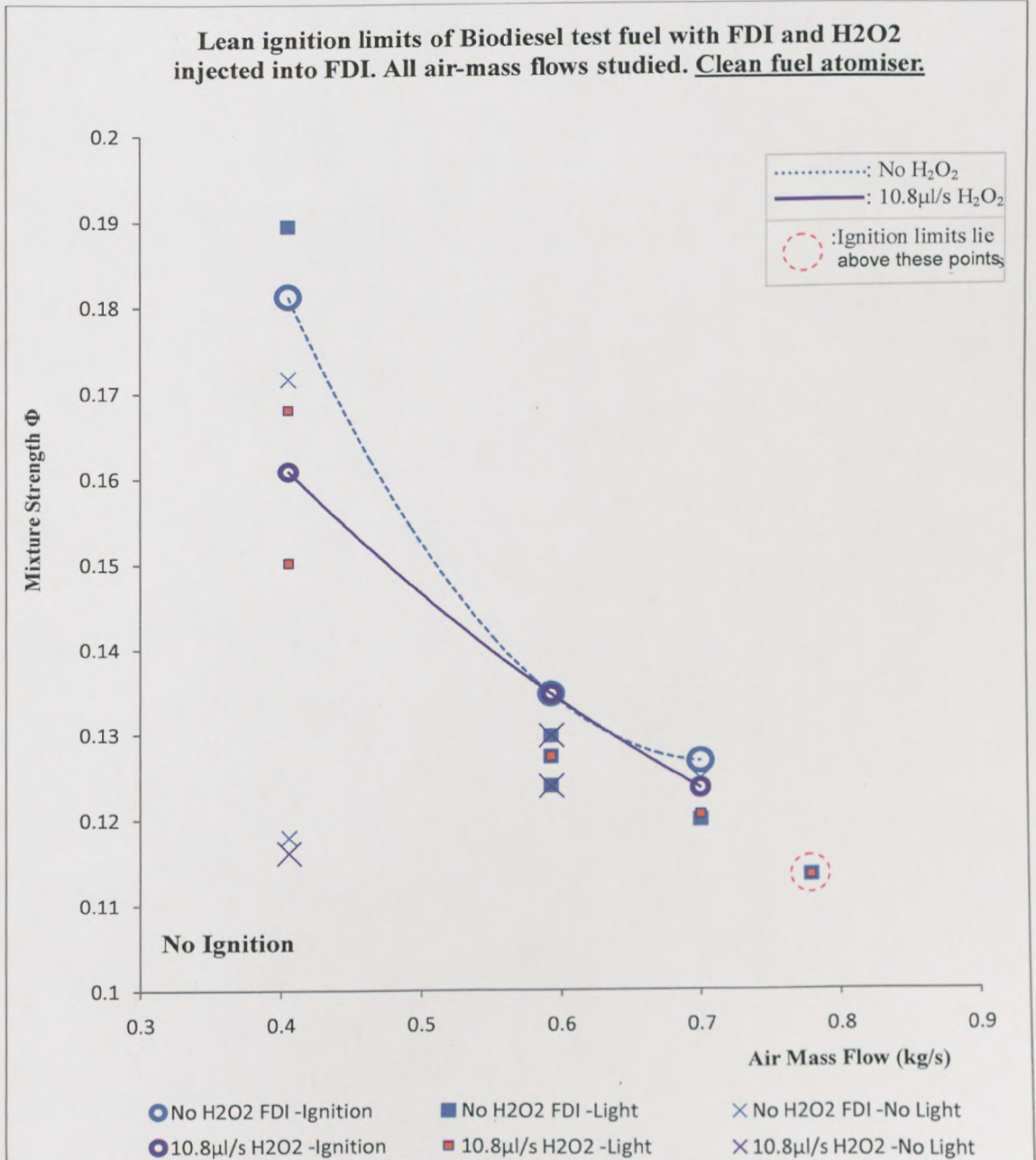


Figure 8.22: Lean ignition limits of F.A.M.E. Biodiesel test fuel for all air mass flow studied using the modified igniter with 0 and 10.8 μ l/s H₂O₂ additive injected into its cavity. The circles indicate the average of 3 consecutive successful ignitions (60% probability of ignition criterion) at the limit of ignition for each case. The red dashed circle indicates that successful ignitions were achieved for both cases and that the ignition limit lies above these points. Test conditions are ambient. Experimental set-3: Clean fuel atomiser- FDI igniter

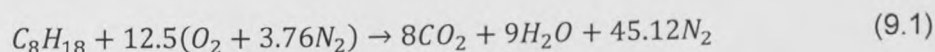
Figure 8.22 presents the results obtained from the ignition experiments that were carried using the F.A.M.E. (Fatty Acid Methyl Ester) Biodiesel test fuel in experimental set-3. The graph shows the behaviour of the lean ignition limits (in terms of fuel to air ratio f against air flow) of the biodiesel with $0\mu\text{l/s}$ and $10.8\mu\text{l/s}$ of H_2O_2 pumped into the modified focus discharge igniter. The air mass flow rates studied were 0.4 , 0.6 and 0.7kg/s . It can be seen in [Figure 8.22](#) that the lean limits were reduced by the use of the hydrogen peroxide for two of the three air mass flow rates studied.

DISCUSSION PART-A:

**IGNITION EXPERIMENTS IN THE STIRRED FAN REACTOR
(BOMB) - ISOOCTANE**

9.1 EQUIVALENCE RATIO ϕ CALCULATIONS FOR THE 'BOMB'
EXPERIMENTS

The stoichiometric burning of isooctane is chemically expressed by the following formula:



The equivalence ratio ϕ has the general equation:

$$\phi = \frac{\left(\frac{m_f}{m_{air}}\right)_{actual}}{\left(\frac{m_f}{m_{air}}\right)_{stoich}} \quad (9.2)$$

The calculations of the equivalence ratio, of the fuel to air mixture, involve the known quantity of the fuel to air pressure ratio. The experimental procedure that was followed, allowed for a manual recording of the partial fuel pressure inside the rig, by adding first the fuel and then the air into the vacuumed vessel. The total pressure of the vessel was pre-selected as near atmospheric as already mentioned in the experimental procedures (Section 5.1.4).

$$P_f + P_{air} = 1 \quad (bar) \quad (9.3)$$

Due to the pressure ratio being equal to its corresponding mole fraction, the equivalence ratio equation (9.2) is reduced to (9.4). Moreover the volume of the injected liquid fuel or its molar quantity could be calculated by noting that the density of the isooctane is known: $V_{C_8H_{18}} = \frac{m_f}{\rho_{C_8H_{18}}} = \frac{114.224n_f}{688} \cong 166 \times 10^3 n_f (ml)$.

$$\Phi = \frac{\left(\frac{n_f M_f}{n_{air} M_{air}} \right)_{actual}}{\left(\frac{M_f}{12.5 M_{air}} \right)_{stoich}} = \frac{12.5 n_f}{n_{air}} = \frac{12.5 P_f}{1 - P_f} \quad (9.4)$$

9.2 IMAGES OF THE PROPAGATION OF THE IGNITION FLAME

Shown in Figures 6.1-6.4 are pairs of images of the early stages of the initiated developing flame, with and without the addition of H₂O₂. Each set of photos is at same equivalence ratio and initial conditions. For Figure 6.1, the images were taken with the high speed cine camera running at 36000 frames per second, giving about 0.0278ms between frames. For Figures 6.2-6.4 the frame rate of the camera was decreased to 15000 frames per second, thus recording a photo at every ~0.0667ms.

Shown in Figure 6.1 is the highly reactive material of the propagating kernel, before it detaches from the igniter at about 0.16ms; with and without H₂O₂ addition. At this instance, ignition has not yet taken place and therefore the images are recorded inside the ignition delay time. The delay is mainly due to the lag of the kernel in detaching from the igniter tip (Section 4.6.3) and has been studied experimentally for isooctane in reference [85]. Observations of previous researchers have indicated that there is a path of ions between the

developing kernel and the igniter end (Section 4.7.1). This path will exist even when the kernel detaches from the igniter and the plum has substantially developed into an ignition flame (Figures 6.2-6.3). The path is preferred by the plasma ions because the hot medium created by the passing of the ignition kernel is clearly more conductive than the cold fuel-air mixture. In a dynamic situation of a gas-turbine, it is expected that the observed ion-path will disappear much faster than when it is observed in the 'bomb' (Section 4.7.4).

In Figures 6.1(a,b), each Schlieren image shows the reactive plasma at the very early stages of ignition ($t \sim 0.16\text{ms}$). In this instance, the igniter discharge has initiated the break-down of the spark that created small pockets of extremely active species inside the cavity of the igniter. These pockets release a rapid and dramatic increase in the temperature and the pressure of the medium, inside the FDI cavity (Section 4.7.1). A shockwave is also initiated as a result of the electromagnetic discharge of the igniter. The shockwave is captured to travel away from the igniter in each of the Figures 6.1(a,b) at time $t \sim 0.16\text{ms}$. Each captured shockwave is travelling with a speed of about 297.5m/s and 312.5m/s , that correspond to the 'no H_2O_2 ' and the H_2O_2 plasma ignition cases respectively. The difference in the velocity of the shockwave should mean that the energy released by the spark was higher in intensity at the same discharging time. Further, when comparing the two photos in Figure 6.1, one can see that the area of the highly reactive and highly charged plasma is much larger for the ignition case with the hydrogen peroxide addition. This observation favours the possibility that the intensity of the discharge was higher

for this case. Whatever the mechanism, it can be seen that there is some kind of enhancement due to the presence of the hydrogen peroxide during ignition.

In a later stage of the ignition process, Figure 6.2 shows a pair of photos of two ignition flames at an equivalence ratio of $\phi=0.71$, without and with the addition of H_2O_2 . In Figure 6.3(a) and (b) the same initial conditions were kept, as in Figure 6.2 but two different ignition attempts are shown. The time is stopped at about 6ms again from the time of the ignition initiation. Once more, it can be deduced that the propagating flame, initiated with the presence of the H_2O_2 , has a larger flame area compared to the 'no H_2O_2 ' case -when averaging and then comparing the relevant photos. Moreover it can be observed that in Figures 6.2(b) and 6.3(b), both flame fronts have travelled further away from the focus discharge igniter, than the comparing cases of 'no hydrogen peroxide' ignition. The break-away of the ignition flame from the igniter's tip is also seen, in both photographs (H_2O_2 ignition cases) to proceed with a faster rate, probably due to the momentum of the ignition kernel. Hence, the photographic results suggest that the velocity of the ignition kernel is faster due to the presence of the H_2O_2 additive and that the reaction rate of the ignition flame is higher for the ignition cases with H_2O_2 addition.

A closer inspection of Figure 6.2(c) reveals that between the ignition flame and the igniter end, there are some traces of liquid that travel slowly away from the igniter. These traces are also observed in Figure 6.4(c). The travelling liquid is surely a result of the placement of the H_2O_2 droplet above the igniter at the wire

fitment. The upward motion of this liquid should be due to the proximity of the liquid droplet above the cavity. The pressure difference that drives the plasma outward and particularly the momentum carried by the plasma into the path of the droplet -due to this driving force- will create some motion.

These 'flying' traces of fluid do not take any later part in the ignition process after the plasma passes through the H_2O_2 droplet. There is one main plausible reason that could explain this behaviour. The passing of the reactive plasma - created by the focus discharge igniter- through the H_2O_2 droplet, resulted in the dissociation of some of the hydrogen peroxide into H_2O with the other products being a combination of O_2 (oxygen) and O free radicals. The observed travelling liquid could be the water created during this process. The composition of the H_2O_2 throughout the 'bomb' experiments was a 60% by weight solution. In such concentration, the H_2O_2 is very unstable and therefore the decomposition of a droplet is quite possible.

The above behaviour was observed only when the H_2O_2 droplet was placed at the wire fitment above the igniter and not when the H_2O_2 was situated at the site where the spark breaks down (Figure 6.3(b)). It is suggested that this is due to the high reactivity of the spark, the high temperatures and pressures inside the cavity that will form a different plasma that will include all the H_2O_2 additive.

9.3 POST PROCESSING OF THE IMAGE DATA FOR THE FLAME RADIUS GROWTH CALCULATIONS

The Schlieren image data from the stirred fan reactor work were post-processed in order to calculate the flame radius growth, from the time of ignition until the flame boundaries expand away from the viewing window. The 'Find-Edge' program was used for post processing the images. This is a program that was created by R. Wooley [82] using Fortran 77. The role of the program is to calculate the number of white pixels in a black and white image. The user has to input the scaling characteristics of the image; i.e. how many pixels are equal to one millimetre in length.

Processing of each image prior to running the Find-Edge code was necessary in order to reduce the Schlieren image to a white coloured flame with black background. Processing was done using the Adobe Photoshop image processor. The boundaries of the flame front in each picture were drawn, using a black brush, by following the visible edges of the flame. Examples of this step are found in Figure 9.1. All pictures were later colour-burned, after completing the previous step for all pictures; i.e. the backgrounds were removed and the threshold was set to a pre-set value, enough to have the desired black and white effect. Examples of this step are found in Figure 9.2. The area inside the drawn perimeter was then filled with white paint. All steps after drawing the flame perimeter were done automatically using the record and play function of the Photoshop environment.

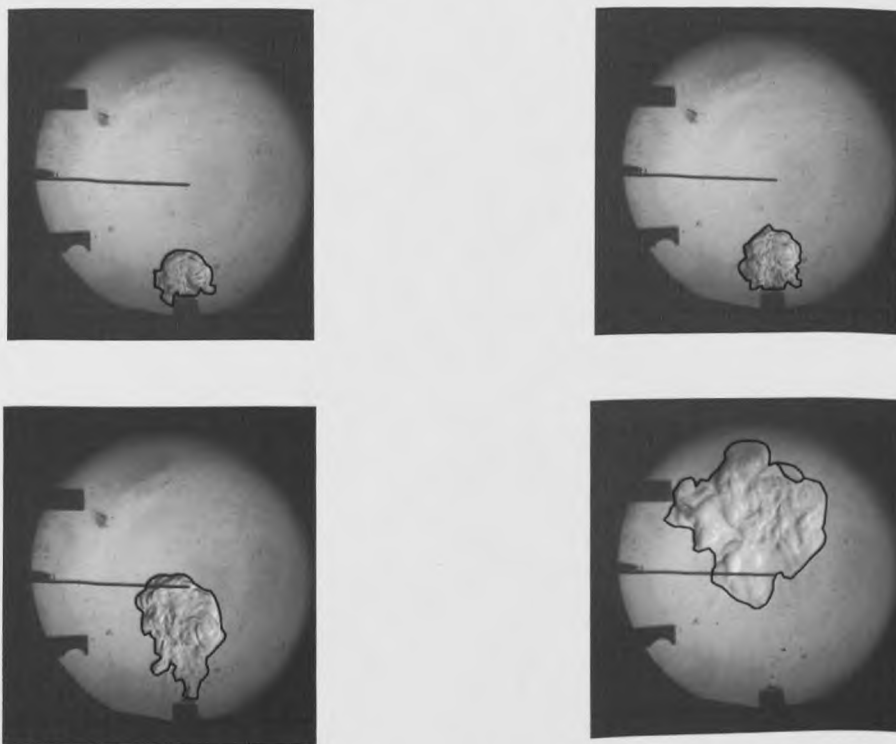


Figure 9.1: Examples of drawing the boundaries of an ignition flame front at different instances as it evolves.

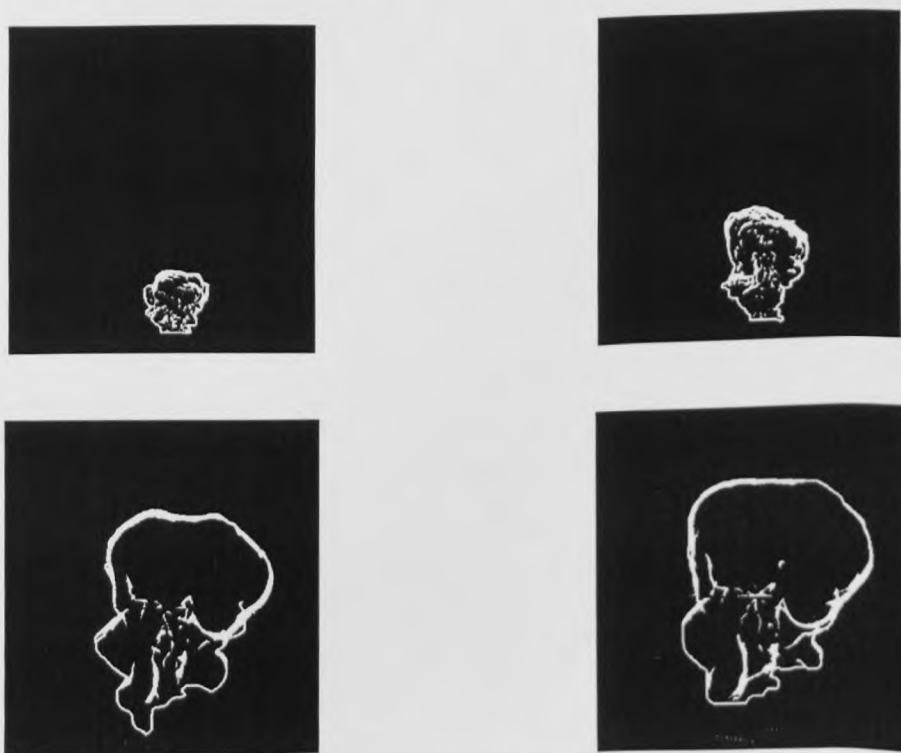


Figure 9.2: Examples of further processing of the image data. These pictures have been colour-burned so as to keep only a black background and the white trace of the boundary of the flame. The three dimensional characteristics of the flame are clearly visible.

By running the Find-Edge code, the program finds the area that the white pixels would occupy if they were connected together. It then calculates a flame radius by assuming that the calculated white pixel area describes the area of a circle. The flame area calculator is run for all the images selected for the study and therefore a flame area is measured for each instance of the development of the flame. Hence, the graphs in Figures 6.5 and 6.6 show the radius growth of flames that are assumed to be two-dimensional and circular.

9.4 FLAME RADIUS GROWTH

Figures 6.5 and 6.6 show the flame radius growth (in millimetres) against time for an isooctane-air mixture at equivalence ratios of $\phi=0.8$ and $\phi=0.6538$ respectively, with and without the addition of H_2O_2 . The plots show averaged values of at least two randomly selected cases of same initial conditions. In particular in Figure 6.5 ($\phi=0.8$) the ignition flame which was aided by the presence of the hydrogen peroxide shows an increase of a maximum of 12% in the growing flame radius, when compared to the no additive case at same times. For the $\phi=0.6538$ case (Figure 6,4), there is a maximum of 6% difference in the radius between the H_2O_2 and the no-additive ignition flames. Moreover, in In Figure 6.4 the green line slope expresses the average flame radius in time, when adding water instead of H_2O_2 . The flame that is created by the H_2O addition is growing slower than the two other cases by a maximum of 6.8%. Moreover Figure 6.6 shows the kernel growth when there is no fuel present in the 'bomb'. It is clear from this graph that without H_2O_2 addition the kernel develops at a slower pace. The maximum difference in the radius of the

developing ignition kernel, between the best H_2O_2 and the 'no H_2O_2 ' case and without the presence of isooctane, is about 12%. It can be deduced that the addition of the hydrogen peroxide affects the ignition process in a positive way and helps the reaction to proceed faster.

9.5 ERRORS IN THE FLAME RADIUS GROWTH CALCULATIONS

Due to the fact that the visual data are two-dimensional images of a three-dimensional flame, the error in the assumption that the flame is circular and flat, cannot be accounted for but it is bound to exist. However, due to the fact that the calculations for the hypothetical flame radius were done in the same way for all images that were processed and because the visual data were taken from the same angle, the assumption is considered valid for this initial study. On the other hand, the flame front is highly three dimensional and this is particularly true during the initiation period.

The drawing of the flame perimeter by hand, as it evolves, adds a human error factor to the calculations of the flame radius growth. This human error was minimised by processing the images in an ordered way; so as to make sure that the flame front was followed correctly.

Although the post-processing technique of the visual data (Section 9.3) involves two identifiable errors, it is considered more accurate compared to other methods, as it employs the pixel as a tool for dimensioning the flame. In general

these errors are difficult to be avoided by other imaging methods. Of course increasing the quality of the schlieren image or the pixel quality recorded by the camera increases the accuracy of the data.

9.6 STIRRED FAN REACTOR WORK – SUMMARY

The experimental method followed is considered acceptable for the initial study of ignition with the addition of H_2O_2 but no conclusive remarks can be drawn. The potential for the enhancement of ignition by the addition of small amounts of H_2O_2 has been clearly demonstrated in Figure 6.5. A better understanding of the plasma ignition process was gained and showed that the use of the hydrogen peroxide with the focus discharge igniter is feasible. A safety protocol on handling the hydrogen peroxide on confined spaces was created and successfully followed during the experiments. The need for decreasing the safety procedures and thus time and experimental costs, when moving to more complex experiments in an industrial facility, was stressed. Knowledge was also gained on the behaviour of the igniter that was later used to design the modifications described in Section 7.2.

DISCUSSION PART-B:

IGNITION EXPERIMENTS IN THE OLYMPUS GAS-TURBINE RIG - KEROSENE JET-A₁

9.7 DATA POST PROCESSING USING FORTRAN-95

9.7.1 PROGRAM 1 - EQUIVALENCE RATIO AND FUEL ENERGY CALCULATOR - POST PROCESSING

A program was written in fortran-95 to post process the data that were acquired by the Labview platform; the program which controlled the engine. The complete code for the post processing is shown in Appendix-B with explanatory comments for each step. The program serves two main purposes: To sort the data according to the experiments and to commence the required calculations.

9.7.2 SORTING THE DATA

The raw data were recorded initially in a matrix format by Labview. Each initial data file corresponds to a single hydrogen peroxide volume rate setting for each experimental set. Each column in this file represents a single function and each row represents a forward step in time. The data collected by Labview, in order of appearance in the data file, are: time, atmospheric pressure, inlet air mass flow rate, orifice ΔP , upstream air temperature, fuel flow rate, temperature (thermocouple 1), temperature (thermocouple 2), ΔP , Pump On, Pump Off.

At first, the calculator reads the data file and counts the rows of zeros as M . Each zero row corresponds to a different ignition experiment (or else ignition attempt). The data between the zero rows represent the data of a single experiment that start from zero. The number of data points is also recorded as a function of the experiment number: $K(M)$. The program assigns a function of dimensions $(M, K(M))$ to each column, to name the values. Hence, if A is the number of rows in the initial data matrix then $[M \times K(M)] = [1 \times A]$.

FINDING THE IGNITION POINT AND THE H_2O_2 VOLUME PUMPED TO IGNITION

There are two important rows of data for each experiment. These are the point of ignition and the point when the hydrogen peroxide pump starts.

The ignition point or row $iK(M)$ is determined by searching the temperature data and by finding a sudden temperature increase. This temperature increase should be higher than the recorded temperature at two time steps backwards plus $5^\circ C$.

The row, in the data matrix, where the hydrogen peroxide pump is turned-on, for each ignition experiment, is easily found by mining the point where the $PUMPon(M)$ function changes from 0 to 1. This row number is recorded as a function of the ignition experiment number: $oTH_2O_2(M)$. The total volume of the

hydrogen peroxide that is injected at the time of ignition can be calculated by deducting the time at $iK(M)$ from $oTH_2O_2(M)$ and by using the pump calibrations of Section 7.5, depending on the pump volume rate setting.

CALCULATIONS

The calculations are done by the program in order to determine the equivalence ratio and the system's available (chemical) net energy at the time of ignition, for each ignition attempt. The derivations for the equations used are explained in detail in Sections 9.8 and 9.12.1. It should be noted that there are one equivalence ratio $FI(M)$ and two available (chemical) net energy values $TotEN(M)$ and $TotEN2(M)$ that correspond to each of the M ignition experiments.

9.7.3 **PROGRAM 2** - TEMPERATURE INCREASE AFTER IGNITION AT SIMILAR EQUIVALENCE RATIOS - POST PROCESSING

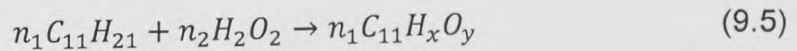
A similar to the above (Section 9.7.2), but more complex, program was devised to search the initial data files for similar equivalence ratios ϕ , only at a similar air mass flow rates (Appendix C). This program is more complex because the search to find similar equivalence ratios cases, involves processing all the initial data files of one experimental set. The program was used only in experimental set-2 because in set-3 a more dedicated experimental procedure was devised to study the temperature increase after ignition at almost same equivalence ratios but at different H_2O_2 injection rates. Set-1 was not included in this study

because of the continuous steady H_2O_2 injection (CSI) procedure that was followed (Section 7.1.1).

Hence the program does the following: It first reads all the initial data matrixes and sorts the order of the data. Afterwards, it does the required calculations in a similar way as the previous program and finds the experiments that, at ignition, have similar equivalence ratio ϕ values. Finally it writes to the output file the temperature increase, in each experiment, from the time of ignition until the data end. It sorts the order of the output data according to the ϕ values from larger to smaller. The program writes in the output file the following data in order of appearance: experiment number, H_2O_2 pump rate setting, time (from ignition), temperature, Equivalence ratio and air mass flow rate. The H_2O_2 pump rate setting is determined by the file that the program writes. The equivalence ratio function FI and other functions that are unique for each experiment have dimensions (M,K(M),MD), with M being the experiment no, K(M) the data number of the experiment M and MD the hydrogen peroxide rate setting.

9.8 EQUIVALENCE RATIO CALCULATIONS

The simplified chemical formula of $C_{11}H_{21}$ [84] is considered as an acceptable approximation for the Jet A₁ kerosene fuel. Since the hydrogen peroxide is highly flammable, in order to calculate the new equivalence ratio, the amount of H_2O_2 that was injected into the combustor was counted as extra hydrogen and oxygen to the original kerosene fuel. In other words the kerosene was assumed to be enhanced by the H_2O_2 additive:



$$x = 21 + 2 \frac{n_2}{n_1} \quad , \quad y = 2 \frac{n_2}{n_1}$$

The mass flow rate of the kerosene fuel is $\dot{m}_f = 153 \dot{n}_1$ (kg) and the volume rate of the infused hydrogen peroxide is $\dot{V}_{H_2O_2} = 34 \frac{\dot{n}_2}{0.59} \times 10^6$ (μ l). Taking the mass of the enhanced fuel $m_f = n_1(132 + x + 16y)$ (kg), the mass of air needed for stoichiometric burning of this fuel can be calculated as $m_{air} = 137.28 n_3$ (kg), with $n_3 = n_1(11 + \frac{x}{4} - \frac{y}{2})$ (kmol). In this case the equivalence ratio with the general expression $\Phi = \frac{[\frac{m_f}{m_{air}}]_{Actual}}{[\frac{m_f}{m_{air}}]_{Stoich}}$ will be:

$$\Phi = \frac{\frac{\dot{m}_f}{\dot{m}_{air Actual}}}{\frac{m_f}{m_{air stoich}}} = \frac{\frac{\dot{m}_f + \dot{m}_{H_2O_2}}{\dot{m}_{air Actual}}}{\frac{132 + x + 16y}{137.28(11 + \frac{x}{4} - \frac{y}{2})}} \quad (9.6)$$

It should be noted that the mass of hydrogen peroxide $\dot{m}_{H_2O_2}$ used in all calculations here was taken as the half of the total mass infused; because of the 50% by weight liquid solution of H_2O_2 in water. The density was given by the manufacturer as $\rho_{H_2O_2} = 1.18 \text{ kg/l}$.

9.9 IGNITION LIMITS OF KEROSENE JET-A₁

9.9.1 EXPERIMENTAL SET-1 – USED FUEL INJECTOR AND CONTINUOUS STEADY H₂O₂ INJECTION (CSI)

Figure 8.1 is a summary of the results acquired in experimental set-1. Shown in this Figure are the ignition limits of the kerosene Jet-A₁ fuel by using a Surface discharge igniter and the modified focus discharge igniter (FDI), with and without H_2O_2 . These limits are found using the 60% probability of ignition criterion out of a total of 5 ignition attempts. In the modified FDI, H_2O_2 is continuously injected into the cavity of the igniter at $0 \mu\text{l/s}$ and $0.54 \mu\text{l/s}$ volume rates. Each circle indicates the equivalence ratio ϕ that represents one ignition limit (60% probability of ignition criterion), for each air mass flow rate studied. The crosses represent failed ignition attempts and the squares show all other attempts where combustion was initiated (light attempts) but were either above the lean limit or, if below, did not pass the 60% probability of ignition criterion. Hence, each point in the graph represents at least three ignition attempts and indicates the average value of the corresponding equivalence ratios ϕ . The tests were conducted using the engine's standard fuel injector being in 'under normal service' state; hence, it is herein called a 'used fuel injector'. The experiments are conducted under ambient conditions.

Between the SDI (surface discharge igniter) and the modified FDI (focus discharge igniter) with 'no hydrogen peroxide' cases, the difference in terms of ignition performance is found small. At three of the four air mass flow rates studied, the difference in the ignition limits of the kerosene fuel lies between 0.5 to 6% and therefore is considered insignificant. It is only at a high air mass flow, where ignition is considered more difficult, that the difference in performance between the two igniters is visible. This difference is about 21% in favour of the modified focus discharge igniter (FDI), at an air mass flow of about 0.7kg/s. Hence, the modified FDI is at least as efficient as the widely used surface discharge igniter and in some cases a little bit superior, as it is capable of igniting more turbulent mixtures. This observation is relevant because of two important reasons:

- It shows that by changing the standard igniter to the modified FDI, without H_2O_2 , the performance of the engine is not compromised.
- It provides an indirect route for comparison between the performances of the modified FDI and the SDI (the standard engine's igniter) and thus, eliminates the need for repeating the ignition tests with the SDI in the other experimental sets.

More importantly, the graph in Figure 8.1, indicates that a marked improvement in the ignition limits of the Jet-A₁ fuel was achieved by the use of the hydrogen peroxide additive. Table 9.1 (above) summarises the ignition limits that were found in the first experimental set when using the modified focus discharge

igniter with and without hydrogen peroxide addition. In particular the ignition limits of the kerosene fuel were reduced by a maximum of 33.9% in terms of equivalence ratio Φ , when continuously pumping (CSI) 0.54 μ l/s of hydrogen peroxide into the modified igniter. The results show that the ignition process was positively affected by the introduction of the hydrogen peroxide to the site where the spark initiates. It should be stressed how such a large improvement in the ignition performance was achieved by such a low additive infusion rate.

Inlet Air mass flow rate (kg/s)	FDI – 0 μ l/s H ₂ O ₂ Lean Limits in Φ	FDI – 0.54 μ l/s H ₂ O ₂ Lean Limits in Φ	% Ignition Improvement in Φ
0.199 (\pm 0.004)	0.2318 (\pm 2E-4)	0.1787 (\pm 1E-4)	22.907%
0.405 (\pm 0.001)	0.1598 (\pm 2E-4)	0.1224 (\pm 4E-4)	23.404%
0.6 (\pm 0.003)	0.133(\pm 3E-4)	0.0879 (\pm 1E-4)	33.9%
0.802 (\pm 0.003)	0.1405 (\pm 4E-4)	0.1358 (\pm 8E-4)	3.345% *

Table 9.1: Ignition improvement in the lean limits of the kerosene Jet-A₁ fuel in terms of mixture strength Φ . Experimental Set-1 with 0 and 0.54 μ l/s of H₂O₂ injected into the cavity of the modified focus discharge igniter. Summary of Figure 8.1. Test conditions are ambient. (*There is uncertainty in the improvement of this point due to a piece of tube that broke away from the cavity of the igniter. See also section 9.13 and Appendix A

9.9.2 EXPERIMENTAL SET-2 – USED FUEL INJECTOR AND CONTROLLED CONTINUOUS STEADY H₂O₂ INJECTION (CCSI)

Figure 8.2 and Figures 8.7-8.10 show the lean ignition limits of the kerosene Jet-A₁ fuel that were found by experimental set-2. Figures 8.7 to 8.10 shows the lean limit of ignition with 0, 2.7, 5.4 and 10.8 μ l/s (CCSI) H₂O₂, each at 0.194(\pm 0.003), 0.409(\pm 0.008), 0.604(\pm 0.009) and 0.805(\pm 0.012)kg/s air mass flows rates respectively. Figure 8.2 is a graphical summary of all ignition results for all the air mass flows stated. The limits are represented by circles and these were found experimentally using the 60% probability of ignition criterion out of a total of 5 attempts –thus there are three circles for one ignition limit. These are expected to coincide or to be very close as it is shown in Figure 8.2(b) and Figures 8.7 to 8.10. The crosses represent failed ignition attempts and the squares show all other attempts where combustion was initiated (light attempts) but were either above the lean limit or, if below, did not pass the 60% probability of ignition criterion. For the reader's convenience the results are also shown in average values of ϕ (equivalence ratios) against air mass flows in Figure 8.2(a). The tests were conducted using the engine's standard fuel injector being in an 'under normal service' state; hence, it is called a 'used fuel injector', as in experimental set-1.

One can observe in all Figures 8.7-8.10 that the presence of the H₂O₂, at the site where ignition takes place, has resulted in the lowering of the fuel-air mixture strength ϕ which is required for sustainable ignition. In other words:

- A small amount of additive has aided the ignition process at equivalence ratios much lower than the normal lean limit.

In particular, in Figure 8.7 at an air mass flow of $0.194(\pm 0.003)$ kg/s the lean ignition limit with no additive was at an equivalence ratio of $0.2736(\pm 8E-04)$. By changing the hydrogen peroxide rate, at intervals of 2.7, 5.4 and $10.8\mu\text{l/s}$ for each case, the limit was changed to $0.2348(\pm 5E-04)$, $0.218(\pm 14E-04)$ and $0.2168(\pm 3E-04)$ respectively. Thus the result, which can be seen in Figure 8.7, is at least a 20% improvement in the ignitability limit by the insertion of 5.4 and $10.8\mu\text{l/s}$ of hydrogen peroxide. A summary of the graphs in Figures 8.7-8.10 for the four air mass flow cases can be found in Table 9.2 and as a graphical representation in Figure 8.2(a) (or 8.2(b) in non-averaged values).

Furthermore the ability of the modified FDI to ignite fuel mixtures which would otherwise not ignite is emphasized in Table 9.2. Even with only the addition of small volumes of hydrogen peroxide, there was considerable improvement achieved in the ignition system.

- With the presence of hydrogen peroxide as a plasma medium, the same igniter can achieve ignition at lower lean limits and at higher air flows.

Moreover, at higher air flows, where the energy losses are increasing with turbulence, the differences in the igniter performance become more enhanced. Normally increasing the air mass flow -hence the velocity inside the combustor- would resolve in a richer mixture with a higher burning velocity being needed. Figure 8.2(a) and Figures 8.7-8.10 show that:

- With the addition of the hydrogen peroxide at ignition, the mixture strength was decreased by at least 20% even at increased air mass flow rates.

- The results indicate without doubt an enhancement effect that originates to the fact that liquid hydrogen peroxide was added into the ignition mechanism.

Air mass Flow (kg/s)	H ₂ O ₂ volume rate (μl/s)	Lean ignition limit in Φ	% Ignition improvement in Φ
0.194(±0.003)	0	0.2736(±8E-04)	-
0.194(±0.003)	2.7	0.2348(±5E-04)	14.181%
0.194(±0.003)	5.4	0.218(±14E-04)	20.322%
0.194(±0.003)	10.8	0.2168(±3E-04)	20.76%
0.409(±0.008)	0	0.1515(±16E-04)	-
0.409(±0.008)	2.7	0.1417(±3E-04)	6.469%
0.409(±0.008)	5.4	0.141(±4E-04)	6.93%
0.409(±0.008)	10.8	0.137(±1E-04)	9.57%
0.604(±0.009)	0	0.1605(±2E-04)	-
0.604(±0.009)	2.7	0.1133(±17E-04)	29.408%
0.604(±0.009)	5.4	0.1159(±6E-04)	27.788%
0.604(±0.009)	10.8	0.0901(±1E-04)	43.863%
0.805(±0.012)	0	0.158(±3E-04)	-
0.805(±0.012)	2.7	0.1154(±4E-04)	26.962%
0.805(±0.012)	5.4	0.1159(±18E-04)	26.645%
0.805(±0.012)	10.8	0.1252(±7E-04)	20.759%

Table 9.2: Ignition improvement in terms of fuel mixture strength Φ at the lean ignition limits. Summary of Figures 8.7 to 8.10, each corresponding to a different air mass flow rate case. Experimental set-2- used fuel injector. Test conditions are ambient [65]

When comparing between the injection rates of $2.7\mu\text{l/s}$ and $5.4\mu\text{l/s}$ in Figure 8.2(a), the differences in the improvement of the ignition limits tend to become small as the air mass flow rate is increased. In the same Figure, the $10.8\mu\text{l/s}$ H_2O_2 injection rate contributes to a significant improvement of about 44% of the ignition limit at about 0.604kg/s of the engine's air mass flow. On the other hand, at the lowest air mass flow (about 0.194kg/s), the same H_2O_2 injection rate of $10.8\mu\text{l/s}$ does not produce a significant enhancement (stays to about 20%) in the ignition limit when compared with the lower H_2O_2 injection rate of $5.4\mu\text{l/s}$. Moreover, at the highest air mass flow (about 0.805kg/s) the $10.8\mu\text{l/s}$ H_2O_2 injection rate is less efficient than the two other H_2O_2 injection rates.

- This behaviour suggests that there is an optimum combination of hydrogen peroxide injection rate and engine's air mass flow rate.

9.9.3 EXPERIMENTAL SET-3 – CLEAN FUEL INJECTOR AND CONTROLLED CONTINUOUS STEADY H_2O_2 INJECTION (CCSI)

Figure 8.3 and Figures 8.11-8.14 show the lean ignition limits of the kerosene Jet-A₁ fuel that were found by experimental set-3. Figures 8.11 to 8.14 shows the lean limit of ignition with 0, 2.7, 5.4 and $10.8\mu\text{l/s}$ (CCSI) H_2O_2 , each at $0.398(\pm 0.004)$, $0.603(\pm 0.007)$, $0.709(\pm 0.005)$ and $0.776(\pm 0.001)\text{kg/s}$ air mass flows rates respectively. Figure 8.3 is a graphical summary of all ignition results for all the air mass flows stated. The limits are represented by circles and these were found experimentally using the 60% probability of ignition criterion out of a total of 5 attempts. The crosses represent failed ignition attempts and the squares show all other attempts where combustion was initiated (light attempts)

but were either above the lean limit or, if below, did not pass the 60% probability of ignition criterion. There are at least three ignitions attempts shown in each point in the graphs, as in experimental set-1. The equivalence ratio ϕ was averaged for these graphs although the fuel injector was controlled automatically. The automation of the fuel injection allowed for better precision on the fuel rate for each of the ignition attempts that represent one point in the graph. The differences between the equivalence ratios of each point in the plots are very small. In this case a standard error is introduced of 1E-04 to show that the results are accurate up to the fourth decimal point (it should be added that the fuel reading was taken in grams per second). Therefore there was no need for averaging the equivalence ratio values in this case. Moreover, the tests were conducted using the engine's standard fuel injector just after being serviced; hence, it is called a 'clean fuel injector'. The experiments were conducted under ambient conditions. From the relevant Figures:

- It should be highlighted that the use of the clean fuel injector alone, has resulted in reducing the lean ignition limits to very low values of mixture strengths ϕ .

Even the lowest ignition limits, found in experimental set-2 by the use of the H₂O₂ additive, could not reach so low values such as the ones achieved by the FDI igniter without H₂O₂ in experimental set-3. In particular the best ignition performance in experimental set-2 (used fuel injector) was achieved at an air mass flow rate of 0.604(±0.009) where the ignition limit was found at a mixture strength of 0.0901(±1E-04) (10.8µl/s H₂O₂ injection case, Table 9.2). At a

similar mass flow rate of $0.603(\pm 0.007)$, in experimental set-3 (clean fuel injector), the ignition limit without H_2O_2 was found at a mixture strength of $0.0682(\pm 1.3E-04)$ (Table 9.3). The difference in ϕ is $\sim 24\%$. Furthermore, at the same mass flow rate, in the clean fuel injector case, the ignition limit was reduced further by up to about 20% ($\phi = 0.0545$), by injecting $10.8\mu\text{l/s}$ of the H_2O_2 medium into the igniter.

In all Figures 8.11-8.14, it can be observed that the presence of the H_2O_2 , at the site where ignition takes place, has resulted in the reduction of the fuel-air equivalence ratio ϕ which is required for sustainable ignition. It follows that:

- Even at such low mixture strengths ϕ , a small amount of H_2O_2 additive has enhanced the ignition process to equivalence ratios lower than the lean limit set without the H_2O_2 additive.
- A maximum improvement of 11% to 20% is shown to be possible by using the modified FDI igniter with a H_2O_2 plasma injection of $10.8\mu\text{l/s}$, depending on the air mass flows used, at the highest FSQ.

The performance of the igniter increases by increasing the hydrogen peroxide rate of the pump and we anticipate a higher improvement in the lean ignition limits by increasing the H_2O_2 injection rate even further. This would be an interesting future study at such very low fuel to air ratios.

Once again, the highest improvement in terms of lean ignition limits is experienced at the 0.6kg/s air mass flow rate. This persistent result could be a good guide for future experiments:

- It suggests that if one ignition system out-performs a different system at the ~0.6kg/s air mass flow rate, with kerosene Jet-A₁ as the fuel, then it is in overall a more efficient ignition system (for the Olympus liner).
- With this suggestion in mind, there is potential to cut the experimental costs to a high extent. Lower costs could encourage the testing of more ideas in the Olympus experimental gas turbine.

Air mass Flow (kg/s)	H ₂ O ₂ volume rate (μl/s)	Lean ignition Limits in Φ	% Ignition Improvement in Φ
0.398(±0.004)	0	0.098(±1E-04)	-
0.398(±0.004)	2.7	0.095(±1E-04)	3.061%
0.398(±0.004)	5.4	0.0899 (±1E-04)	8.265%
0.398(±0.004)	10.8	0.087(±1E-04)	11.224%
0.603(±0.007)	0	0.0682(±1E-04)	-
0.603(±0.007)	2.7	0.0599(±1E-04)	12.17%
0.603(±0.007)	5.4	0.0589(±1E-04)	13.636%
0.603(±0.007)	10.8	0.0545(±1E-04)	20.088%
0.703(±0.005)	0	0.0674(±1E-04)	-
0.703(±0.005)	2.7	0.0683(±1E-04)	-1.335%
0.703(±0.005)	5.4	0.0601(±1E-04)	10.83%
0.703(±0.005)	10.8	0.0584(±1E-04)	13.353%
0.776(±0.001)	0	0.0771(±1E-04)	-
0.776(±0.001)	2.7	-	-
0.776(±0.001)	5.4	0.0733(±1E-04)	4.928%
0.776(±0.001)	10.8	0.0637(±1E-04)	17.38%

Table 9.3: Ignition improvement in terms of fuel mixture strength Φ at the lean ignition limits. Summary of Figures 8.11 to 8.14, each corresponding to a different air mass flow rate case. Experimental set-3- clean fuel injector. Test conditions are ambient

It should be highlighted that in the lean ignition limits obtained in experimental set-3 (shown in Figure 8.3 and Figures 8.11-8.14, summarised in Table 9.3), the differences between the equivalence ratios at same air mass flow rates are very small (between the second and third decimal). However, it should be pointed that a more sophisticated plasma igniter with a dedicated hydrogen peroxide delivery system, supplying an optimum rate of H_2O_2 medium at an optimum position inside the igniter, should be more efficient than the current modified igniter. From the low ϕ values of the ignition limits in Table 9.3 it can be deduced that:

- There is limited space for improving the lean ignition limits at high fuel spray qualities (FSQ)

Furthermore, looking at the differences between the ignition limits, of experimental set-2 and set-3, one realises that the limits are very subjective. In theory they depend on the overall combustor aerodynamics, the diffuser, the primary aerodynamic zone, the fuel, the fuel spray quality (FSQ), the atmospheric conditions and the igniter unit. The results of experimental-set 1 imply that the placement of the additive into the optimum location inside the cavity of the igniter is crucial to extract extra performance (conclusion discussed in Section 9.13). The cleaning of the fuel atomiser part, improves greatly the characteristics of the whole combustor system. It follows that:

- In general, the whole combustor system is very prone to changes and this is indicated by experimental set-2 and set-3.

- In the case of the hydrogen peroxide injection during ignition, it is positive to note that, the novel igniter exhibits higher performance as the fuel spray quality (FSQ) deteriorates, with only a low injection flow rate of H_2O_2 additive in the order of $\mu\text{l/s}$ (this conclusion is discussed in Section 9.10.2).

9.10 THE EFFECT OF THE FUEL SPRAY QUALITY (FSQ)

9.10.1 FUEL SPRAY QUALITY (FSQ) WITH 'NO H_2O_2 ' PLASMA IGNITION

Figure 8.4 shows how the fuel spray quality affects the lean ignition limits of the kerosene Jet-A₁ fuel when using the modified igniter with $0\mu\text{l/s}$ of H_2O_2 , in the Rolls Royce Olympus combustor testing facility.

The experimental sets were spaced between long periods of time. During this time other experiments were conducted in the gas-turbine rig. It is safe to assume that at each set the fuel atomiser is at a different 'used' state and that the fuel spray quality (FSQ) will depend mostly on the device's condition and less on the atmospheric conditions; the tests were all conducted during winter time and the air was heated externally before entering the combustor. Using this assumption and looking at the ignition limits of Figure 8.4, it can be deduced that the quality of the fuel spray was at its lowest when conducting the experimental set-2. Moreover, experimental set-3 was conducted just after servicing the fuel atomiser and therefore the FSQ is considered to be at its highest possible.

Most importantly, the plot in Figure 8.4 shows that the ignition behaviour of a fuel is largely different between a low and a high fuel spray quality case. As mentioned in Chapter 4, the fuel spray quality (FSQ) is a key parameter in producing a uniform, well mixed fuel-air fluid. As the FSQ decreases, the ignitability of the mixture is bound to decrease. The quality of the fuel spray may deteriorate because of two main reasons: a) Partial or total blockage of all or some of the nozzle veins of the fuel injector as the device reaches service time. b) Low pressures at high attitudes that affect the spray distribution quality.

It is interesting to compare the lean ignition limits of each experimental set with set-2 (which is assumed as the lowest FSQ case) at the ~ 0.4 and ~ 0.6 kg/s inlet air rates when not injecting H_2O_2 into the modified focus discharge igniter (Figure 9.3(b)). Figure 9.3(a) is a plot of the differences in the improvement of the ignition limits when comparing set-1 with set-2 (points 1 and 2 in the graph) and set-3 with set-2 (points 3 and 4) at the mentioned air mass flow rates. It is interesting to note that there is a form of linearity between the two comparisons. This linearity implies that the improvement in the ignition limits, due to a superior FSQ, is the same for each of the two air mass flow rate cases and that the FSQ is the major parameter that changes the behaviour of the ignition limits, when using the same ignition system in the same engine. Assuming this is true for all engine's air mass flows, an empirical correlation can be found to calculate the effect of the fuel spray quality to the ignition limit loop.

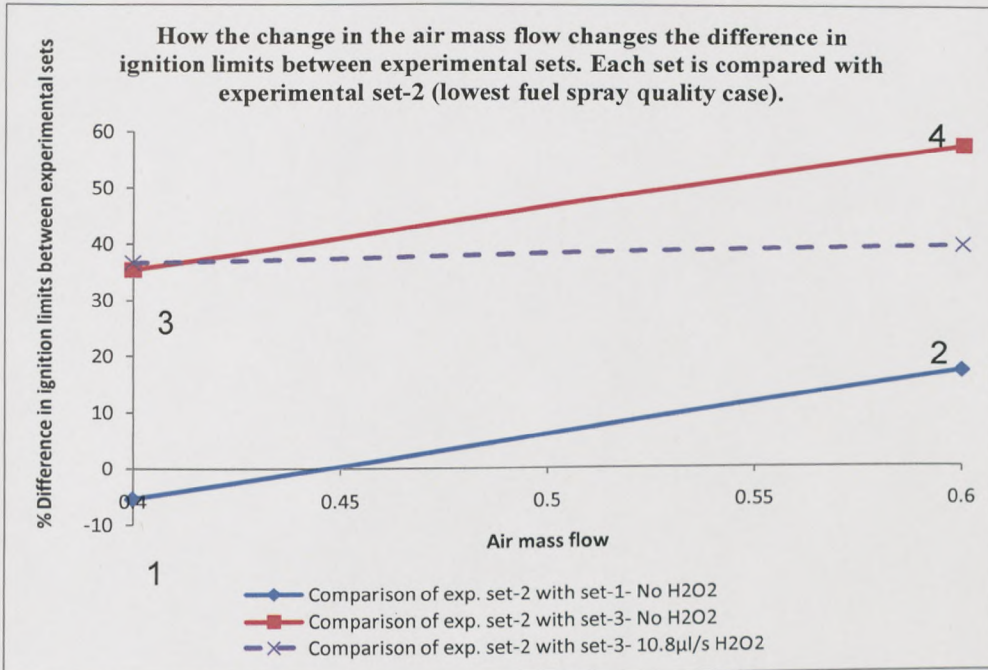


Figure 9.3(a): % improvement in the ignition limits when comparing experimental set-1 with set-2 and set-3 with set-2 at ~ 0.4 and ~ 0.6 kg/s. Figure 9.3(b) explains what the points 1, 2, 3 and 4 represent.

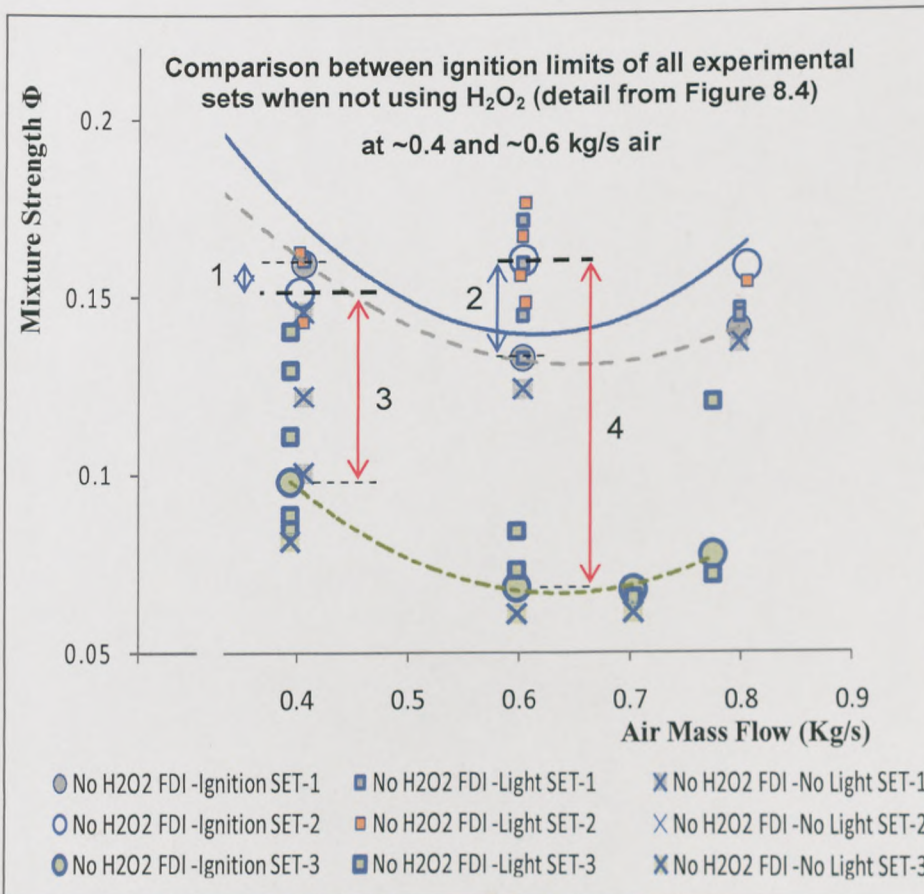


Figure 9.3(b): Detail from Figure 8.4. The arrows explain which ignition limits are compared in order to obtain the points shown in Figure 9.3(a). Each circle indicates the average of 3 successful ignition attempts. Comparison is done only at these air mass flows where enough data are available (~ 0.4 and ~ 0.6 kg/s).

Hence, the empirical formulas below are found by using the above assumption:

$$\left[\frac{\Phi_C - \Phi_B}{\Phi_C} - \frac{\Phi_C - \Phi_A}{\Phi_C} \right]_{AMF_1} \approx \left[\frac{\Phi_C - \Phi_B}{\Phi_C} - \frac{\Phi_C - \Phi_A}{\Phi_C} \right]_{AMF_2} \approx \dots \approx C_{FSQ}$$

$$C_{FSQ} \approx \left[\frac{\Phi_A - \Phi_B}{\Phi_C} \right]_{AMF} \quad (9.7)$$

Therefore:

$$[\Phi_B \approx \Phi_A - C_{FSQ}\Phi_C]_{AMF} \quad (9.8)$$

And:

$$[\Phi_A = \Phi_B + C_{FSQ}\Phi_C]_{AMF} \quad (9.9)$$

Φ : Average equivalence ratio on the lean ignition limit

A – C: Highest to lowest fuel spray quality

AMF: Engine Air mass flow rate

C_{FSQ} : Fuel spray quality constant

Using first equation (9.7), the C_{FSQ} is calculated at an air mass flow rate where the ignition limits are known for two fuel spray quality (FSQ) cases (i.e. experimental set-2 (low FSQ) and experimental set-3 (high FSQ) at the known ~0.6kg/s air mass flow rate) and by taking a random ignition point below the low FSQ line. Then using equation (9.8) the ignition limits can be found at the specific FSQ for the other air mass flows (figure 9.4).

Figure 9.4 shows the results obtained by using the suggested equations (9.7) to (9.8). The green slope represents a second order polynomial trendline of the calculated ignition limits for experimental set-3 using equation (9.9) with the ignition limits of set-1 and set-2 and the C_{FSQ} found at ~ 0.6 kg/s of inlet air.

For comparison reasons, it is common practice to do a full standard igniter test before testing the improvements that can be made to the same igniter -for example by different plasma additives or by different FDI nozzles etc. By using the proposed equations (9.7) to (9.9) , a full test to find the lean ignition limits at a fixed FSQ is not required. The ignition limit line, of the same igniter at a particular fuel spray quality state, can be calculated by finding only one ignition limit at one inlet air mass flow rate. If the proposed formulas are proved valid, they could dramatically reduce the time and hence the costs of ignition experiments.

The effect of the fuel spray quality (FSQ) to the lean ignition limits of Kerosene Jet-A₁. Mixture strength Φ vs. air mass flow rate. FDI with 'No H₂O₂' injection cases.

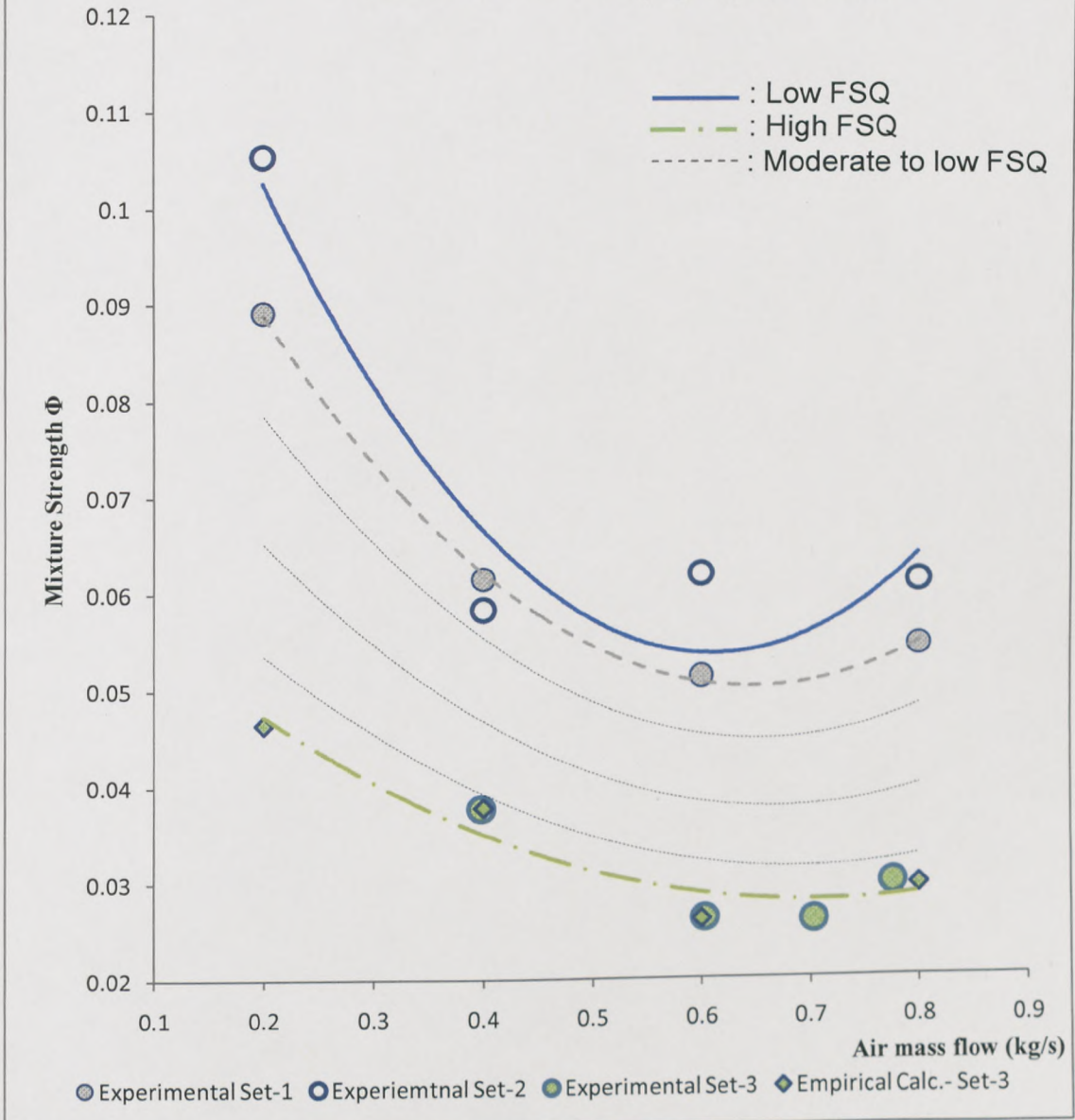


Figure 9.4: The effect of the fuel spray quality (FSQ) in the lean ignition limits of kerosene jet-A₁. Experimental and calculated results at different air mass flow rates. Calculated using equations 11.7 and 11.8. In the calculations it assumed that the fuel spray quality has the same effect to the ignition limits at different air mass flow rates when compared to the low FSQ experimental case (set-2).

9.10.2 FUEL SPRAY QUALITY (FSQ) AND H₂O₂ PLASMA IGNITION

In Figure 9.3 it is shown that the same constant C_{FSQ} (equation (9.7)) to the 'no H₂O₂' is not found in the case of the 10.8μl/s H₂O₂ injected into the focus discharge igniter. The same observation can be deduced by comparing Figures 8.4-8.5(a,b) (or Tables 9.2-9.3) where the Jet-A₁ ignitability is seen to improve with reducing FSQs, at same cases of hydrogen peroxide ignition plasma rates. Moreover the 2.7 and 5.4μl/s H₂O₂ injection rates result in almost same ignition performance in each experimental set-2 and set-3 (at different FSQs) implying that the two H₂O₂ rates behave in the same manner in terms of ignition (Figure 8.5(a)). However, in each of the two experimental sets the ignition improvement is different with the highest ignition performance being at the lowest FSQ.

- There is an optimum H₂O₂ plasma rate depending on the engine's air mass flow rate. This conclusion is in agreement with the observation made in Section 9.9.2.
- The ignition limit is not so depended to the FSQ (and the fuel-air mixing) when injecting small amounts of H₂O₂ into the igniter.
- The improvement in the ignition limits of the kerosene Jet A₁ is higher at lower fuel spray qualities (FSQs) when comparing between the high and low FSQ cases (Sections 9.9.2- 9.9.3).

Note the important extra observation, that at a same fuel spray quality (FSQ) the ignition limits are reduced by the use of the H₂O₂ additive, as there was a different ignition plug (or system). The same observation is supported by the

results obtained from the available energy at ignition calculations that are discussed in 9.12:

- The behaviour of the lean ignition limits with and without H_2O_2 plasma ignition at different FSQs, implies that it is the igniter's efficiency that improves by the supply of the H_2O_2 plasma medium (in line with Section 9.12.2)

9.11 THE EFFECT OF ADDING H_2O INSTEAD OF H_2O_2

Water plasma ignition was previously studied by Vince et al [74]. In their work, they observed that water has no effect when injected during ignition. For clarification reasons, their findings on the water additive (only) were tested during experimental set-3. Other plasma mediums were studied by previous researchers and were referred in Section 4.7.7.

Figure 8.6 shows how the lean ignition limits of the kerosene Jet-A₁ fuel are affected by adding water instead of hydrogen peroxide to the cavity of the igniter at a volume flow rate of 10.8 μ l/s. These tests were conducted during experimental set-3. In the Figure, the comparison is made with the 'no H_2O_2 ' case (the modified igniter with no additive in experimental set-3). In this graph the circles indicate the lean ignition limits that were found again experimentally using the 60% probability of ignition criterion out of a total of 5 attempts. The crosses represent failed ignition attempts and the squares show all other attempts where combustion was initiated (light attempts) but were either above

the lean limit or, if below, did not pass the 60% probability of ignition criterion. The experimental conditions are ambient.

A summary of the ignition limits, with and without the water additive is shown in Table 9.4 below. The tests on the water additive are in agreement with the findings of Vince et al [74]. Moreover, in two of the four air mass flow rates studied, at ~ 0.603 and ~ 0.776 kg/s of air, the performance of the igniter was degraded. It can then be deduced that:

- The lean ignition limits of the fuel remain virtually unchanged with the water plasma additive.
- This study along with the consistent results acquired in experimental sets one, two and three, highlights the importance of the H_2O_2 medium in improving the efficiency of the igniter.

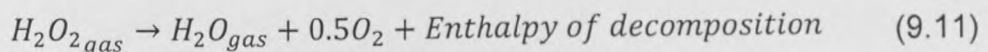
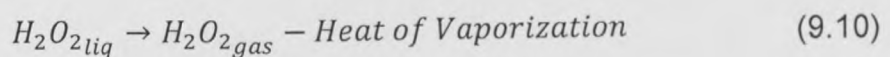
Inlet Air mass flow rate (kg/s)	FDI – $0\mu\text{l/s } H_2O_2$ Lean Limits in Φ	FDI – $10.8\mu\text{l/s } H_2O$ Lean Limits in Φ	% Ignition Improvement in Φ
0.398 (± 0.004)	0.098	0.0888	9.387%
0.603 (± 0.007)	0.0682	0.0731	-7.184%
0.703 (± 0.005)	0.0674	0.0674	0%
0.776 (± 0.001)	0.0771	0.0797	-3.372%

Table 9.4: Ignition improvement in the lean limits of the kerosene Jet-A₁ fuel in terms of mixture strength Φ . Experimental Set-3 with 0 and 10.8 $\mu\text{l/s}$ of H_2O injected into the cavity of the modified focus discharge igniter. Summary of Figure 8.4. Test conditions are ambient.

9.12.1 ENERGY CALCULATIONS

Adding H₂O₂ to the mixture adds also energy. So, it is considered important to calculate the maximum energy that was added to the fuel. This case study, investigates the energy gained by the dissociation of the hydrogen peroxide which is promoted by the spark. Although the study concerns all the experiments that were done in the Rolls Royce Olympus combustor rig, it is concentrated around the results obtained in experimental set-2. The reasons for focusing in one set are discussed in the last paragraph of the next section.

The calculations involve the maximum net energy that would be possible to exist, by the addition of H₂O₂ to the kerosene fuel, at the time of ignition, if there were no energy losses. It is assumed as a possible scenario here that when the hydrogen peroxide is ejected into the cavity of the igniter the liquid vaporizes (3) and then dissociates (4) to give away the energy that the H₂O₂ carries:



The heat of vaporization of H₂O₂ was taken from the literature as 481.1 (Cal/g) [86] and the enthalpy of decomposition as 2.78 (MJ/Kg).

Although the amount of hydrogen peroxide that is present at ignition cannot accurately be quantified, the highest energy gain which will occur if the whole amount of H_2O_2 were to reside inside the combustor, as hydrogen peroxide vapour, can be calculated. In such a case the total amount of H_2O_2 from the start of ejection ($t_{H_2O_2}$) until the time of ignition is assumed to be present inside the combustion chamber. In this way a high value of maximum energy can be calculated which is the total of the net energy of the Jet A₁ plus the energy gained by the dissociation of the total infused hydrogen peroxide vapour at the time of each successful ignition t_{ign} :

$$E_{High}^{max} = E_{net}^{fuel} + E_1^{H_2O_2} \quad (9.12)$$

$$E_1^{H_2O_2} = 2.78m_1^{H_2O_2} \text{ and } m_1^{H_2O_2} = 1.18\dot{V}_{H_2O_2}\Delta t \text{ with } \Delta t = t_{ign} - t_{H_2O_2}$$

To account for a low value of maximum net energy with the above assumptions, a second scenario is studied. In this scenario the hydrogen peroxide amount present at the time of each successful ignition depended on the maximum residence time of a streamline which had as start point the location of the igniter. This residence time was calculated to be 0.147s by using the commercial CFX-5 code and by modelling the fluid dynamics of the air flowing inside the combustor; before ignition and assuming a steady state condition (Appendix D).

$$E_{Low}^{max} = E_{net}^{fuel} + E_{H_2O_2} \quad (9.13)$$

$$E_{H_2O_2} = 2.78m_{H_2O_2} \text{ and } m_{H_2O_2} = 1.18\dot{V}_{H_2O_2}\Delta t \text{ with } \Delta t = 0.147s$$

As described above these two values are devised to account for the energy gain by the hydrogen peroxide decomposition in two different cases but with no energy losses. It should be noted that in the experiments there will be heat losses so that the additional energy gain from the hydrogen peroxide will be lower than the calculated values. ($E_{net}^{fuel} = 43.21$ in Section 7.8)

9.12.2 DISCUSSION ON THE ENERGY ADDITION BY INTRODUCING H₂O₂ DURING IGNITION

The difference between the calculated maximum high and maximum low net energy values for each ignition point at the lean limit lies below 0.2%. The difference is negligible compared to the 15%-20% reduction achieved in the energy that is present at the lean ignition limits, when adding H₂O₂ (Figure 8.15). The energy gained by the dissociation of the added H₂O₂ is almost insignificant and this is due to the very small volumes of H₂O₂ injected which are of the order of μl/s. For this reason only one of the two calculated maximum net energy values was plotted when comparing the available energy at ignition for each hydrogen peroxide injection rate case. In particular, Figure 8.15 shows the calculated high value of maximum net energy of the system at the time of ignition, against air mass flow rate for all hydrogen peroxide settings. Comparing the corresponding values at the same air mass flows in Figure 8.15,

it can be deduced that ignition with the addition of hydrogen peroxide is achieved at lower values of maximum net energy than without. This observation is enhanced by the fact that the calculations do not account for any energy losses, as mentioned above. Therefore the additional energy gain by the dissociation of hydrogen peroxide, if it exists, it should be lower than either value calculated by the two methods. Figure 8.15 indicates that:

- The system with the additional H_2O_2 required less energy to ignite the combustible mixture at the same initial conditions.

Although the dissociation of H_2O_2 adds some energy to the local system, this energy gain is very small when compared to the energy decrease accompanying the lowering of the fuel supply and while the mixture is still able to ignite with the help of the hydrogen peroxide. Therefore the result in terms of energy is that the requirement for the mixture to successfully ignite (using the 60% probability of ignition criterion) has been decreased. Hence:

- The improvement in the ignition performance is not due to an energy directly being supplied by the injection of H_2O_2 , but due to the actual increase in the ignitor's performance.
- The study clearly shows that the net available energy at ignition decreases due to the lowering of the ignition limits by the H_2O_2 addition.
- The hydrogen peroxide dissociation plays an insignificant role in increasing the chemical net energy of the system, during the ignition process, due to the low infusion rates and the decrease of the fuel flow rate requirement.

- It is suggested that similar results can be obtained for the experimental set-1 and set-3 in terms of energy addition.

Moreover, in experimental set-1, where the pumping of the hydrogen peroxide was continuous throughout the study at a rate of $0.54\mu\text{l/s}$, the maximum net energy available at ignition cannot be measured. Instead it is assumed that the hydrogen peroxide will stay at the combustor before ignition for a maximum time of 0.147s ; the maximum combustor residence time with the lowest air mass flow rate $\sim 0.2\text{kg/s}$. From the energy calculations of experimental set-2 it was suggested that the combustor residence time is a good approximation for calculating the maximum available energy. Hence, because of the very low H_2O_2 infusion rate of experimental set-1 compared with the ones in set-2, the additional energy at ignition will be insignificant. It follows that:

- The ignition improvement (by a maximum of 34%) obtained in experimental set-1 cannot be explained by the difference in the experimental procedure followed, which was continuous steady H_2O_2 injection (CSI) instead of controlled CSI, although the improvement is certainly due to the presence of H_2O_2 .

9.13 DISCUSSION ON THE DIFFERENCES OF SET-1 WITH SET-2

In Section 9.12.2 (above) it was concluded that the different experimental procedure, followed in set-1 compared to set-2, while using the same used fuel injector, cannot explain the high improvement in the lean ignition limits of the Jet

A₁ that are obtained by the addition of only 0.54µl/s of H₂O₂. This rate is an order of magnitude less than the rates used in set-2. It is characteristic to say that the improvement in the ignition limits by a maximum of 34% at an air mass flow rate of 0.6kg/s in set-1, using 0.54µl/s of H₂O₂ (Table 9.1 and Figure 8.1), could not be reached by the 2.7 or 5.4µl/s H₂O₂ rates employed in set-2 (Table 9.2 and Figure 8.2). Hence, another explanation must exist for such a difference.

After examination of the focus discharge igniter following the conduction of the experimental set-1, it was noticed that a small piece of the hypodermic tube was detached and blown away due to the high temperatures reached inside the igniter cavity and by the outward motion of the plasma. The end of the hypodermic tube was initially bent in order to position the hydrogen peroxide medium deep inside the cavity of the igniter. The piece, before the detachment, is shown in drawing no.5 of Appendix A This piece is most likely to have been blown-away while conducting the ignition experiments of set-1 at the ~0.8kg/s air mass flow rate. This could explain why there is such a small improvement in the ignition limit at that point (3.3% shown in Table 9.1 and Figure 8.1), which was unexpected. A revised drawing of the modified FDI igniter that was used in experimental set-2 and set-3 is included in Appendix A. This design difference along with the relevant results obtained in set-1 and set-2, implies that:

- An improved design of a dedicated hydrogen peroxide plasma igniter, which will deliver the medium deeper inside the cavity of the igniter and therefore at a location where the spark is more reactive, may increase further the igniter's

overall performance in terms of lean ignition limits and hydrogen peroxide usage.

The possibility of decreasing the required hydrogen peroxide rate by an order of magnitude, without compromising the improvements in the ignition limits, could make the proposed ignition system even more appealing to the gas-turbine industry.

9.14 TEMPERATURE EVOLUTION AS THE ENGINE PULLS AWAY TO IDLE

Usually, in a gas turbine engine there are a number of combustion chambers. The ignition sequence can be divided into three distinct phases [10, 11]. (i) At first a hot kernel must be initiated. (ii) The hot kernel produced by the igniter heats the mixture and initiates the first flame in the burner and (iii) after the first ignition the flame front must propagate to the neighbouring combustors until all of them are active. In the previous paragraphs attention was given to phases (i) and (ii). Although the propagation of the flame (iii) is difficult to be assessed, an attempt is made here by showing the rate of change of the combustion temperature -pulling away to idle.

This case study investigates the temperature increase with time after ignition. For this purpose similar equivalence ratio cases, which showed successful ignition, were selected that corresponded to a range of hydrogen peroxide

volume rates. For each setting an average temperature profile was calculated from cases of similar equivalence ratios. Comparison was then made between the average temperature profiles of the different H₂O₂ insertion rates but at similar values of equivalence ratio and at the same air mass flows. Only average temperature profiles were compared in this study and the position of the thermocouples remained unchanged.

Figures 8.16-8.18 are examples of such plots from the results acquired in experimental set-2. The raw data were post-processed for this particular study using the Fortran-95 program 2 (Section 9.7.3). In Figure 8.16, it can be deduced that for an air mass flow of 0.194(±0.003)kg/s, the average temperature after ignition, is increasing faster when injecting 5.4µl/s of H₂O₂ than without. The equivalence ratios investigated in Figure 8.16 were 1.05E-01(±1E-04) and 1.02E-01(±1E-04). Similar results are also shown in Figures 8.17-8.18, where the air mass flows are 0.604(±0.009)kg/s and 0.805(±0.012)kg/s respectively and the equivalence ratio for each Figure is 4.47E-02(±2E-04) and 4.68E-02(±8E-04). It is characteristic that

- In all plots, the higher hydrogen peroxide rate results in higher temperature gradients when compared with a lower rate or 'no H₂O₂' case.
- The above observation, along with the previous results, suggests that the presence of the hydrogen peroxide plays a key role in enhancing ignition.

To support the above further, another relevant study was devised. In experimental set-3 the temperature increase after ignition was recorded at a fixed air-fuel mixture strength ϕ -by keeping the fuel flow at a constant rate of 0.0069kg/s- at 0.4, 0.6, 0.7kg/s of inlet air and at 0, 2.7, 54 and 10.8 μ l/s of H₂O₂ and H₂O plasma medium. There was only one successful ignition run for each air mass flow rate at each hydrogen peroxide volume rate. The data obtained were averaged between the two thermocouples. The results of the temperature increase inside the combustor plotted against time, at the fixed fuel flow, are presented in Figures 8.19 to 8.21. Each Figure corresponds to one inlet air mass flow rate and each temperature slope describes a different hydrogen peroxide or water plasma volume rate.

Figure 9.8 is a graphical summary of all the results obtained from the temperature tests, in terms of maximum exhaust temperature gradients against H₂O₂ and H₂O plasma additive flow rates, at the early stages of ignition as the engine pulls away to idle and under a fixed Jet-A₁ flow rate of 0.069kg/s. The maximum temperature gradients were found (using a single thermocouple in this case) by drawing the tangent of each temperature line at the point where the temperature increase with time is highest, as it is shown in Figures 9.5 to 9.7.

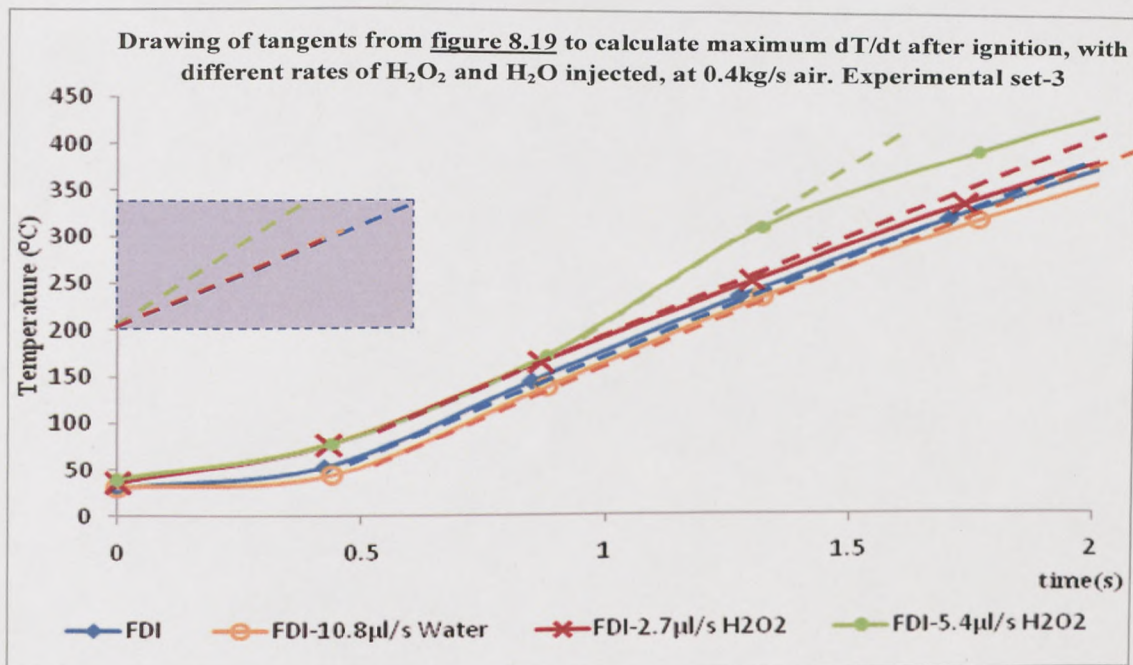


Figure 9.5: Drawing of tangents from Figure 8.19 and comparison (purple box). Temperature and time data at the early stages of ignition (pulling away from idle) when supplying 0, 2.7, 10.8µl/s of H₂O₂ and 10.8µl/s of H₂O plasma medium into the cavity of the FDI igniter. The air mass flow rate is ~0.4kg/s and the mixture strength is $\Phi=0.099(\pm 2E-03)$. Experimental set-3: Clean fuel atomiser. Note: the mixture strength Φ decreases by a small margin (2E-03) when the hydrogen peroxide rate is increased from 0 to 10.8µl/s and when the fuel flow is kept constant at this air mass flow.

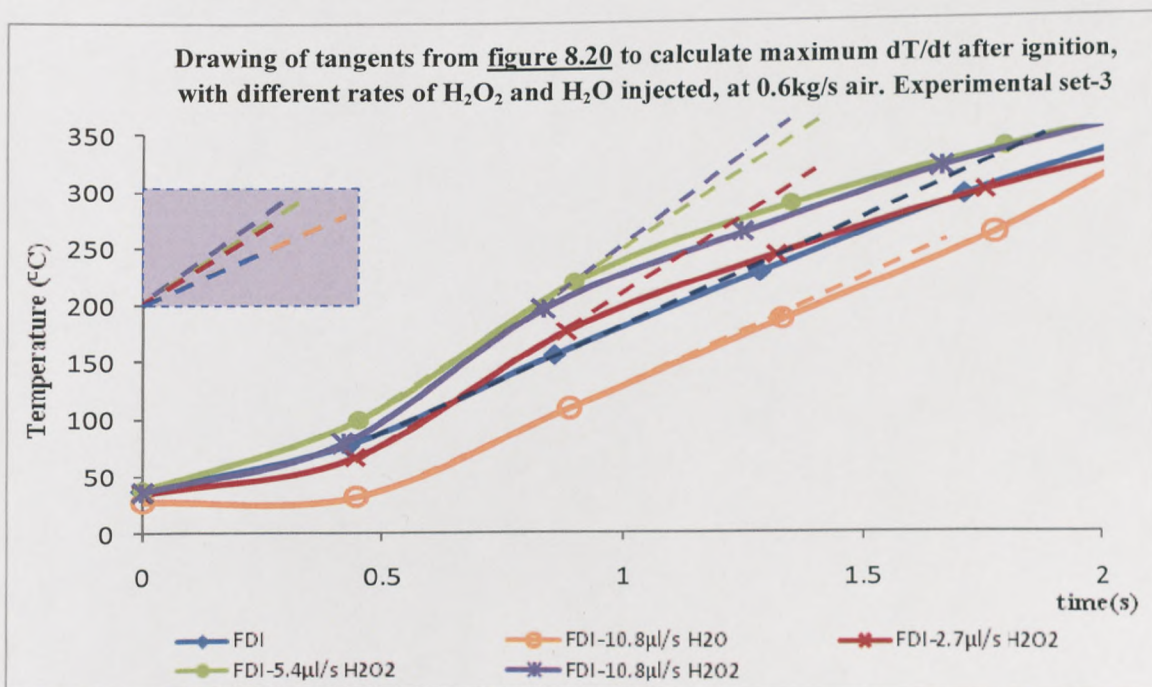
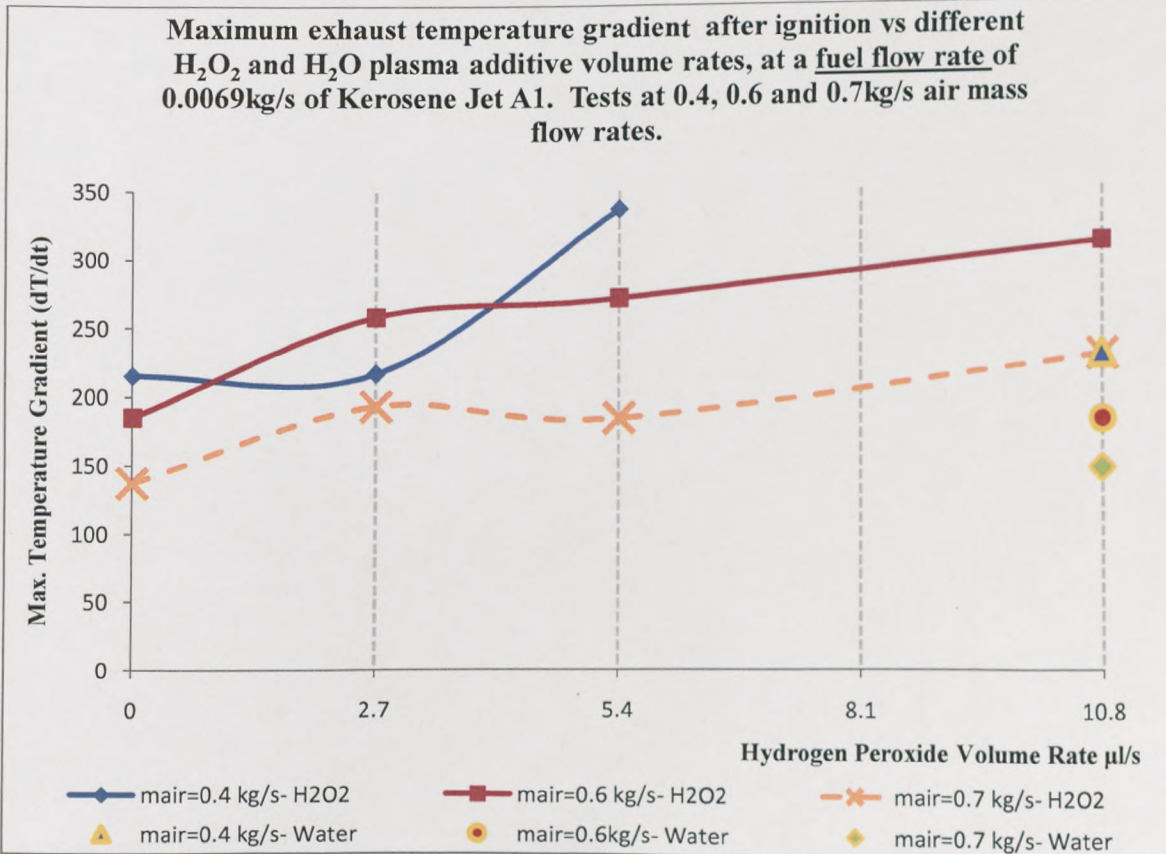
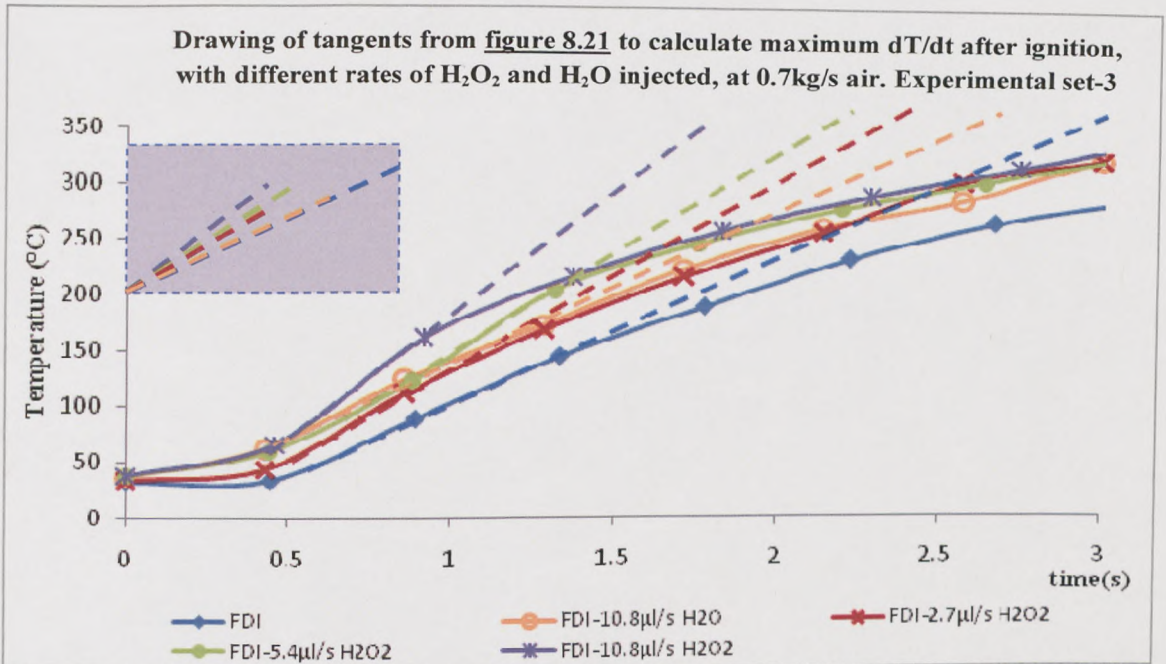


Figure 9.6: Drawing of tangents from Figure 8.20 and comparison (purple box). Temperature and time data at the early stages of ignition (pulling away from idle) when supplying 0, 2.7, 10.8µl/s of H₂O₂ and 10.8µl/s of H₂O plasma medium into the cavity of the FDI igniter. The air mass flow rate is ~0.6kg/s and the mixture strength is $\Phi=0.065(\pm 2E-03)$. Experimental set-3: Clean fuel atomiser. Note: the mixture strength Φ decreases by a small margin (2E-03) when the hydrogen peroxide rate is increased from 0 to 10.8µl/s and when the fuel flow is kept constant at this air mass flow.



The points below are drawn from the interpretation of Figure 9.8:

- The maximum exhaust temperature gradient decreases with increasing air mass flow rates as it is expected.
- The hydrogen peroxide produces a noticeable effect in increasing the maximum temperature gradient of the combustor's exhaust gas as the engine pulls away from idle.
- The maximum exhaust temperature gradient was changed by the addition of 0, 2.7, 5.4 and 10.8 μ l/s of H₂O₂ into the cavity of the igniter. This behaviour is changed in a similar way for the ~0.6 and the ~0.7kg/s of inlet air.

Most importantly:

- The H₂O plasma additive does not affect the maximum temperature gradient of the exhaust gas as the engine pulls away from idle.
- Figure 9.8 suggests that the combustion (reaction) rate of the kerosene-air mixture increases with the use of the H₂O₂ plasma additive.
- The ignition performance of the modified focus discharge igniter was enhanced by the supplied H₂O₂ plasma medium and this is evident by the increase in the maximum temperature gradients of the exhaust gases during the early stages of ignition (Figure 9.8).

9.15 STATISTICAL CALCULATIONS – IGNITION TIME AND ADDITIONAL COSTS FROM HYDROGEN PEROXIDE USAGE

9.15.1 IGNITION TIME

Table 9.5 compares statistically the time to ignition -from the time the igniter was started- for each hydrogen peroxide injection rate used: 0, 2.7, 5.4 and 10.8 μ l/s. This study presents the results obtained in experimental set-2. The maximum, minimum and mean times to ignition, as recorded during the experiments, were found for the cases that correspond to the lean ignition limits. From Table 9.5 it can be deduced that:

- The mean time to ignite the kerosene-air mixture, at the lean limits of ignition, was decreased by about 47.4%, 40% and 76.3% by using 2.7, 5.4 and 10.8 μ l/s of H₂O₂ respectively.
- The maximum and minimum ignition times were both reduced at the lean ignition limits.
- Note the important extra observation that, at points where without hydrogen peroxide, the fuel: air mixtures lie inside the cold region (i.e. are not ignitable), by introducing the H₂O₂ not only are they now ignitable but the time-to-ignition is also reduced compared to the no H₂O₂ cases.

In another study of experimental set-2, the mean ignition time of all light attempts, including the ignition limits, was calculated and compared between the different hydrogen peroxide injection rate cases. From Table 9.5:

- The mean ignition time was again decreased by ~45%, 32.7% and 54.2% by the introduction of 2.7, 5.4 and 10.8 μ l/s of H₂O₂ respectively (Table 9.5).

	0	2.7	5.4	10.8
AT LEAN LIMITS ONLY	($\mu\text{l/s}$)			
Max. Time for ignition (s)	11.328	7.578	9.64	5.344
% Difference	0	33.103	14.901	52.824
Min. Time for ignition(s)	1.875	1.047	1.016	0.625
% Difference	0	44.16	45.813	66.666
Mean Time for ignition(s)	5.919	3.116	3.553	1.404
% Difference	0	47.356	39.972	76.28
FOR ALL 'LIGHT' CASES				
Mean Time for ignition(s)	4.868	2.681	3.275	2.227
% Difference	0	44.926	32.724	54.252

Table 9.5: Statistical comparison of the maximum, minimum and mean ignition times of the kerosene fuel from the start of the ignition sequence between the four hydrogen peroxide injection rate cases 0, 2.7, 5.4 and 10.8 $\mu\text{l/s}$. The first comparison is being done at the lean limits only. The second comparison considers all cases that a flame was achieved and shows their mean ignition time with respect to the hydrogen peroxide injection rate setting. All results are from interpretation of experimental set-2: Used fuel injector case.

9.15.2 ADDITIONAL COSTS FROM HYDROGEN PEROXIDE USAGE – CALCULATIONS FROM EXPERIMENTAL DATA

The total volume of H_2O_2 that was injected inside the combustor was calculated in order to show how much it was used during all the experiments of experimental set-2. The total time of the experiments was found by summing all the individual times for each experiment. Each experimental time includes the time to ignition t_0 plus 10s to burn the fuel plus 10s to cool the engine for each case as described in Section 7.6. The volume of hydrogen peroxide used was found to be 9.35ml for 2 hours of ignition experiments. The cost of the hydrogen

peroxide for 2 hours of ignition experiments was £0.65 by today's price, which is £34.60 per 500ml delivered.

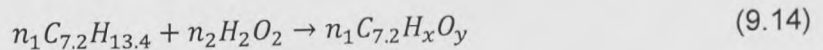
- The cost therefore is minimal when considering the advantages from the decrease in the lean ignition limits.

DISCUSSION PART-C:

IGNITION EXPERIMENTS IN THE OLYMPUS GAS-TURBINE RIG – F.A.M.E. BIODIESEL

9.16 EQUIVALENCE RATIO CALCULATIONS FOR THE F.A.M.E. BIODIESEL

The chemical formula of the biodiesel test fuel was obtained by lab analysis (Section 7.8). The equivalence ratio calculations were done according to the same approach that was used in the calculations of the kerosene fuel (Section 9.8). According to this approach the biodiesel fuel was enhanced by the H_2O_2 additive:



The following equation for calculating the equivalence ratio can be obtained following the same steps as for kerosene in Section 9.8:

$$\Phi = \frac{\frac{\dot{m}_f}{2}}{\dot{m}_{air\ Actual}} \bigg/ \frac{\frac{m_f}{2}}{m_{air\ stoich}} = \frac{\frac{\dot{m}_f + \dot{m}_{H_2O_2}}{1}}{\dot{m}_{air\ Actual}} \bigg/ \frac{86.4 + x + 16y}{137.28(7.2 + \frac{x}{4} - \frac{y}{2})} \quad (9.15)$$

9.17.1 EXPERIMENTAL SET-3 – CONTROLLED CONTINUOUS STEADY H₂O₂ INJECTION (CCSI) AND CLEAN FUEL INJECTOR

Figure 8.22 is a graphical summary of the ignition results obtained in experimental set-3 for the biodiesel fuel, when injecting 0 and 10.8 μ l/s H₂O₂ into the cavity of the modified focus discharge igniter. The experiments were conducted under ambient conditions in the Olympus combustor rig. The engine's air mass flow rates studied were about 0.4, 0.6, 0.7 and 0.775kg/s. The ignition limits are indicated by circles and these were obtained using the 60% probability of ignition criteria out of five consecutive ignition attempts (as in the kerosene experiments). The crosses indicate failed ignition attempts and the squares indicate ignitions where a light was initiated but in less than three consecutive ignition attempts out of the total five. The red dashed circle in the graph, at the 0.775kg/s air flow rate, indicates a point where the ignition limits lie at a higher value of equivalence ratio. The limit at the ~0.775kg/s air flow could not be found due to a fuel pressure issue that arose and due to higher fuel flow rates needed at this air mass flow.

Table 9.6 shows the equivalence ratio values of the ignition limits of the biodiesel fuel with and without hydrogen peroxide at the air mass flow rates studied. It should be highlighted that, in this short study, the igniter with the H₂O₂ additive, not only matched the performance of the FDI, but in two out of the three study air flow rates this performance was improved.

- o As Table 9.6 shows, an improvement in the ignition limits of the biodiesel fuel was achieved between about 0 to 11 per cent, by using a 10.8 μ l/s H₂O₂ injection rate.

Moreover, the low fuel pressure problem arose towards the end of the 'no H₂O₂; ignition experiments. The fuel spray quality (FSQ) therefore, during the experiments with H₂O₂ (commenced after the ignition experiments with 'no H₂O₂') should have deteriorated. This statement emphasizes the importance of the 11 per cent improvement in the lean ignition limits at the 0.406kg/s air flow rate and of the igniter performance in the other two air flows.

It is therefore suggested that a more thorough study should be conducted before concluding on the values of the ignition limits of the biodiesel with H₂O₂ addition. In the author's opinion the ignition limits of the biodiesel fuel could be reduced further. It should be also be mentioned that there may be a different - from the one used - optimum H₂O₂ rate for extracting the maximum reduction in the ignition limits.

Inlet Air mass flow rate (kg/s)	FDI – 0 μ l/s H ₂ O ₂ Lean Limits in Φ	FDI – 10.8 μ l/s H ₂ O ₂ Lean Limits in Φ	% Ignition Improvement in Φ
0.406 (\pm 0.001)	0.1812 (\pm 1E-4)	0.1606 (\pm 1E-4)	11.336%
0.593 (\pm 0.001)	0.1345 (\pm 1E-4)	0.1344 (\pm 4E-4)	0.086%
0.7 (\pm 0.001)	0.1264(\pm 1E-4)	0.1232 (\pm 1E-4)	2.536%

Table 9.6: Ignition improvement in the lean limits of the bio-diesel test fuel in terms of mixture strength Φ . Experimental Set-3 (clean fuel injector) with 0 and 10.8 μ l/s of H₂O₂ injected into the cavity of the modified focus discharge igniter. Summary of Figure 8.22. Test conditions are ambient.

DISCUSSION PART-D:

FEASIBILITY STUDY OF THE PROPOSED H₂O₂ PLASMA IGNITION SYSTEM – AN OPTIONAL SYSTEM FOR PRODUCING H₂O₂

9.18 FEASIBILITY STUDY

9.18.1 H₂O₂ SAFETY

In terms of safety and handling, the hydrogen peroxide is known to be an unstable chemical. The following remarks were taken from [87]. When it comes to contact with a flammable substance the H₂O₂ will decompose to water and oxygen. In this case, it is likely that the fuel-oxygen mixture will auto-ignite by the exothermic reaction (of the decomposition) when the oxygen is enough for the mixture to reach the flammability limits. The decomposition rate increases with temperature at about 2.3 times per 10°C [87]. Due to the unstable nature of the H₂O₂, care should be taken when storing the chemical in large quantities. The escaping oxygen can result in a high pressure build-up during long periods of time. According to [87], 20 tonnes of H₂O₂ at a 70% by weight solution, losing 0.3% of oxygen per year will result in 13dm³ of extra oxygen per day inside the storage vessel. It should be stressed that hydrogen peroxide at a solution of above 40% by weight can form highly explosive mixtures with organic compounds Table 9.7 [87]. Furthermore, a H₂O₂ vapour concentration of above 39% by weight, at a temperature above about 140°C, when introduced to the atmospheric pressure is expected to be explosive (Figure 9.9 [87]). It should be mentioned that oxygen enriched flammable environments (due to the hydrogen

peroxide decomposition) greatly reduce the minimum ignition energy requirement to initiate combustion(Figure 9.8 [87]).

Substance	Explosive power	Sensitivity (kg cm)
Nitroglycerine	52	2-5
85% m/m hydrogen peroxide/glycerol	46	10-15
70% m/m hydrogen peroxide/polyethylene	30	22
Picric acid	32	75
Trinitrotoluene	30	150
97% m/m hydrogen peroxide	17	Insensitive

Table 9.7: Explosive power and sensitivity of various substances [87]

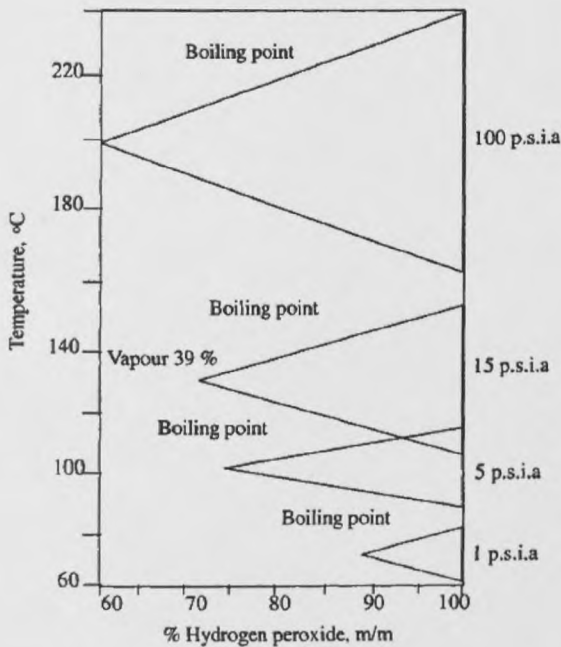


Figure 9.9: Compositions of H₂O₂ that form ignitable vapour [87]

Substance	In air	In oxygen
Methane	0.3	0.003
Acetone	1.15	0.0024
Diethyl ether	0.20	0.0013

Table 9.8: Minimum ignition energies in air and oxygen in mJ [87]

9.18.2 FEASIBILITY OF THE PROPOSED IGNITION SYSTEM AND AN OPTIONAL SYSTEM FOR PRODUCING H₂O₂

According to the experimental results of this research, the injection of H₂O₂ into the cavity of a focus discharge igniter improves the ignition efficiency of the igniter. It was shown that notable improvements from 6.5 to 44%, to the ignition limits of kerosene, were attainable by using only a small amount of a 50% by weight solution of hydrogen peroxide during the ignition process. The injected amount was varied from 0.54 to 10.8µl/s. Moreover, in experimental set-2, where the volume flow rate of the additive was varied from 2.7 to 10.8µl/s during two hours of ignition experiments, the total volume of H₂O₂ that was used was 9.35ml. This amount translates to about 100 hours or 4 days of repeated ignition attempts being achieved from a 500ml bottle of H₂O₂, which when delivered currently costs £34.60. Furthermore, assuming in an extreme case that the gas-turbine flame stays within the stability loop at 50% of the times during continuous operation, it is worth noting that a monthly supply of 2 litres of H₂O₂ would be enough to keep the engine running. Therefore in terms of storage, supply and costs the requirements of the proposed ignition system are minimal for industrial use. The potential improvements in the ignition loop and hence, the characteristics of a gas-turbine are expected to be high in this case.

The low monthly storage requirements and the usage of small amounts of H₂O₂ together with low cost precautionary measures should ensure that the proposed ignition system is safe enough and easy to integrate to the current industrial gas-turbines.

In the aircraft industry, the safety requirements will be more demanding. In the case of one aircraft carrying 2 litres of liquid H_2O_2 the safety concerns should not be raised. In an emergency the hydrogen peroxide could be instantly diluted to water to make an emergency landing safer. However, in the case of using the H_2O_2 plasma ignition in a large scale, like the civil aircraft industry, the high demand would increase the risks of hazards exponentially. The risks are more likely to increase in international airports that would need to store and handle large quantities of the chemical in order to supply the airlines. In this regard, safety procedures and supporting infrastructure should be planned to reduce the risks of accidents. The cost of these procedures coupled with the risk of a high explosion could make the proposed ignition system not viable for civil aircrafts.

To make this ignition system more attractive an optional system could be deployed to produce in-situ hydrogen peroxide whenever required, by passing some of the fuel of the gas-turbine through a catalyst and then injecting it into the igniter. According to the experimental study the amount of the H_2O_2 medium that is required, is small in the order of $\mu\text{l/s}$ and therefore the proposed optional system would not need to produce the optimum amount of H_2O_2 . It is possible that the H_2O_2 could be one of the bi-products of the fuel catalyst reaction. It is also possible that all the products of the fuel catalyst reaction are instantly injected into the ignition system if they improve ignition. With such an optional system, the need for supplying and storing the hydrogen peroxide would be eliminated.

Figure 9.10, shows an igniter system that is proposed by C.Wilson and A.C.McIntosh. The system has a hypodermic tube passing below the outer electrode and over the insulation of a focus discharge igniter. At the end of the tube there is a suitable catalyst with the exit being inside the cavity of the igniter. Propane fuel is infused into the hypodermic tube and the fuel passes through the catalyst. The fuel-catalyst reaction produces some hydrogen peroxide while the igniter is fired with a pulsed plasma ignition (PPI) mode.

According to this research the first part of the hypothesis of the above proposal, that the hydrogen peroxide will augment the combustion initiation process, is correct. The advantages and the improvements in the ignition limits, when using a small amount of hydrogen peroxide during ignition, are evident in all the experimental results in the Olympus rig. The second part of the hypothesis is beyond the scope of this study but an initial study is presented to encourage further research.

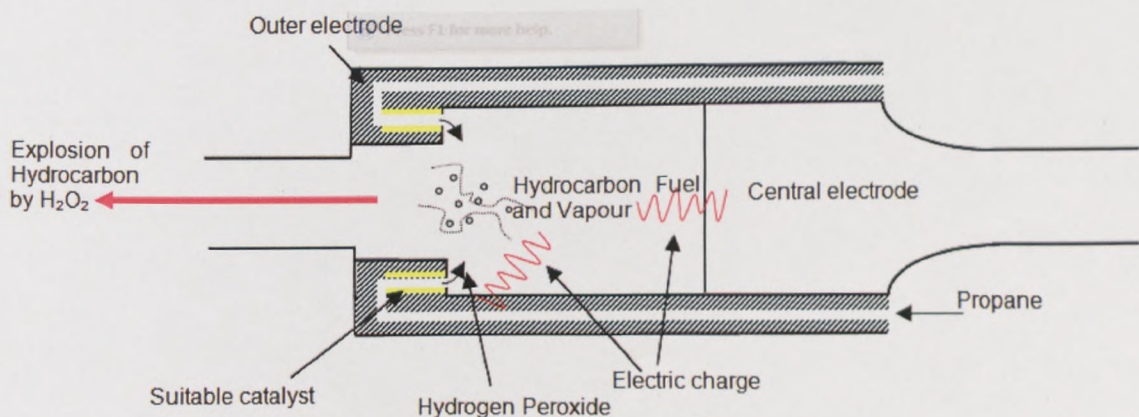


Figure 9.10: Proposed ignition system with propane passing over a suitable catalyst and the product infused into the cavity of a focus discharge igniter. This igniter design was proposed by C. Wilson and A.C. McIntosh.

10.1 CHAPTER OUTLINE

10.1.1 BIO-INSPIRATION FROM THE BOMBARDIER BEETLE

In the introductory chapter, it was highlighted that a connection exists between this research of a new ignition system and the Bombardier beetle's defence mechanism. The author recognises that the link between the two is somewhat indirect. Many ideas though, are the result of observation and 'creative inspiration'. The main connection between the ignition system proposed and the beetle's chemical mechanism, is the need for producing hydrogen peroxide internally and in a small scale. But, looking further into the matter, one will observe that the current technology in large scale production of H₂O₂ has interesting similarities with the chemicals and the procedure that the insect is believed to use to produce hydrogen peroxide. It is interesting to note that both chemical procedures use a catalyst at some point. The two mechanisms are discussed in Section 10.2.

10.1.2 SIMULATION WORK

An initial attempt is made to prove that the idea of passing a hydrocarbon fuel through a catalyst will produce some quantity of hydrogen peroxide within the right conditions. For this reason the Chemkin Pro 2010 platform was deployed to run the simulations. This simulation work is an important aspect of the overall project because an on-site production of H₂O₂ will resolve some concerns, e.g. the need for supplying hydrogen peroxide by an external source and the safety

concerns involved in the alternative case of storing it next to a gas turbine (Section 9.18)

10.2 COMMON INDUSTRIAL PRODUCTION OF H₂O₂ TODAY

Almost all large scale production of H₂O₂ today is based on the auto-oxidation process (AO) of organic compounds [88]. The AO method uses indirect oxidation of H₂ to H₂O₂ [89].

10.2.1 A SIMPLE H₂O₂ PRODUCTION SCHEME

The most usual AO method is the anthraquinone (AQ) process [90]. In this process, at first, an alkyl anthraquinol (for example 2-ethyl anthraquinol) is oxidized by air or oxygen and forms the corresponding quinone (anthraquinone) and H₂O₂. The anthraquinone then is reduced back to the anthraquinol (illustrated in Figure 10.1) or anthrahydroquinone (AHQ) using pressurized hydrogen in the presence of a hydrogenation catalyst (such as supported Pd or Pt).

10.2.2 A MORE COMPLEX H₂O₂ PRODUCTION SCHEME

If the product of the hydrogenated anthraquinone is anthrahydroquinone (AHQ) then a separate step is done. The AHQ undergoes further hydrogenation to produce the tetrahydroanthrahydroquinone (THAHQ). Finally, the THAHQ is oxygenated to produce more H₂O₂ and tetrahydroanthraquinone (TAHQ). This process is illustrated in Figure 10.2.

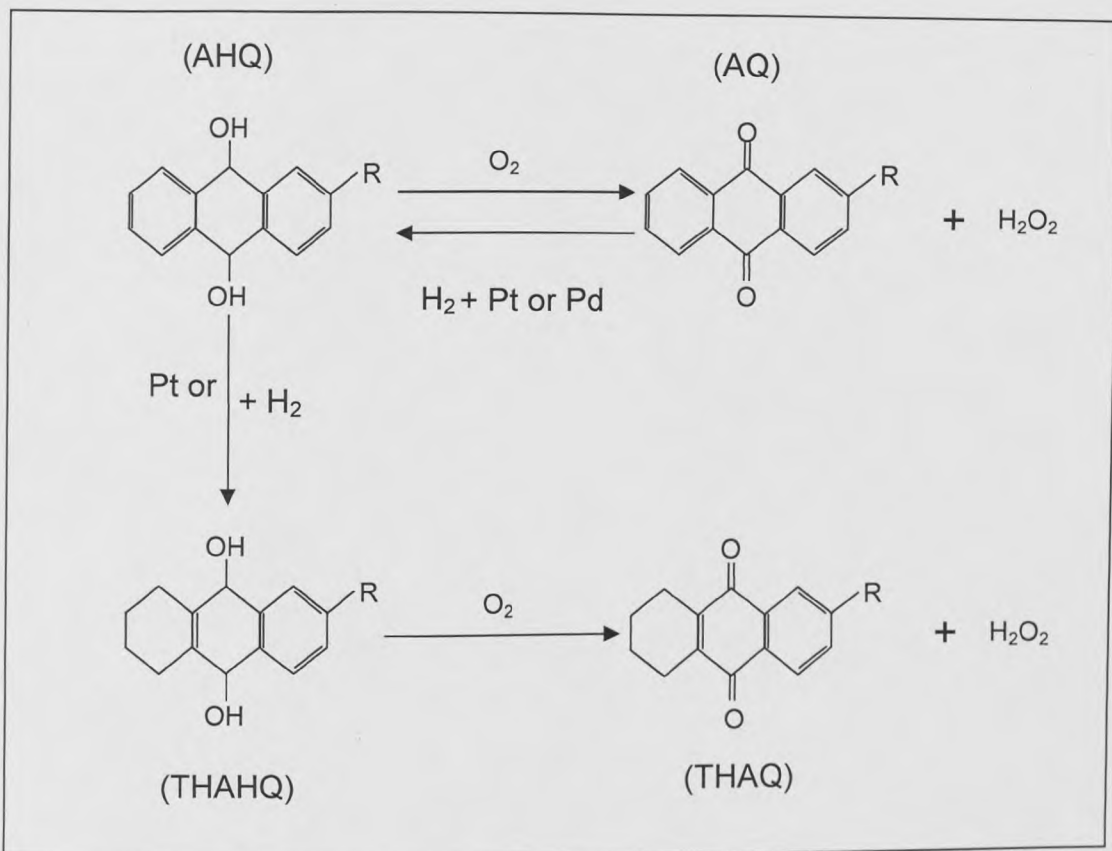


Figure 10.1: Production of H₂O₂ through the anthraquinone auto-oxidation (AQ) process. R denotes a hydrocarbon compound. [88]

The AO process is considered the most common for the industrial production of H₂O₂ because it avoids explosive H₂/O₂ gas mixing. It requires high capital and has high operating costs so therefore it is used only for large-scale H₂O₂ production (> 40x10³ tones per year) [88]. Safety concerns arise from the need to transport the hydrogen peroxide from the plant to the end users as it can be highly explosive if it violently decomposes. Some toxic chemicals that are used in the production process induce further safety issues[88].

10.3 THE BOMBARDIER BEETLE'S DEFENCE MECHANISM

Thomas Eisner's and Daniel J. Aneshansley's pioneering work of the 'Spray aiming in the bombardier beetle: Photographic evidence' [13] in 1999, amongst others, has brought the beetle's defence mechanism to the attention of a large portion of the scientific community. The detailed photographs showed for the first time the ejection mechanism and what it really does. It was also the first time that the moveable and rotating nozzle at the tip of the abdomen was shown in such detail. Many that see these photographs are impressed by the insect's unique system which is able to eject a hot caustic spray with high aiming accuracy when it is being attacked.

10.3.1 REACTION CHAMBER AND MECHANISM

The beetle possesses two reaction chambers, shaped like a boxing glove (Figure 10.2C), that exhaust either in tandem or each separately after the other. Each system consists of a gland [91] with two compartments; a reservoir (Figure 10.2A) and the reaction chamber which are connected through an inlet valve (Figure 10.2B).

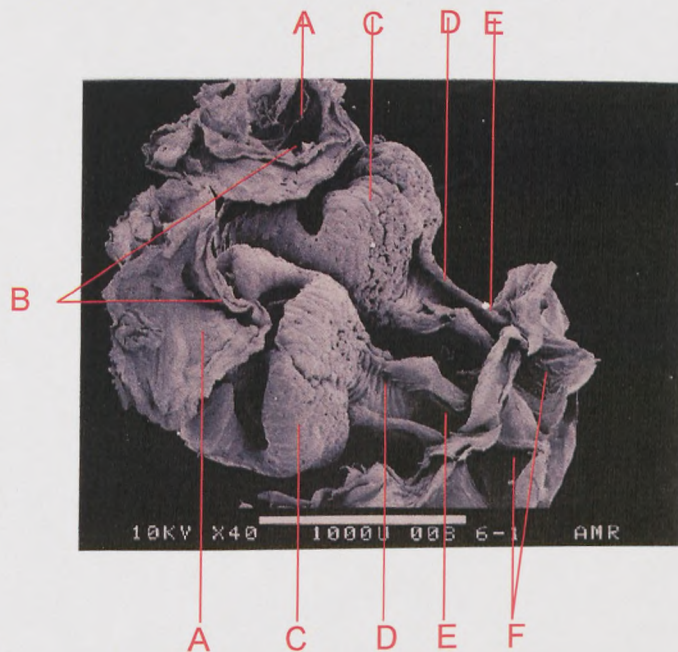


Figure 10.2: Electron photograph of the ejection mechanism inside the bombardier beetle. The photograph clearly shows that it is a twin ejection system. The similarities of the system with man-made engines are impressive. A: reservoir, B: inlet valve, C: reaction chamber (boxing glove shaped), D: outlet valve, E: outlet nozzle, F: exit at the tip of the abdomen.

BOXING GLOVE SHAPED REACTION CHAMBER AND INLET VALVE

The boxing glove shape of the reaction chamber (Figures 10.2C and 10.3D) is a clever mechanism that is used to block the inlet valve which seats between the two 'fingers' of the glove. The outer walls of the reaction chamber are quite rigid but not at the inlet. The inlet valve (Figures 10.2B and 10.3B) therefore closes when the pressure increases and when the reaction takes place inside the chamber. It then reopens when the pressure decreases after an ejection.

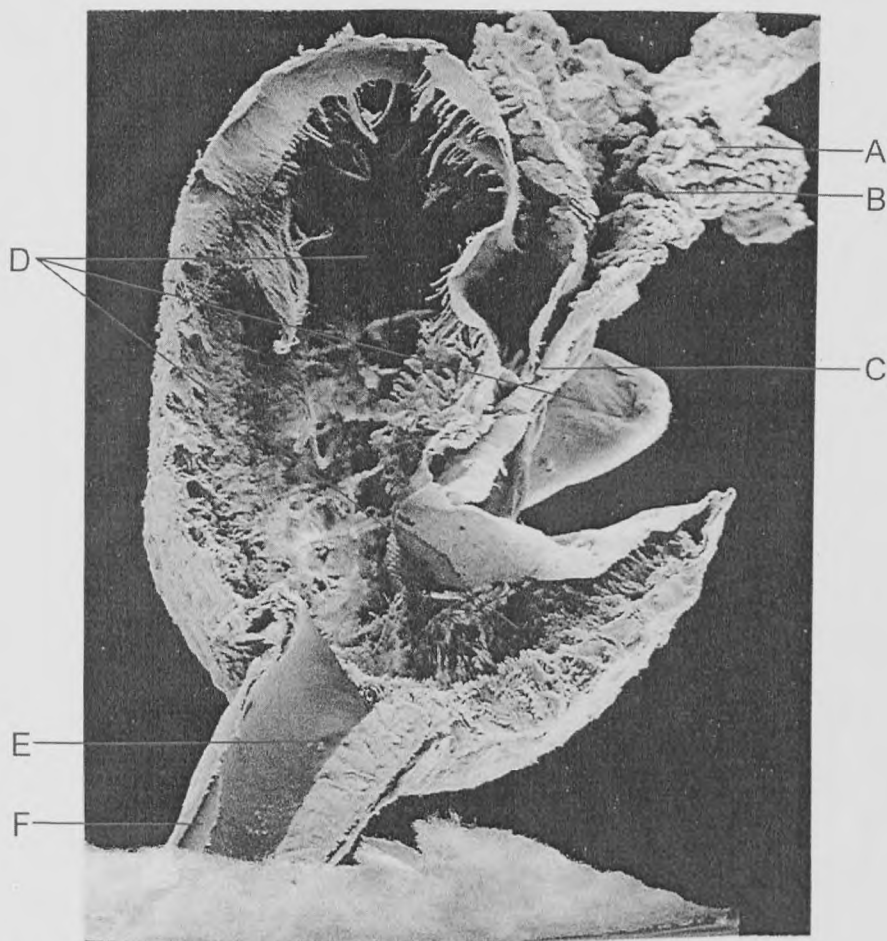
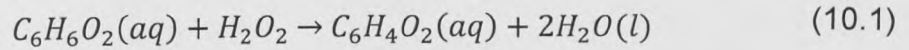


Figure 10.3: Electron photograph of a dissected gland. A: thin long tube, B: reservoir, C: inlet valve, D: reaction chamber and its fibrous wall, E: exit of reaction chamber, F: membrane part of the outlet valve.

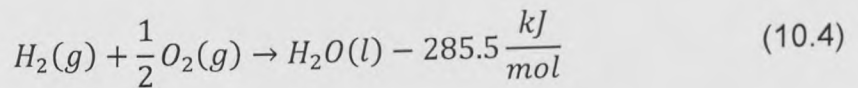
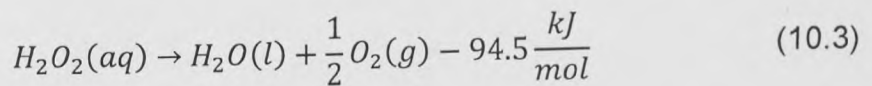
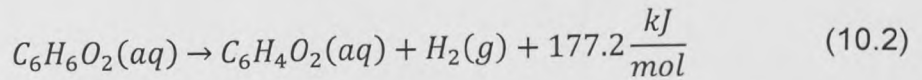
RESERVOIR AND THIN LONG TUBE

In the reservoir (Figure 10.2A and 10.3B) an aqueous solution of hydroquinones (or else quinols) $C_6H_6O_2$ and hydrogen peroxide is stored for using it when required. The hydrogen peroxide and hydroquinones are produced within an extremely narrow tube of $1\mu m$ in diameter and $5cm$ in length (Figure 10.3A), which is about 1.7 times the beetle's length (about 2-3cm).

The reaction mechanism in the chamber when the chemicals come to contact and at the instance before ejection was first reported by Aneshansley et al [12]:



The reaction is described by three stages:



The overall heat released by the reaction (2.46) is: $-202.8 \frac{kJ}{mol}$. The heats of reaction for each step were calculated by Schildneckt and Holoubek [91] at a reference temperature of 25°C. Experiments on bombardier beetles at the reference temperature have shown similar values of heat released. The consistency of the experimental with the theoretical results, suggest that the reaction mechanism shown above is the main mechanism used by the beetle.

The chamber walls have a fibrous texture, shown in Figure 10.3D. The chamber is filled with a mixture of catalase and peroxidase that is dissolved in water. It is thought that the secretion of these organic catalysts is a key feature for

accelerating the reaction. It is also believed that these chemicals are secreted through the fibres of the reaction chamber.

OUTLET VALVE

At the exit of the reaction chamber (Figure 10.3E) exists an outlet valve (Figure 10.2D and 10.3F). This valve is similar to a pressure release system. It opens only above a certain pressure and closes below it. The outlet valve is a very important part of the whole mechanism because it allows for a pressure increase at the reaction chamber. When the reaction occurs, the fluid inside the chamber is at a certain temperature ($\sim 100^{\circ}\text{C}$) and pressure. At that instance the outlet valve opens and the reacted fluid is introduced to the outside temperature and pressure. The pressure drop results in an explosive vaporization of the fluid -which is in most parts water- as it exits the reaction chamber. CFD simulations by the Leeds Group, using two face flow models with the CFX platform, proved that it is the explosive vaporization that produces the high outlet speeds of the ejected caustic spray. This explains the fact that the beetle is able to eject with such intensity and at such long distances compared to the length of the reaction chamber.

The spray producing mechanism of the outlet valve was patented by the Leeds Group [92-95]. The technology is being developed as the μ mist platform technology [96] and is supported by Swedish Biomimetics 3000, a company dedicated to biomimetics.

10.3.2 H₂O₂ PRODUCTION MECHANISM

A possible chemical route of how the beetle produces the chemicals that are stored in the reservoir is suggested in [4]. This route was suggested after noticing that current H₂O₂ production technology involves anthraquinol in the process [88]. The hydroxyl groups from the phenol compound are well known to release the two hydrogens easily in the presence of oxygen. By introducing air, the hydrogens from the phenol react with the air and they form hydrogen peroxide. It is likely that there is a catalyst inside the beetle's thin long tube that enables such reaction to occur. The presence of a catalyst (a metal or mineral) may also explain the reason why all the bombardier beetles that were studied lost their ability to eject their hot spray after a short period in captivity.

10.4 SIMULATIONS ON THE PRODUCTION OF H₂O₂

10.4.1 CHEMKIN PRO

Simulations were done using the Chemkin-Pro platform, release 15082 (September 2008). As Chemkin is used in a wide variety of chemical simulations, the mechanisms that come with the platform are basic and are used mostly for training and educational purposes. Chemkin provides researchers with a tool that solves complex chemical reactions. Besides the Chemkin Language, it requires advanced knowledge of chemistry and the inputting of the relevant experimental and chemical data in order to create a chemical mechanism. Moreover, chemkin mechanisms are in some cases not readily available to the public. Usually, because of the related costs -it requires time, specialized equipment and specialized researchers-, the work is

sponsored and therefore under right-protection agreements. It was found that this applied mostly to the mechanisms that were needed to validate this project's idea; to run different hydrocarbon fuels under different catalysts in order to produce some quantity of H_2O_2 . It is representative to say, that there is none recommended database from the Chemkin website that uploads catalytic mechanisms.

10.4.2 DETCHEM MECHANISMS

Detchem is a company specialised in chemistry CFD [97]. Some of the company's catalytic work is available to download online. One of the Detchem chemical mechanisms matched some of the criteria set by this project and therefore was used to do the simulations. In this mechanism, the three way catalytic converter (Pt/Rh) [97, 98], a fuel can be passed through a platinum - rhodium catalyst. The highest hydrocarbon that could be passed was propane C_3H_8 . It is not as high in carbons and hydrogens as a kerosene fuel, but it is nevertheless a widely used fuel and therefore because of the small availability of catalytic reaction mechanisms, it fits the criteria of this initial study.

10.4.3 SIMULATION INPUTS IN CHEMKIN

A simple reaction scheme was used in the Chemkin interface. An inlet was connected to a honeycomb catalyst and then to an exit as it is shown in the diagram (Figure 10.4).

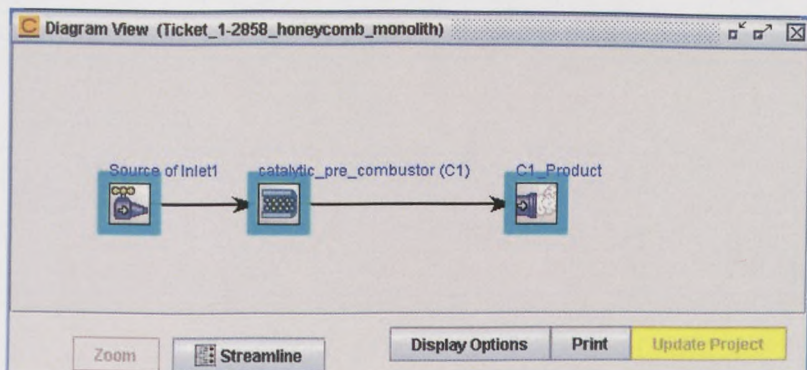


Figure 10.4: The Chemkin diagram interface.

HONEYCOMB CATALYST PROPERTIES AND SIMULATION PROBLEM

Some of the physical properties of the platinum/ rhodium catalyst were already inputted by running the mechanism in the Chemkin platform. These were taken as default values for this initial study and are shown in Table 10.1 and 10.2 together with the stagnation pressure and temperature parameters that were varied between simulations. The stagnation pressure expresses the pressure drop through the catalyst.

Problem Type:	Solve Gas Energy Equation
Momentum Equation:	Off
Residence Time:	On
Temperature	Variable 1
Pressure (i.e. stagnation pressure)	Variable 2
Surface Temperature:	Same as gas temperature

Table 10.1: Physical properties of the catalyst.

CATALYST PROPERTIES

Catalyst Weight	5.2 g
Metal Surface Area	1.89E6 cm²/g
Metal Surface Dispersion	70 %

Table 10.2: Catalyst properties.

HONEYCOMB PROPERTIES

The catalyst used is of cylindrical shape. The properties of the honeycomb are shown in Table 10.3.

Diameter	10 cm
Length	10 cm
Cell Density	400 cell/in²
Cell Wall Thickness	0.018 cm

Table 10.3: Honeycomb properties.

CATALYST SPECIES SPECIFIC PROPERTIES

Species	Surface Fraction
H(Solid)	0.05
O(Solid)	0.94
PD(Solid)	0.01

Table 10.4: Catalyst Species.

SOURCE INLET

Inlet mass flow rate	Variable 3	
Equivalence Ratio	Variable 4	
Fuel	Variable 5	
Oxidizer mixture	Air:	Fraction of total oxidizer mixture
		0.79 O_2
		0.21 N_2

Table 10.5: Inlet Inputs.

PRODUCT SETTINGS

The complete combustion products were set as usual: CO_2, H_2O, N_2

10.4.4 SIMULATION PROCEDURE AND INITIAL CONDITIONS

The procedure for numerically studying the production of H_2O_2 was by first setting an initial run condition run and then by conducting a study by setting one study variable whilst keeping all other variables steady at the initial condition. The selection of the initial condition values depended on their effectiveness in producing some H_2O_2 within the maximum catalyst distance, which was kept stable at 10cm. Table 10.7 presents the initial conditions. Each study investigates how the production of the hydrogen peroxide chemical is affected by increasing or decreasing one study variable (parameter study).

The variables were presented in Section 10.4.3. These are namely: (1) the catalyst temperature, (2) the catalyst stagnation pressure (i.e. the catalyst pressure drop), (3) the catalyst mass flow rate, (4) the fuel-air mixture equivalence ratio and (5) the fuel studied. The catalyst length and catalyst diameter variables were kept constant for this initial investigation. This was done on purpose as the simulations were concerned mostly with the effect of passing different fuels into the platinum/rhodium catalyst and not with the characteristics of the catalyst. Furthermore, it should be expected that the effectiveness of the fuel, when compared to another fuel, is not depended on the catalyst length and diameter.

Two fuels were studied in the simulations using the Detchem catalyst scheme. Table 10.6 shows some properties of these fuels.

PROPANE C_3H_8

According to the simulation, the program passes a mixture of propane and air into the platinum-rhodium catalyst, at the predefined mixture strength. In Section 10.4.2 it was explained why this fuel was selected (i.e. It is a wide used fuel and the highest hydrocarbon fuel that could be selected in the Detchem mechanism).

Methane was selected as the lighter fuel, for comparing another fuel with the propane simulation results. It is the simplest alkane and the main component of the natural gas. The wide use of the natural gas in industrial gas turbines and the ease in the supply of the fuel are two good reasons for investigating this fuel into the study of the production of H_2O_2 .

Name	Propane (gas)	Methane (gas)
Chemical Formula	C_3H_8	CH_4
%vol stoichiometric air	5/6	2/3
Molecular Weight ($\frac{g}{mol}$)	44.1	16.04
Density ($\frac{kg}{m^3}$)	2.0098	0.717
Melting point (K)	85.5	90.7
Boiling point (K)	231.1	111.6
Flash point(K)	169	85.15
Auto-ignition temperature (K)	723.15	313.15
Heat of reaction ($\frac{MJ}{m^3}$) (Per stoichiometric unit volume)	3.7	3.9
Heat of combustion ($\frac{MJ}{kg}$)	46	47

Table 10.6: Fuel properties for propane and methane

Catalyst Variable	Units	Propane	Methane
Stagnation Pressure	P_0 (atm)	4	4
Temperature	T (K)	1225	1225
Inlet Mass Flow Rate	\dot{m}_{in} ($\frac{kg}{s}$)	0.2	0.2
Fuel-air Equivalence Ratio	ϕ (-)	0.4	0.4
Distance	x (cm)	10	10

Table 10.7: Initial conditions for the Chemkin simulations on the production of H_2O_2 by passing fuel over a Pt/Rh catalyst.

CHAPTER 11 - CHEMKIN SIMULATIONS ON THE PRODUCTION OF H₂O₂ - RESULTS

Chapter 11 presents the outcome of the Chemkin simulation runs. Each simulation parameter was varied separately to study its influence on the production of H₂O₂ according to the procedure explained in Section 10.4.4. The results of both the C₃H₈ and the CH₄ simulated fuels are presented in each of the sections that describe a particular parameter study. These results show only the relationship between the simulation variables and the rate of production of H₂O₂, which is the principal objective of this study.

11.1 VARYING THE CATALYST STAGNATION PRESSURE

In Figures 11.1-11.2, the catalyst stagnation pressure was varied by keeping the air-fuel mixture parameters, namely the temperature, mass flow rate and equivalence ratio ϕ fixed.

11.1.1 PASSING PROPANE FUEL THROUGH THE PT/RH CATALYST

For the propane fuel, the catalyst stagnation pressures that were selected for the numerical investigation were 3, 4, 4.5 and 5 atmospheres. The temperature was set at 1225K (951.85°C). The mass flow rate of the fuel-air mixture was 0.2kg/s and the mixture's equivalence ratio was set to 0.4.

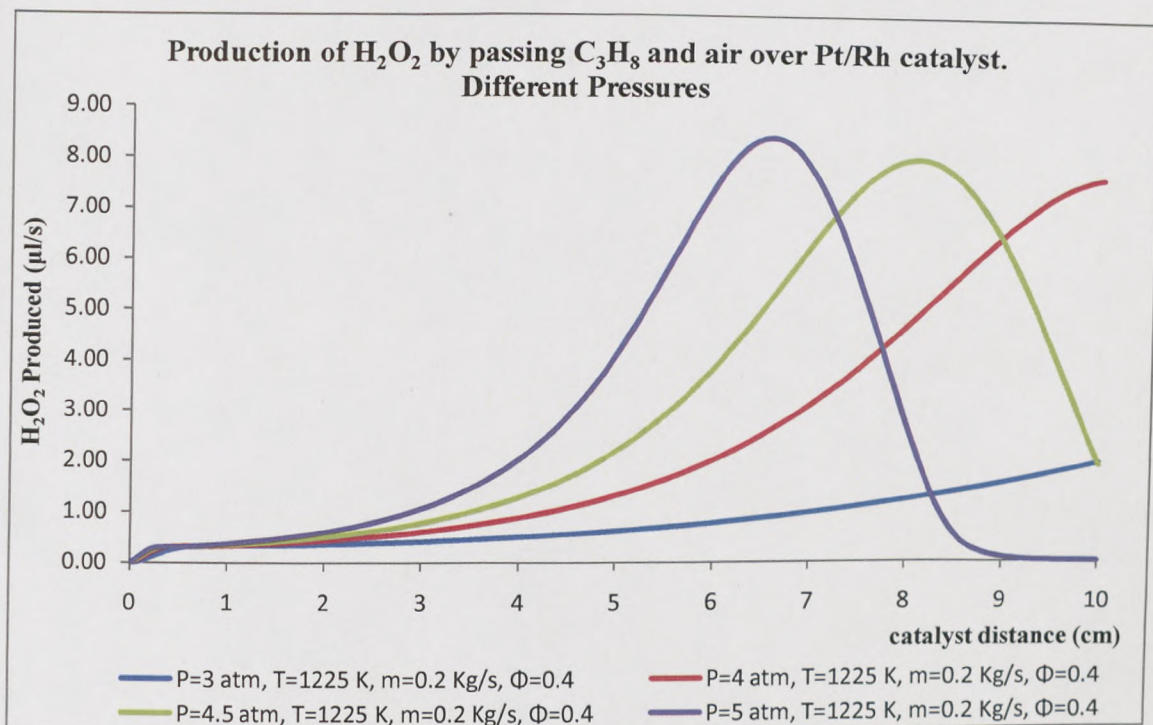


Figure 11.1: Graph of H_2O_2 production volume rate against catalyst distance, exhibiting the effect of varying the catalyst stagnation pressure. The fuel passing through the catalyst is propane-air.

11.1.2 PASSING METHANE FUEL THROUGH THE PT/RH CATALYST

For methane the catalyst stagnation pressure was simulated at 3, 4, 5, 6 and 7 atmospheres. All other parameters were kept the same as in the propane simulation. Figure 11.2 presents the results of this study.

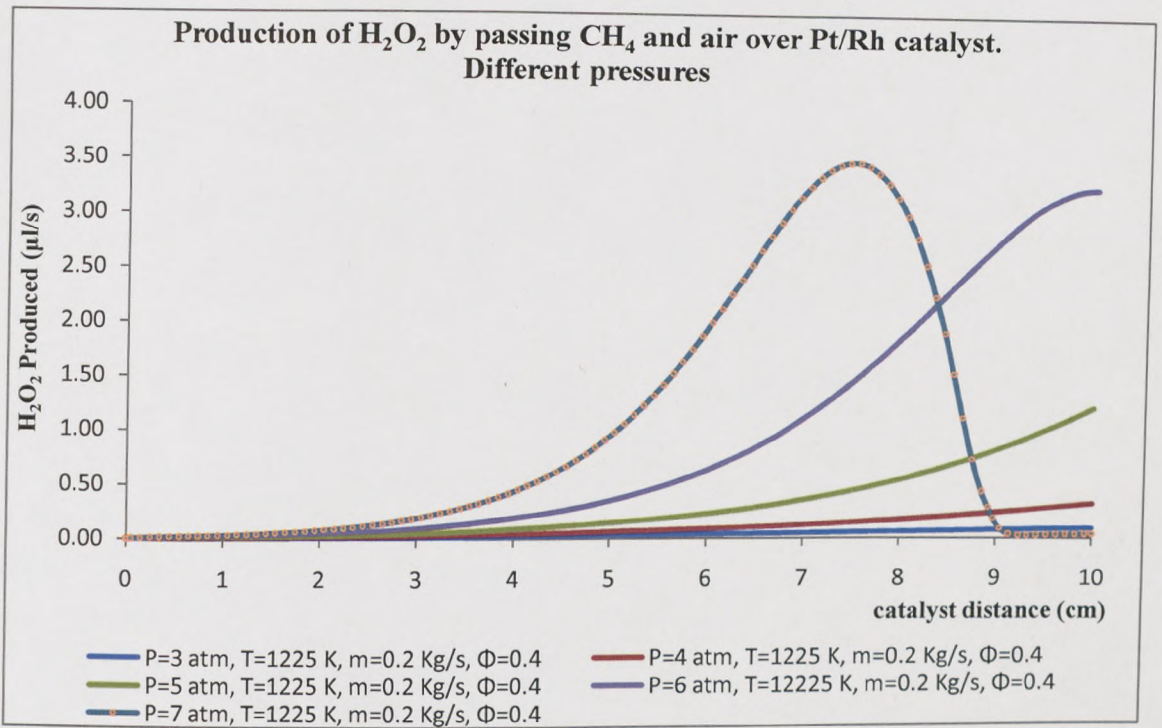


Figure 11.2: Graph of H_2O_2 production volume rate against catalyst distance, exhibiting the effect of varying the catalyst stagnation pressure. The fuel passing through the catalyst is

11.2 VARYING THE CATALYST TEMPERATURE

11.2.1 PASSING PROPANE FUEL THROUGH THE PT/RH CATALYST

Figures 11.3-11.4 are demonstrating the relationship between the catalyst temperature and the H_2O_2 production, at different catalyst pressures. The catalyst stagnation pressures were selected to be 3 and 4 atmospheres respectively for each study. The fuel-air mixture mass flow rate was kept steady at 0.2kg/s and the mixture was again at an equivalence ratio of 0.4.

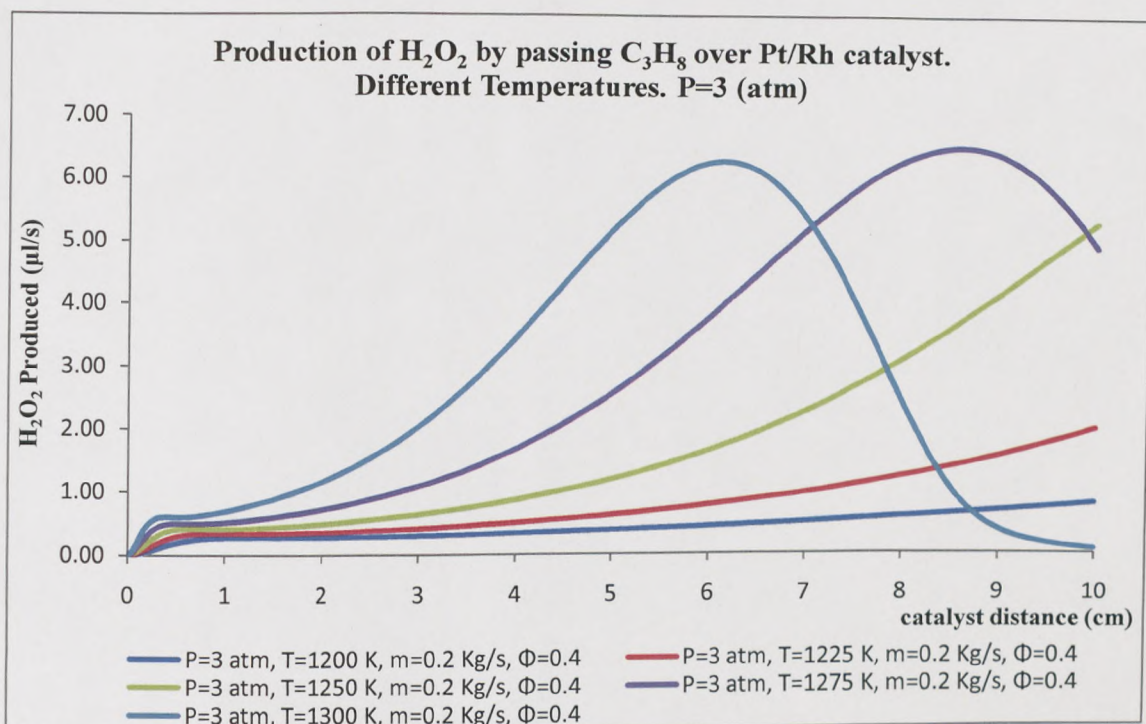


Figure 11.3: Hydrogen peroxide production volume rate against catalyst distance. The graph shows the effect of changing the catalyst temperature at a catalyst stagnation pressure of 3atm. The fuel passing through the catalyst is propane-air.

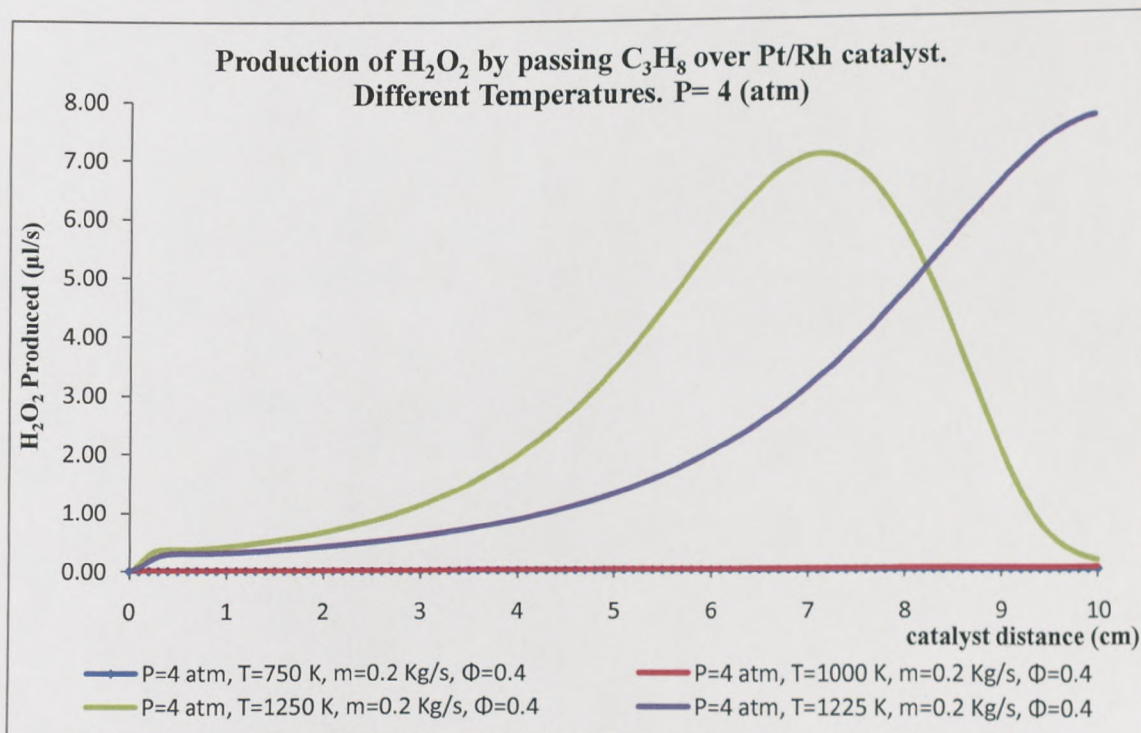


Figure 11.4: Hydrogen peroxide production volume rate against catalyst distance. The graph shows the effect of changing the catalyst temperature at a catalyst stagnation pressure of 4atm. The fuel passing through the catalyst is methane-air

11.2.2 PASSING METHANE THROUGH THE Pt/RH CATALYST

In Figure 11.5, the methane-air mixture was passed through the Pt/Rh catalyst at different catalyst temperatures, at a catalyst stagnation pressure of 4 atmospheres. The catalyst temperatures selected for these runs were 750, 1225 and 1250 Kelvin respectively for each simulation. Figure 11.5 presents the outcome of this study.

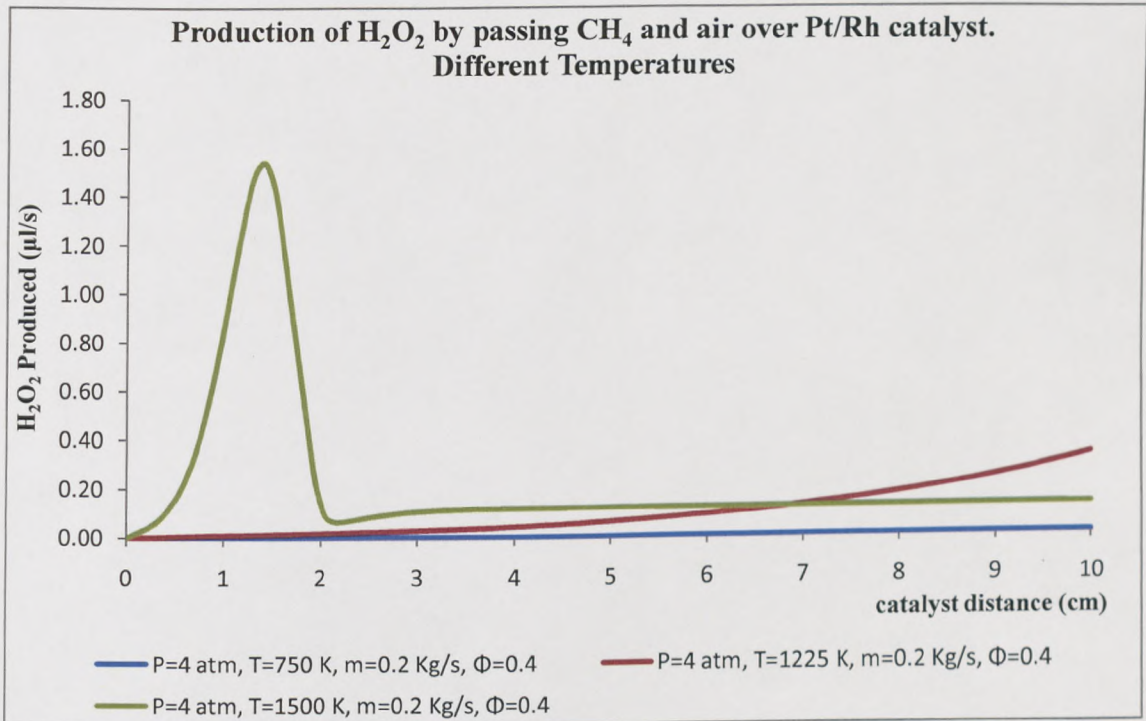


Figure 11.5: Hydrogen peroxide production volume rate against catalyst distance. The graph shows the effect of changing the catalyst temperature at a catalyst stagnation pressure of 4atm. The fuel passing through the catalyst is methane-air

11.3 VARYING THE CATALYST INLET MASS FLOW RATE

Figures 11.6-11.7 show the dependence of the hydrogen peroxide production by the Pt/Rh catalyst on the system's mass flow rate. All other variables were kept constant as previously mentioned. The pressure, temperature and ϕ values were 4atm, 1225K and 0.4 respectively.

11.3.1 PASSING PROPANE FUEL THROUGH THE Pt/RH CATALYST

In Figure 11.6, the fuel mixture's mass flow rate was increased from 0.05kg/s to 0.4kg/s but not at constant intervals. In particular, the values of the mass flow rates studied were 0.05, 0.1, 0.18, 0.2, 0.3 and 0.4kg/s.

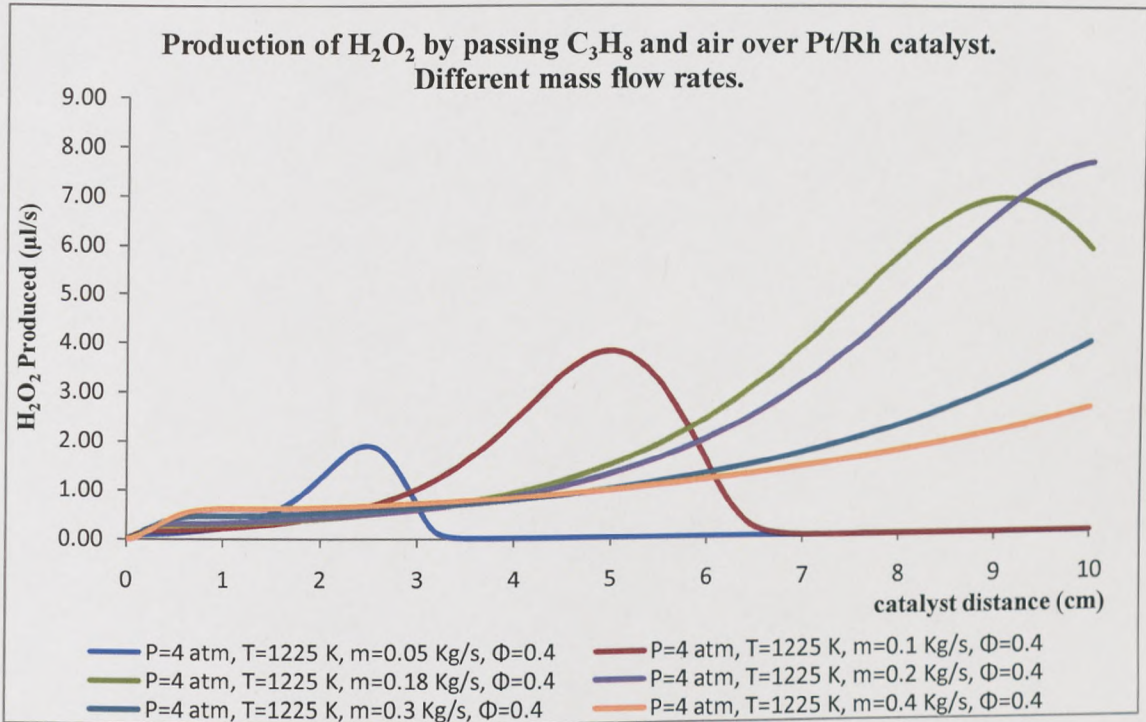


Figure 11.6: Graph of hydrogen peroxide production volume rate against catalyst distance, summarising the effect of different catalyst inlet mass flow rates. The fuel passing through the catalyst is propane-air

11.3.2 PASSING METHANE FUEL THROUGH THE PT/RH CATALYST

The values of the catalyst inlet mass flow rates selected for these simulations were 0.05, 0.1, 0.3, 0.4, 0.5, 0.9kg/s. Figure 11.7 presents the outcome of this study.

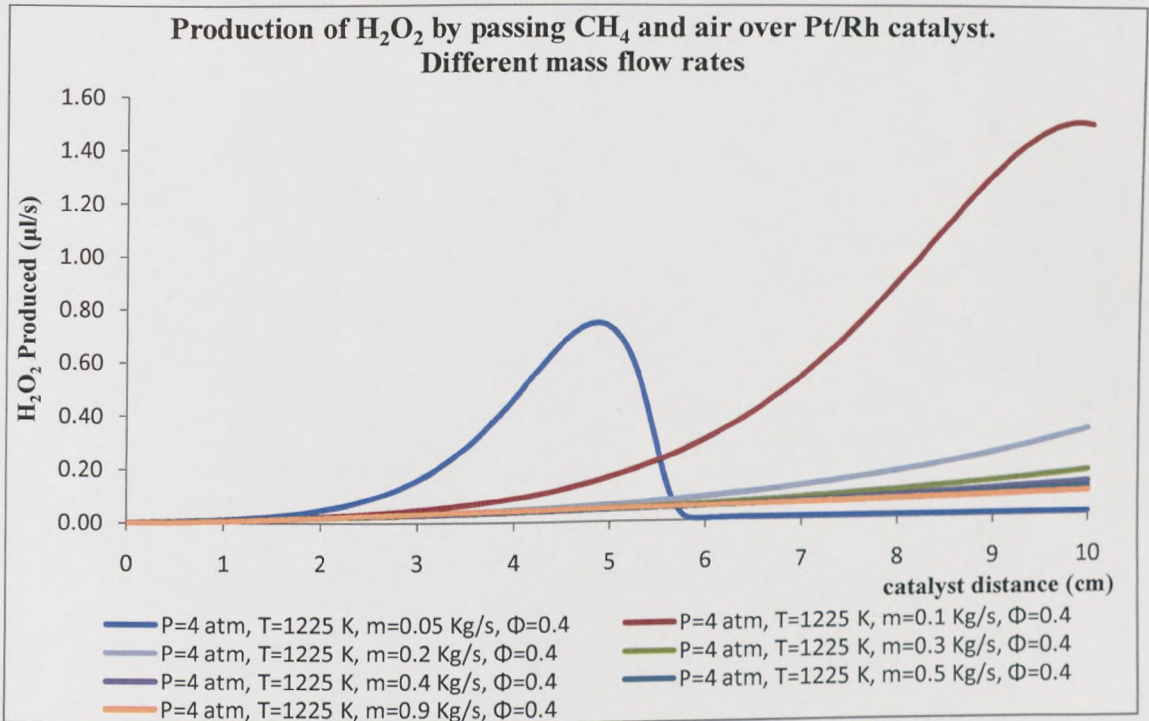


Figure 11.7: Graph of hydrogen peroxide production volume rate against catalyst distance, summarising the effect of different catalyst inlet mass flow rates. The fuel passing through the catalyst is methane-air

11.4 VARYING THE FUEL MIXTURE'S EQUIVALENCE RATIO Φ

This study involved passing the fuel-air mixture inside the catalyst at different compositions. All other parameters were kept to the initial simulation values. The catalyst pressure was at 4 atmospheres, the catalyst temperature was 1225K and the mixture's mass flow rate at the inlet of the catalyst was 0.2kg/s

11.4.1 PASSING PROPANE FUEL THROUGH THE PT/RH CATALYST

The effect of changing the mixture composition to the production of the hydrogen peroxide is shown in Figure 11.5. The values of the mixture strength ϕ for the particular study were 0.1, 0.2, 0.3, 0.4, 0.5, 0.6 and 0.9.

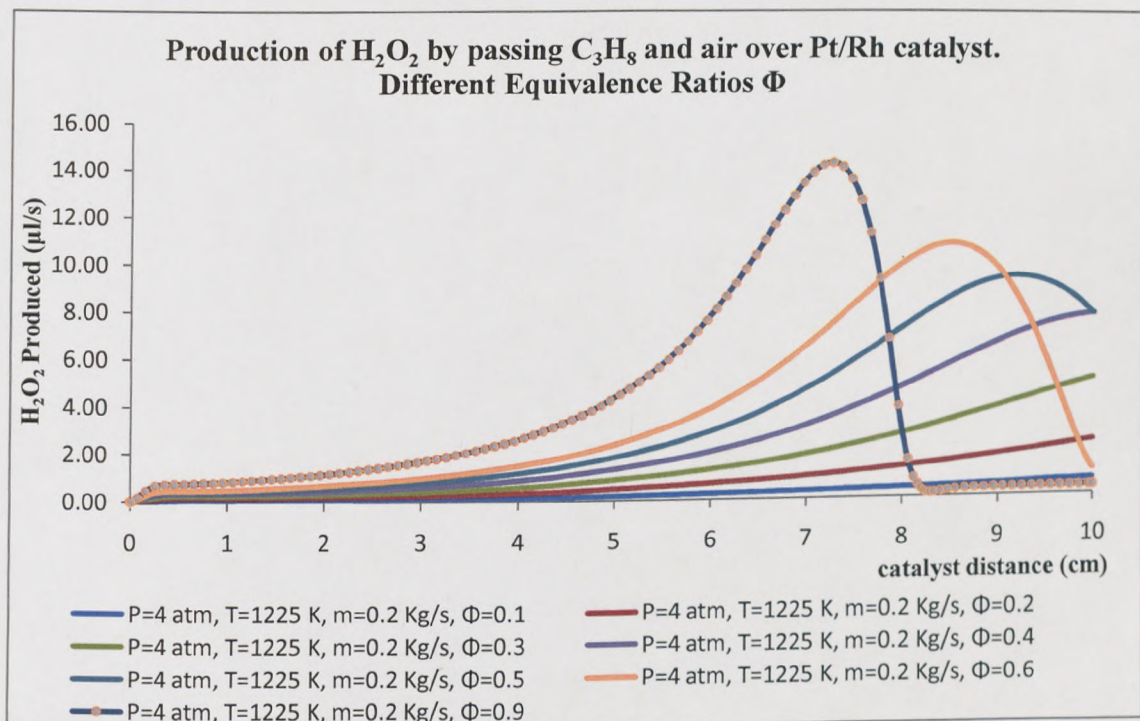


Figure 11.8: Graph of hydrogen peroxide production volume rate against catalyst distance, exhibiting the effect of varying the equivalence ratio. The fuel passing through the catalyst is propane-air.

11.4.2 PASSING METHANE FUEL CH_4 THROUGH THE Pt/RH CATALYST

For the methane-air mixture, the equivalence ratios Φ that were studied were 0.1, 0.2, 0.3, 0.4, 0.5, 0.6, 0.7, 0.9, 1.2 and 1.5. Figure 11.9 shows the findings of this study.

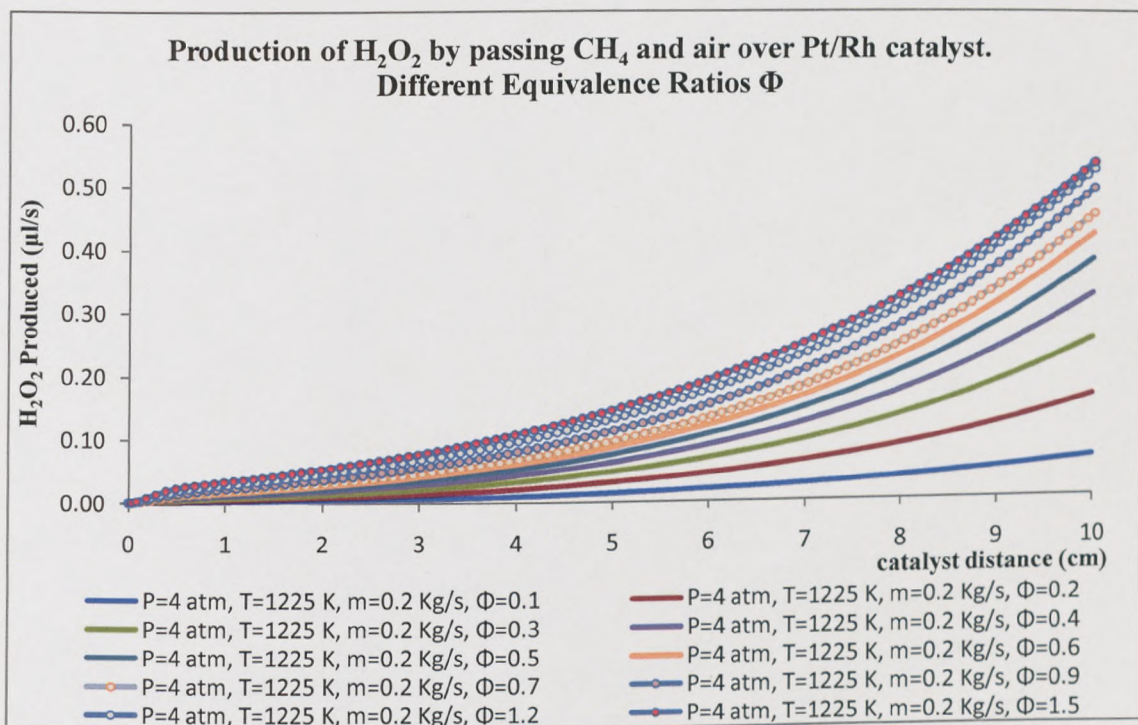


Figure 11.9: Graph of hydrogen peroxide production volume rate against catalyst distance, exhibiting the effect of varying the equivalence ratio. The fuel passing through the catalyst is methane-air.

CHAPTER 12 - DISCUSSION OF SIMULATION RESULTS ON THE PRODUCTION OF H₂O₂

12.1 STUDY OUTLINE

To support the ignition system proposal, the production of hydrogen peroxide was investigated numerically by looking at the effect of passing separately propane and methane over a catalyst. For this purpose, simulations were conducted in the Chemkin platform using a Pt/Rh catalyst scheme, as described in Chapter 10. In this initial study the catalyst distance was kept stable at 10cm.

It is encouraging to note that in the simulations, hydrogen peroxide production was found possible at rates above 10.8 μ l/s. This rate was the maximum H₂O₂ rate injected in the gas-turbine experimental studies (Chapters 7-9) that, when injected to the cavity of the modified focus discharge igniter, resulted in a maximum of 44% improvement in the lean ignition limits of the kerosene jet A₁ fuel.

12.2 THE EFFECT OF CATALYST STAGNATION PRESSURE TO THE PRODUCTION OF H₂O₂

The increase in the stagnation pressure means that the fuel passes through the catalyst with a higher velocity. Hence, there are less energy losses related with the passing of the fluid into the catalyst matrix. Moreover it should be noted that the pressure increase simply translates to more moles of fuel per unit volume are available and thus the location of the maximum H₂O₂ production is closer to the inlet and reflects the greater rapidity of the products (due to more fuel being available per unit time). An interesting point in the graph is the similarity of the H₂O₂ production rate peaks and how a peak depends on the catalyst distance when changing the stagnation pressure. The H₂O₂ production rate peaks become smoother as the stagnation pressure decreases.

Figure 11.1, shows how the pressure drop inside the catalyst affects the production of the hydrogen peroxide when propane is used. When the stagnation pressure is large the pressure drop inside the catalyst is small. It is suggested in Figure 11.1 that if the pressure drop inside the catalyst is decreased the production of H₂O₂ should increase within the constant catalyst distance. Moreover, it suggests that at a higher pressure drop, a similar but slightly lower H₂O₂ production rate could be obtained if the catalyst distance was increased. The graph indicates that at a low stagnation pressure of $P_0 = 3(atm)$ the H₂O₂ production rate would be low to about 2.5-3.5 μ l/s even if the catalyst distance was increased. The maximum H₂O₂ production rate was found to be 8.38 μ l/s at a catalyst distance of 6.57cm. This result was obtained

by increasing the stagnation pressure of the initial condition by 1atm to $P_0=5$ atm.

A similar behaviour is found to exist between the pressure drop and the H_2O_2 production when methane is used as the fuel (Figure 11.2). As the stagnation pressure increases, the H_2O_2 production also increases. It should be noted that the H_2O_2 production rate peaks in the graph of Figure 10.2 become smoother again as the pressure drop increases. Moreover the maximum H_2O_2 production rate was found to be $3.47\mu\text{l/s}$ at a stagnation pressure of $P_0=7\text{atm}$ and at a catalyst distance of 7.45cm.

The catalyst pressure drop can be reduced by using more efficient catalyst shapes. More efficient catalyst shapes will allow less energy to be lost when the fluid passes through the catalyst bed. There are three main catalyst shapes: The pellet type, the ring type and the ribbed or daisy type. These are shown in Figure 12.1[99].



Figure 12.1: Main catalyst shapes. a) pellet type catalyst, b) ring type catalyst, c) ribbed or daisy type[99]

12.3 THE EFFECT OF CATALYST TEMPERATURE TO THE PRODUCTION OF H_2O_2

Figures 11.3 and 11.4 show the relationship between the catalyst temperature and the H_2O_2 production rate, when passing propane through the catalyst, at $P_0 = 3(atm)$ and $P_0 = 4(atm)$ respectively.

At the $P_0 = 3(atm)$ stagnation pressure, the temperature was varied from 1200(K) to 1300(K). In Figure 11.3 it is interesting to note that the maximum H_2O_2 production rate is found at $T=1275(K)$ and at a catalyst distance of 8.55(cm) and not at a higher temperature. This rate is 7.62(μ l/s) of H_2O_2 . Moreover, the graph indicates that as the temperature decreases, the H_2O_2 production rate will increase but at a longer than 10(cm) catalyst distance.

At the $P_0 = 4(atm)$ stagnation pressure, the temperature was varied from 750(K) to 1300(K). A similar behaviour to Figure 11.3 is shown in Figure 11.4. In Figure 11.4 the maximum H_2O_2 production rate is found at $T=1225(K)$ at the maximum catalyst distance of 10(cm). This rate is 7.62(μ l/s) of H_2O_2 . Moreover, in the same plot, it is shown that when the catalyst temperature is above $T=1225(K)$ the H_2O_2 production rate decreases. At a catalyst temperature of $T=1000(K)$ the maximum H_2O_2 production rate is 0.037(μ l/s) at the maximum catalyst distance studied. At this temperature the H_2O_2 production rate increases slowly with catalyst distance. Therefore, there is an optimum temperature for maximum H_2O_2 production depending on the catalyst distance.

Figure 11.5 shows the results obtained when passing methane over the Pt/Rh catalyst at different temperatures. The graph indicates that the production of the H_2O_2 is very sensitive to temperature changes. Although the run at $T=1500(K)$ was converged the result is considered questionable. More simulations would need to be conducted near this temperature before conclusions can be drawn.

12.4 THE EFFECT OF THE FUEL-AIR INLET MASS FLOW RATE TO THE PRODUCTION OF H_2O_2

In Figure 11.6 the catalyst mass flow rate of the propane air mixture was varied to study how this affects the hydrogen peroxide production. The mass flow rates studied were 0.05, 0.1, 0.18, 0.2, 0.3 and 0.4(kg/s) with the 0.2(kg/s) run being the initial condition. The graph clearly shows that the H_2O_2 production rate increases when increasing the propane-air mass flow rate through the catalyst. The results indicate that the hydrogen peroxide production depends on the propane-air mixture. This observation should be expected after realising that the particular fuel mixture is producing H_2O_2 by passing it through a Pt/Rh catalyst. As the mass flow rate is increased inside the catalyst, a larger number of molecules of the mixture will react with the catalyst per unit time resulting in an increased production rate. The distance of the catalyst plays once again an important role in the production of the H_2O_2 . The maximum H_2O_2 production rate in this study is $7.62\mu l/s$ and is found using the initial condition $\dot{m} = 0.2(kg/s)$ at the maximum catalyst distance. Hence, the graph reveals that the hydrogen peroxide production will increase with increasing mass flow rates at longer catalyst distances. It should be highlighted that when increasing the mass flow rate by a factor of 2 the H_2O_2 production rate doubles.

A similar behaviour is shown in Figure 11.7 for the methane fuel. When increasing the mass flow rate of the fuel-air mixture, inside the catalyst, from 0.05 to 0.1kg/s the H₂O₂ production rate again doubles. As the methane fuel is less effective than the propane fuel, in producing H₂O₂, the maximum production rate is lower. The maximum production rate is found to be 1.5µl/s at the maximum catalyst distance of 10cm with a mixture mass flow rate of 0.1kg/s. This rate is expected to increase by increasing the methane-air mass flow rate and/or the catalyst distance.

12.5 THE EFFECT OF THE FUEL-AIR EQUIVALENCE RATIO TO THE PRODUCTION OF H₂O₂

The fuel flow rate that is required to pass through the catalyst can be calculated from the equivalence ratio of the mixture and by knowing the mixture's mass flow rate at the inlet of the catalyst. The equation below is obtained from the general equivalence ratio equation (9.2):

$$\dot{m}_f = \dot{m}_{in} \frac{\Phi \left(\frac{\dot{m}_f}{\dot{m}_{air}} \right)_{stoich}}{1 + \Phi \left(\frac{\dot{m}_f}{\dot{m}_{air}} \right)_{stoich}} \quad (10.5)$$

\dot{m}_f : fuel mass flow rate

\dot{m}_{in} : total mass flow rate at catalyst inlet. $\dot{m}_{in} = 0.2kg/s$

Φ : equivalence ratio of fuel air mixture passing through the catalyst

$\left(\frac{\dot{m}_f}{\dot{m}_{air}}\right)_{stoich}$: stoichiometric fuel to air mass flow ratio.

For propane: $\left(\frac{\dot{m}_f}{\dot{m}_{air}}\right)_{stoich} = \frac{1}{11.964}$. For methane: $\left(\frac{\dot{m}_f}{\dot{m}_{air}}\right)_{stoich} = \frac{1}{13.6}$.

Table 12.1 presents the fuel mass flow rates that were used in the equivalence ratio study according to equation (10.5). It is shown that for the methane case, at the same equivalence ratios as the propane, the fuel flow rate is higher for the same total inlet mass flow rate. Therefore, even with higher fuel flow rates, methane does not produce as high H₂O₂ rates as the propane fuel. It is suggested that higher hydrocarbons are more effective in producing the desired chemical compound.

$m_{in} = 0.2$	ϕ	0.1	0.2	0.3	0.4	0.5	0.6	0.7	0.9	1.2	1.5
(C ₃ H ₈) Propane	$\dot{m}_f \left(\frac{g}{s}\right)$	1.658	3.288	4.892	6.470	8.023	9.551	-	13.993	-	-
(CH ₄) Methane	$\dot{m}_f \left(\frac{g}{s}\right)$	1.460	2.899	4.317	5.714	7.092	8.451	9.790	12.414	16.216	19.868

Table 12.1: Calculated fuel mass flow rate depending on the equivalence ratio used in the simulations

Figures 11.8 and 11.9 show how the fuel-air equivalence ratio, of the mixture that passes through the catalyst, affects the production of the hydrogen peroxide. As the mass flow rate of the fuel is increased and the total mass flow rate is kept constant, the H₂O₂ production rate also increases. The relationship indicates that it is the fuel that dictates the production of the H₂O₂ when the mixture reacts with the Pt/Rh catalyst. In Figure 11.8 the maximum H₂O₂

production rate is found to be $14.18\mu\text{l/s}$ at the highest equivalence ratio $\phi=0.9$ that was studied with propane at a catalyst distance of 7.26cm . In Figure 11.9 with methane as the fuel, a peak in the H_2O_2 production could not be found within the predefined catalyst distance of 10cm . The maximum equivalence ratio that was studied with methane was $\phi=1.5$ but the maximum H_2O_2 production rate that could be achieved was $0.531\mu\text{l/s}$ at the maximum catalyst distance. Clearly, with a lower mass flow rate and a higher stagnation pressure this value will increase.

12.6 SUMMARY OF DISCUSSION ON CHEMKIN SIMULATIONS ON THE PRODUCTION OF H_2O_2

The subject of this study was to evaluate the hypothesis that hydrogen peroxide can be produced by passing a fuel over a suitable catalyst. The evaluation was done numerically in this initial study. The simulations investigated the passing of propane and methane over a Pt/Rh catalyst in the Chemkin platform using the Detchem Mechanism. The simulations suggest that the reactions of the fuel-air mixtures with the Pt/Rh catalyst will lead to the production of some H_2O_2 . The runs indicate that the highest hydrocarbon fuel, the propane, is more suitable for the production of the required chemical and that it will result in better yields of H_2O_2 .

Figure 12.2 shows the maximum hydrogen peroxide rates that were numerically produced by simulating the passing of the propane fuel over a fixed distance of

10cm of the Pt/Rh catalyst. A similar behaviour is observed when passing methane through the catalyst. In this case though, even with higher fuel flow rates, methane fails to achieve as high H_2O_2 production rates as the propane fuel. It is indicative to say that the highest H_2O_2 production rate, obtained by using methane as the fuel, is $1.5\mu\text{l/s}$ at the maximum catalyst distance of 10cm and at a mixture mass flow rate of 0.1kg/s . The highest H_2O_2 production rate that was achieved by the propane fuel is $14.8\mu\text{l/s}$ at a catalyst distance of 7.26cm and at a mixture mass flow rate of 0.2kg/s .

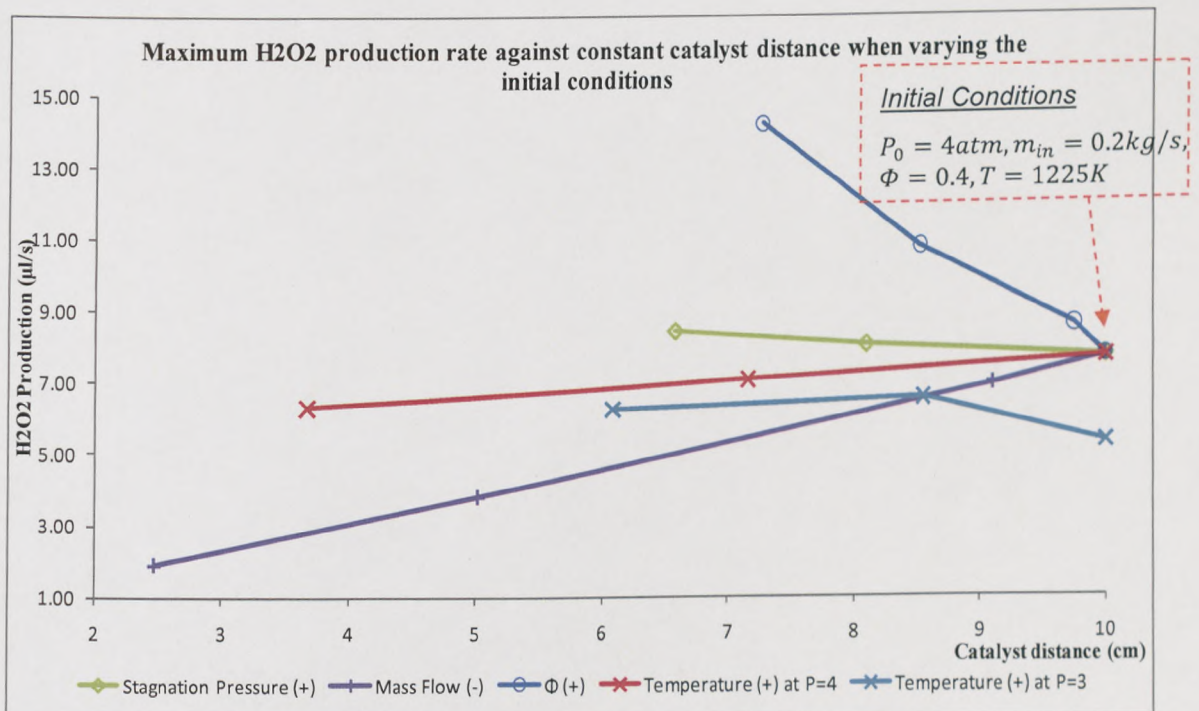


Figure 12.2: Maximum H_2O_2 production rates, within a specific catalyst length of 10cm, obtained by the Chemkin simulations in the passing of propane-air over a Pt/Rh catalyst. The maximum H_2O_2 yield is investigated by changing the initial conditions (shown in the graph by the orange arrow). (+): Increase. (-): decrease of the specified variable.

13.1 CONCLUSIONS FROM THE EXPERIMENTAL WORK

A number of experiments were conducted on a conventional Olympus liner at air mass flows of about 0.2, 0.4, 0.6, 0.7 and 0.8 kg/s. For each air mass flow, hydrogen peroxide was injected to the cavity of a modified focus discharge igniter (FDI) at various volume rates of 0, 0.54, 2.7, 5.4 and 10.8 μ l/s. The experimental results showed good consistency throughout this work. More importantly, repeatability was not only shown throughout the different experimental cases studied by using a serviced (clean) and an 'under normal service' (used) fuel injector, but it was also ensured by the use of the 60% probability of ignition criterion which was employed to determine the lean ignition limits. The following are the conclusions drawn.

CONCLUSIONS FROM THE EXPERIMENTS WITH THE USED FUEL INJECTOR DEVICE AND WITH KEROSENE AS THE TEST FUEL

- The addition of small volumes of hydrogen peroxide helped to extend the lean operational limits of the engine.
- Although a higher equivalence ratio was calculated by assuming enhancement of the fuel by the H₂O₂ addition, the strength of the mixture was decreased at the lean ignition limit.
- A maximum of 44% improvement, in terms of ϕ , in the lean ignition limit was achieved at an air mass flow of 0.604(\pm 0.009)kg/s with the insertion of 10.8 μ l/s hydrogen peroxide at a 50% by weight solution in water.

- Whilst lower lean ignitability limits were achieved, the net energy of the fuel that was present in the combustor at the instant of ignition was also decreased.
- The energy that was added to the fuel by the decomposition of hydrogen peroxide is not the full explanation of the improvement in ignition. The implication of these experiments is that ignition was aided by the presence of radicals formed by the dissociation of H_2O_2 during the spark breakdown, as it is indicated by other researchers.
- The exhaust temperature graphs highlight further the improvement in ignition experienced by the addition of hydrogen peroxide. The increased temperature gradients suggest that the reaction rate of the kerosene-air mixture, at the same equivalence ratios, was increased by the addition of hydrogen peroxide.
- The maximum, minimum and mean ignition times at the limits of ignition were decreased by the introduction of the hydrogen peroxide. The mean time for ignition at the limit was decreased by 76.28% with $10.8\mu\text{l/s H}_2\text{O}_2$.
- The mean ignition time of all experiments was also reduced for each hydrogen peroxide injection rate case. The maximum reduction of the mean time for ignition was 54.2% by using $10.8\mu\text{l/s H}_2\text{O}_2$.
- The insertion of hydrogen peroxide played a key role in the chemical process of ignition.

CONCLUSIONS FROM THE EXPERIMENTS WITH THE CLEAN FUEL INJECTOR DEVICE AND WITH KEROSENE AS THE TEST FUEL

- The use of the clean fuel injector alone, has resulted in reducing the lean ignition limits to very low values of mixture strengths ϕ . The improvement depends on the air mass flow and was found to be 35% and 57% at about 0.4 and 0.6kg/s of air respectively. The comparison is done between the highest and lowest fuel spray quality (FSQ) cases,
- Even at such low mixture strengths ϕ , a small amount of H_2O_2 additive has enhanced the ignition ability to equivalence ratios lower than the lean limit set without the H_2O_2 additive.
- A maximum improvement of 11% to 20% is shown to be possible by using the modified FDI igniter with a H_2O_2 plasma injection of $10.8\mu\text{l/s}$, depending on the air mass flows used, at the highest FSQ case.
- The ignition performance of the modified focus discharge igniter was enhanced by the supplied H_2O_2 plasma medium and this is also evident by the increase in the maximum temperature gradients of the exhaust gases during the early stages of ignition (Figure 9.8).
- In the case of the hydrogen peroxide injection during ignition, it is very positive to note that, the novel igniter exhibits higher performance as the fuel spray quality (FSQ) deteriorates, with only a low flow rate of H_2O_2 additive in the order of $\mu\text{l/s}$.
- The lean ignition limits of the kerosene fuel remain virtually unchanged by using a water plasma additive (instead of H_2O_2) when compared with the 'no H_2O_2 ' FDI case.

- The H₂O plasma medium fails to increase the maximum temperature gradient of the exhaust gas as the engine pulls away from idle.

CONCLUSIONS FROM THE SHORT EXPERIMENTS WITH THE CLEAN FUEL INJECTOR DEVICE AND WITH F.A.M.E. BIODIESEL AS THE TEST FUEL

- An improvement in the lean ignition limits of the biodiesel fuel between 0% and 11% was achieved by using a 10.8 μ l/s H₂O₂ injection rate into the FDI igniter at the studied air mass flow rates of about 0.4, 0.6 and 0.7kg/s.

13.2 SIMULATIONS ON THE PRODUCTION OF H₂O₂

The production of H₂O₂, by passing separately propane-air or methane-air mixtures through a platinum/rhodium catalyst, was numerically studied using the Chemkin Pro platform. This work focused on parameter studies to investigate the effect of different simulation variables with a fixed catalyst distance of 10cm.

The following remarks can be drawn from the simulation runs:

- Fuel study

Both methane and propane fuels were effective in producing some small amount of H₂O₂ when passing them through the Pt/Rh catalyst. The results indicate that the propane fuel is more effective in producing H₂O₂ over the same catalyst length.

- Fuel-air equivalence ratio study

The fuel flow rate across the catalyst was increased by increasing the equivalence ratio, whilst keeping the mass flow rate constant. Increasing fuel flow rate is the most effective way in increasing the H_2O_2 production rate. Most importantly, the study suggests that some hydrocarbon fuels can be used as reactants for generating H_2O_2 , alongside the use of a suitable catalyst.

- Catalyst stagnation pressure study

Increasing the stagnation pressure, hence decreasing the pressure drop inside the catalyst, increases the H_2O_2 production rate.

- Catalyst temperature study

There is an optimum temperature for obtaining a high H_2O_2 yield at a specific catalyst length. It was shown that increasing the temperature will slightly decrease the maximum H_2O_2 production rate. The study suggests that the catalyst temperature is more important for selecting the correct catalyst length at a given mixture mass flow rate.

- Catalyst mass flow rate study

Increasing the mass flow rate, of the fuel-air mixture that passes through the catalyst, results in higher H_2O_2 yields. The inlet mass flow rate should determine the selection of the catalyst length at a particular catalyst temperature.

13.3 SUGGESTIONS FOR FUTURE RESEARCH

In the feasibility study it was shown that the costs and the safety issues of installing and using the proposed ignition technology in industrial gas turbines

are minimal. Due to the demonstrated reduction in the lean limits of the kerosene, the market for this technology is wide and hence the possibilities for immediate application should be exploited.

There is evidence to suggest that the improvement in the ignition limits shown in this work with the kerosene and the F.A.M.E. biodiesel fuel can be achieved with other fuel-air mixtures, when burned in gas turbine engines. Future research should investigate this hypothesis. Other experimental research should concentrate on determining optimum H_2O_2 rates depending on fuels, air mass flow rates, combustors, fuel injectors, different plasma igniter designs and last but not least pressures and temperatures at simulated different altitude re-light conditions.

From the consistent results obtained throughout the experimental study -with the kerosene fuel on the Olympus gas turbine rig,- it is shown that the improvements achieved in the lean ignition limits are most highlighted at the ~ 0.6 kg/s air mass flow rates. It is therefore suggested that new ignition systems could be evaluated first at this air mass flow rate before conducting complete experimental studies.

From the discussion on the effect of the fuel spray quality (FSQ) with 'no H_2O_2 ' plasma ignition, it was shown, using the available data only, that the fuel spray quality improves the ignition limits of the kerosene fuel by a constant factor. Assuming this is true, an empirical formula was obtained to predict the standard focus discharge igniter's behaviour at different FSQs (using data available at two other FSQs and one ignition limit at the new FSQ). This formula should be evaluated further at different air mass flow rates and FSQs. If the assumption is

correct then the direct consequence would be to dramatically decrease the time for obtaining the base lean limits -that depend on the condition of the fuel injector- and hence the costs of ignition experiments of new systems.

From the initial simulation runs, a more specialised study is suggested in the chemistry of the production of H_2O_2 from gas turbine fuels. A cost effective method of an onsite H_2O_2 production in small amounts would be an ideal topic for further study. A novel ignition system that will produce the required H_2O_2 medium by passing some fuel through a catalyst and then directly infusing the products into the cavity of a focus discharge or plasma igniter, during the ignition sequence, was proposed. The study should look further into the feasibility of the catalytic ignition system which is proposed at the end of Section 9.12 (Figure 9.10).

REFERENCES

1. Weinberg, F.J. *The significance of reaction of low activation energies to mechanism of combustion.* in *Proceedings of the Royal Society of London.* 1955b: Mathematical and Physical Sciences. A230, p.331-342
2. Wilson, C.W., Novel ignition systems and the effect of primary zone aerodynamics on the ignition of aircraft gas turbines, Ph.D. Thesis, Mechanical Engineering, University of Leeds
3. Cardiner, W.C.J., *Gas-Phase combustion chemistry.* 2000, New York: Springer-Verlag. p.
4. McIntosh, A.C. and Prongidis, A. *Further biomimetic challenges from the bombardier beetle- the intricate chemical production system.* in *Conference on Design and Nature.* 2010. Pisa, Italy: C.A. Brebbia and Carpi, A. Design and Nature V. p.265-272
5. McIntosh, A.C. *Biomimetic inspiration from fire and combustion in nature including the bombardier beetle, Invited paper in session 7401.* in *Proceedings of SPIE.* 2009. San Diego: M.-P. R.J. and Lakhtakia, A. SPIE Bellingham 74010F.
6. McIntosh, A.C. and Beheshti, N., *Insect inspiration.* Physics World (Inst. of Physics), 2008. **21**(4): p. 29-31.
7. Low, H.C., Wilson, C.W., Abdel-Gayed, R.G., and Bradley, D. *Paper No. 89-29244.* in *25th Joint Propulsion Conference.* 1989. Monterey: AIAA.
8. Carleton, F.B., Vince, I.M., and Weinberg, F.J. *Energy and radical losses from plasma jet igniters to solid surfaces.* in *Nineteenth symposium on combustion.* 1982. Haifa, Israel: T.c. institute. p.1523-1531
9. Smy, P.R., Clements, R.M., Dale, J.D., Simeoni, D., and Topham, D.R., *Plasma expulsion from the plasma jet igniter* J. Physics D: Applied Physics 1982. **15**(11).
10. Boileau, M., Staffelbach, G., Cuenot, B., Poinso, T., and Berat, C., *LES of an ignition sequence in a gas turbine.* Combustion and flame, 2008. **154**(1): p. 2-22.
11. Neophytou, A., Spark ignition and flame propagation in flames, Ph.D. Thesis, Department of Engineering, Cambridge University
12. Aneshansley, D.J., Eisner, T., Widom, M., and Widom, B., *Biochemistry at 100°C.: Explosive secretory discharge of Bombardier Beetles (Brachinus)* Science, 1969. **165**: p. 61-63.
13. Aneshansley, D.J. and Eisner, T. *Spray aiming in the Bombardier Beetle: Photographic Evidence.* in *Proceedings Natural Academy of Science.* 1999. USA. 96,
14. Aneshansley, D.J., Edgerton, H.E., and Eisner, T., *Defensive spray of the bombardier beetle: A biological pulse jet.* Science, 1990. **248**: p. 1219-1221.

15. McIntosh, A.C. and Forman, M. *The efficiency of the explosive discharge of the bombardier beetle with possible biomimetic applications.* in *Design and Nature II*, C.A. 2004. Southampton and Boston: WIT Press.
16. Beheshti, N. and McIntosh, A.C., *A biomimetic study of the explosive discharge of the bombardier beetle.* *Int. J. Design and Nature*, 2007. **1**: p. 61-69.
17. Beheshti, N. and McIntosh, A.C., *The bombardier beetle and its use of a pressure relief valve system to deliver a periodic pulsed spray.* *Bioinspiration and Biomimetics*, (Inst. of Physics), 2007. **2**: p. 57-64.
18. Beheshti, N. and McIntosh, A.C. *A novel spray system inspired by the bombardier beetle.* in *Design and Nature IV*, C.A. 2008. Southampton and Boston: WIT Press. p.13-22
19. Lefebvre Arthur, H., *Gas turbine combustion.* 1983, U.S.A.: Hemisphere Pub. Inc.
20. Rolls-Royce, *The Jet Engine; 5th Edition.* 5th ed. 1996: Rolls-Royce plc 1986; Derby, U.K. p.
21. Anderson John, D., Jr., *Aerodynamics some fundamental principles and equations- Chapter 2*, in *Fundamentals of aerodynamics.* 2001, McGraw-Hill Inc: N.Y. p. 85-176.
22. Kanury Murty, A., *Appendix A: Review of thermodynamics of gases*, in *Introduction to combustion phenomena*, I. Glassman, Editor. 1982, Gordon and Breach: N.Y. p. 321-339.
23. Anderson John, D., Jr., *Compressible Flow- Chapter 7*, in *Fundamentals of aerodynamics.* 2001, McGraw-Hill Inc. p. 435-464.
24. Hill, P.G. and Peterson, C.R., *Air breathing engines- Part 2*, in *Mechanics and thermodynamics of propulsion.* 1992, Addison-Wesley: Wokingham. p. 139-466.
25. Anderson John, D., Jr., *Normal shock waves and related topics- Chapter 8*, in *Fundamentals of aerodynamics.* 2001, McGraw-Hill Inc. p. 465-502.
26. Anderson John, D., Jr., *Compressible flow through nozzles, diffusers and wind tunnels- Chapter 10*, in *Fundamentals of aerodynamics.* 2001, McGraw-Hill Inc: N.Y. p. 555-585.
27. Farokhi, S., *Engine Thrust and performance parameters & Gas turbine engine cycle analysis- Chapters 3-4*, in *Aircraft propulsion.* 2009, John Wiley&Sons Inc.: U.S. p. 97-214.
28. Jenkinson Lloyd, R., Simpkin, P., and Rhodes, D., *Powerplant and instalation- Chapter 9*, in *Civil Jet Aircraft Design.* 1999, Arnold: London. p. 181-222.
29. Gorla, R.S.R. and Khan, A.A., *Turbomachinery design and theory*, ed. M.D. Inc. 2003, New York.
30. Saravanamuttoo, H.I.I., Rogers, G.F.C., and Cohen, H., *Compressors- Chapters 4-5*, in *Gas Turbine Theory.* 1996, Pearson Education limited: Essex. p. 126-231.

31. Farokhi, S., *Compressors- Chapters 7-8*, in *Aircraft propulsion*. 2009, John Wiley&Sons Inc.: U.S. p. 389-524.
32. Turns, S.R., *Thermal - Fluid Sciences: An Integrated Approach*. 2006, Hong Kong, Golden Cup Printing Co. Ltd., Cambridge University Press.
33. Zucker, R.D. and Biblarz, O., *Fundamentals of Gas Dynamics*. 2nd ed. 2002, New Jersey: John Wiley & Sons, Inc. p.
34. NASA. *Visible earth*. [cited; Available from: www.visibleearth.nasa.gov/].
35. Rolls-Royce, *Combustion Chambers- Part 4*, in *The jet engine*. 1966, Rolls-Royce Limited: Derby, U.K. p. 25-34.
36. Rahm, S., Goldmeer, J., Moliere, M., and Eranki, A. *Addressing gas turbine fuel flexibility*. in *Power-Gen*. 2009. Manama, Bahrain. p.1-10
37. Annamalai, K. and Puri Ishwar, K., *Fuels- Chapter 4*, in *Combustion science and engineering*. 2007, CRC Press: Boca Raton, FL.
38. Casamassa Jack, V. and Bent Ralph, D., *Fuels: JP-4*, in *Jet aircraft power systems*. 1957, McGraw-Hill Inc: London. p. 99-101.
39. Rolls-Royce, *Starting and ignition- Part 14*, in *The jet engine*. 1966, Rolls-Royce Limited: Derby, U.K. p. 105-114.
40. Saravanamuttoo, H.I.I., Rogers, G.F.C., and Cohen, H., *Combustion systems- Chapter 6*, in *Gas Turbine Theory*. 1996, Pearson Education limited: Essex. p. 233-267.
41. Bradley, D. and Critchley, I., *Electromagnetically induced motion of spark ignition kernels*. *Combustion and flame*, 1974. **22**: p. 143-152.
42. Clements, R.M., Smy, P.R., and Dale, J.D., *An experimental study of the ejection mechanism for typical plasma jet igniters*. *Combustion and flame*, 1981. **42**: p. 287-295.
43. Orrin, J.E., Vince, I.M., and Weinberg, F.J., *Ignition by radiation from plasmas*. *Combustion and flame*, 1980. **37**: p. 91-93.
44. Gettel, L.E. and Tsai, K.C., *The effect of enhanced ignition on the burning characteristics of methane air mixtures*. *Combustion and flame*, 1983. **54**: p. 183-193.
45. Cheriyan, G.K., Krallis, K., and Weinberg, F.J., *Adapting continuous- flow plasma jets for intermittent ignition in gas turbine combustors*. *Combustion Science and Technology*, 1990. **70**: p. 171-185.
46. Cetegen, B., Teichman, K.Y., Weinberg, F.J., and Oppenheim, A.K., SAE Paper no: 800042, 1980.
47. Penner, S. and Mullins, B.P., *Principles of ignition and Spark ignition- Chapters 7-8*, in *Explosions, detonations, flammability and ignition*. 1959, Pergamon Press: London. p. 85-191.
48. Williams Forman, A., *Ignition, extinction and flammability limits- Chapter 8*, in *Combustion Theory*. 1985, Perseus Books: U.S.A. p. 265-293.
49. Griffiths, J.F., *Combustion Hazards- Chapter 12*, in *Flame and combustion*. 1995, Blackie: London. p. 227-245.

50. Annamalai, K. and Puri Ishwar, K., *stoichiometry and thermochemistry of reacting systems- Chapter 3*, in *Combustion science and engineering*. 2007, CRC Press: Boca Raton, FL.
51. Sepherd, J.S., Krok, C., and Lee, J., *Spark ignition energy measurements in Jet A*, in *Explosion Dynamics Laboratory Report FM97-9*. 200, Graduate Aeronautical Laboratories.
52. Semenov Nikolay, N., *Some problems relating to chain reactions and to the theory of combustion*. Nobel Lecture, 1956: p. 487-511.
53. Fitzgerald, D.F. and Breshears, R.P., *Patent no:4,122,816*: U.S.
54. Annamalai, K. and Puri Ishwar, K., *Chemical kinetics- Chapter 5*, in *Combustion science and engineering*. 2007, CRC Press: Boca Raton, FL.
55. Mullins, B.P., *General theoretical considerations- Chapter 2*, in *Spontaneous ignition of liquid fuels*, Butterworths Pub. LTD: London. p. 5-12.
56. Griffiths, J.F., *Thermal ignition- Chapter 8*, in *Flame and combustion*. 1995, Blackie: London. p. 145-161.
57. McMurry, J., *Organic Chemistry*. Vol. 1. 2009, Swindon: Mary Finch. p. 139
58. Behbahani, H.F., Fontijn, A., Muller-Dethlefs, K., and Weinberg, F.J., *The destruction of nitric oxide by nitrogen atoms from plasma jets*. *Combustion Science and Technology*, 1982. **27**: p. 123-132.
59. Behbahani, H.F., Warris, A., and Weinberg, F.J., *The destruction of nitric oxide by nitrogen atoms from plasma jets: Designing for thermal stratification*. *Combustion Science and Technology*, 1983. **30**: p. 289-302.
60. Ballal, D.R. and Lefebvre, A.H., *Ignition of liquid fuel sprays at subatmospheric pressures*. *Combustion and flame*, 1978. **31**: p. 115-126.
61. Pascoe, A.G., *Start systems for aero gas turbines*. *Aircraft Engineering and Aerospace Technology: An international journal*, 2005. **77**(6): p. 448-454.
62. Smy, P.R. and Clements, R.M., *Efficiency and erosion of plasma jet igniters-variation with voltage*. *Combust. Sci. and Tech.*, 1985. **42**: p. 317-324.
63. Dale, J.D., Smy, P.R., and Clements, R.M., *Combustion and flame*, 1978. **31**: p. 173.
64. Clements, R.M., Smy, P.R., Topham, D.R., Vince, I.M., Vovelle, C., and Weinberg, F.J., *Chemical activity and transport processes in the vicinity of a plasma jet igniter*. *Combustion and flame*, 1984. **57**: p. 265-274.
65. Weinberg, F.J., Hom, K., Oppenheim, A.K., and Teichman, K.Y., *Ignition by plasma jet*. *Nature*, 1978. **272**: p. 341-343.

66. Lee, A.J.J. and Weinberg, F.J., *A novel ignition device for the internal combustion engine*. *Nature*, 1987. **311**: p. 738-740.
67. Grant, J.F., Marram, E.P., and McIlwain, M.E., *Optimization of Plasma Jet Ignition Properties: Ignition of Lean-Quiescent Mixtures of Propane*. *Combustion Science Technology*, 1983. **30**: p. 171-184.
68. Fitzgerald, D.J., SAE paper 760764, 1976.
69. Kimura, T., Aoki, H., and Kato, M., *The use of plasma jet for flame stabilization and promotion of combustion in supersonic flows*. *Combustion and flame*, 1981. **42**: p. 297-305.
70. Topham, D.R., Smy, P.R., and Clements, R.M., *An investigation of a coaxial spark igniter with emphasis on its practical use*. *Combustion and flame*, 1975. **25**: p. 187-195.
71. Ridley, J.D., Pitt, P.L., and Clements, R.M., *The effect of feed gasses on plasma jet ignition*. *Combustion Science Technology*, 1985. **43**: p. 39-47.
72. Takita, K., *Ignition and flame-holding by oxygen, nitrogen, argon plasma torches*. *Combustion and flame*, 2002. **128**: p. 301-313.
73. Prongidis, A., McIntosh, A.C., Wilson, C.W., and Dolmansley, T., *Enhancement of ignition of a gas turbine by the addition of small amounts of H₂O₂*. Institute Mechanical Engineers, Part A: Journal of Power and Energy, (In press), 2011.
74. Vince, I.M., Vovelle, C., and Weinberg, F.J., *The effect of plasma jet ignition on flame propagation and sooting at the rich limit of flamability*. *Combustion and flame*, 1984. **56**: p. 105-112.
75. Sloane, T.M., *The effect of selective energy deposition on homogeneous ignition of methane and its implication for flame initiation and combustion enhancement*. *Combustion Science and Technology*, 1985. **42**(3): p. 131-144.
76. Zxhang, J.X., Clements, R.M., and Smy, P.R., *An experimental investigation of the effect of a plasma on a freely expanding methane-air flame*. *Combustion and flame*, 1983. **50**: p. 99-106.
77. Takita, K., *Ignition by H₂/N₂ plasma torch in supersonic air flow*. *Combustion Science and Technology*, 2003. **175**: p. 743-758.
78. Vince, I.M. and Weinberg, F.J., *Hydrogen atom distribution in pulsed plasma jet igniters*. *Combustion and flame*, 1987. **67**: p. 259-264.
79. Orrin, J.E., Vince, I.M., and Weinberg, F.J. *A study of plasma jet ignition mechanisms*. in *Eighteenth Symposium (International) on combustion*. 1981. Pittsburg: The combustion institute. p.1755-1765
80. Sloane, T.M., Ratcliffe, J.W., and Dobosiu-Halalai, I., *Effects of plasma chemistry and charge stratification in plasma jet ignition*. *Combustion Science and Technology*, 1986. **50**: p. 61-77.
81. Mullins, B.P., *Bomb methods- Chapter 6*, in *Spontaneous ignition of liquid fuels*, Butterworths Pub. LTD: London. p. 32-33.

82. Wooley, R., *Personal communications*: Mechanical Engineering Department, University of Leeds.
83. Abdel-Gayed, R.G., Bradley, D., Hamid, M.N., and Lawes, M. *Lewis number effects on turbulent burning velocity*. in *Twentieth Symposium (International) on Combustion*. 1984b: The combustion institute. p.505-512
84. Edwards and Maurice, *Surrogate mixtures to represent complex aviation and rocket fuels* J. Propulsion and Power, 2001. **17**: p. 461-466.
85. He, X., Donovan, M.T., Zigler, B.T., Palmer, T.R., Walton, S.M., and Wooldridge, M.S., *An experimental and modeling study of iso-octane ignition delay times under homogeneous charge compression ignition conditions*. Combustion and flame, 2005. **142**: p. 266-275.
86. Schumb, W.C., Satterfield, C.N., and Wentworth, R.I., *Hydrogen peroxide*. 1955, N.Y., London: Chapman&Hall ltd. p.
87. Jones Graig, W., *Applications of hydrogen peroxide and derivatives*. 1999: Royal society of chemists. p.
88. Samantha, C., *Direct synthesis of hydrogen peroxide from hydrogen and oxygen: An overview of recent developments in the process*. Applied Catalysis A: General, 2008. **350**: p. 133-149.
89. Reidl, H.J. and Pfeiderer, G., *Patent no:2,158,525*. 1939, I.G. Farbenindustrie AG: US.
90. Thernard, L.J., Ann. Chim. Phys., 1818. **8**.
91. Schildknecht, H. and Holoubrek, K., *Die Bombardierkäfer und ihre Explosionschemie V. Mitteilung über Insekten-Abwehrstoffe*. Angew. Chem., 1961. **73**: p. 1-7.
92. McIntosh, A.C. and Beheshti, N., *Vapour explosion device- Patent no:60/720,716 (UOL Ref: UOL 05012/US/P1)*. 2005.
93. McIntosh, A.C. and Beheshti, N., *Patent Cooperation Treaty : Fire extinguisher- Patent no:PCT/GB2006/003568*. 2006.
94. McIntosh, A.C. and Beheshti, N., *Patent Cooperation Treaty : Drug delivery- Patent no:PCT/GB2006/003576* 2006.
95. McIntosh, A.C. and Beheshti, N., *Patent Cooperation Treaty : Fuel injector- Patent no:PCT/GB2006/003582* 2006.
96. *Swedish Biomimetics 3000. Current Technologies: μ mist® platform technology*. 2011 [cited; Available from: <http://www.swedishbiomimetics.com/umist.htm>].
97. Detchem. *Detailed Chemistry in CFD, Surface reactions:Three way catalytic converter(Pt/Rh)*. [cited; Available from: <http://www.detchem.com/>].
98. Chatterjee, D., Deutschmann, O., and J., W., *Detailed Surface Reaction Mechanism in a Three-way. Catalyst*. Faraday Discussions, 2001. **119**: p. 371-384.

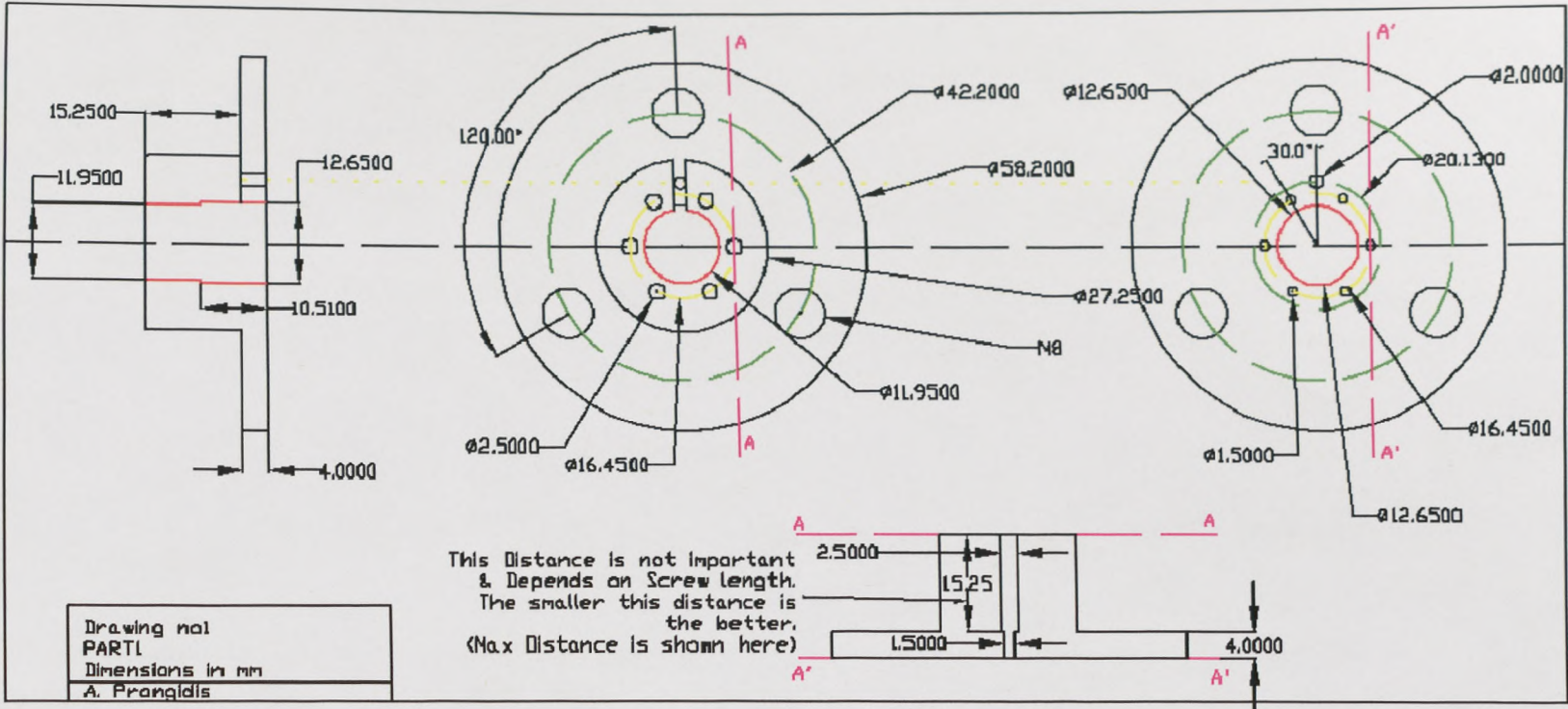
99. *DKL Engineering Inc.* [cited; Available from: www.sulphuric-acid.com/techmanual/contact/contact_catalysts.htm].

APPENDIX – A

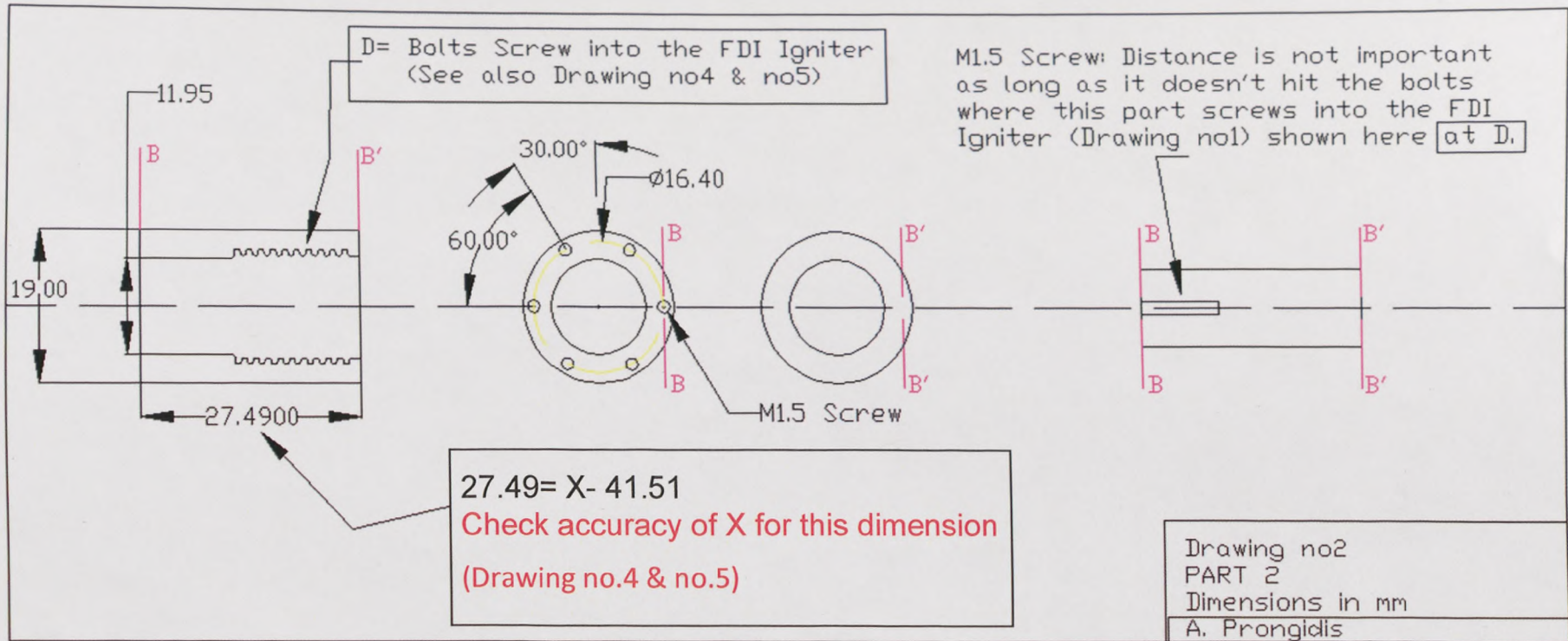
FOCUS DISCHARGE IGNITER (FDI) MODIFICATIONS

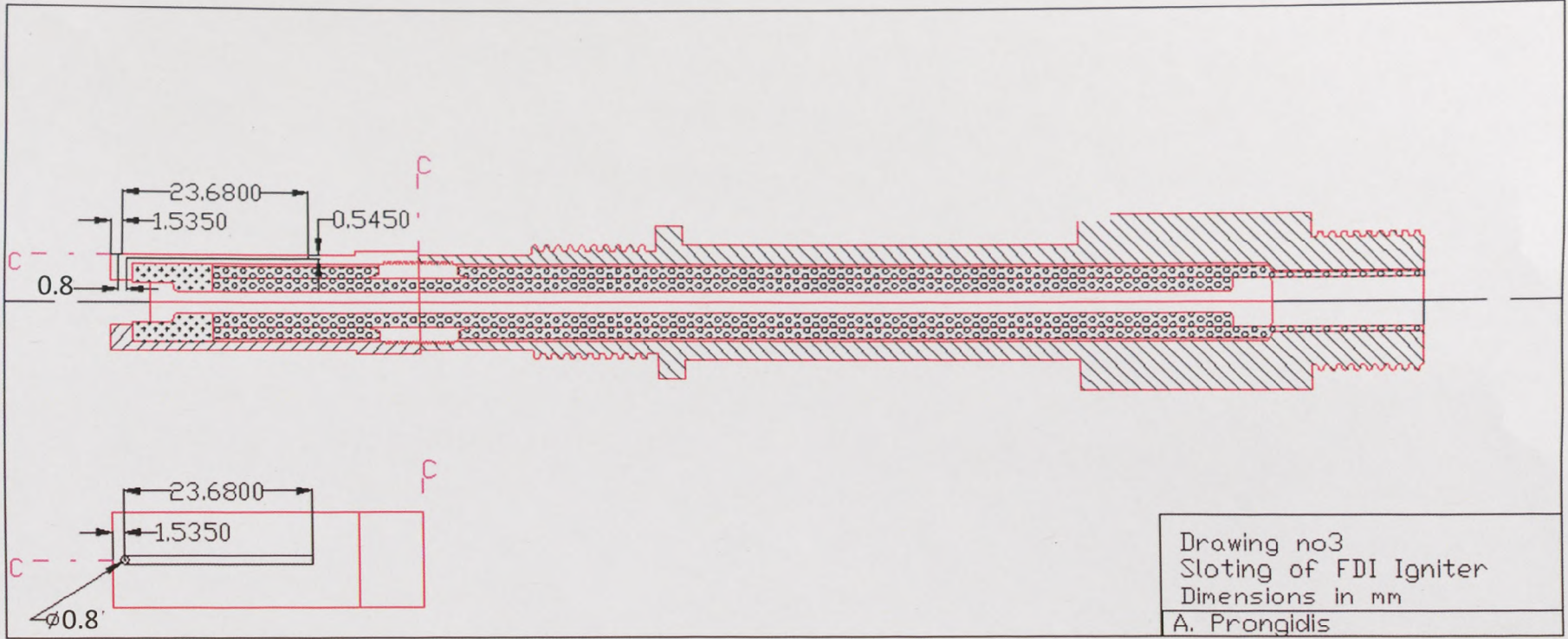
FDI MODIFICATIONS – CAD DRAWINGS NO: 1, 2, 3 & 5

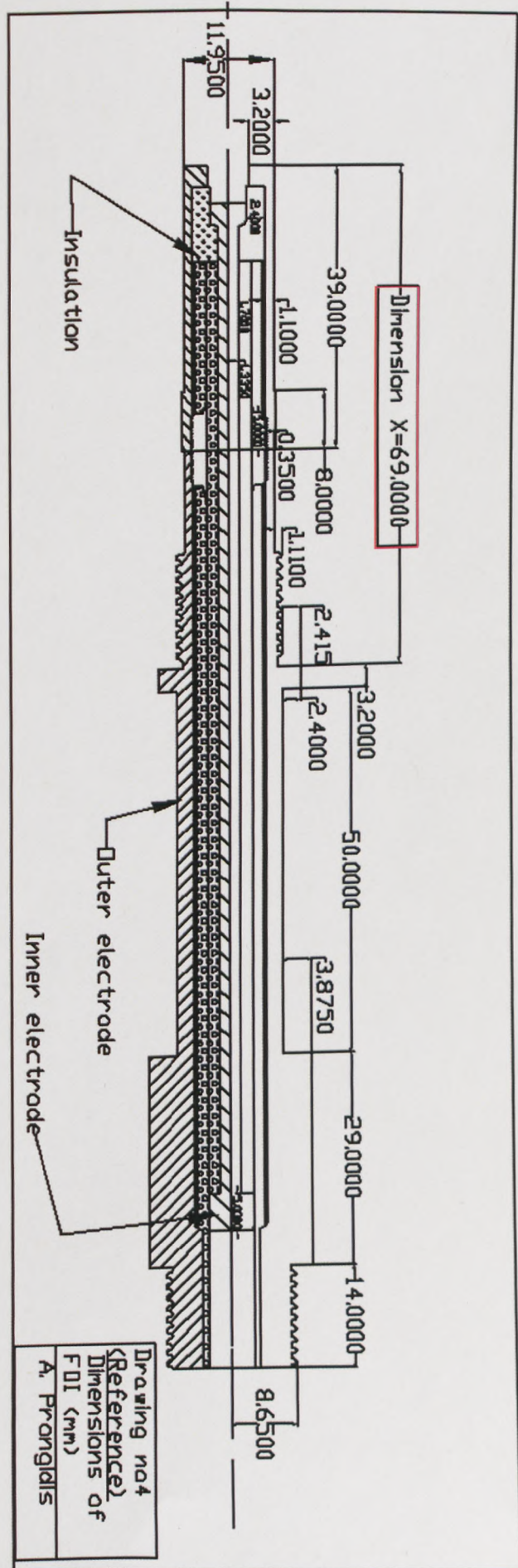
FDI ORIGINAL DIMENSIONS – CAD DRAWING NO 4



Drawing no1
PART1
Dimensions in mm
A. Prangidis

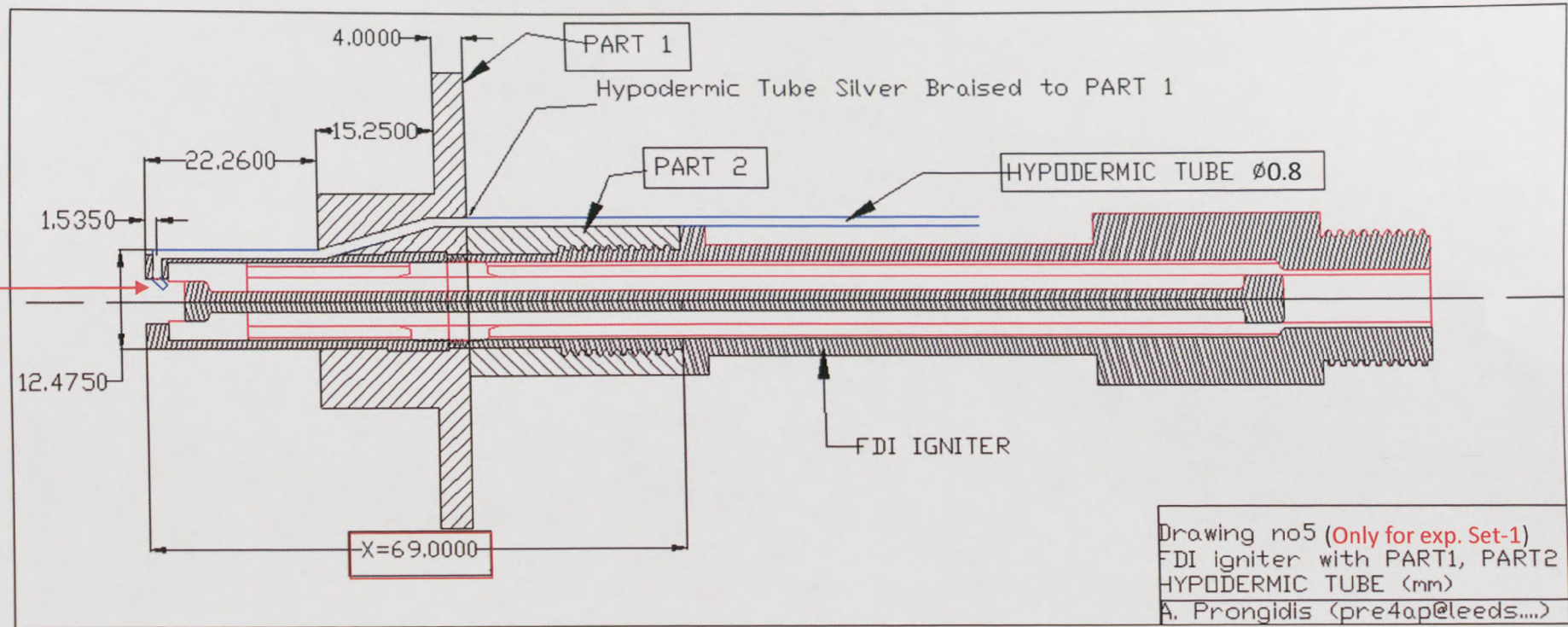


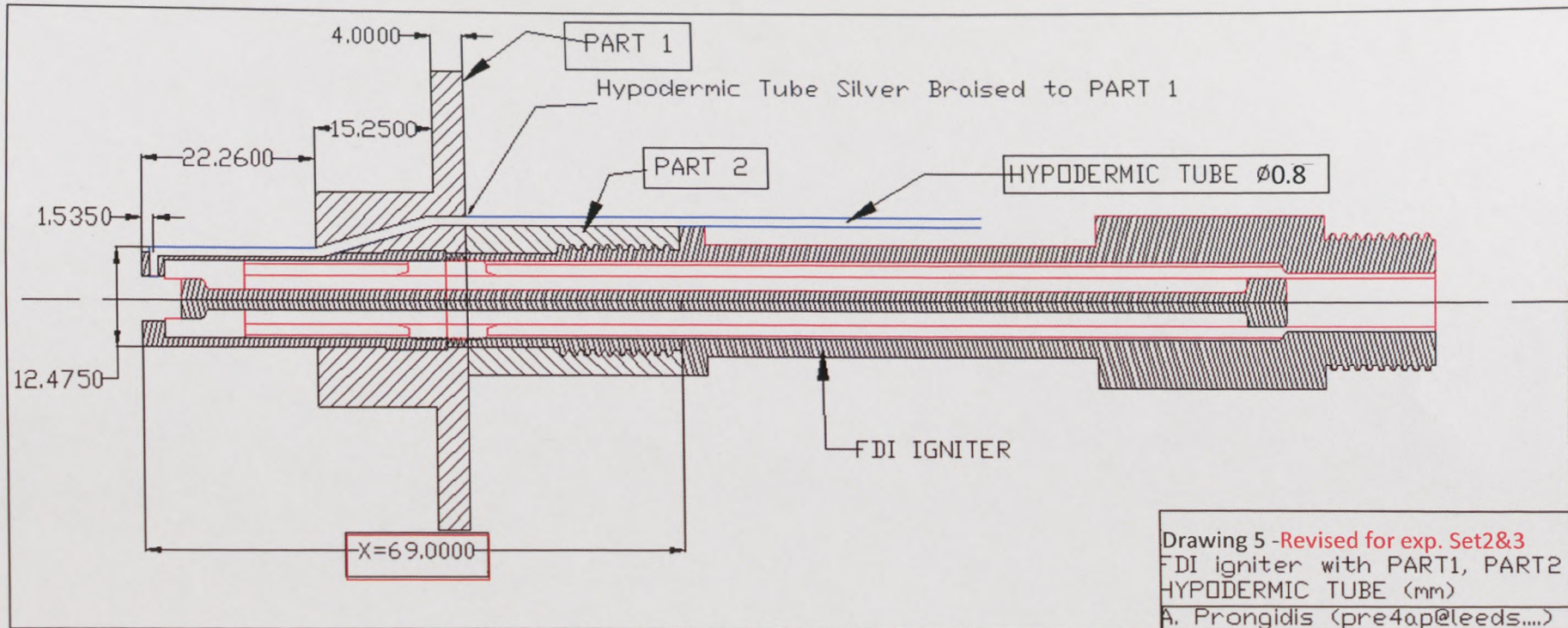




Bended protuberance of the hypodermic tube into the cavity of the FDI igniter.

This nozzle broke-away during the conduction of experimental set-1. A revised drawing no.5 for exp. Set-2 and set-3 is shown on the next page.





APPENDIX - B

FORTRAN POST PROCESSING PROGRAM 1

C-----**PROGRAM NAME:** OLYMPUS FI AND ENERGY CALCULATOR

C-----Creator: A. Prongidis

IMPLICIT REAL*8 (A-H,O-Y)
CHARACTER LINE

C===== **USER INPUT** =====

C **LINE NUMBER IN INPUT FILE**

PARAMETER(KK=789,N=KK-1)

C **MM MAX NUMBER OF EXPERIMENTS, KM MAX NUMBER OF DATA**

C **(RANDOM HIGH NUMBERS!)**

PARAMETER(MM=200,KM=300)

C **ENTER HYDROGEN PEROXIDE PUMP RATE**

PARAMETER(NN=10)

C-----**FUNCTION MATRIX DIMENSIONS**-----

DIMENSION t(MM,0:KM), Atm(MM,0:KM), Am(MM,0:KM), OrP(MM,0:KM),
& OrDP(MM,0:KM), ATup(MM,0:KM), F(MM,0:KM)
DIMENSION RigT1(MM,0:KM), RigT2(MM,0:KM), DP(MM,0:KM),
& PUMPOn(MM,0:KM), K(0:MM)
DIMENSION A(N), B(N), C(N), D(N), E(N), G(N), H(N), O(N), P(N), QQ(N),
& TotEN(MM), eF(MM), eH2O2v(MM), eH2O2d(MM), mH2O2(MM), mH2O(MM),
& OH2O2(MM), OH2O(MM), TotEN2(MM),
& V2H2O2(MM), O2H2O(MM), O2H2O2(MM), e2H2O2v(MM), e2H2O2d(MM),
& oIGN(MM), oAm(MM), oF(MM), oT(MM), oTH2O2(MM), vH2O2(MM), iH2O2(KM),
& iK(KM), AFR(MM), oN1(MM), oN2(MM), X1(MM), Y1(MM), FI(MM), TIME(MM, KM)

C **INPUT FILE NAME**

OPEN(unit=10, file='OLYMPUS_SET-2_EXPER.dat', status='UNKNOWN')

C **OUTPUT FILE NAMES**

OPEN(unit=11, file='Energy-Calc-IGN.dat', status='unknown')

OPEN(unit=12, file='EXPERIMENTnumber.dat',

& status='unknown')

OPEN(unit=14, file='FlvsAMF_0MLperH-IGNITION.dat',

& status='unknown')

OPEN(unit=15, file='FlvsAMF_0MLperH-NoIGNITION.dat',

& status='unknown')

C===== **DATA ORDERING** =====

M=0

DO I=1,N

IF(NN.EQ.0) THEN

READ(10,*) A(I), B(I), C(I), D(I), E(I), G(I), H(I), O(I), P(I)

ELSE

```

READ(10,*)A(I),B(I),C(I),D(I),E(I),G(I),H(I),O(I),P(I),QQ(I)
ENDIF
IF(C(I).EQ.0.D0)THEN
IF(D(I).EQ.0D0)THEN
IF(G(I).EQ.0D0)THEN
IF(O(I).EQ.0.D0)THEN

```

When data row is zero count one experiment

C M=NUMBER OF EXPERIMENTS (or No of Ignition Attempts)

```
M=M+1
```

C K(M) NUMBER OF DATA FOR EACH EXPERIMENT

```

K(M)=0
ENDIF
ENDIF
ENDIF
ELSE

```

When data row is not zero count number of rows in the current experiment

```
K(M)=K(M)+1
```

C PUT EXP. VALUES IN ORDER ACCORDING TO NAMES

```

t(M,K(M))=A(I)
Atm(M,K(M))=H(I)
Am(M,K(M))=C(I)
OrDP(M,K(M))=O(I)
ATup(M,K(M))=P(I)
F(M,K(M))=B(I)
RigT1(M,K(M))=D(I)
RigT2(M,K(M))=E(I)
DP(M,K(M))=QQ(I)
IF(NN.EQ.0)THEN
PUMPon(M,K(M))=0.D0
ELSE
PUMPon(M,K(M))=G(I)
ENDIF
ENDIF

```

Time
Atmospheric Pressure
Air Mass Flow Rate
Orifice ΔP
Upstream Air Temperature
Fuel Flow Rate
Thermocouple 1
Thermocouple 2
ΔP

Pump (On or Off)

ENDDO

C-----HYDROGEN PEROXIDE PUMP- VOLUME RATE CALIBRATION (in l/s)----

```

IF (NN.EQ.0) THEN
H2O2=0.0D0
ELSEIF (NN.EQ.10) THEN
H2O2=0.0027D0*(10.D0**(-3.D0))
ELSEIF (NN.EQ.20) THEN
H2O2=0.0054*(10.D0**(-3.D0))
ELSEIF (NN.EQ.40) THEN
H2O2=2.D0*0.0054*(10.D0**(-3.D0))

```

C=====CALCULATIONS=====

C-----INITIALIZATION-----

```

DO I=1,M
t(I,0)=0.D0
Atm(I,0)=0.D0
Am(I,0)=0.D0
OrDP(I,0)=0.D0
ATup(I,0)=0.D0
F(I,0)=0.D0
RigT1(I,0)=0.D0
RigT2(I,0)=0.D0

```

```

DP(I,0)=0.D0
PUMPOn(I,0)=0.D0
ENDDO
DO I=1,M

```

C-----FIND IGNITION POINT **iK(I)**-----

```

DO J=3,K(M)
IF(RigT1(I,J).GT.RigT1(I,J-2)+5.D0)THEN
oIGN(I)=1.D0
iK(I)=J
GOTO 200
ELSE
oIGN(I)=0.0D0
iK(I)=1
ENDIF
ENDD

```

C-----FIND HYDROGEN PEROXIDE PUMP START POINT **iH2O2(J)**-----

```

DO J=1,K(M)
IF(NN.NE.0)THEN
IF(PUMPON(I,J).EQ.1.D0)THEN
iH2O2(I)=J
GOTO 200
ENDIF
ELSE
iH2O2(I)=1
ENDIF
ENDDO

```

C-----TIME AT IGNITION **oT(I)**-----

```

200 oT(I)=(t(I,iK(I))-T(I,1))*oIGN(I)

```

C-----H2O2 PUMP START TIME **oTH2O2(I)**-----

```

oTH2O2(I)=(t(I,iH2O2(I))-T(I,1))*oIGN(I)
ENDDO

```

C-----MAX HYDROGEN PEROXIDE AT IGNITION **vH2O2(I) (litres)**-----

C-----H2O2 50%wt DENSITY= 1.18kg/l (Ref: Sigma Aldrich (supplier))----

C-----Assumed that H2O2 Solution vaporizes before decomposing---

C-----but mass(kg) ratio of H2O and H2O2 remains the same-----

```

DO I=1,M

```

```

vH2O2(I)=H2O2*(oT(I)-oTH2O2(I))*oIGN(I)

```

```

OH2O2(I)=0.5D0*vH2O2(I)*1.18

```

```

OH2O(I)=OH2O2(I)

```

C-----MIN H2O2 PEROXIDE WITH STAY TIME=0.147s **v2H2O2(I) (litres)**-----

```

v2H2O2(I)=H2O2*0.147D0*oIGN(I)

```

```

O2H2O2(I)=0.5D0*v2H2O2(I)*1.18

```

```

O2H2O(I)=O2H2O2(I)

```

C-----FUEL FLOW RATE AT IGNITION **oF(I) (kg/s)**-----

```

IF(oIGN(I).EQ.1.D0)THEN

```

C AIR MASS FLOW RATE **oAm(I) AT IGNITION (kg/s)**

```

oAm(I)=Am(I,iK(I))
C FUEL FLOW RATE AT IGNITION (CONVERTED TO Kg/s)
oF(I)=F(I,iK(I))*(10.D0**(-3.D0))

```

C-----FUEL FLOW AT 'No IGNITION'-----

```

ELSEIF(oIGN(I).EQ.0.D0)THEN
TotAm=0.D0
TotF=0.D0
KKK=0
DO J=1,K(M)
IF (F(I,J).GE.F(I,J-1).AND.F(I,J).LE.F(I,J-1)+0.1)THEN
TotAm=TotAm+Am(I,J)
TotF=TotF+F(I,J)
KKK=KKK+1
ENDIF
ENDDO

```

```

C AIR MASS FLOW AT 'NO IGNITION' oAm(I) Kg/s
oAm(I)=TotAm/KKK

```

```

C FUEL RATE AT 'NO IGNITION' (CONVERTED TO Kg/s)
oF(I)=TotF/KKK*(10.D0**(-3.D0))
ENDIF
ENDDO

```

C=====ENERGY CALCULATIONS=====

```

C---HYDROGEN PEROXIDE HEAT OF VAPORIZATION HEATv(MJ/Kg) -----
C---HEAT OF VAPORIZATION FOR 50%wt H2O2=481.1 Cal/g
C---(Ref:HYDROGEN PEROXIDE (Schumb, W.C.;Satterfield, C.N.;Wentworth, R.L., C---
p.233,1955)
HeatV=48.1D0*4.19002D0*(10.D0**(-3.D0))

```

```

C-ENTHALPY OF DECOMPOSITION FOR HYDROGEN PEROXIDE ENTH(MJ/Kg)
C-----H2O2(g)-->H2O(g)+0.5*O(g)-----
C-----ENTHALPY=94500(KJ/Kmol) (Ref:McIntosh,A.C. PAPER 2007)-----
ENTH=94500*(10.D0**(-3.D0))/34.D0

```

DO I=1,M

```

C-----FUEL ENERGY eF(I)(MJ)-----
C---NET SPECIFIC ENERGY=43.2 MJ/Kg (Ref:Shell kerosene Jet-A1 supplier)
eF(I)=43.2*oF(I)*oIGN(I)

```

C---HYDROGEN PEROXIDE HEAT OF VAPORIZATION AT IGNITION

```

C---eH2O2v(I)(MJ)-----
C-----HEAT OF VAPORIZATION FOR 50%wt= HeatV (MJ/Kg)
eH2O2v(I)=HeatV*(OH2O2(I)+OH2O(I))*oIGN(I)
e2H2O2v(I)=HeatV*(O2H2O2(I)+O2H2O(I))*oIGN(I)

```

C---HYDROGEN PEROXIDE DECOMPOSITION ENERGY AT IGNITION

C---eH2O2d(I)(MJ)-----

C-----ENTHALPY OF DECOMPOSITION OF 100% H2O2 GASS-----

eH2O2d(I)=ENTH*oH2O2(I)*oIGN(I)

e2H2O2d(I)=ENTH*o2H2O2(I)*oIGN(I)

C----TOTAL ENERGY AT IGNITION TotEN(I)(MJ)-----

C--TotEN(I)=FUEL ENERGY-VAPORIZATION ENERGY+DECOMPOSITION

C--ENERGY-----

C----MAXIMUM

TotEN(I)=eF(I)-eH2O2v(I)+eH2O2d(I)

C----MINIMUM WITH STAY TIME 0.147s

TotEN2(I)=eF(I)-e2H2O2v(I)+e2H2O2d(I)

C-----AIR-FUEL RATIO-----

AFR(I)=oAm(I)/oF(I)

ENDDO

C=====EQUIVALENCE RATIO CALCULATIONS FI(I)=====

DO I=1,M

oN1(I)=oF(I)/153.D0

oN2(I)=(0.59D0*H2O2)/34.D0

X1(I)=((21.D0*oN1(I)+2.D0*oN2(I))/oN1(I))

Y1(I)=((2.D0*oN2(I))/oN1(I))

FI(I)=((oF(I)+oN2(I)*34.D0)/oAm(I))/((132.D0+X1(I)+16.D0*Y1(I))

& /(137.28D0*(11.D0+(0.25D0*X1(I))-0.5D0*Y1(I))))

ENDDO

C=====WRITE RESULTS IN ORDER IN DATA FILES=====

C----Write Equivalence Ratio Fi, Air mass Flow and Fuel Flow Rates

DO I=1,M

WRITE(*,*)oIGN(I),I

IF(oIGN(I).EQ.1.D0)THEN

WRITE(*,*)'SUCCESS',oIGN(I)

WRITE(14,100) oAm(I),FI(I),oF(I)

ELSE

WRITE(15,100) oAm(I),FI(I),oF(I)

ENDIF

ENDDO

C----Write Air mass Flow, Max. Energy High, Max. Energy Low

DO I=1,M

IF(oIGN(I).EQ.1.D0)THEN

WRITE(11,100)oAm(I) TotEN(I) TotEN2(I)

C----Write Experiment Numbers when Ignition was successful

WRITE(12,*) I

ENDIF

ENDDO

100 FORMAT(6F12.6)

STOP

END

APPENDIX - C
FORTRAN 95 POST PROCESSING PROGRAM 2

C-PROGRAM NAME: OLYMPUS-TEMPERATURE INCREASE AT SIMILAR
C--FI

C-----Creator: A. Prongidis

IMPLICIT REAL*8 (A-H,O-Y)
CHARACTER LINE

C=====USER INPUT=====

C LINE NUMBER IN INPUT FILE

PARAMETER(KK=789,N=KK-1)

C MM MAX NUMBER OF EXPERIMENTS, KM MAX NUMBER OF DATA
C (RANDOM HIGH NUMBERS!)

PARAMETER(MM=200,KM=300)

C-----FUNCTION MATRIX DIMENSIONS-----

DIMENSION t(MM,0:KM,4), Atm(MM,0:KM,4), Am(MM,0:KM,4),
& OrP(MM,0:KM,4),OrDP(MM,0:KM,4),ATup(MM,0:KM,4),F(MM,0:KM,4)
DIMENSION RigT1(MM,0:KM,4),RigT2(MM,0:KM,4),DP(MM,0:KM,4),
& PUMPOn(MM,0:KM,4),K(0:MM,4)
DIMENSION A(N),B(N),C(N),D(N),E(N),
& G(N),H(N),O(N),P(N),QQ(N),
& TotEN(MM,4),eF(MM,4),eH2O2v(MM,4),
& eH2O2d(MM,4),mH2O2(MM,4),mH2O(MM,4),
& oIGN(MM,4),oAm(MM,4),oF(MM,4),oT(MM,4),
& oTH2O2(MM,4),vH2O2(MM,4),iH2O2(KM,4),
& iK(KM,4),AFR(MM,4),oN1(MM,4),oN2(MM,4),
& X1(MM,4),Y1(MM,4),FI(MM,4),TIME(N,N,N),
& Ni(4),M(0:4),H2O2(4),I1(N),MB1(N),I2(N),MB2(N),I3(N),MB3(N),
& I4(N),MB4(N),IS1(N),MS1(N),FIo(N,N),MM1(N),ORDERfi(0:N),
& MMM1(N),MDD1(N),AVEGRAD(N),GRAD(N,KM),ORDERGRAD(N,0:KM)
& ,oFI(N),ooFI(N),ooAM(N),MD2(N),ooIGN(N),I5(N),LL(N),LM(N),
& IJ(N)

C INPUT FILE NAMES

C-----EACH FILE CONTAINS DATA FOR DIFFERENT H2O2 RATES**----**

OPEN(unit=10,file='EPTEC_DEC08_EXPER_0H2O2.dat',
& status='UNKNOWN')
OPEN(unit=20,file='EPTEC_DEC08_EXPER_10H2O2.dat',
& status='UNKNOWN')
OPEN(unit=30,file='EPTEC_DEC08_EXPER_20H2O2.dat',
& status='UNKNOWN')
OPEN(unit=40,file='EPTEC_DEC08_EXPER_40H2O2.dat',
& status='UNKNOWN')

C OUTPUT FILE NAMES

```
OPEN(unit=13,file='TemperatureGRAD-AMF0.2a.dat',  
& status='unknown')  
OPEN(unit=14,file='FlinORDER-AMF0.2a.dat',  
& status='unknown')  
OPEN(unit=15,file='TemperatureGradCalculations-AMF0.2a.dat',  
& status='unknown')
```

```
AMF=0.2  
AMF1=AMF-0.02  
AMF2=AMF+0.02
```

Change Air Mass Flow Rate for Study
and Change Output File Names

C=====DATA ORDERING=====

```
C-----NUMBER OF DATA FOR EACH FILE Ni -----  
C-----EACH FILE CONTAINS DATA FOR DIFFERENT H2O2 RATES----  
Ni(1)=2159  
Ni(2)=789  
Ni(3)=2370  
Ni(4)=1958
```

```
C---- MD=Hydrogen Peroxide Pump Rate Setting-----  
C----MD=1----> 0ml/hr Pump Rate  
C----MD=2----> 10ml/hr Pump Rate  
C----MD=3----> 20ml/hr Pump Rate  
C----MD=4----> 40ml/hr Pump Rate  
MD=1
```

```
210 M(MD)=0
```

DO I=1,Ni(MD)-1

```
IF(MD.EQ.1)THEN  
  READ(10,*)A(I),B(I),C(I),D(I),E(I),G(I),H(I),O(I),P(I)  
ELSEIF(MD.EQ.2)THEN  
  READ(20,*)A(I),B(I),C(I),D(I),E(I),G(I),H(I),O(I),P(I),QQ(I)  
ELSEIF(MD.EQ.3)THEN  
  READ(30,*)A(I),B(I),C(I),D(I),E(I),G(I),H(I),O(I),P(I),QQ(I)  
ELSEIF(MD.EQ.4)THEN  
  READ(40,*)A(I),B(I),C(I),D(I),E(I),G(I),H(I),O(I),P(I),QQ(I)  
ENDIF  
IF(C(I).EQ.0.D0)THEN  
  IF(D(I).EQ.0.D0)THEN  
    IF(O(I).EQ.0.D0)THE
```

C M=NUMBER OF EXPERIMENTS (or No of Ignition Attempts)

```
M(MD)=M(MD)+1
```

C K(M) NUMBER OF DATA FOR EACH EXPERIMENT

```
K(M(MD),MD)=0  
ENDIF  
ENDIF  
ELSE
```

K(M(MD),MD)=K(M(MD),MD)+1

C PUT EXP. VALUES IN ORDER ACCORDING TO NAMES

```
t(M(MD),K(M(MD),MD),MD)=A(I)
Atm(M(MD),K(M(MD),MD),MD)=H(I)
Am(M(MD),K(M(MD),MD),MD)=C(I)
OrDP(M(MD),K(M(MD),MD),MD)=O(I)
ATup(M(MD),K(M(MD),MD),MD)=P(I)
F(M(MD),K(M(MD),MD),MD)=B(I)
RigT1(M(MD),K(M(MD),MD),MD)=D(I)
RigT2(M(MD),K(M(MD),MD),MD)=E(I)
DP(M(MD),K(M(MD),MD),MD)=QQ(I)
IF(MD.EQ.1)THEN
PUMPon(M(MD),K(M(MD),MD),MD)=0.D0
ELSE
PUMPon(M(MD),K(M(MD),MD),MD)=G(I)
ENDIF
ENDIF
ENDDO
```

C-----CHECK IF ALL DATA WERE READ ELSE GO BACK TO 210

```
IF(MD.NE.4)THEN
MD=MD+1
GOTO 210
ELSE
ENDIF
```

C-----HYDROGEN PEROXIDE PUMP- VOLUME RATE CALIBRATION (in l/s)-

```
H2O2(1)=0.0D0
H2O2(2)=0.0027D0*(10.D0**(-3.D0))
H2O2(3)=0.0054*(10.D0**(-3.D0))
H2O2(4)=0.0081*(10.D0**(-3.D0))
```

C=====CALCULATIONS=====

C-----INITIALIZATION-----

```
DO MD=1,4
DO I=1,M(MD)
t(I,0,MD)=0.D0
Atm(I,0,MD)=0.D0
Am(I,0,MD)=0.D0
OrDP(I,0,MD)=0.D0
ATup(I,0,MD)=0.D0
F(I,0,MD)=0.D0
RigT1(I,0,MD)=0.D0
RigT2(I,0,MD)=0.D0
DP(I,0,MD)=0.D0
PUMPon(I,0,MD)=0.D0
ENDDO
ENDDO
```

C-----FIND IGNITION POINT iK(I,MD)-----

DO MD=1,4

```
DO I=1,M(MD)
DO J=3,K(M(MD),MD)
```

```
IF(RigT1(I,J,MD).GT.RigT1(I,J-2,MD)+5.D0)THEN
oIGN(I,MD)=1.D0
iK(I,MD)=J
GOTO 200
ELSE
oIGN(I,MD)=0.0D0
iK(I,MD)=1
ENDIF
ENDDO
```

```
C-----FIND HYDROGEN PEROXIDE PUMP START POINT iH2O2(J,MD)
DO J=1,K(M(MD),MD)
IF(MD.NE.1)THEN
IF(PUMPON(I,J,MD).EQ.1.D0)THEN
iH2O2(I,MD)=J
GOTO 200
ENDIF
ELSE
iH2O2(I,MD)=1
ENDIF
ENDDO
```

```
C-----TIME AT IGNITION oT(I,MD)-----
200 oT(I,MD)=(t(I,iK(I,MD),MD)-T(I,1,MD))*oIGN(I,MD)
```

```
C-----H2O2 PUMP START TIME oTH2O2(I)-----
oTH2O2(I,MD)=(t(I,iH2O2(I,MD),MD)-T(I,1,MD))*oIGN(I,MD)
ENDDO
ENDDO
```

```
C-----MAX HYDROGEN PEROXIDE AT IGNITION vH2O2(I,MD) (litres)----
C-----H2O2 50%wt DENSITY= 1.18kg/l (Ref: Sigma Aldrich (supplier))----
C-----Assumed that H2O2 Solution vaporizes before decomposing----
C-----but mass(kg) ratio of H2O and H2O2 remains the same-----
```

```
DO MD=1,4
DO I=1,M(MD)
vH2O2(I,MD)=H2O2(MD)*(oT(I,MD)-oTH2O2(I,MD))*oIGN(I,MD)
mH2O2(I,MD)=0.5D0*vH2O2(I,MD)*1.18
mH2O(I,MD)=mH2O2(I,MD)
```

```
C-----FUEL FLOW RATE AT IGNITION oF(I,MD)(kg/s)-----
IF(oIGN(I,MD).EQ.1.D0)THEN
C AIR MASS FLOW RATE oAm(I,MD) AT IGNITION (kg/s)
oAm(I,MD)=Am(I,iK(I,MD),MD)
C FUEL FLOW RATE AT IGNITION (CONVERTED TO Kg/s )
oF(I,MD)=F(I,iK(I,MD),MD)*(10.D0**(-3.D0))
```

C-----FUEL FLOW AT 'No IGNITION'-----

ELSEIF(oIGN(I,MD).EQ.0.D0)THEN

TotAm=0.D0

TotF=0.D0

KKK=0

DO J=1,K(M(MD),MD)

IF (F(I,J,MD).GE.F(I,J-1,MD)

& .AND.F(I,J,MD).LE.F(I,J-1,MD)+0.1)THEN

TotAm=TotAm+Am(I,J,MD)

TotF=TotF+F(I,J,MD)

KKK=KKK+1

ENDIF

ENDDO

C AIR MASS FLOW AT 'NO IGNITION' oAm(I,MD) Kg/s

oAm(I,MD)=TotAm/KKK

C FUEL RATE AT 'NO IGNITION' (CONVERTED TO Kg/s

oF(I,MD)=TotF/KKK*(10.D0**(-3.D0))

ENDIF

ENDDO

ENDDO

C=====ENERGY CALCULATIONS=====

C---HYDROGEN PEROXIDE HEAT OF VAPORIZATION HEATv(MJ/Kg) -----

C---HEAT OF VAPORIZATION FOR 50%wt H2O2=481.1 Cal/g

C---(Ref:HYDROGEN PEROXIDE (Schumb, W.C.;Satterfield, C.N.;Wentworth,
R.L., C---p.233,1955)

HeatV=48.1D0*4.19002D0*(10.D0**(-3.D0))

C-ENTHALPY OF DECOMPOSITION FOR HYDROGEN PEROXIDE

ENTH(MJ/Kg)

C-----H2O2(g)-->H2O(g)+0.5*O(g)-----

C-----ENTHALPY=94500(KJ/Kmol) (Ref:McIntosh,A.C. PAPER 2007)-----

ENTH=94500*(10.D0**(-3.D0))/34.D0

DO MD=1,4

DO I=1,M(MD)

C-----FUEL ENERGY eF(I,MD)(MJ)-----

C---NET SPECIFIC ENERGY=43.2 MJ/Kg (Ref:Shell kerosene Jet-A1 supplier)

eF(I,MD)=43.2*oF(I,MD)*oIGN(I,MD)

C---HYDROGEN PEROXIDE HEAT OF VAPORIZATION AT IGNITION

C---eH2O2v(I,MD)(MJ)-----

C-----HEAT OF VAPORIZATION FOR 50%wt= HeatV (MJ/Kg

eH2O2v(I,MD)=HeatV*(mH2O2(I,MD)+mH2O(I,MD))*oIGN(I,MD)

C---HYDROGEN PEROXIDE DECOMPOSITION ENERGY AT IGNITION

C---eH2O2d(I,MD)(MJ)-----

C-----ENTHALPY OF DECOMPOSITION OF 100% H2O2 GASS-----

eH2O2d(I,MD)=ENTH*mH2O2(I,MD)*oIGN(I,MD)

C---TOTAL ENERGY AT IGNITION TotEN(I)(MJ)-----

C--TotEN(I)=FUEL ENERGY-VAPORIZATION ENERGY+DECOMPOSITION

C--ENERGY-----

C---**MAXIMUM**

$$\text{TotEN}(I,MD)=eF(I,MD)-eH_2O_{2v}(I,MD)+eH_2O_{2d}(I,MD)$$

C-----**AIR-FUEL RATIO**-----

$$\text{AFR}(I,MD)=oAm(I,MD)/oF(I,MD)$$

ENDDO

ENDDO

C===== **EQUIVALENCE RATIO CALCULATIONS FI(I,MD)** =====

J1=0

DO MD=1,4

DO I=1,M(MD)

$$oN_1(I,MD)=oF(I,MD)/153.D0$$

$$oN_2(I,MD)=(0.59D0*H_2O_2(MD))/34.D0$$

$$X_1(I,MD)=((21.D0*oN_1(I,MD)+2.D0*oN_2(I,MD))/oN_1(I,MD))$$

$$Y_1(I,MD)=((2.D0*oN_2(I,MD))/oN_1(I,MD))$$

$$FI(I,MD)=((oF(I,MD)+oN_2(I,MD)*34.D0)/oAm(I,MD))$$

$$\& /((132.D0+X_1(I,MD)+16.D0*Y_1(I,MD))$$

$$\& /((137.28D0*(11.D0+(0.25D0*X_1(I,MD))-0.5D0*Y_1(I,MD))))$$

C===== **RE-ORDER/ RE-NAME EXPERIMENTS** =====

C--- **J1: NUMBER OF ALL EXPERIMENTS WITH TOGETHER**

$$J1=J1+1$$

C---**oFI(J1): Equivalence Ratio of J1 experiment**

C---**ooAm(J1): Air Mass Flow Rate of J1 experiment**

$$oFI(J1)=FI(I,MD)$$

$$ooAm(J1)=oAM(I,MD)$$

C---**I2(J1): ORIGINAL EXPERIMENT NUMBER**-----

$$I2(J1)=I$$

C---**MD2(J1): Hydrogen Peroxide Rate of J1 Experiment**

$$MD2(J1)=MD$$

C---**oolGN(J1): Ignition Point of J1 Experiment**

$$oolGN(J1)=olGN(I,MD)$$

ENDDO

ENDDO

C-----**TIME AFTER IGNITION TIME(I,J,MD)** (time at ignition=0s)-----

J1=0

DO MD=1,4

DO I=1,M(MD)

J1=J1+1

```

DO J=iK(I,MD)-2,K(I,MD)
TIME(I,J,MD)=T(I,J,MD)-T(I,iK(I,MD)-1,MD)
ENDDO
ENDDO
ENDDO

```

```

C FIND SIMILAR FI (oTOL: TOLERANCE) AT SIMILAR AIR FLOWS
C --ONLY WHEN IGNITION OCCURED--
oTOL=0.001D0

```

```

C-----J1: NO OF ALL EXPERIMENTS TOGETHER

```

```

C-----J2:NO OF OCCURENCE OF SIMILAR FI

```

```

C-----I3(1-J2):NUMBERS TAKEN FROM 1-J1 WHERE THE FI IS SIMILAR
C-----FOR EACH OCCURENCE (1-J2)

```

```

C-----I2(I3(1-J2)): EXPERIMENT NUMBER

```

```

C-----MD2(I3(1-J2)): HYDROGEN PEROXIDE RATE

```

```

C-----Initialization
J2=1
I3(1)=0

```

```

C-LOOP STARTS HERE

```

```

DO I=1,J1
J4=1

```

```

C-----CHECK IF THIS IS THE SECOND SWEEP-----
C IF YES GO TO 250
DO KK=1,J2
IF(I.EQ.I3(KK))GOTO 250
ENDDO

```

```

C====FIND SIMILAR EQUIVALENCE RATIOS ooFI(J2)=====
C-----For a specific Air Mass Flow

```

```

C-----Finds the Air Mass Flows ooAM(J1) that lie inside the value studied
C----- (i.e. 0.2kg/s, or 0.4kg/s or 0.6kg/s or 0.8kg/s
IF(ooAM(I).GT.AMF1.AND.ooAM(I).LT.AMF2)THEN

```

```

C-----Search Only When Ignition Occured (Discard 'No Ignition' Cases)
IF(ooIGN(I).EQ.1.D0)THEN

```

```

DO J=I+1,J1
IF(ooAM(J).GT.AMF1.AND.ooAM(J).LT.AMF2)THEN
IF(ooIGN(J).EQ.1.D0)THEN

```

```

C----Check If FI is within Tolerance Limits and assign it to function
ooFI(J2)

```

```

IF(oFI(I)+oTOL.GT.oFI(J).AND.
& oFI(I)-oTOL.LT.oFI(J))THEN

```

C----AVOID COMPARING THE SAME EXPERIMENTS

```

IF(J4.EQ.1)THEN
  ooFI(J2)=oFI(I)
  I3(J2)=I
  J2=J2+1
ENDIF

```

```

  ooFI(J2)=oFI(J)
  I3(J2)=J
  J2=J2+1

```

```

  J4=J4+1

```

```

ENDIF
ENDIF
ENDIF
ENDDO
ENDIF
ENDIF

```

250 ENDDO**C-LOOP ENDS HERE****C=====SORT VALUES IN ORDER=====****C---INITIAL RANDOM HIGH NUMBER:**

```

ORDERfi(0)=100.D0

```

```

J6=0

```

C-LOOP STARTS HERE

```

DO I=1+J6,J2

```

C-----Initialisation

```

  oMAX=0.D0

```

C-----LOOK FOR EXACTLY SAME EQUIVALENCE RATIOS

```

IF(J5.GE.2)THEN

```

```

  J5=0

```

```

  GOTO 260

```

```

ENDIF

```

```

  J5=0

```

```

DO KK=1,J2

```

```

IF(ORDERfi(I-1).EQ.ooFI(KK))THEN

```

```

  J5=J5+1

```

```

  OSAME=ooFI(KK)

```

```

IF(J5.GE.2)THEN

```

```

  J6=J6+1

```

```

  I5(I)=KK

```

```

IF(J6.GT.J2)THEN

```

```

  WRITE(*,*)'ERROR J6>J2 CANNOT EXIST'

```

```

ENDIF

```

```

ENDIF

```

```

ENDIF

```

```

ENDDO

```


C-----**WRITE IN FILE:** Experiment No, H2O2 Pump Rate Setting, Time
C-----From Ignition, Temperature, Equivalence Ratio (in Order), Air mass
Flow

```
WRITE(13,500) LL(I),LM(I),TIME(LL(I),J,LM(I)),  
& RIGT1(LL(I),J,LM(I)),ORDERFI(I),oAM(LL(I),LM(I))
```

ENDDO

```
AvAMF=TotalAMF/LMM
```

```
WRITE(*,*)'AVERAGE AIR MASS FLOW:',AvAMF
```

```
100 FORMAT(6F12.6)
```

```
500 FORMAT(I3,1X,I3,1X,1X,4(E12.5,1X))
```

```
STOP
```

```
END
```

APPENDIX -D

Modelling of the Rolls Royce Olympus Combustion Chamber

The modelling of the Olympus combustion chamber was done using the commercial CFX code. The model was used mostly to better understand the dynamics of the combustor and the flow characteristics at where the spark is introduced. It was also used to determine the maximum residence time of the injected hydrogen peroxide, at an inlet mass flow rate of 0.2kg/s (i.e. the lowest mass flow rate studied in the experiments).

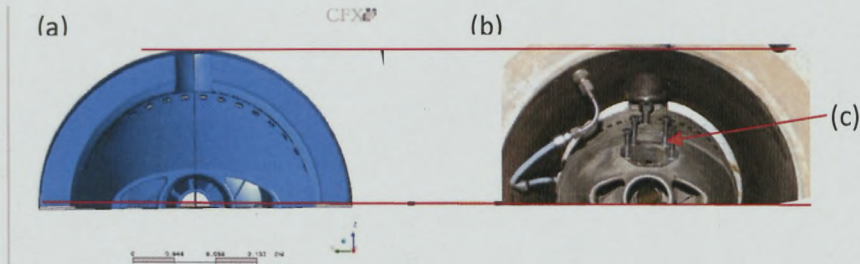


Figure 1: The Olympus Combustor Inside the test pipe together with the inlet piece: (a) Model, (b) Real, (c) Position of Fuel injector at the inlet.

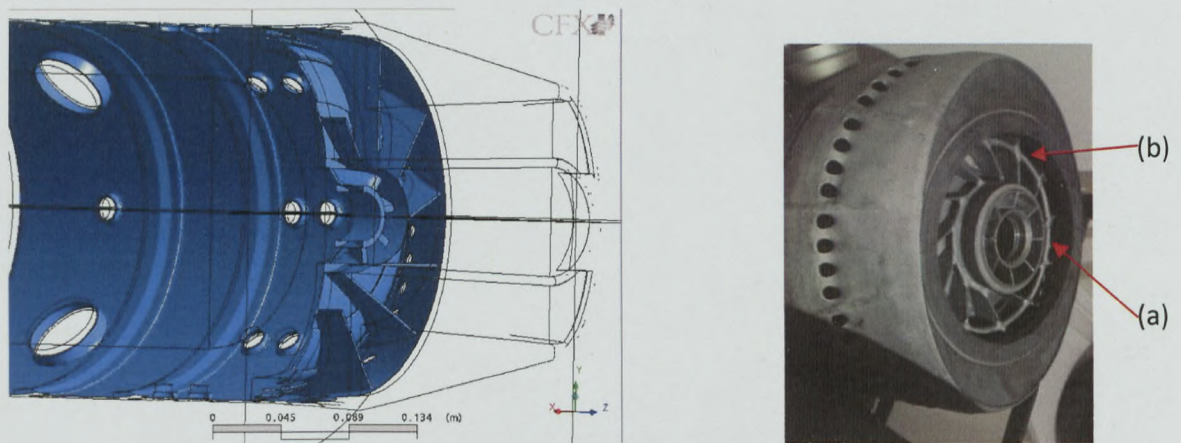


Figure2: Modelling of the Blades: (a) Small Helical Blades, (b) Straight Blades.

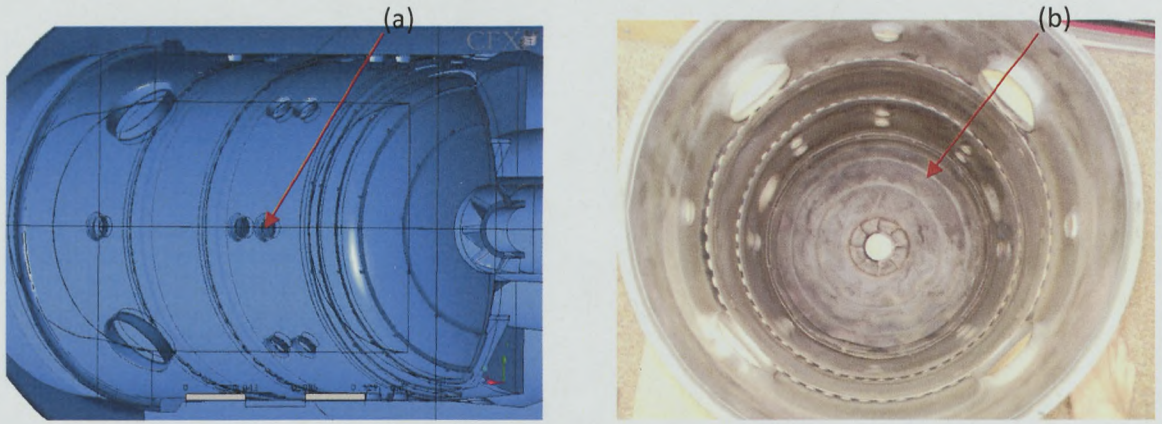


Figure 3: The Combustion Chamber: (a) Igniter position, (b) Inlets.

Converged Run of the Front Part with Turbulence k-ε model

Steady State Solution

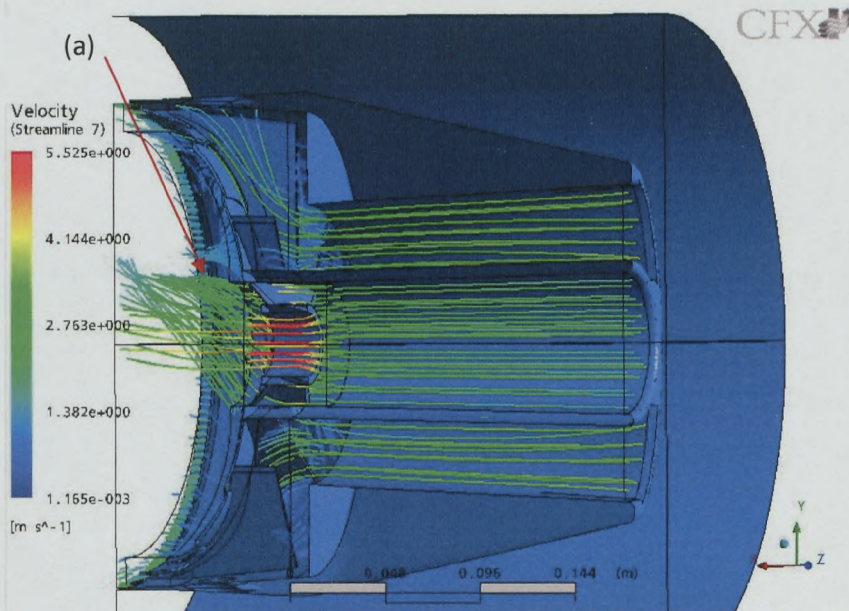


Figure 4: Velocity Streamline over the front part of the Combustion Chamber: (a) Vortex that mixes the fuel with air. The boundary conditions are: (a) at the Pipe before the Inlet $\dot{m} = 0.2 \text{ Kg/s}$ and (b) Opening at the back with a static pressure of 1 atm.

Periodic Boundary Condition

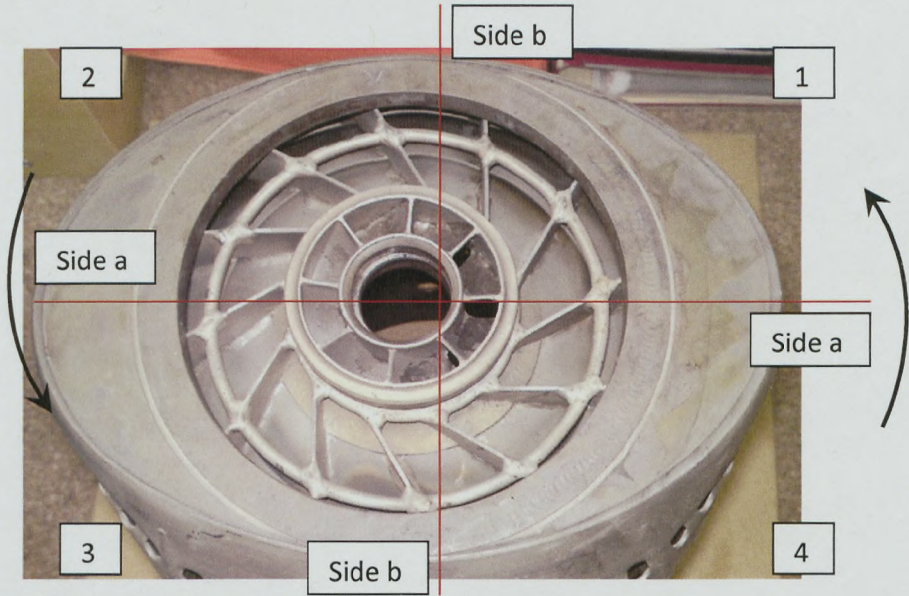


Figure 5: Periodic Geometry. The geometry can be simulated cutting through one of the two periodic planes shown in red. Dividing the geometry in 4 quarters one can observe that: B.C. at Side a 2 is the same as Side a 4 and B.C. at Side b 1= B.C. Side b 3. So the boundary at Side a 2 is the same as the boundary

Convergence Difficulties: Finding Problematic Mesh

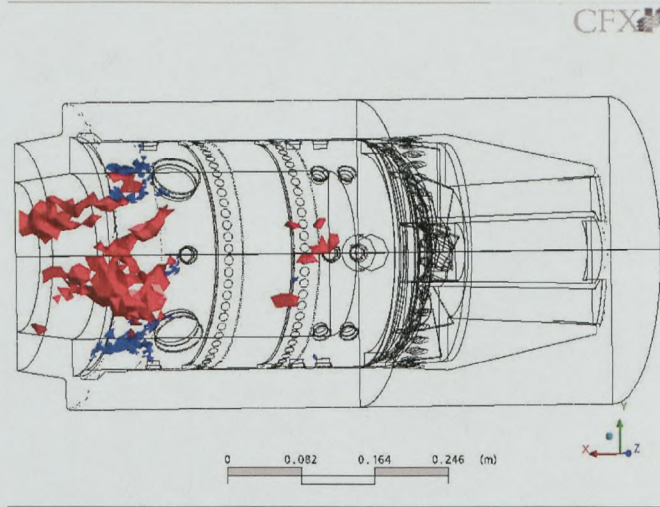


Figure 6: Max RMS residuals. The mesh quality at those regions is poor and the solver is having difficulties to converge to the steady state solution. Better mesh means higher memory requirements but these problems can be surpassed with a parallel simulation.

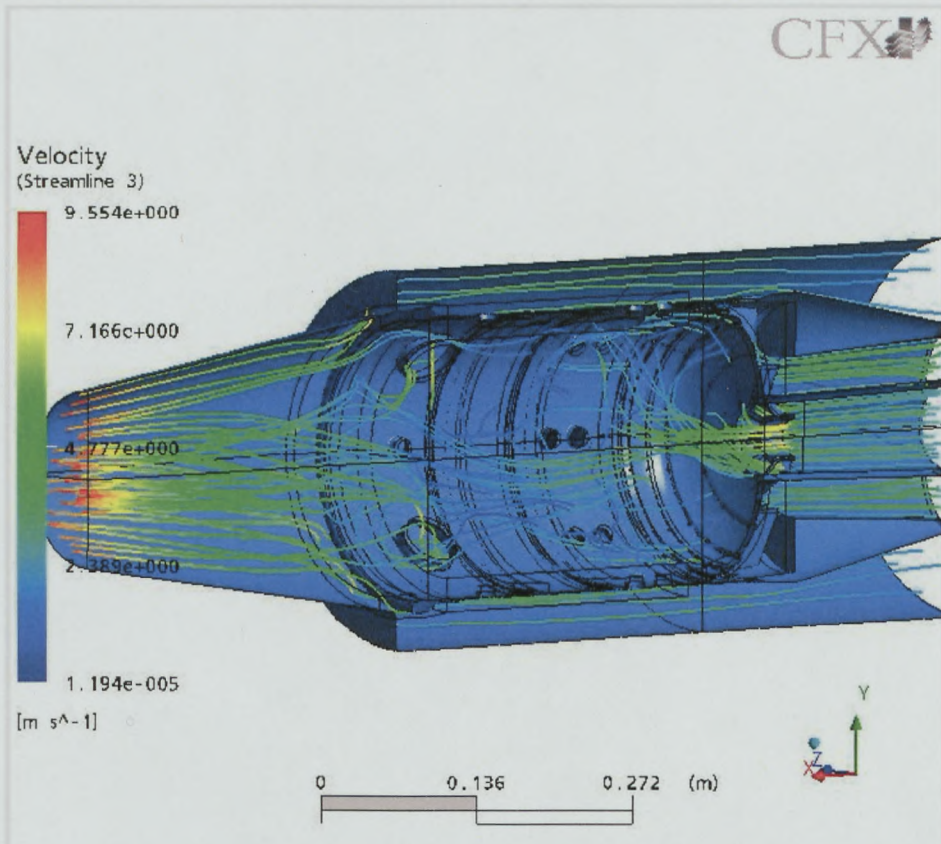


Figure 7: Unconverged run of the whole Olympus Rig. The simulation is good enough for calculating the maximum residence time inside the combustor at the lowest air mass flow rate of 0.2kg/s. The residence time was found to be 0.147seconds.

APPENDIX - E

Contents

LABVIEW 8 – Three Programs for controlling the μ Mist Device.....	291
Program No.1- First edition created May 2006	292
Program No.2 – First edition created June 2006	298
Program No.3 – First edition created July 2007	306
μ Mist Device - High Speed Images of The Ejection Spray.....	27

LABVIEW 8 – THREE PROGRAMS FOR CONTROLLING THE μ MIST DEVICE

Programs 1, 2 and 3 were created by Andreas Prongidis

LabView8 is a powerful programming package which is used here both for data acquisition but also for controlling the μ mist atomiser device. The data are sent as a voltage signal from the temperature and pressure probes to data reading LabView modules that transform the signal to numbers through the program to the computer. A similar but opposite procedure is used to control the device, with modules that send voltage to the valves and the heaters of the system. The procedure is continuous. The feedback is sent to the program with a frequency of 10 kHz. As the data change the response of the program is almost instant and action is taken according to the preset requirements. There are two interfaces that the programmer has to use; one is the graphical interface and the other is used to write the language of the program.

The graphical interface of the program simulates a real control panel and is much more user friendly and easy to understand. Figure 1.1 shows the graphical interface of the initial program created. It is the environment which one sees when the program is running. The control panel gives a continuous feedback from the device through the data values. It also helps the user to read and understand better the real time data by using thermometers for temperature display, a pressure gauge for the pressure and graphs for both. Moreover other helpful features, utilised here, are the progress bar, the placement of relevant information on the same graphical panels and the blinking Booleans that flash only to indicate that a pre-set condition is true. For example in figure 1.1 the chamber pressure is higher than the trigger pressure.

To run the program there are some values that need to be set by the user presented in sections 1.3 for program no.1 and in the relevant sections for all other programs thereafter.

The heater on and heater off times, in seconds, serve as a fail safe feature. The heaters are turned on for a short time and turned off for a longer time continuously, to avoid any deformation or damage to the coil heater. This feature doesn't affect the response of the program so much although a small delay in heating the cylindrical chamber is inevitable in program no. 1. In more recent programs- programs no. 2 and 3- this feature is disabled after the occurrence of the first ejection. It is used mostly to heat up the heaters, the liquid and the walls of the chamber in a uniform way, to prepare the system for the first ejection and to protect the heaters from overheating.

A spray where 90% of its droplets was lower than $5\mu\text{m}$ in diameter was achieved by using programs 2 and 3.



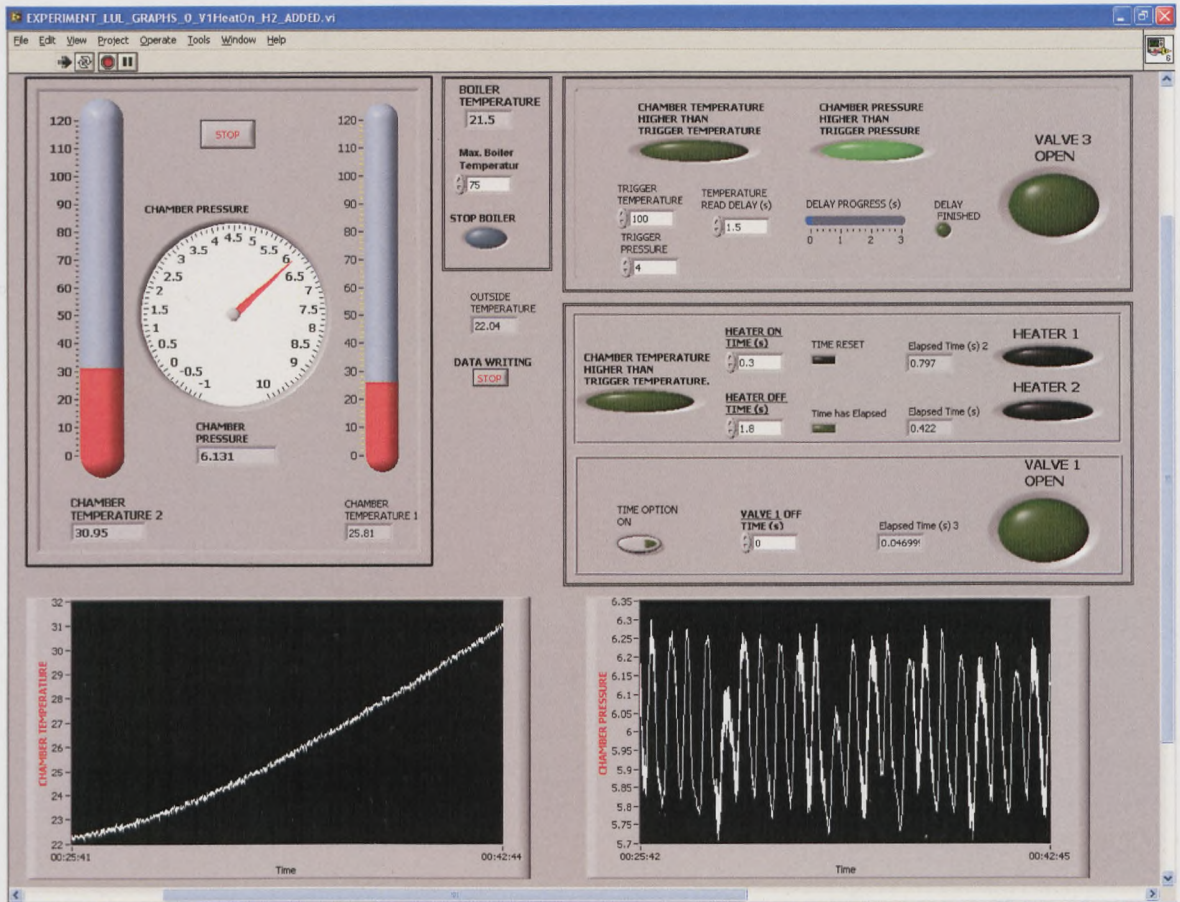


Figure 1.1: Graphical Interface of the LabView8 program for the fuel jet atomiser device.

1. Attributes and terminology used in program no. 1:

1.1 Data available:

- Chamber Temperature 1:** Lower positioned temperature probe inside the chamber.
- Chamber Temperature 2:** Upper positioned temperature probe inside the chamber.
- Boiler Temperature:** Temperature inside the heated liquid (in this case water) reservoir.
- Outside Temperature:** Room temperature.
- Pressure:** Pressure inside the chamber.

1.2 Program Controls:

- Valve 1:** Opening and closing of the Inlet Valve.
- Valve 2:** Opening and closing of the outlet Valve.
- Valve 3:** Opening and closing of the Ejection Valve.

Heater 1:	Coil Heater on and off control. Controls the temperature inside the chamber.
Heater 2:	Cartridge Heater on and off control. Controls the temperature inside the chamber.

1.3 Data that require input by the user:

Trigger Temperature:

Above this temperature set by the user and only if all parameters are met, the program triggers an ejection (Valve 3 opens).

Trigger Pressure:

Above this pressure and only if all set parameters are met, the program triggers an ejection.

Temperature Read Delay (seconds):

Time that is used to delay an ejection and starts when the above two parameters (Trigger temperature and pressure) are met. This parameter was used because the PT100's, the temperature probes installed in the chamber, fail to show the real temperature at the instance an ejection has just occurred. Although the probes sense the temperature drop and that is why the ejection valve closes at that moment the readings show a rise in temperature which does not really exist. The temperature read delay gives time to the program to get more accurate readings before it re-opens the ejection valve.

Heater On Time - Heater Off Time:

Times that control the period that both coil and cartridge heaters are turned on and off.

Max. Boiler Temperature:

The maximum temperature of the liquid (here de-ionised water) running through the pipes which relates directly to the maximum pump operating temperature. This parameter is used to draw the attention of the user to manually turn off the heater of the reservoir.

1.4 Booleans and Statement Connectors

Booleans are denoted in these explanatory notes by **bold** letters. They are true or false statements used as communication centres at different points of the program without the need of any connectors; a feature that keeps the program clean and simple.

Statement Connectors are denoted here by underlined italic letters. The most used connectors are and, or and inverse; the last used to inverse the statement that is connected to.

2. Logical Flow of Program no.1

The program is running in real time and thus it controls a device that sends back feedback on the changes that occur while it is causing them. This enables the program to make appropriate adjustments when they are needed although the set back is that the changes cannot appear instantly, due to the lag of the instruments, and this limits the frequency of the repeated ejections.

2.1 Step 1 – Data Acquisition

Reads the data (Section 1.1) in real time and sends them forward at the required statement assessment points.

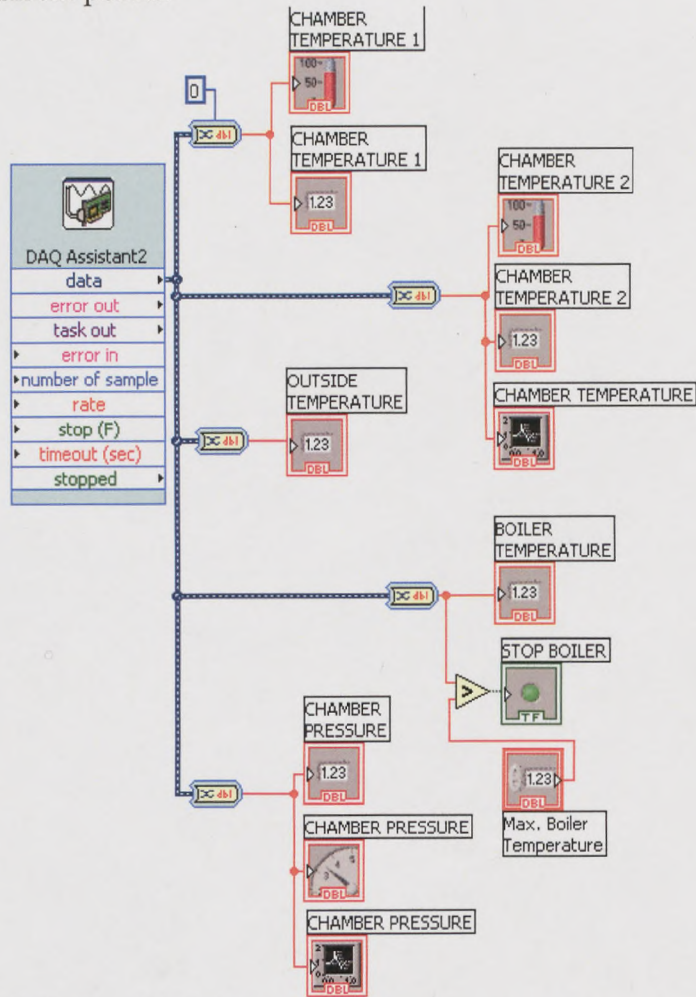


Figure 1.2: Data acquisition loop

2.2 Step 2 – Check Current State of Pressure and Temperature and Advise

2.2.1 Heaters Control

- **Statement 1**- Clock that keeps the heaters off

IF *Temperature 2* lower than the *Trigger temperature* is TRUE

AND

IF **Time Reset** is FALSE *reversed* to show TRUE

IF **Statement 1** returns TRUE THEN

Countdown does not start and **Time has Elapsed** is FALSE.

- **Statement 2**- Clock that turns the heaters on

IF **Time has Elapsed** is FALSE

IF **Statement 2** returns FALSE THEN

Start or Reset the countdown for *Heater On Time* in seconds.

When countdown finishes then **Time Reset** becomes TRUE momentarily.

- **Statement 1**- Clock that turns the heaters off.
IF **Time Reset** is TRUE

IF **Statement 1** returns FALSE THEN
Countdown starts or resets for **Heater Off Time** in seconds.

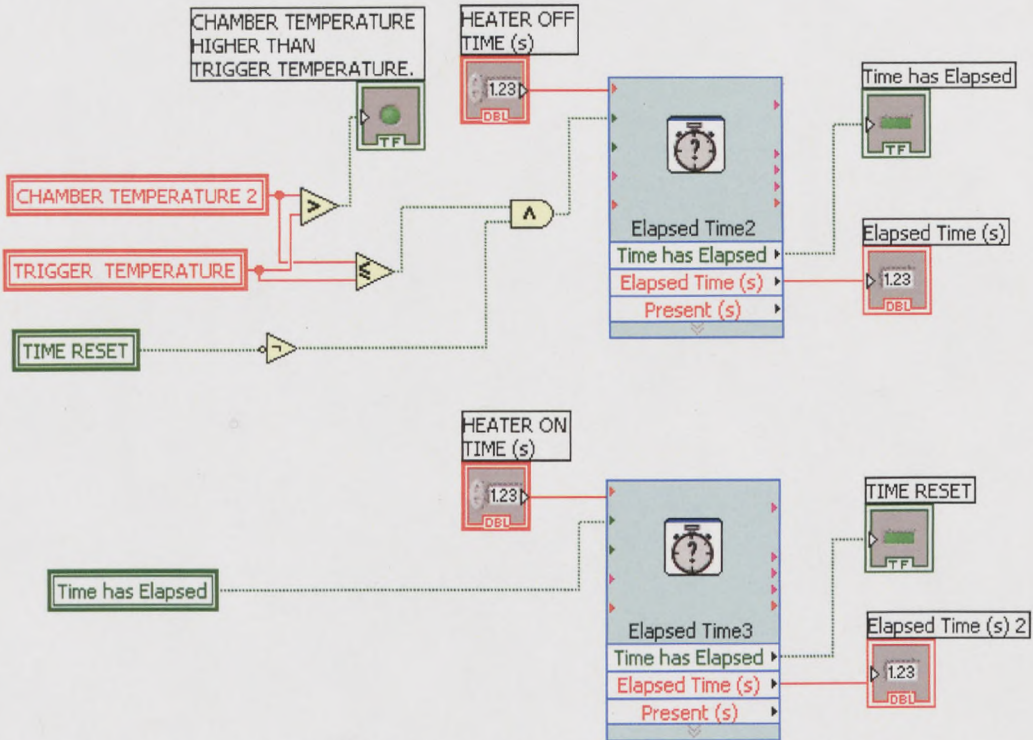


Figure 1.3: Part of the program used to control the heaters on and off time

2.2.2 Inlet Valve Operation

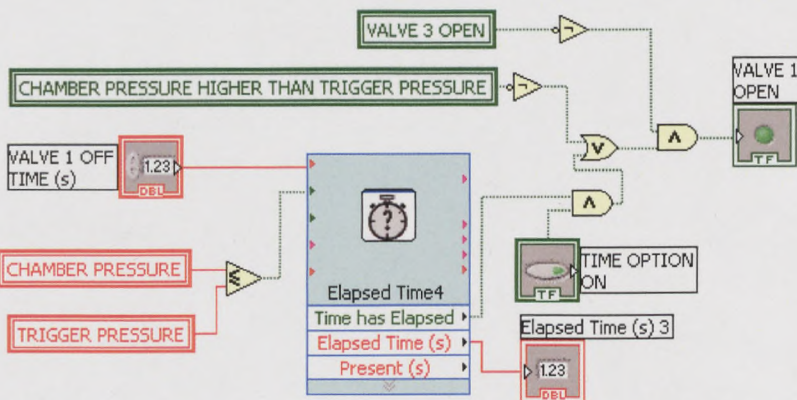


Figure 1.4: Part of the program which controls the inlet valve- V_1 .

- **Statement 3**- Advise if **Valve 1** should open or close
IF **Valve 3 Open** is FALSE *reversed* to TRUE
AND

IF *Chamber Pressure* less than the *Trigger Pressure* is TRUE

IF **Statement 3** returns TRUE THEN
Valve 1 Open is TRUE.

2.2.3 Ejection Valve Operation

- **Statement 4**- Temperature reading delay conditions:

IF **Valve 1 Open** is FALSE

OR

IF *Temperature 2* less than the *Trigger Temperature* is FALSE

IF **Statement 4** returns FALSE THEN

Start or reset countdown for the *Temperature Read Delay* time.

When the countdown ends the **Delay Finished** turns TRUE until **Valve 1 Open** becomes TRUE.

- **Statement 5**- Check *Chamber Pressure*

It checks if the *Chamber Pressure* is higher than the *Trigger Pressure* and if it is it returns a TRUE statement.

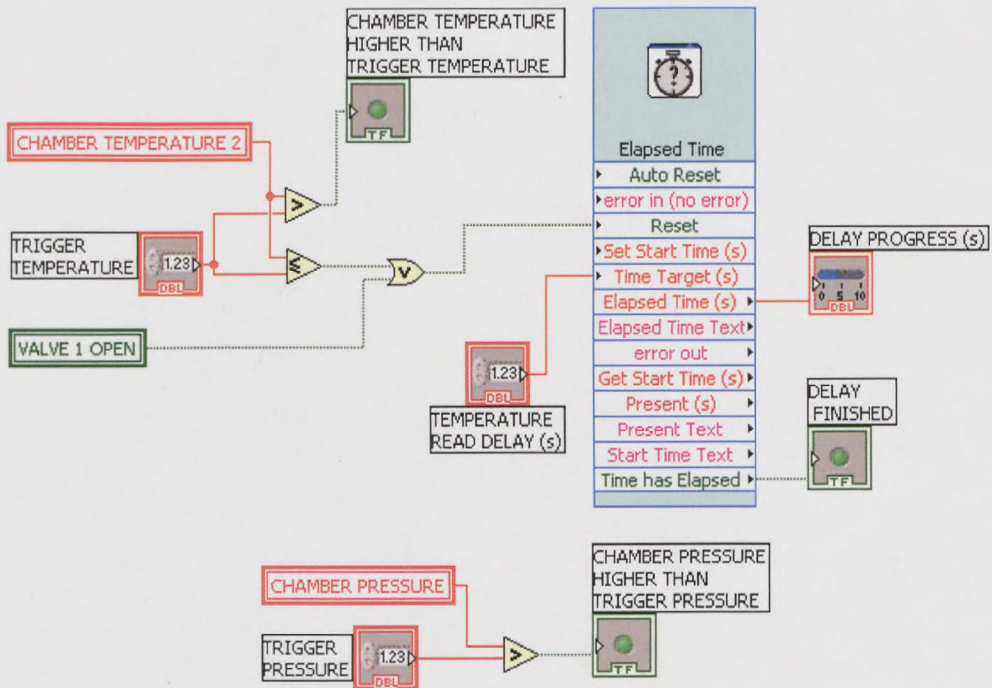


Figure 1.5: Control of ejection valve- V_3 , with time delay to get accurate readings

2.3 Step 3 - Check all Conditions and Command the controls of the device

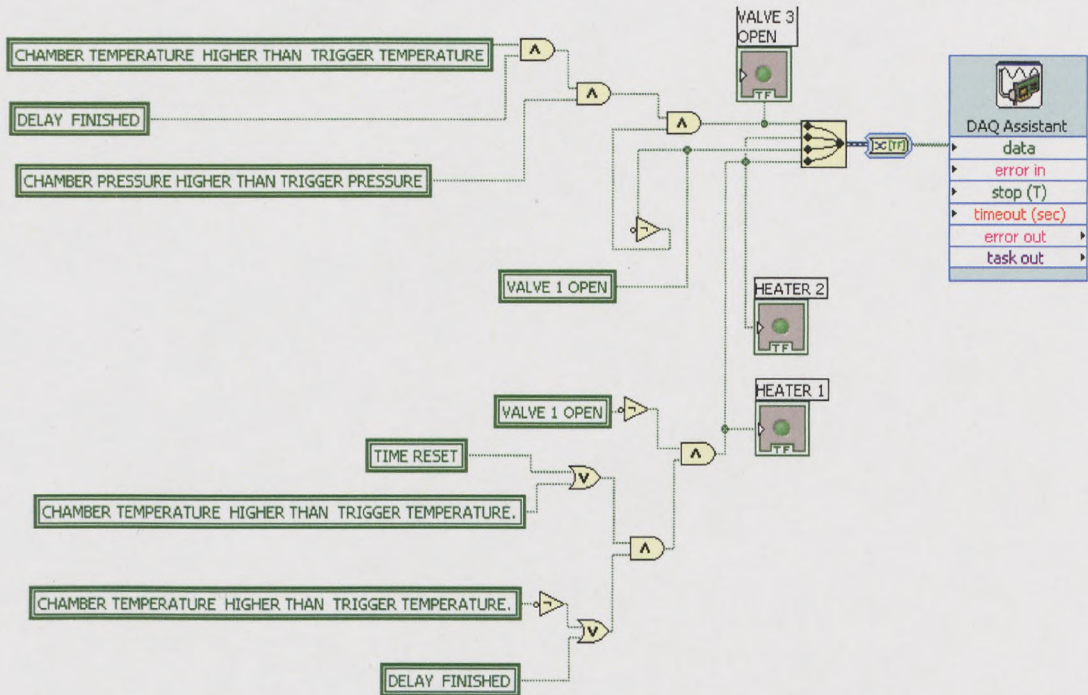


Figure 1.6: Part of the program which is used to command and control the devices of the fuel jet atomiser

2.3.1 Heaters On

The operation of the heaters is *reversed*. This means that when the end result of all statements is false then the heaters are turned on and the opposite. The conditions that turn the heaters on are:

1. **Chamber Temperature 2** higher than the **Trigger Temperature** is FALSE OR
 1. **Time Reset** is FALSE
- AND
2. **Chamber Temperature 2** higher than the **Trigger Temperature** is TRUE *reversed* to FALSE OR
 2. **Delay Finished** is TRUE
- AND
3. **Valve 1 Open** is TRUE *reversed* to FALSE

2.3.2 Opening of the Inlet Valve

The command for the inlet valve to open is given if **Valve 1 Open** is TRUE

2.3.3 Opening of the Ejection Valve

The ejection valve/ **Valve 3** opens if and only if:

1. The **Chamber Temperature 2** higher than the **Trigger Temperature** is TRUE
- AND
2. The **Delay Finished** is TRUE AND
 3. The **Chamber Pressure** higher than the **Trigger Pressure** is TRUE AND

4. Valve 1 Open is FALSE reversed to TRUE.

PROGRAM No.2 – First edition created on June 2006

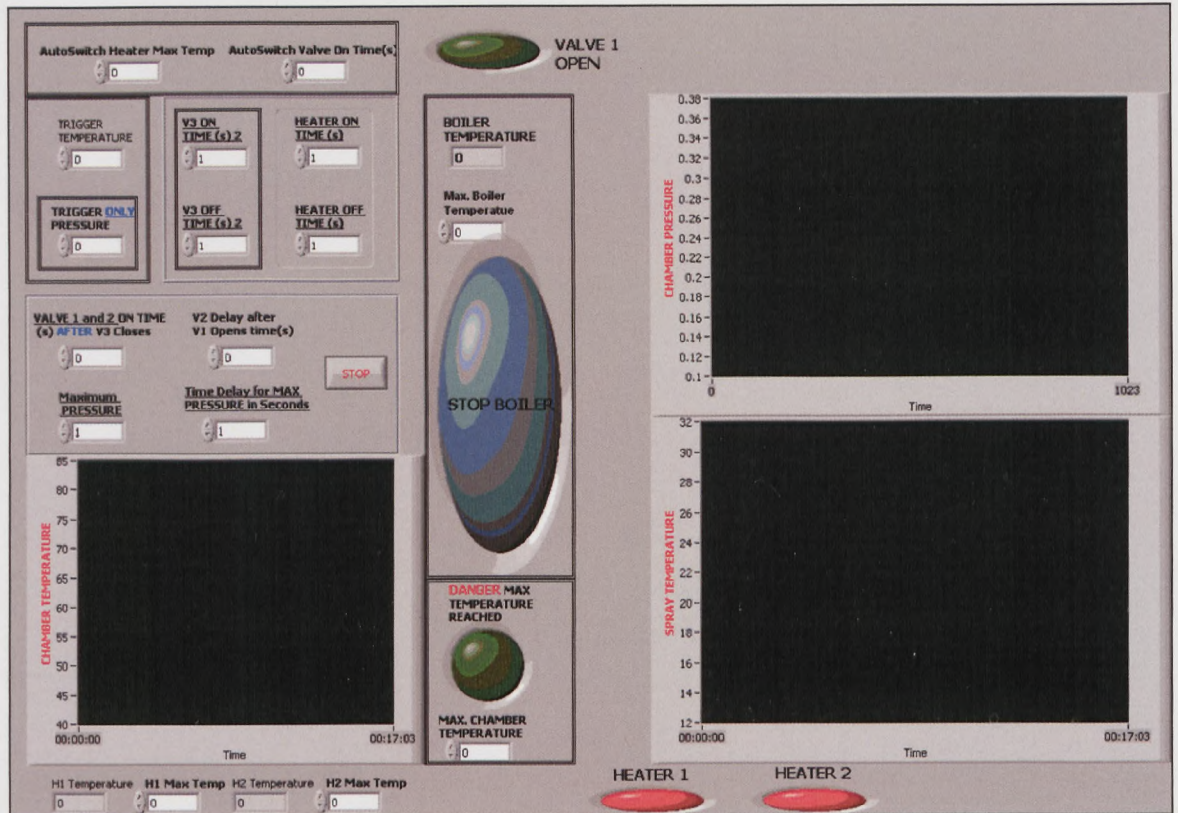


Figure 2.1: Graphical Interface of the LabView8 program no2 for the fuel jet atomiser device.

1. Attributes and terminology used in program no. 2:

1.1 Data available:

Chamber Temperature 1:	Lower positioned temperature probe inside the chamber.
Chamber Temperature 2:	Upper positioned temperature probe inside the chamber.
Boiler Temperature:	Temperature inside the heated liquid (in this case water) reservoir.
Outside Temperature:	Room temperature.
Pressure:	Pressure inside the chamber.
H1 Temperature:	Temperature of the coil heater.
H2 Temperature:	Temperature of the cartridge heater.

1.2 Program Controls:

Same as section 1.2 in Program 1

1.3 Data that require input by the user:

Trigger Temperature:

Above this temperature set by the user and only if all parameters are met, the program triggers an ejection (Valve 3 opens).

Trigger Pressure:

Above this pressure and only if all set parameters are met, the program triggers an ejection.

Heater On Time - Heater Off Time:

Times that control the period that both coil and cartridge heaters are turned on and off. While the program is running these two controls will disable after the first ejection and the heaters are left always on.

AutoSwitch Heater Max. Temp.:

Maximum temperature of the coil heater allowed. This temperature is specified by the manufacturer.

AutoSwitch Valve On Time(s):

When the maximum temperature of the coil heater is reached the inlet valve opens for this time specified by the user and closes momentarily in a periodical mode. The same happens with the outlet valve with a reduced frequency which is set by the V2 Delay After V1 Opens Time.

Valve 1 & 2 On Time After V3 Closes(s):

Time that controls the operation of the inlet and outlet valve at normal conditions and after the ejection valve closes. The time for opening of the outlet valve is not the same as the time for opening the inlet valve; see the setting below.

V2 Delay After V1 Opens Time

When the inlet valve opens for time x then the outlet valve opens with a fixed delay which is controlled by this setting. The inlet and outlet valves close at the same time.

V3 On Time:

Time that controls the opening of the ejection valve when all conditions are met. Once the ejection valve is opened then it will close only when this time elapses overriding all other conditions.

V3 Off Time:

Time that controls the closing of the ejection valve after it has been opened. These two settings control the frequency of the ejections.

Maximum Pressure

The maximum allowed pressure inside the chamber. This value should be lower than the maximum operational pressure specified by the manufacturer; see also the setting below.

Time Delay for Max. Pressure in seconds

Time to wait after the maximum pressure mentioned above is reached to open the outlet valve. This setting is used so as not to release too much pressure from inside the chamber due to delays between reading the pressure and commanding Valve 3 to open and then close.

H1 Max. Temp.

Maximum temperature allowed for the coil heater.

H2 Max. Temp.

Maximum temperature allowed for the cartridge heater.

Maximum Chamber Temperature

Maximum Temperature allowed inside the chamber.

Max. Boiler Temperature:

The maximum temperature of the liquid (here de-ionised water) running through the pipes which relates directly to the maximum pump operating temperature. This parameter is used to draw the attention of the user to manually turn off the heater of the reservoir.

1.4 Booleans and Statement Connectors

Same as section 1.4 in Program 1

2. Logical Flow of Program no. 2:

2.1 Step 1 – Data Acquisition

Reads the data (see Section 1.1) in real time and sends them forward at the required statement assessment points.

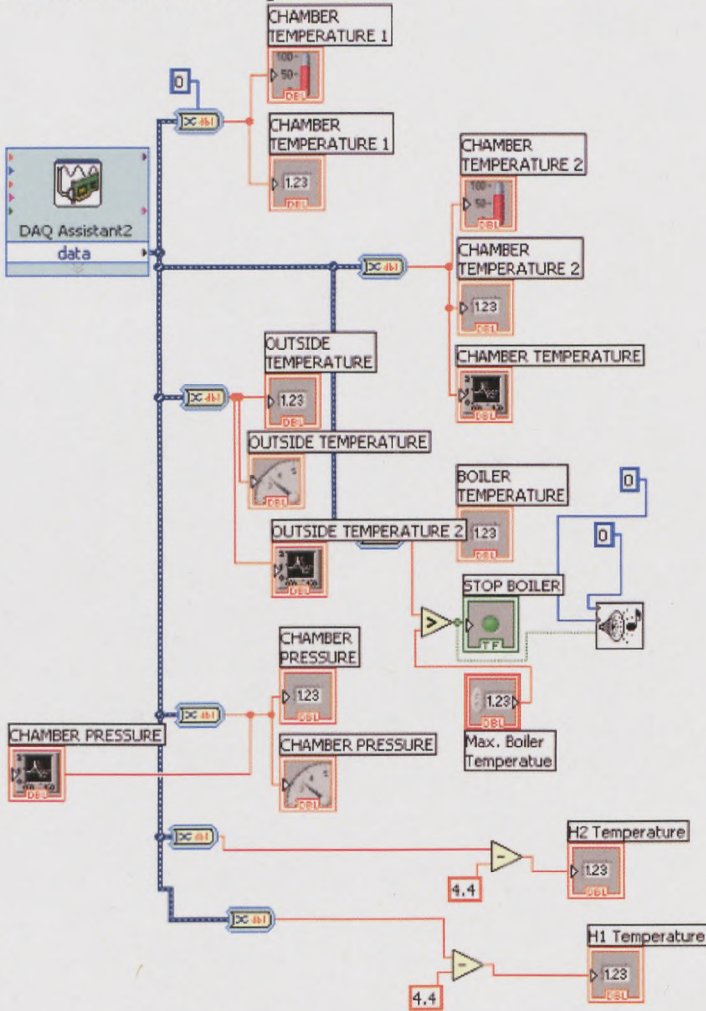


Figure 2.2: Data acquisition sub-program

2.2 Step 2 – Check Current State of Pressure and Temperature and Advise

2.2.1 Heaters Control

Same as section 2.2.1 in program 1. No amendments were made at this feature for program no.2. (Figure 1.3)

2.2.2 Inlet Valve Operation

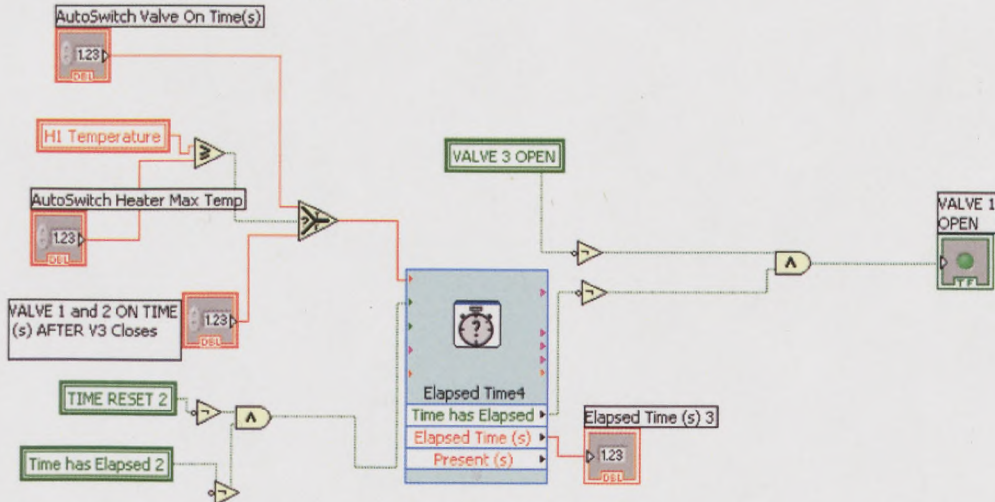


Figure 2.3: sub-program that advises for the desired Valve 1 operation.

- **Statement 1**- Refer also to section 4.3.4 and to its relevant figures for more information.

IF **Time Reset 2** is TRUE reversed to FALSE- see figure 4.5

AND

IF **Time has Elapsed 2** is TRUE reversed to FALSE- see figure 4.6

Note: **Time Reset 2** and **Time has Elapsed 2** turn both TRUE only at one instant in time which happens only when **Valve 3** closes after the opening time **V3 On Time**, set by the user, has expired.

IF **Statement 1** is FALSE THEN

Start or reset a countdown. The countdown time depends on the temperature of the coil heater- **Statement 2** below.

- **Statement 2**

IF **HI Temperature** higher or equal to **Auto-switch Max Temperature** TRUE THEN the time for countdown is taken as the **Auto-switch Valve on Time**.

IF **Statement 2** is FALSE THEN the time for countdown is set as the **Valve 1 and 2 On Time After V3 Closes**.

- **Statement 3**

IF **Valve 3 Open** is FALSE *reversed* to TRUE

AND

IF **Time has Elapsed** is FALSE *reversed* to TRUE

IF **Statement 3** returns TRUE THEN
Valve 1 Open turns TRUE.

2.2.3 Outlet Valve Operation

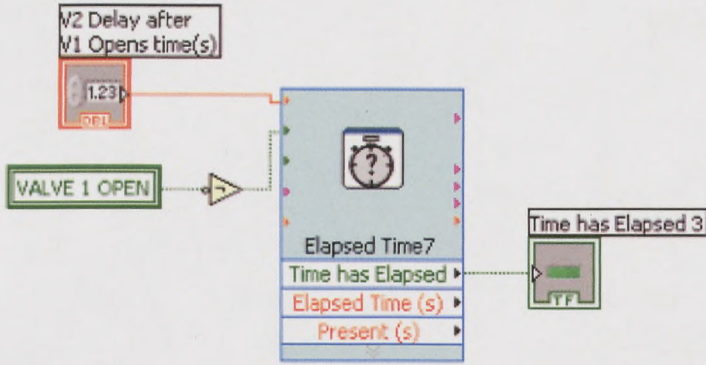


Figure 2.4: Section that advises for Valve 2 Operation.

IF **Statement 3** is TRUE *reversed* to FALSE THEN
 Start a countdown for **V2 Delay after V1 Opens Time** in seconds.
 When the countdown ends **Time has Elapsed 3** becomes TRUE.

2.2.4 Ejection Valve Operation

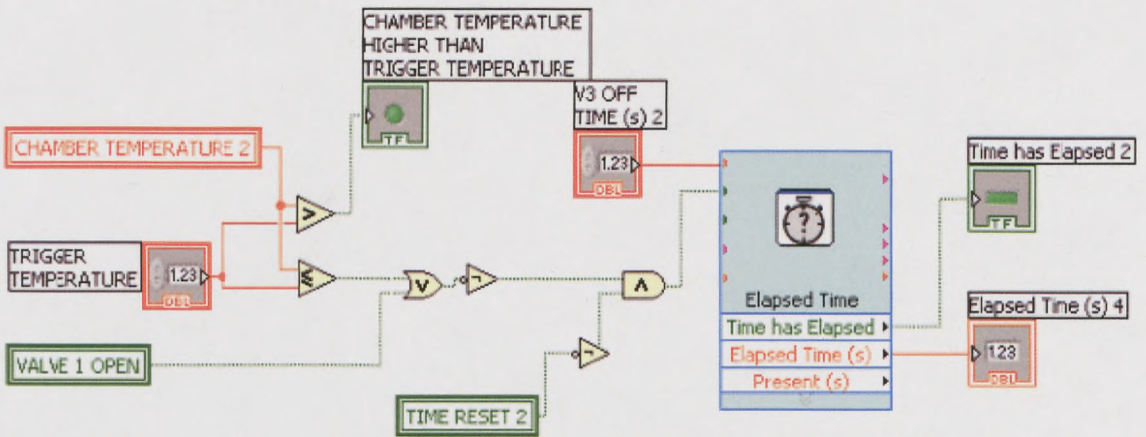


Figure 2.5: Section that controls the ejection valve closing time.

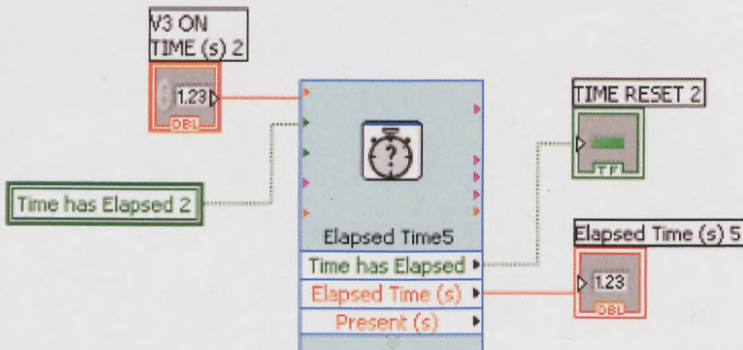


Figure 2.6: Section that controls the ejection valve opening time.

2.2.5 Advise *Valve 3* to Open:

- **Statement 4**- See Figure 4.5

IF *Chamber Temperature 2* lower than *Trigger Temperature* is FALSE
OR
IF **Valve 1 Open** is FALSE

- **Statement 5**

IF **Statement 4** becomes FALSE *reversed* to TRUE
AND
IF **Time Reset 2** is FALSE *reversed* to TRUE

IF **Statement 5** becomes TRUE THEN
Time has Elapsed 2 remains FALSE

- **Statement 6**- See Figure 4.6

If **Time has Elapsed 2** is FALSE THEN
Start or reset a countdown for **V3 On Time** in seconds.
When the countdown finishes **Time Reset 2** becomes TRUE.

2.2.6 Advise *Valve 3* to close

- **Statement 5**- See figures 4.5 and 4.6

IF **Statement 4** is FALSE *reversed* to TRUE
AND
IF **Time Reset 2** is TRUE *reversed* to FALSE

IF **Statement 5** becomes FALSE THEN

Start a countdown for **V3 Off Time** in seconds.

When the countdown ends **Time has Elapsed 2** becomes TRUE and thus **Time Reset 2** turns FALSE.

Note: If **Statement 4** (*Chamber temperature 2* lower than *Trigger temperature*) turns FALSE *reversed* to TRUE AND **Time Reset 2** is TRUE *reversed* to FALSE at any given moment (meaning that the ejection valve is closed at that time) then the clock in figure 3.6 will continue to countdown until the set **V3 Off Time** expires. The opposite happens for the opening time of *Valve 3*. If *Valve 3* opens then it remains open even if the *Chamber Temperature 2* falls below the *Trigger Temperature* until **V3 On Time** expires.

2.2.7 Report the Occurrence of the First Ejection

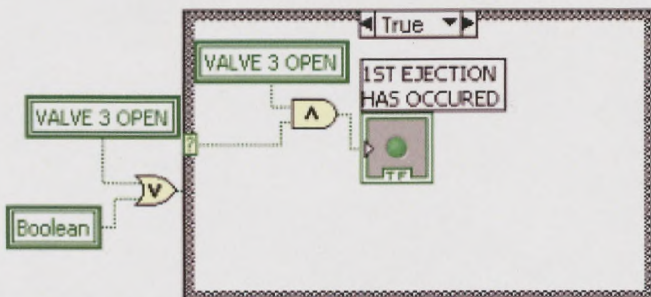


Figure 2.7: sub-program that reports the occurrence of the first ejection

- **Statement 7**

IF **Valve 3 Open** is TRUE

OR

Boolean is TRUE

Note: The Boolean here is used to initialise the program and to denote that time $t=0$ has just passed. When starting the program, time $t=0$ has already passed. The clock in figure 4.8 will never be equal to zero so this will start the countdown module for an infinitely small countdown time set here to be 0 seconds. The Boolean turns to TRUE at the instance the program starts to run as the countdown time is 0s and then **resets** back to FALSE. The option to **reset** the Boolean was chosen here to make sure that the only time the Boolean is TRUE it is at the instance that time $t=0$ has just passed.

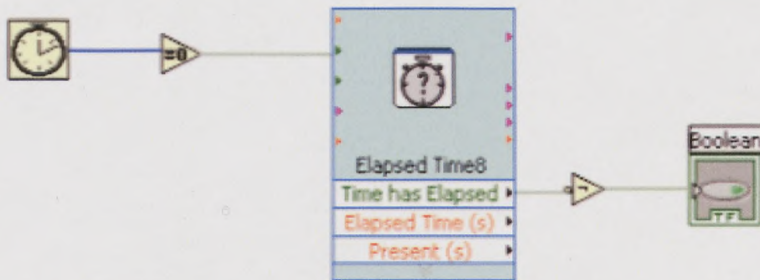


Figure 2.8: When $t=0$ has just passed Time has Elapsed will become instantly TRUE. The elapsed time module gives the option of resetting the Time has Elapsed statement and thus the Boolean.

IF **Statement 7** is FALSE THEN

The program waits until it becomes TRUE.

- **Statement 8**

IF **Statement 7** is TRUE

AND

Valve 3 Open is TRUE

IF **Statement 8** is TRUE THEN

The first ejection has happened-**1st Ejection has Occurred** is TRUE

IF **Statement 8** is FALSE THEN

This denotes that time $t=0$ has just occurred and the program has just initialised and **1st Ejection has Occurred** should be FALSE.

2.3 Step 3 - Check all Conditions and Command the controls of the device

2.3.1 Heaters On

The operation of the heaters is *reversed* like in program no.1. The conditions that turn the heaters on are:

1. **Chamber Temperature higher than Trigger Temperature** is FALSE OR
1. **Time Reset** is FALSE

AND

2. **Chamber Temperature higher than Trigger Temperature** is TRUE reversed to FALSE OR

2. **Valve 3 Open** is FALSE

AND

3. **Valve 1 Open** is TRUE reversed to FALSE

AND

4. **1st Ejection Has Occurred** is TRUE reversed to FALSE

OR

1. **Chamber Temperature 2** higher or equal to **Max. Chamber Temperature** is FALSE

OR

a) For the Coil Heater:

1. **H1 Temperature** higher than **H1 Max. Temp.** is FALSE

b) For the Cartridge Heater:

1. **H2 Temperature** higher than **H2 Max. Temp.** is FALSE

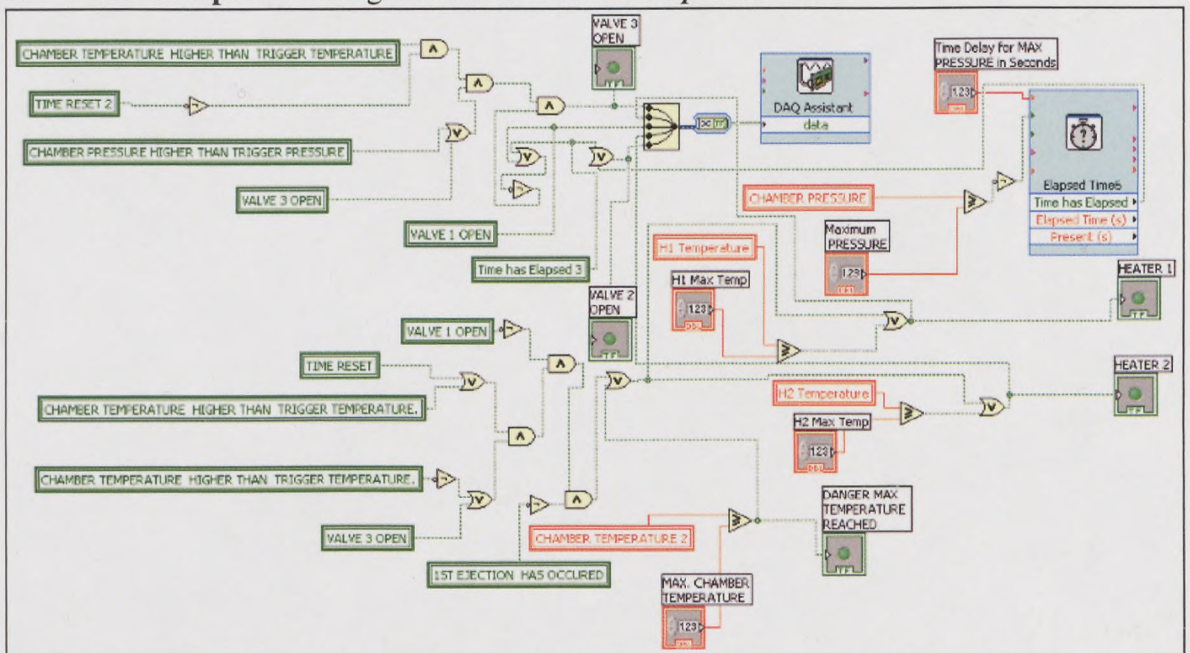


Figure 2.9: Check all conditions and control the device.

2.3.2 Opening of the Inlet Valve

The command for the inlet valve to open is given if **Valve 1 Open** is TRUE

2.3.3 Opening of the Outlet Valve

Valve 2 opens if and only if:

1. **Time has Elapsed 3** is TRUE

OR

1. The **Chamber Pressure** is higher or equal to the **Maximum Pressure**. This statement when TRUE reversed here to FALSE starts a countdown for **Time Delay for**

Max Pressure in seconds. When this time expires it returns a TRUE statement which opens *Valve 2*.

2.3.4 Opening of the Ejection Valve

Valve 3 opens if and only if:

1. **Chamber Temperature higher than Trigger Temperature** is TRUE AND
2. **Time Reset 2** is FALSE reversed to TRUE

AND

3. **Chamber Pressure Higher than Trigger Pressure** is TRUE OR

3. **Valve 3 Open** is TRUE

AND

4. **Valve 1 Open** is FALSE reversed to TRUE OR

4. **Time has Elapsed 3 (Valve 2 control)** is FALSE reversed to TRUE.

PROGRAM No.3 – First edition created on July 2007

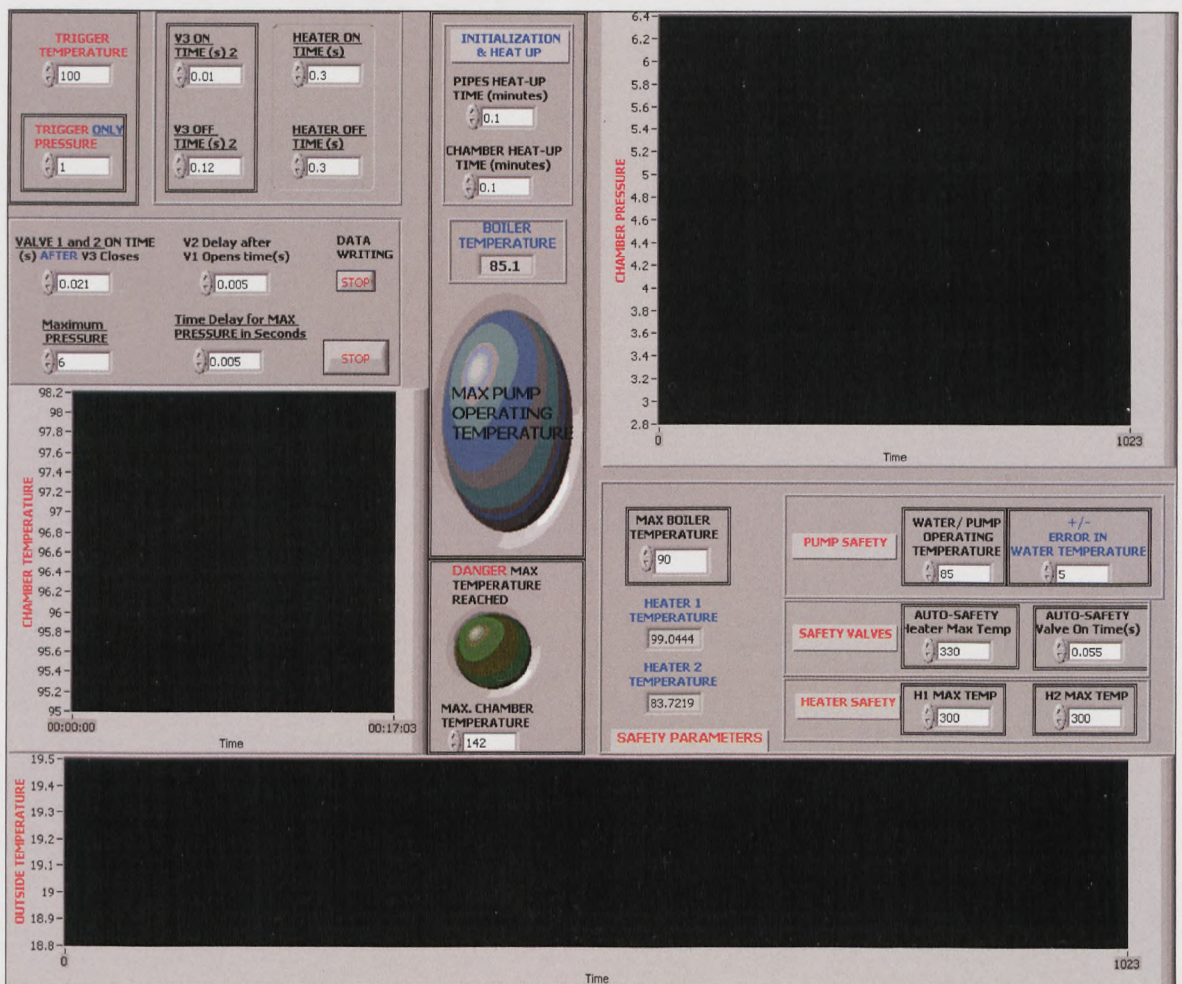


Figure 3.1: Graphical Interface of the LabView8 program no.3 for the fuel jet atomiser device.

1. Attributes and terminology used in program no. 3:

1.1 Data available:

Chamber Temperature 1:	Lower positioned temperature probe inside the chamber.
Chamber Temperature 2:	Upper positioned temperature probe inside the chamber.
Boiler Temperature:	Temperature inside the heated liquid (in this case water) reservoir.
Outside Temperature:	Room temperature.
Pressure:	Pressure inside the chamber.
H1 Temperature:	Temperature of the coil heater.
H2 Temperature:	Temperature of the cartridge heater.

1.2 Program Controls:

Same as section 1.2 in Program 1 with one extra control:

Reservoir Heater: Heater on and off control. Controls the temperature of the circulating liquid.

1.3 Data that require input by the user:

Trigger Temperature:

Above this temperature set by the user and only if all parameters are met, the program triggers an ejection (Valve 3 opens).

Trigger Only Pressure:

Above this pressure and only if all set parameters are met, the program triggers an ejection. If an ejection is triggered and the pressure drops the valve will not close until the ejection time- set by the user- elapses.

Water/Pump Operating Temperature:

Temperature at which the water in the reservoir should reach. This setting is used also to control the operation of the pump; see setting below.

+/- Error in Water Temperature:

Plus and minus value from the value of the setting above. Between these values the pump should operate.

Pipes Heat Up Time(minutes):

Time that is used by the program to circulate the hot water around the pipes. Before this time elapses the program will not start operating any controls related to the chamber.

Chamber Heat Up Time(minutes):

Time that is used by the program to pass the hot water through the chamber. Before this time elapses the program will not start operating any controls related to the chamber except the inlet and outlet valves.

Heater On Time - Heater Off Time(s):

Times that control the period that both coil and cartridge heaters are turned on and off. While the program is running these two controls will disable after the first ejection and the heaters are left always on.

Auto-Safety Heater Max. Temp.:

Maximum temperature of the coil heater allowed. This temperature is specified by the manufacturer.

Auto-Safety Valve On Time(s):

When the maximum temperature of the coil heater is reached the inlet valve opens for this time specified by the user and closes momentarily in a periodical mode. The same happens with the outlet valve with a reduced frequency which is set by the V2 Delay After V1 Opens Time.

Valve 1 & 2 On Time After V3 Closes(s):

Time that controls the operation of the inlet and outlet valve at normal conditions and after the ejection valve closes. The time for opening of the outlet valve is not the same as the time for opening the inlet valve; see the setting below.

V2 Delay After V1 Opens Time

When the inlet valve opens for time x then the outlet valve opens with a fixed delay which is controlled by this setting. The inlet and outlet valves close at the same time.

V3 On Time:

Time that controls the opening of the ejection valve when all conditions are met. Once the ejection valve is opened then it will close only when this time elapses overriding all other conditions.

V3 Off Time:

Time that controls the closing of the ejection valve after it has been opened. These two settings control the frequency of the ejections.

Maximum Pressure

The maximum allowed pressure inside the chamber. This value should be lower than the maximum operational pressure specified by the manufacturer; see also the setting below.

Time Delay for Max. Pressure in seconds

Time to wait after the maximum pressure mentioned above is reached to open the outlet valve. This setting is used so as not to release too much pressure from inside the chamber due to delays between reading the pressure and commanding Valve 3 to open and then close.

H1 Max. Temp.

Maximum temperature allowed for the coil heater.

H2 Max. Temp.

Maximum temperature allowed for the cartridge heater.

Maximum Chamber Temperature

Maximum Temperature allowed inside the chamber.

Max. Boiler Temperature:

The maximum temperature of the liquid (here de-ionised water) running through the pipes which relates directly to the maximum pump operating temperature. This parameter is used to draw the attention of the user to manually turn off the heater of the reservoir.

1.4 Booleans and Statement Connectors

Same as section 1.4 in program 1

2. Logical Flow of Program no.3:

2.1 Step 1 – Data Acquisition

Reads the data (see Section 1.1) in real time and sends them forward at the required statement assessment points.

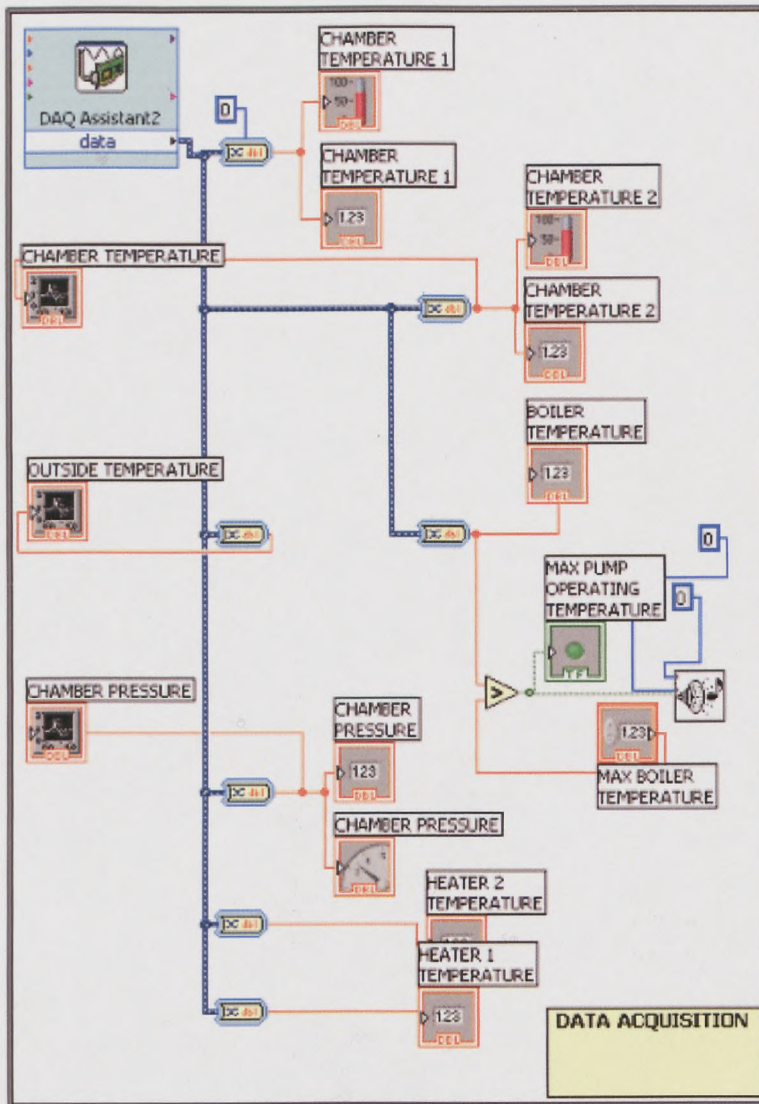


Figure 3.2: Data acquisition sub-program

2.2 Step 2 – Check Parameters

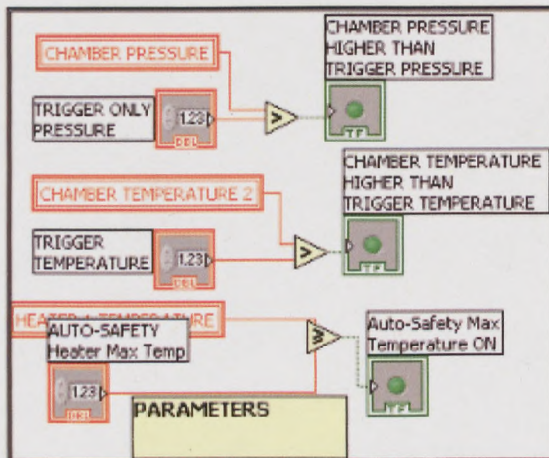


Figure 3.3: Section of the program that checks important parameters.

This section checks parameters that are used throughout the program. The booleans turn TRUE if:

1. The *Chamber Pressure* is higher than the *Trigger Only Pressure – Chamber Pressure Higher than Trigger Pressure* boolean.
2. The *Chamber Temperature 2* is higher than the *Trigger Temperature – Chamber Temperature Higher than Trigger Temperature* boolean.
3. The *Heater 1 Temperature* is higher of equal than the *Auto-Safety Heater Max. Temp. – Auto-Safety Max. Temperature On* boolean.

2.3 Step 3 – Preparation and Pipes Heat Up

The sub-program in figure 6.3 decides whether to turn on the pump, to circulate the water around the pipes at first and whether to pass the water through the chamber afterwards. It then gives the signal that the device is ready for step 4 which prepares the conditions for ejection.

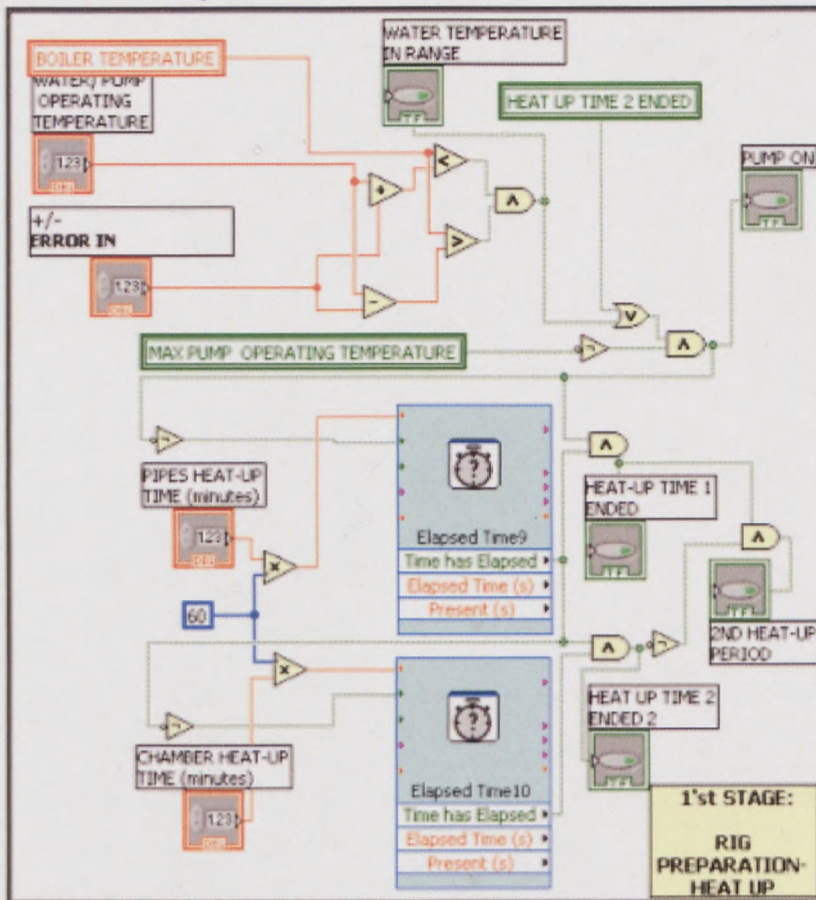


Figure 3.4: Sub-program that prepares the heat-up of the device.

- **Statement 1**

IF *Boiler Temperature* less than the *Water/ Pump Operating Temperature* plus the *Error in Water Temperature* is TRUE

AND

IF *Boiler Temperature* higher than the *Water/Pump Operating Temperature* minus the *Error in Water Temperature* is TRUE

IF **Statement 1** is TRUE THEN
Water Temperature in Range is TRUE

- **Statement 2**

IF **Statement 1** is TRUE

OR

IF **Heat Up Time 2 Ended** is TRUE

- **Statement 3**

IF **Statement 2** is TRUE

AND

IF **Max Pump Operating Temperature** is FALSE *reversed* to TRUE

IF **Statement 3** is TRUE THEN

Pump On is TRUE

Then **Statement 3** is *reversed* to FALSE, which starts a countdown for **Pipes Heat Up Time** in minutes. When this countdown expires the resulting statement (**Statement (a)**) turns TRUE (upper clock). **Statement (a)** is reversed to show FALSE to start a countdown on the bottom clock for **Chamber Heat Up Time** in minutes.

- **Statement 4**

IF **Statement (a)** (upper clock) is TRUE

AND

IF **Statement 3** is TRUE

IF **Statement 4** is TRUE THEN

Heat Up Time 1 Ended is TRUE

- **Statement 5**

IF **Statement (a)** is TRUE

AND

IF bottom clock has finished counting down for **Chamber Heat Up Time** in minutes is TRUE

IF **Statement 5** is TRUE (i.e. if both clocks have finished their countdown) THEN
Heat Up Time 2 Ended 2 is TRUE

- **Statement 6**

IF **Heat Up Time 1 Ended** is TRUE

AND

IF **Heat Up Time 2 Ended 2** is TRUE reversed to FALSE

IF **Statement 6** is FALSE THEN

2nd Heat Up Period is FALSE

2.3.1 Report that the Heat Up Time has Ended

This feature in figure 6.4 is used to make sure that after heating up the pipes and the chamber the program will move on to step 4. In the case the pump stops operating due to a high temperature in the liquid reservoir (in this case water), the program will not

start heating up again the chamber after the water temperature drops back to an operational value.

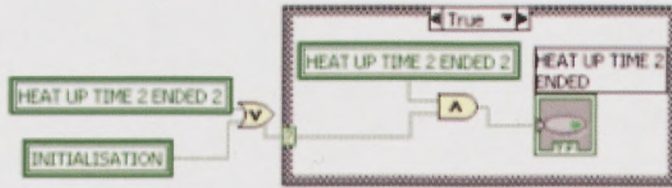


Figure 3.5: Sub-program that reports that the preparation of the device has ended.

- **Statement 7**

IF **Heat Up Time 2 Ended 2** is TRUE

OR

Initialisation is TRUE (time $t=0$ has just passed; see figure 6.7)

IF **Statement 7** is FALSE THEN

Do nothing until it becomes TRUE

- **Statement 8**

IF **Statement 7** is TRUE

AND

Heat Up Time 2 Ended 2 is TRUE

IF **Statement 8** is FALSE THEN

Time $t=0$ has just passed.

IF **Statement 8** is TRUE THEN

Heat Up Time 2 Ended turns TRUE and will never turn FALSE even when the program is terminated by the user. It will turn FALSE again when the user starts the program again when time $t=0$ has just passed.

2.4 Step 4 – Check Current State of Pressure and Temperature and Advise

2.4.1 Heaters Control

The heaters control section is the same as section 2.2.1. The only change that was made to this section is in the bottom clock of figure 6.5. When the bottom clock starts a countdown, for Heater on Time in seconds, and until that time expires the resulting statement (**Statement (b)**) -where the Boolean **Time Reset** was connected in the previous programs i.e. see sections 2.2.1 and 4.2.1- remains FALSE; this sends an advice that the heaters should turn on. A new statement is connected at that point with an *OR* connector:

Statement 9

If countdown has not passed the *Heater on Time* in seconds- **Statement (b)** is FALSE

OR

Heat Up Time 2 Ended is TRUE *reversed* to FALSE

AND

1st Ejection Has Occurred is TRUE *reversed* to FALSE

IF **Statement 9** is FALSE THEN
Time Reset becomes FALSE

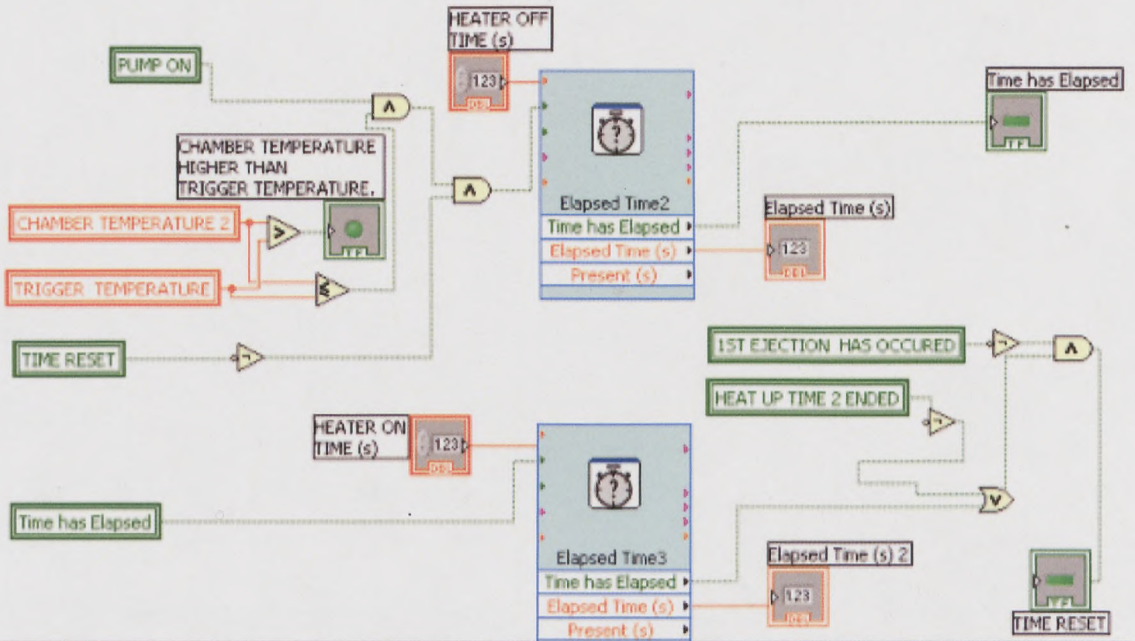


Figure 3.6: Section that controls the heaters.

2.4.2 Inlet Valve Operation

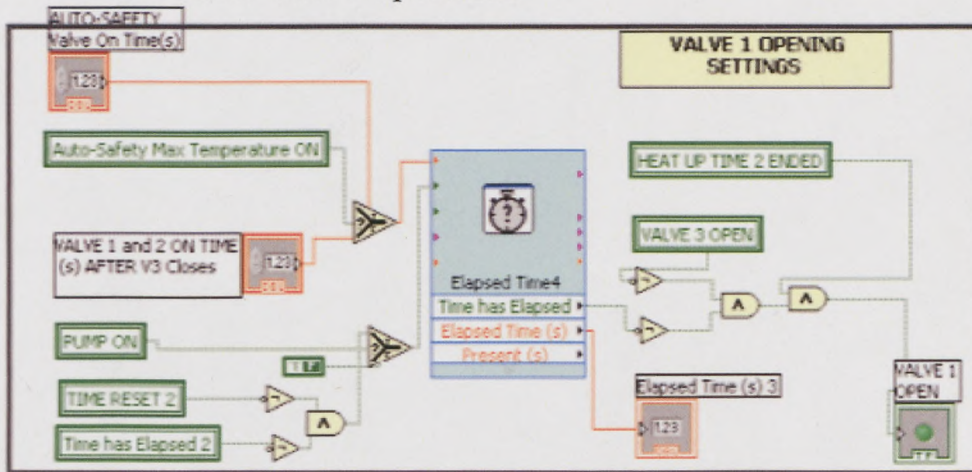


Figure 3.7: sub-program that advises for the desired Valve 1 operation.

This sub-program, that advises for the operation of the inlet valve, is almost the same as in program no.2 and has undergone very small changes. The reader should refer also to section 4.2.2:

Change 1: The countdown for either *Auto Safety Valve On Time* or *Valve 1 and 2 On Time After V3 Closes* in seconds will start or reset only when **Pump On** is TRUE.

Change 2: **Heat Up Time 2 Ended** is connected with an AND before the resulting boolean **Valve 1 Open**

2.4.3 Outlet Valve Operation

This section of the program was left unchanged. Refer to section 2.2.3 in program no. 2.(Figure 2.4)

2.4.4 Ejection Valve Operation

This part of the program was left unchanged. Refer to section 2.4.4 of program no. 2. (Figures 2.5-2.6)

2.4.5 Report the Occurrence of the First Ejection

This part of the program in figure 6.7 is left the same as in program no.2. The reader should note only that the name of the **Boolean** in program no. 2 is changed here to **Initialisation**, which is a more appropriate name and indicates its use; to show that time $t=0$ has just passed.

2.5 Step 5 - Check all Conditions and Command the controls of the device (Figure 6.8)

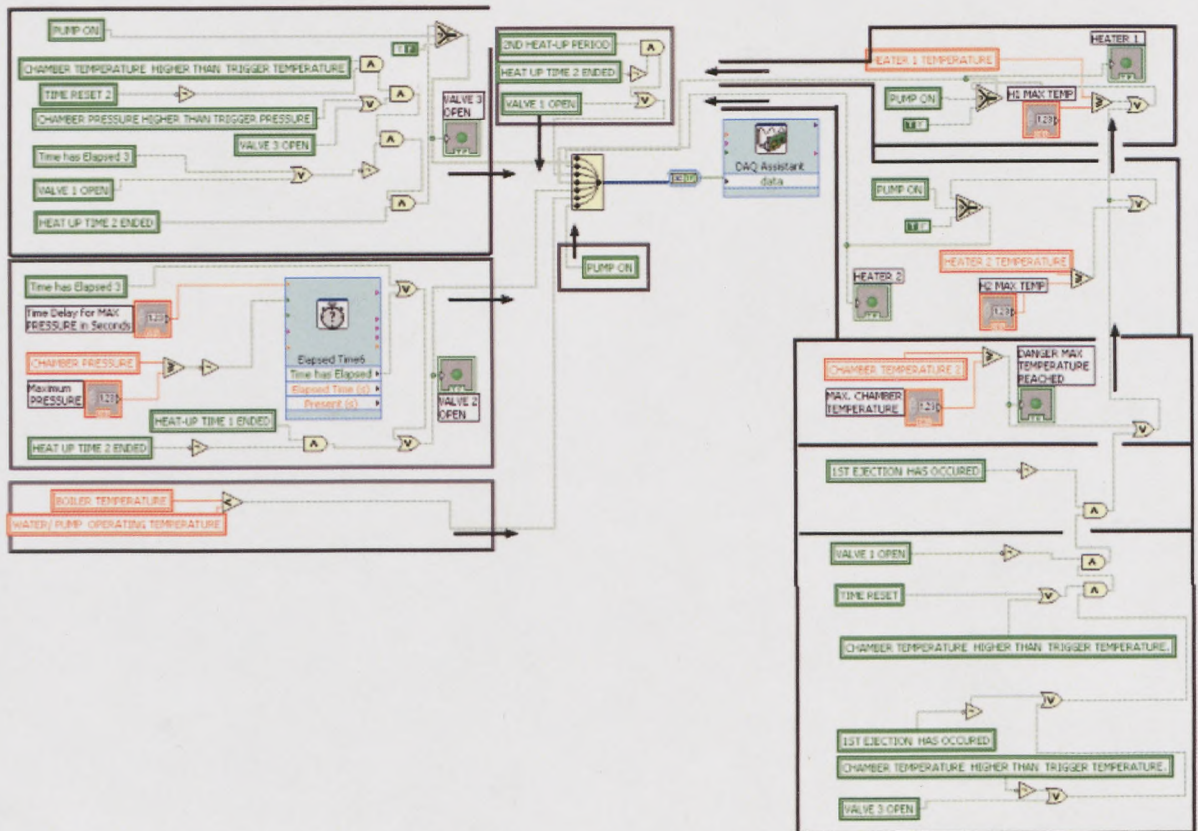


Figure 3.8: sub-program that checks all conditions and controls the device at step 5.

2.5.1 Reservoir Heater- Boiler On

The heater in the Boiler is turned on if:

1. The **Boiler Temperature** is lower than the **Water/Pump Operating Temperature**

2.5.2 Pump Operation:

The Pump turns on when:

1. **Pump On** turns TRUE

2.5.3 Heaters On

The operation of the heaters is *reversed* like in program no.1. The conditions to turn the heaters on are:

1. **Chamber Temperature higher than Trigger Temperature** is FALSE *OR*

1. **Time Reset** is FALSE

AND

2. **Chamber Temperature higher than Trigger Temperature** is TRUE *reversed* to FALSE *OR*

2. **Valve 3 Open** is TRUE

AND

3. **Valve 1 Open** is TRUE *reversed* to FALSE

AND

4. **1st Ejection Has Occurred** is TRUE *reversed* to FALSE

OR

1. **Chamber Temperature 2** higher or equal to *Max. Chamber Temperature* is FALSE

OR

a) For the Coil Heater:

1. **H1 Temperature** higher than *H1 Max. Temp.* is FALSE while **Pump On** is TRUE.

b) For the Cartridge Heater:

1. **H2 Temperature** higher than *H2 Max. Temp.* is FALSE while **Pump On** is TRUE

2.5.4 Opening of the Inlet Valve

The command for the inlet valve to open is given if:

1. **2nd Heat Up Period** is TRUE *AND*

2. **Heat Up Time 2 Ended** is FALSE *reversed* to TRUE

OR

1. **Valve 1 Open** is TRUE

2.5.5 Opening of the Outlet Valve

Valve 2 opens if and only if:

1. **Time has Elapsed 3** is TRUE

OR

1. **Chamber Pressure** is higher or equal to the *Maximum Pressure*. This statement when TRUE *reversed* here to FALSE starts a countdown for *Time Delay for Max Pressure* in seconds. When this time expires it returns a TRUE statement which opens *Valve 2*.

2.5.6 Opening of the Ejection Valve

The Conditions that Open *Valve 3* are:

IF **Pump On** is TRUE THEN IF:

1. **Chamber Temperature higher than Trigger Temperature** is TRUE AND
2. **Time Reset 2** is FALSE reversed to TRUE

AND

3. **Chamber Pressure Higher than Trigger Pressure** is TRUE OR
3. **Valve 3 Open** is TRUE

AND

4. **Valve 1 Open** is FALSE reversed to TRUE OR
 4. **Time has Elapsed 3** (*Valve 2* control) is FALSE reversed to TRUE.
-

The following images were recorded from one single ejection using Program 1.

The velocity of some droplets in the spray, were measured to be between ~ 13.5 to $14.5 \left(\frac{m}{s}\right)$. The time difference between each frame is $\sim 0.83333(ms)$

